

**CHARACTERIZATION OF THE FLOW QUALITY IN THE BOEING
SUBSONIC WIND TUNNEL**

by
Claire Diffey

A Thesis

*Submitted to the Faculty of Purdue University
In Partial Fulfillment of the Requirements for the degree of*

Master of Science in Aeronautics and Astronautics



School of Aeronautics & Astronautics

West Lafayette, Indiana

August 2019

**THE PURDUE UNIVERSITY GRADUATE SCHOOL
STATEMENT OF COMMITTEE APPROVAL**

Dr. John Sullivan, Co-Chair

Department of Aeronautics and Astronautics

Dr. Sally Bane, Co-Chair

Department of Aeronautics and Astronautics

Dr. Steven Schneider

Department of Aeronautics and Astronautics

Approved by:

Dr. Weinong Chen

Head of the Graduate Program

ACKNOWLEDGMENTS

I would like to thank my advisors Professors John Sullivan and Sally Bane for their constant guidance, advice and knowledge during my time here at Purdue and for providing the opportunity to work on this project. I would also like to thank Professor Steven Schneider for his many helpful discussions related to this work. I would also like to thank the professors at Purdue who taught my engineering courses with both a high level of knowledge and enthusiasm. Funding for this project was provided by the Boeing Company.

The machinists in the ASL machine shop were some of the biggest contributors to the completion of this work. Thanks to Jerry Hahn for making many of my random tunnel repair parts and Jim Younts for replacing the tiny wires on the multiple hot-wire probes that I broke. Robin Snodgrass helped me with almost every upgrade I had to do on the wind tunnel, stopped me from making needlessly convoluted part designs and helped to fix the ones that I did make. Thanks also to John Phillips for making up for my severe lack of electrical knowledge when getting the wind tunnel door to work.

I would also like to my parents Terry and Grace Diffey for their continued support, especially to my mum, for spending a lot of her time editing this thesis; without her help, it would be unintelligible. Thanks also to Aaron Blacker, Tim Gurshin and Jakob Hardtl for the friendship and introducing me to the American diet.

TABLE OF CONTENTS

LIST OF TABLES	6
LIST OF FIGURES	7
SYMBOLS	10
ABBREVIATIONS	11
ABSTRACT	12
1. INTRODUCTION	13
1.1 Background	13
1.2 Motivation	16
1.3 Low-Turbulence Wind-Tunnel Flow Characteristics	17
2. WIND TUNNEL DESIGN	19
2.1 General Description	19
2.2 Main Components	20
2.2.1 First Diffuser	20
2.2.2 Breather	22
2.2.3 Turning Vanes	23
2.2.4 Wind Tunnel Fan	23
2.2.5 Stilling Section – Screens and Honeycomb	24
2.2.6 Contraction	26
2.3 Wind Tunnel Performance	28
3. INSTRUMENTATION AND DATA REDUCTION	29
3.1 Reference Velocity	29
3.2 Hot-Wire Anemometry	32
3.2.1 Theory of Operation	32
3.2.2 Instrumentation	33
3.2.3 Probe Calibration	34
3.3 Temperature Measurement	35
3.4 Traverse System	35
3.5 Survey Grid	36
3.6 Measurement Parameters	38

3.7	Correlating tests	39
4.	RESULTS AND DISCUSSION	40
4.1	Velocity Distribution	40
4.2	Turbulence Intensity	43
4.2.1	Sampling Length	43
4.2.2	High-Pass Filter	44
4.2.3	Turbulence Variation with Tunnel Speed	46
4.2.4	Turbulence Intensity Distribution	47
4.2.5	Effect of Dirty Screens	48
4.3	Turbulence Power Spectral Density.....	49
4.3.1	Hot-wire Signal Noise	50
4.3.2	Blade-Passing Frequency	51
4.4	Boundary Layer	53
4.5	Temperature Variation	54
4.5.1	Temporal Temperature Variation.....	54
4.5.2	Spatial Temperature Variation	55
5.	CONCLUSIONS AND RECOMMENDATIONS	56
	APPENDIX A. TEST SETUP	60
	APPENDIX B. SUPPLEMENTARY FLOW QUALITY DATA.....	64
	APPENDIX C. BOEING SUBSONIC WIND TUNNEL MANUAL	72

LIST OF TABLES

Table 1.1: Summary of low-turbulence wind-tunnel data	18
Table 2.1: Stilling section screen sizes [2].....	25
Table 3.1: Sample hot-wire calibration results	35
Table A.1: Cross-section survey measurement locations	61

LIST OF FIGURES

Figure 1.1: Original Purdue subsonic wind tunnel (1950s)	13
Figure 1.2: 1988 version of the wind tunnel. (a) and (b) show a top view of the tunnel, (c) shows the closed test section, and (d) shows the open test section.....	14
Figure 1.3: Schematic of the 1988 wind tunnel	15
Figure 1.4: Current wind tunnel test-section installed in 1991	16
Figure 2.1: Schematic of the Boeing Subsonic Wind Tunnel; in the front view of the tunnel the flow moves from left to right	19
Figure 2.2: Side view of the first diffuser plate arrangement (units in inches)	21
Figure 2.4: Breather hole arrangement.....	22
Figure 2.5: Top view of corner turning-vanes showing flow direction	23
Figure 2.6: Wind tunnel motor power curve.....	24
Figure 2.7: Honeycomb and screen configuration used in the stilling section of the tunnel	25
Figure 2.8: Contraction dimensions	26
Figure 2.9: Contraction contour profile	27
Figure 2.10: Contraction wall fiberglass construction.....	27
Figure 2.11: Wind tunnel test-section flow speed	28
Figure 3.1: Pitot-static tube placement and contraction pressure tap locations	29
Figure 3.2: Test-section reference velocity vs contraction pressure drop	31
Figure 3.3: Hot-wire sensor operation schematic	32
Figure 3.4: Schematic of the wind tunnel measurement system.....	33
Figure 3.5: 90° hot-wire probe used for boundary layer and cross-section survey measurements [16].....	34
Figure 3.6: Straight hot-wire probe used for measuring turbulence over the entire tunnel speed range [16].....	34
Figure 3.7: Traverse probe mounting configuration used for center measurements	36

Figure 3.8: Location of measurement instruments in the wind tunnel	37
Figure 3.9: Flow measurement grid, each colored box contains the points measured in a single test	38
Figure 3.10: Overlapping test regions where the red box is first old and the blue box is new test, (•) overlapping points.....	39
Figure 4.1: Cross-section velocity contour (core region) at 20m/s. The red lines show the boundary of the covered hole in the top of the tunnel	41
Figure 4.2: Schematic of the floor of the test section showing the model mounting hole cover. Note that during tests the slots in both the cover and the test section floor were sealed.....	41
Figure 4.3: Percentation deviation of the mean velocity across the BSWT test section for a free-stream speed of 20 m/s, 86” from the test-section inlet.....	42
Figure 4.4: Percentation deviation of the mean velocity across the NDF test section for a free-stream speed of 20 m/s, 8” inches from the test-section inlet [7]	43
Figure 4.5: Turbulence intensity for various sampling times, at a free-stream speed of 20 m/s ..	44
Figure 4.6: Turbulence intensity vs high-pass filter frequency for $U_{\infty} = 20\text{m/s}$	45
Figure 4.7: Tunnel center turbulence intensity across the entire range of wind tunnel speeds	46
Figure 4.8: Cross-section turbulence intensity contour – core region	47
Figure 4.9: Cross-section turbulence intensity contour with high turbulence spot before screen cleaning	48
Figure 4.10: Higher turbulence intensity spot – before cleaning.....	49
Figure 4.12: Comparison of velocity power spectral densities at 20 m/s for the KSWT and the BSWT [5].....	51
Figure 4.13: Blade-passing frequency noise at a tunnel motor frequency of 30 Hz (20 m/s)	52
Figure 4.14: Bottom-wall boundary-layer profile and turbulence intensity	53
Figure 4.15: Temperature rise measured in the stilling section of the tunnel.....	54
Figure 4.16: Spatial temperature variation – core region – temperature measured in Celcius.....	55
Figure A.1: Comparrision of the effect of including different correction factors on the reference velocity using Equation 3.4.....	60
Figure A.2: Hotwire calibration curve showing 95% confidence interval	61

Figure A.3: Probe holding configuration for measurement locations where $Y \leq -13.5''$ or $Y \geq 13.5''$	62
Figure A.4: Probe holding configuration for measurement locations where $-18.0'' \leq Y \leq 18.0''$	62
Figure A.5: Probe holding configuration for boundary layer measurements	63
Figure B.1: Preliminary test data of tunnel running at 20 m/s for 1 minute	64
Figure B.2: Preliminary test data of tunnel running for 1 minute for a sampling rate of 10 kHz.	64
Figure B.3: Cross-section velocity contour – complete test section.....	65
Figure B.4: Cross-section turbulence intensity contour – complete test section	65
Figure B.5: Cross-section temperature contour – complete test section.....	66
Figure B.6: Velocity profiles for varying height locations over the cross-section core region	66
Figure B.7: Velocity profiles for varying spanwise locations over the cross-section core region	67
Figure B.8: Velocity profiles for varying height locations over the entire cross-section	67
Figure B.9: Velocity profiles for varying spanwise locations over the entire cross-section	68
Figure B.10: Comparison of the PSDs for two different probe configurations. Data was measured at the center of the test section for $U_\infty = 20$ m/s	68
Figure B. 11: Percent of turbulent energy lying between different frequency bands. Data was measured at the center of the test section for $U_\infty = 20$ m/s.....	69
Figure B.12: Power spectrum at a tunnel motor frequency of 20 Hz	69
Figure B.13: Power spectrum at a tunnel motor frequency of 30 Hz	70
Figure B.14: Power spectrum at a tunnel motor frequency of 40 Hz	70
Figure B.15: Power spectrum at a tunnel motor frequency of 50 Hz	71
Figure B.16: Power spectrum at a tunnel motor frequency of 60 Hz	71

SYMBOLS

A	Area
f	Frequency
H	Equivalent radius
k	Loss coefficient
K	Contraction coefficient
N	Number of samples
P	Pressure
q	Dynamic pressure
T	Temperature
U	Velocity
\bar{u}	Mean velocity
u'	Velocity fluctuations
V	Voltage

Greek Symbols

δ_{99}	Boundary layer thickness
δ^*	Boundary layer displacement thickness
Δ	Change in a quantity
η	Subsection correlation multiplication factor
λ	Wavelength
ρ	Density
θ^*	Boundary layer momentum thickness

ABBREVIATIONS

ASL	Aerospace Sciences Laboratory
BPF	Blade passing frequency
BSWT	Boeing Subsonic Wind Tunnel
HP	Horse power
IIT	Illinois Institute of Technology
KSWT	Klebanoff-Saric Wind Tunnel
NDF	National Diagnostic Facility
PSD	Power spectral density
RMS	Root mean square
RPM	Revolutions per minute
RTD	Resistance temperature detectors
Tu	Turbulence intensity
T-S	Tommlein-Schlichting

ABSTRACT

Author: Diffey, Claire, S. MSAAE

Institution: Purdue University

Degree Received: August 2019

Title: Characterization of the Flow Quality in the Boeing Subsonic Wind Tunnel

Committee Chairs: Dr. John P. Sullivan and Dr. Sally Bane

Good wind-tunnel flow quality characteristics are vital to using test data in the aerodynamic design process. Spatially uniform velocity profiles are required to avoid yaw and roll moments that would not be present in real flight conditions. Low turbulence intensity levels are also important as several aerodynamic properties are functions of turbulence intensity. When measuring mean flow and turbulence properties, hot-wire anemometry offers good spatial resolution and high-frequency response with a fairly simple operation, and the ability to make near-wall measurements. Using hot-wire anemometry, flow quality experiments were conducted in a closed-circuit wind tunnel with a test section that has a cross section area of 1.2 m x 1.8 m (4 ft. x 6 ft.). The experiments included measurements of flow velocity and turbulence intensity variation over the test section cross-section, spatial and temporal temperature variation, and boundary layer measurements. The centerline velocity and turbulence intensity were also measured for flow speeds ranging from 13 to 43 m/s.

1. INTRODUCTION

1.1 Background

The Boeing Subsonic Wind Tunnel (BSWT), located at Purdue University, has been used by industry, researchers and students for more than 60 years. Designed and built in the 1950s by Professor George Palmer, the original wind tunnel shown in Figure 1.1 has undergone many upgrades, ranging from single-component replacements to large section redesigns.

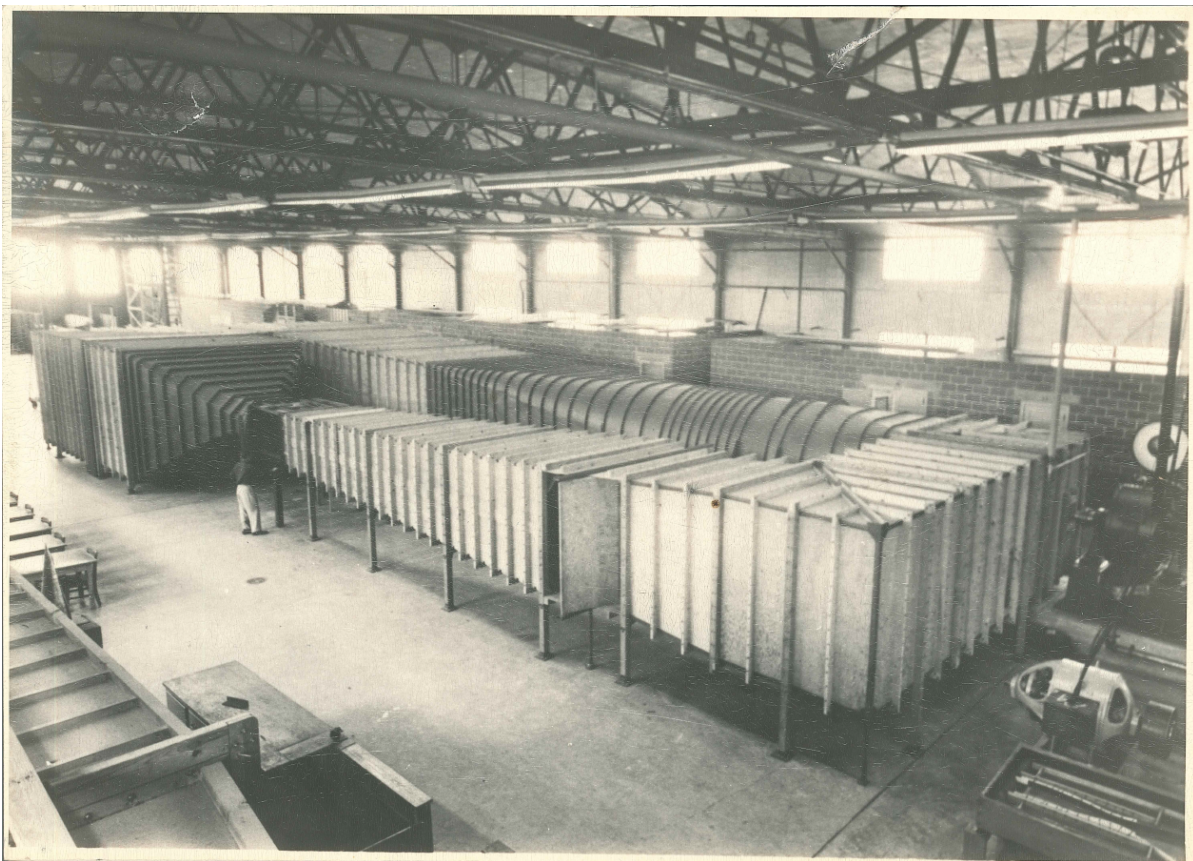


Figure 1.1: Original Purdue subsonic wind tunnel (1950s)

In 1988, Ricky Behrens [1] conducted experiments on the modified Boeing Subsonic Wind Tunnel shown in Figure 1.2 to determine the airflow quality in the test-sections. The wind tunnel was a closed-circuit, single-return tunnel. This tunnel featured a 1.5 m x 2.2 m (4.8 ft. x 7.2 ft.) open test-section, with a maximum speed of 45 m/s (150 ft/s) [2]. The tunnel was also equipped with a 0.9 m

x 1.4 m (3 ft. x 4.5 ft.), closed, octagonal test-section. The octagonal closed test-section was capable of reaching air speeds of up to 137 m/s (450 ft/s).

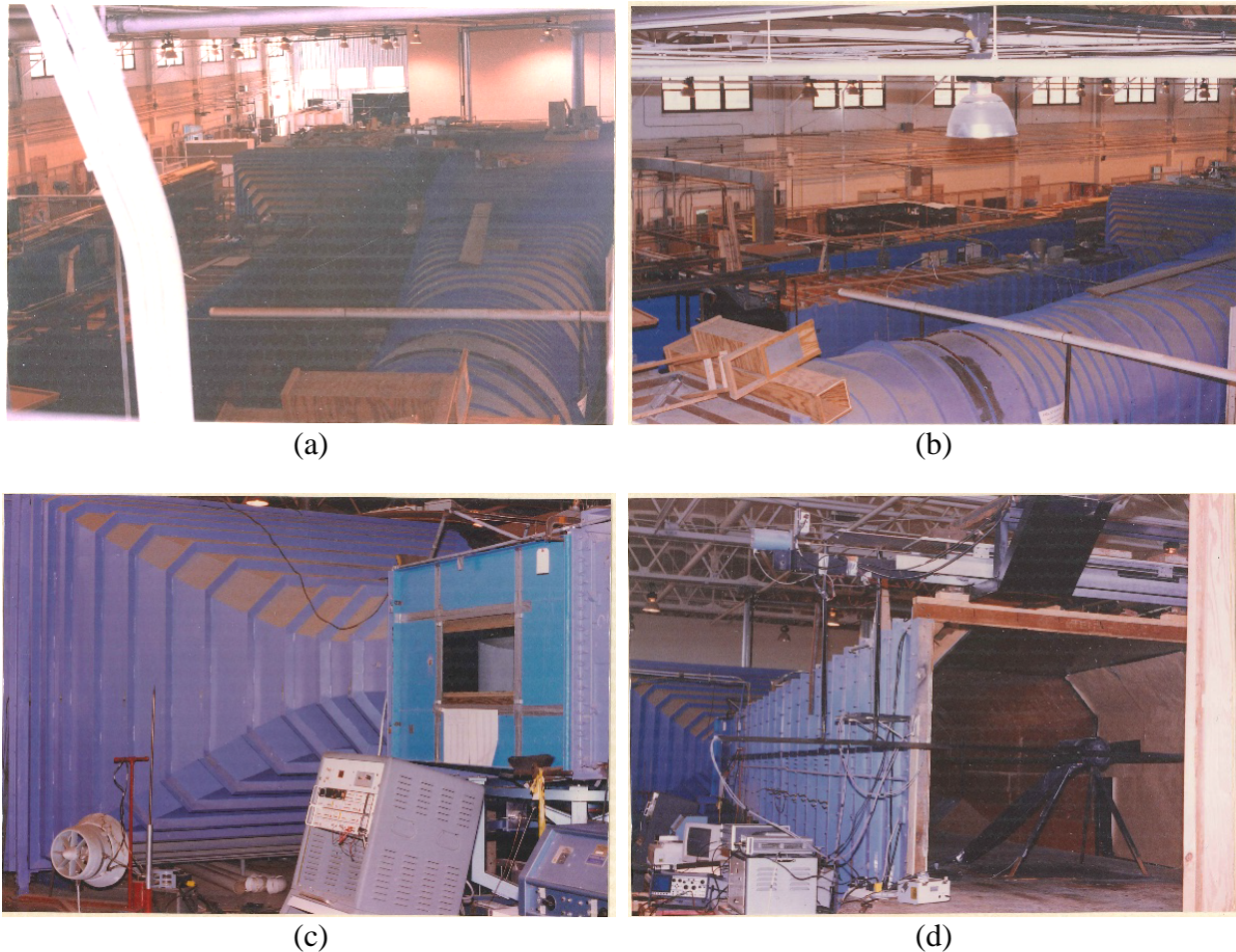


Figure 1.2: 1988 version of the wind tunnel. (a) and (b) show a top view of the tunnel, (c) shows the closed test section, and (d) shows the open test section

These experiments showed the open section shown in Figure 1.3, to have a turbulence intensity of 1.9% at the diffuser exit. The closed section had turbulence intensities across the test-section of 0.7% at 34 m/s to 1.35% at 58 m/s, with a 3% difference in the velocity profile gradient. The results of Behrens' study were used to make suggestions for improving the tunnel's flow quality.

Behrens's main recommendations to reduce turbulence in the tunnel were to replace the single screen in the stilling section with a combination of multiple honeycombs and screens, and to redesign the contraction.

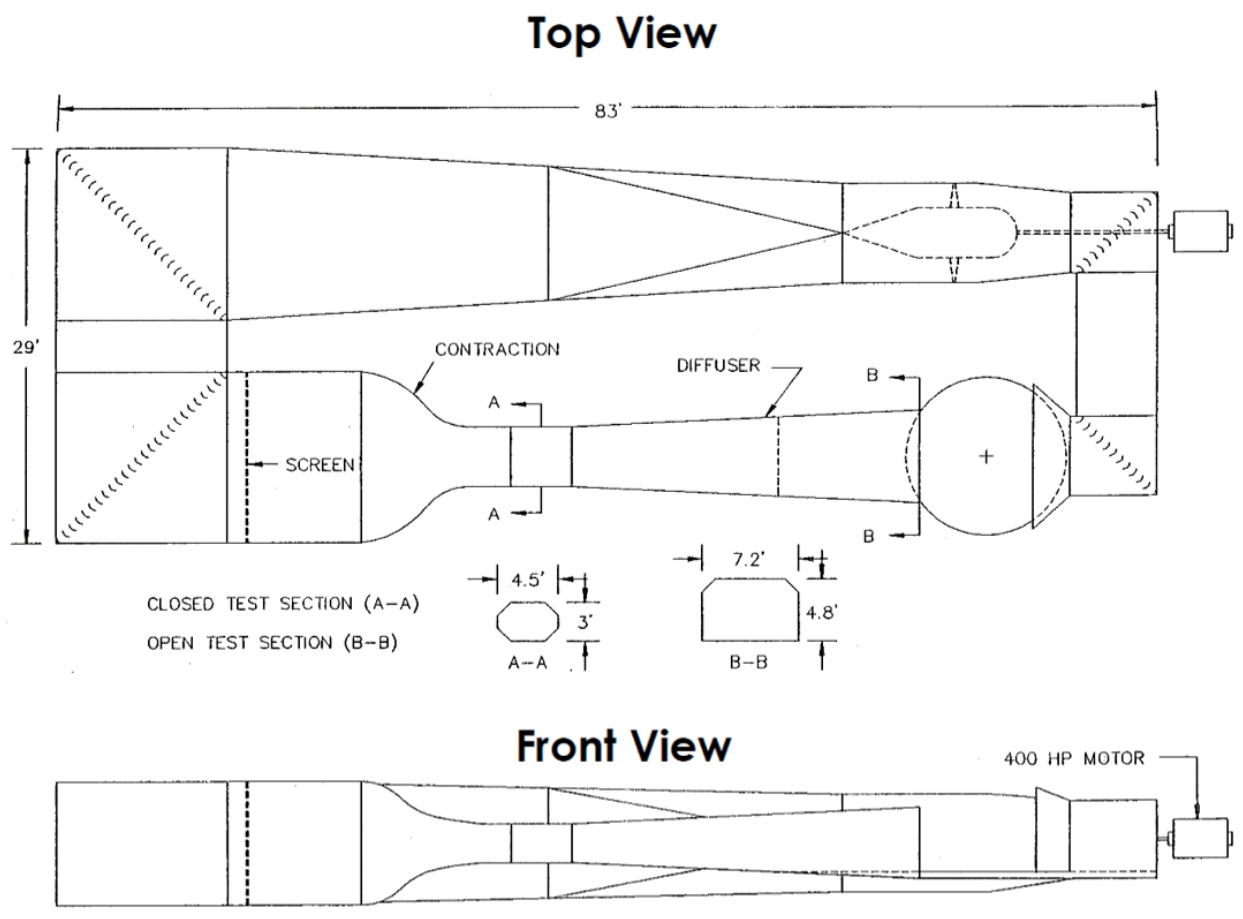


Figure 1.3: Schematic of the 1988 wind tunnel

In the most-recent major tunnel modification in 1991, Behrens's changes were implemented, along with others that would improve the tunnel flow quality. This upgrade included installing a new stilling section with a honeycomb and seven screens and a four-piece fiberglass contraction section. The test-section was replaced with a larger closed, 2.4 m (8 ft.) long 1.2 m x 1.8 m (4 ft. x 6 ft.) test section as shown in Figure 1.4, and a new diffuser was also installed [2].



Figure 1.4: Current wind tunnel test-section installed in 1991

1.2 Motivation

Subsonic wind tunnel tests are commonly used to accurately determine the flow physics of aircraft. Currently wind tunnel research is being conducted to allow for better understanding of small-scale flow physics and small-aircraft design configuration changes rather than large-component redesigns. With such research, free-stream flow properties in wind-tunnel tests play a more significant role. Specifically, low turbulence is required because several aerodynamic properties, such as drag, are functions of turbulence intensity. Uniform flow is also needed because non-uniform flow can cause yaw and roll moments that would not be present in real flight conditions. For example, research is being conducted on the effect that boundary-layer flows (and the control of these flows) have on drag [3]. Since high turbulence levels can cause transition to occur earlier, it is advantageous to have low free-stream turbulence that better matches real flight conditions.

As discussed in the previous section, the Boeing Subsonic Wind Tunnel was upgraded to improve flow quality in the tunnel in 1991. In the intervening three decades, no study has been conducted into the effect the upgrades had on the tunnel flow quality. Thus, the purpose of this project is both to determine the quality of flow in the tunnel and propose future tunnel modifications.

1.3 Low-Turbulence Wind-Tunnel Flow Characteristics

Wind tunnels have been designed and characterized for over 50 years, yet better ways to lower the turbulence levels or actively control the turbulence into a specified region are still being studied. Saric [4] suggested that when considering frequencies above 0.1 Hz the turbulence levels in low-turbulence wind tunnels should be below a 0.05% limit for stability experiments. It was also suggested that the turbulent spectra should decrease monotonically in the range of Tommelein-Schlichting (T-S) wave frequencies.

The Klebanoff-Saric Wind Tunnel (KSWT) (Texas A&M) [5] has a stated streamwise turbulence intensity range of 0.027% to 0.125% over free-stream speeds of 5 – 25 m/s, where a 1 Hz – 10 kHz band pass filter was used. At the Royal Institute of Technology (Stockholm), the MTL tunnel [6] had similar turbulence intensities of 0.025% with an unfiltered value of 0.08%. These values were reported only for the core region (47% test-section area), at 25 m/s and with a high pass cut-off frequency $\left(f_c = \frac{U_\infty}{\lambda_c}\right)$ equal to the free-stream velocity divided by the sum of the test-section side lengths (λ_c). Evaluation of the flow quality at the National Diagnostic Facility (NDF) at Illinois Institute of Technology (IIT) [7] was shown to have free-stream turbulence intensities ranging between 0.02% at a free-stream speed of 16 m/s to 0.05% at 26 m/s.

Table 1.1 gives a brief overview of the turbulence characteristics of some low-turbulence closed circuit wind tunnels, and the conditions under which these measurements were made. The Boeing subsonic tunnel was not built to be a low-turbulence tunnel and will not have turbulence levels as low as those outlined in Table 1.1. Research tunnels similar to the Boeing wind tunnel have turbulence intensity levels which fall within the range of 0.14% - 1.0% [8].

Table 1.1: Summary of low-turbulence wind-tunnel data

Tunnel Name	Cross section (m)	Streamwise turbulence intensity (%)	Free-stream Speed (m/s)	Filtering
Klebanoff-Saric Wind Tunnel	1.4 x 1.4	0.091	20	Band-pass 1Hz – 10 kHz
MTL tunnel	0.8 x 1.2	0.025	25	High-pass 12.5 Hz
National Diagnostic Facility	1.22 x 1.52	0.04	26	Band-pass 1Hz – 4 kHz
Tōhoku University Wind Tunnel [9]	1 m wide octagon	0.025	20	Not reported
PennState Low-Speed, Low-Turbulence Wind Tunnel [10]	1.5 x 1.85	0.04	23	Band-pass 1 Hz – 4 kHz

2. WIND TUNNEL DESIGN

The following section is a brief overview of the Boeing Subsonic Wind Tunnel. For a more complete and in depth report on the design and operation of the wind tunnel see Appendix C.

2.1 General Description

A drawing of the Boeing Subsonic Wind Tunnel is shown in Figure 2.1. The tunnel, located in the Aerospace Sciences Laboratory (ASL) at Purdue University, is a closed-return, closed test-section wind tunnel with a 1.2 m x 1.8 m (4 ft. x 6 ft.) test-section that is 2.4 m (8 ft.) long, followed by a straight duct section that is 7.3 m (24 ft.) long. With an empty test-section, the wind tunnel is able to reach speeds of up to 43 m/s.

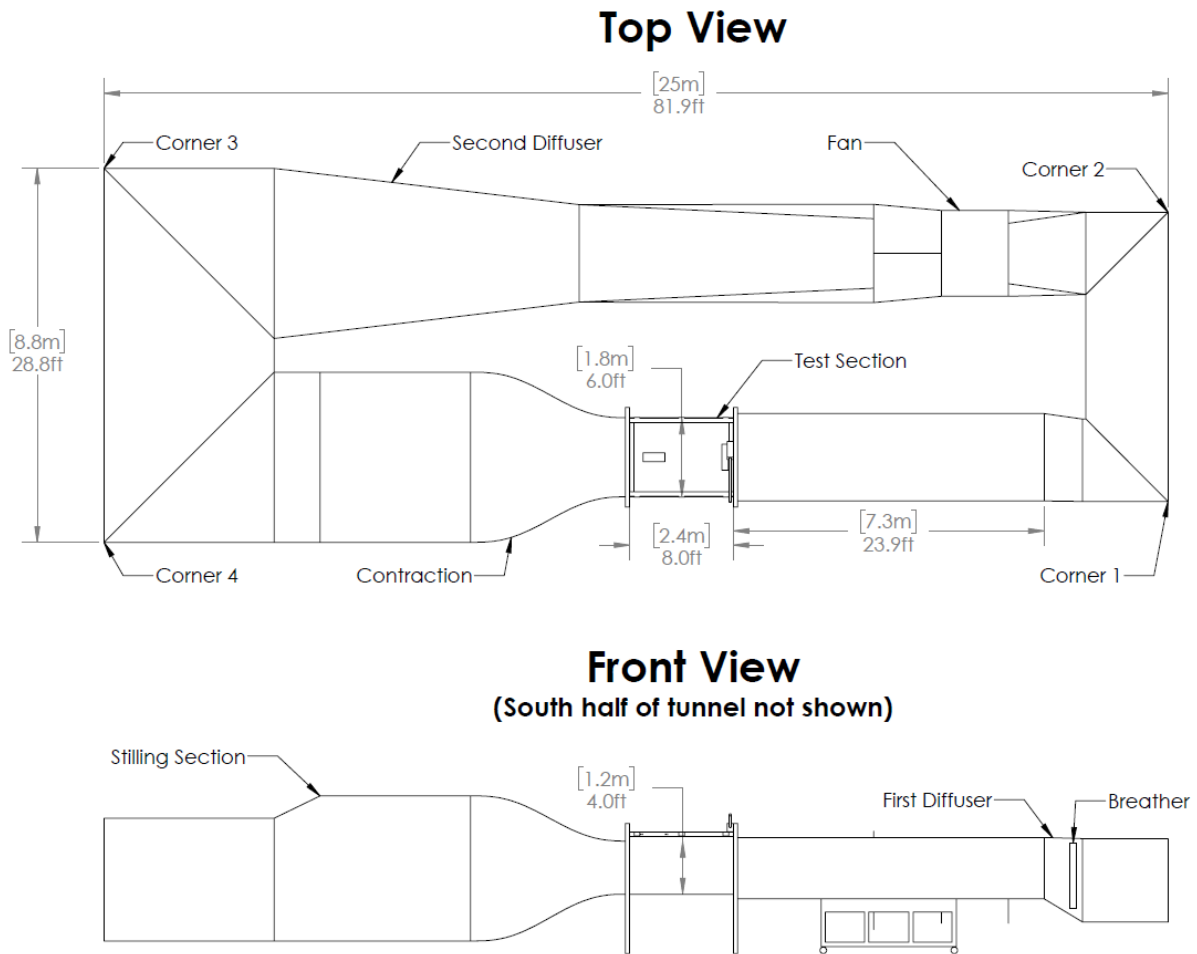


Figure 2.1: Schematic of the Boeing Subsonic Wind Tunnel; in the front view of the tunnel the flow moves from left to right

Starting at Corner 1, the flow goes around Corner 2, and passes through a 2 m inner diameter fan. After the fan, the flow expands through a diffuser into a square duct before going through Corners 3 and 4. Corners 1, 2 and 3 are equipped with turning vanes. Downstream of Corner 4, the flow passes through the stilling section where a set of honeycombs and screens are used to reduce any large swirl components in the flow, reduce turbulence and establish a uniform test-section profile [11]. The now more-uniform flow enters the contraction section of the tunnel where it accelerates until it reaches the test-section inlet. After the test-section, the flow moves through a straight duct that is 7.3 m (24 ft.) long, into a diffuser where it expands and slows down. Just as the flow exits the end of the diffuser, it goes through a breather section. This allows air into the tunnel and keeps the static pressure within the tunnel close to atmospheric pressure, thereby reducing air leaks into the test-section of the tunnel.

2.2 Main Components

2.2.1 First Diffuser

The first diffuser is situated between the downstream end of the test-section and the first corner. It contains five angled plates, shown in Figure 2.2, to prevent the flow from separating. If the flow were to separate in the diffuser, it could cause fluctuations to propagate upstream into the test-section.

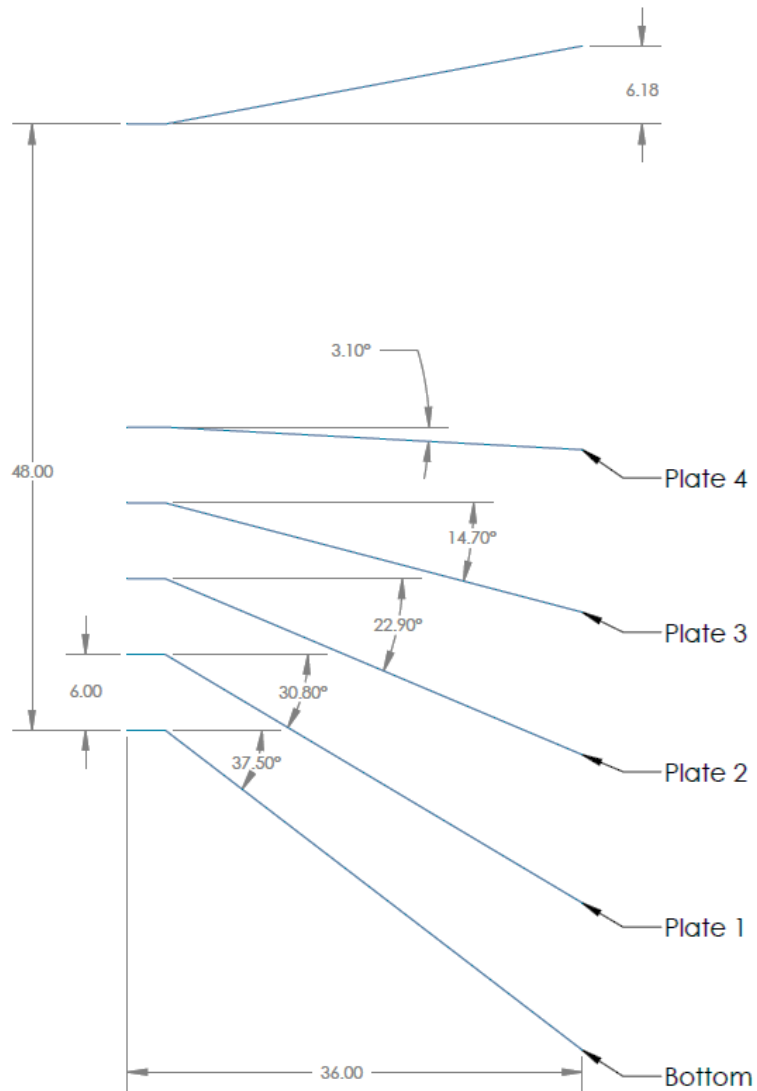


Figure 2.2: Side view of the first diffuser plate arrangement (units in inches)

The flow over the plates was observed using tufts at wind speeds of 5.3, 12.4, and 19.7 m/s. The tufts were placed on plates 1 through 3 and on the bottom of the diffuser and showed no sign of flow separation or reversed flow. The tufts on the bottom of the diffuser at a flow speed of 19.7 m/s are shown in Figure 2.3.

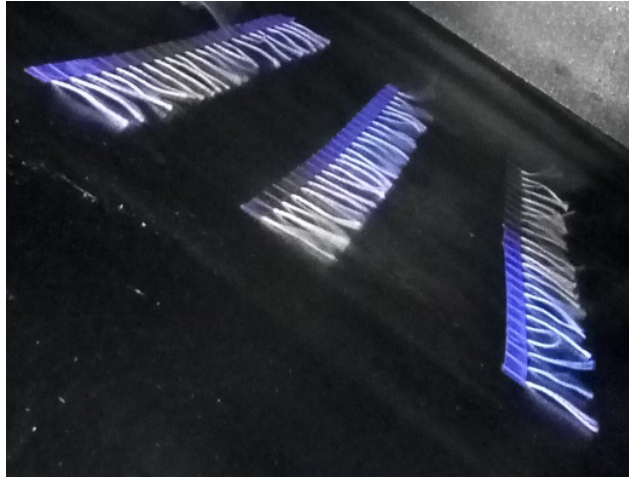


Figure 2.3: Tufts shown on the bottom of the first diffuser at a free-stream speed of 19.7 m/s

2.2.2 Breather

The downstream end of the diffuser contains a breather section, which is constructed from a perforated aluminum sheet shown in Figure 2.4. Holes $3/16$ " in diameter are staggered with $1/4$ " center-to-center spacing with a total open area of 51%. The breather section allows air into the tunnel to set the static pressure within the tunnel close to atmospheric pressure, and also allows for some cooling of the tunnel flow.

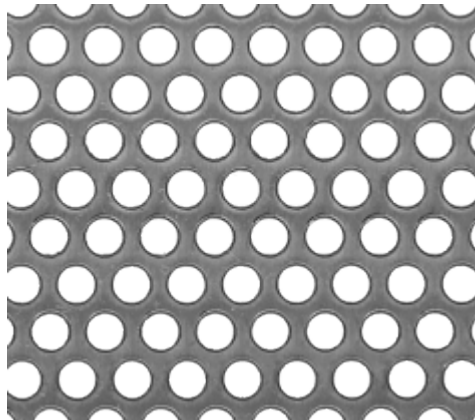


Figure 2.4: Breather hole arrangement

2.2.3 Turning Vanes

In Corners 1, 2, and 3 of the wind tunnel, there are turning vanes that span the entire height, of the tunnel. A schematic of the vanes is shown in Figure 2.5. These turning vanes are used to minimize pressure losses as the air turns the corner, and mitigate separation of the boundary layer through the turn. The turning vanes in Corners 1 and 3 both contain support bars that link the individual turning vanes, to reduce fluttering.

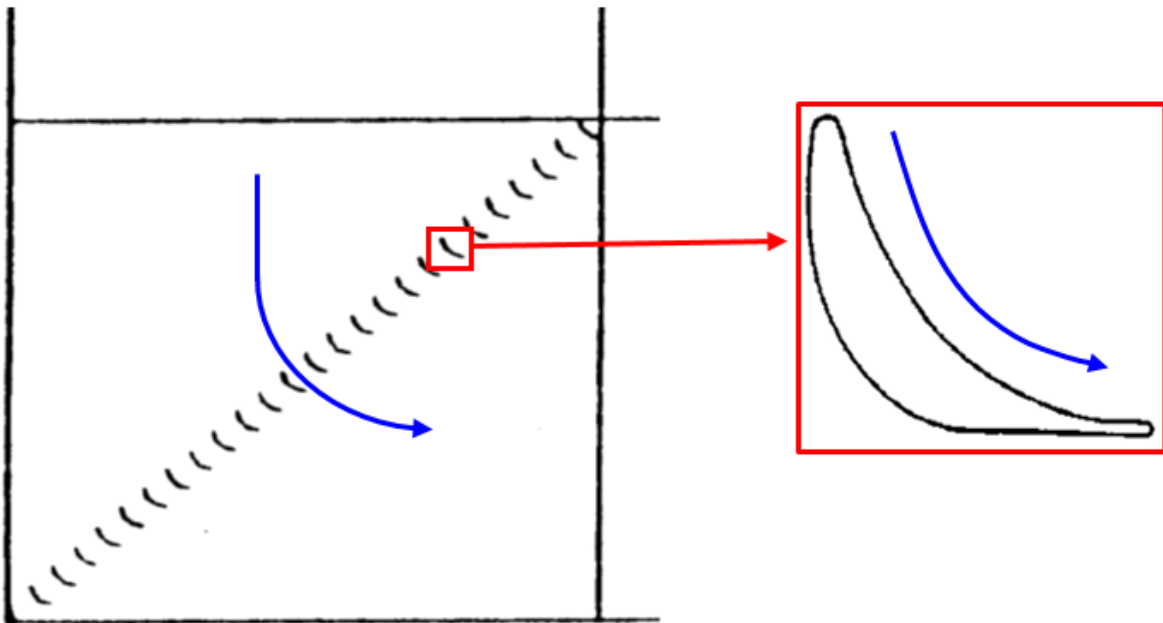


Figure 2.5: Top view of corner turning-vanes showing flow direction

2.2.4 Wind Tunnel Fan

The wind-tunnel fan unit is an Axico Anti-Stall Vaneaxial Fan, run by an MAX-E1 AC Motor with a variable-speed drive. The fan consists of 10 blades with variable pitch, which allows for changing the fan RPM vs. tunnel flow speed curve. The maximum speed for this fan is 1188 RPM at 60 Hz. Per the manufacturer, the motor's maximum power is 300 HP. The wind-tunnel motor power curve is shown in Figure 2.6.

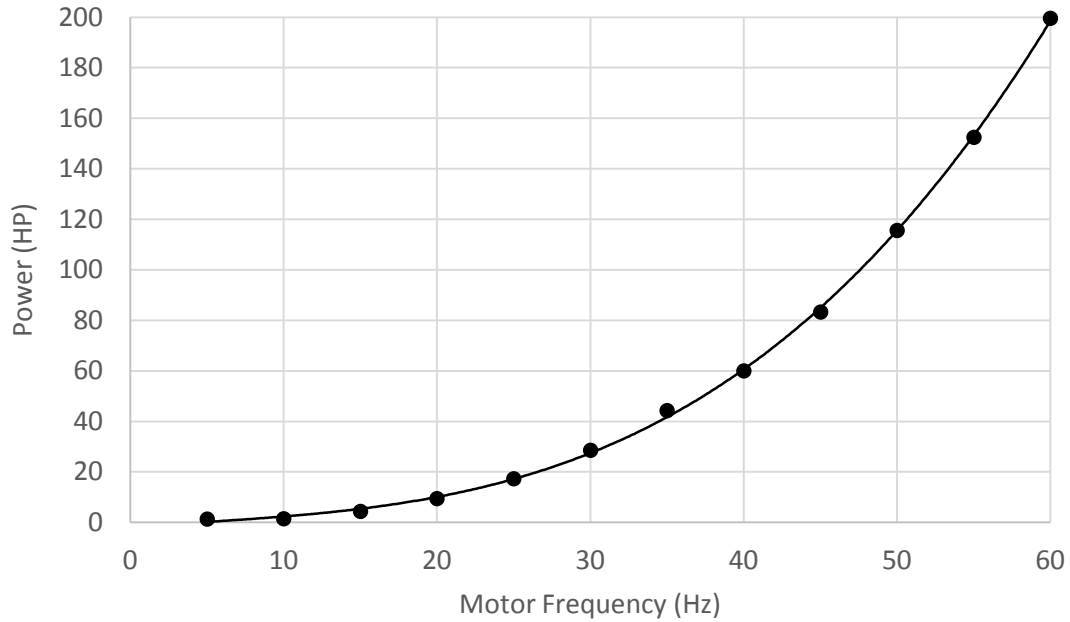


Figure 2.6: Wind tunnel motor power curve

2.2.5 Stilling Section – Screens and Honeycomb

The stilling section of the wind tunnel is designed to reduce the size of the turbulent fluctuations and straighten and increase the uniformity of the flow entering the test-section. The honeycomb is used to reduce any large swirl components of the upstream flow. The screens reduce turbulence and establish a uniform test-section profile [11]. This part of the tunnel is divided into the seven sections as shown in Figure 2.7, where the first two stations are not part of the stilling section, but are part of the diffuser used to increase the tunnel cross section size to the size of the contraction inlet.

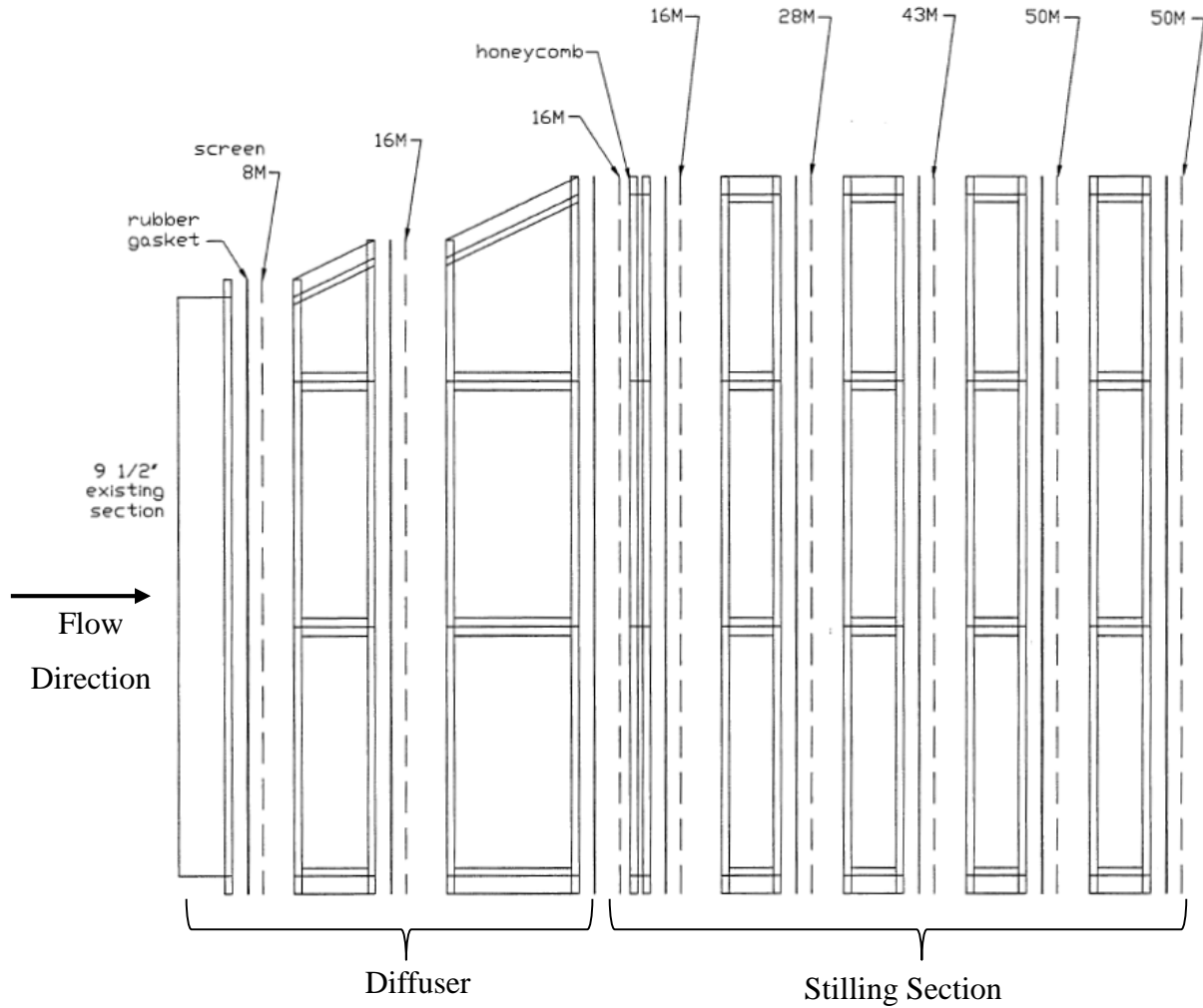


Figure 2.7: Honeycomb and screen configuration used in the stilling section of the tunnel

The honeycomb wall at station 3 is four inches thick and made of polycarbonate, with a 1/2" cell diameter. This honeycomb was supplied by Plascore and has a total density of 3 lbs/ft³. The dotted lines represent screens made from aluminum wire cloth purchased from TSI [2] with the properties listed in Table 2.1.

Table 2.1: Stilling section screen sizes [2]

Mesh Size (M = wires/in)	Wire Diameter (in)	Porosity (%)
8	0.035	51.8
16	0.011	67.9
28	0.0075	62.4
43	0.005	61.6
50	0.0045	60.1

2.2.6 Contraction

The contraction section of the tunnel is used to increase the air speed entering the test-section and has a total contraction ratio (A_{in}/A_{out}) of 5.96:1. It is constructed of four individual fiberglass sides, which are fastened together at the corners.

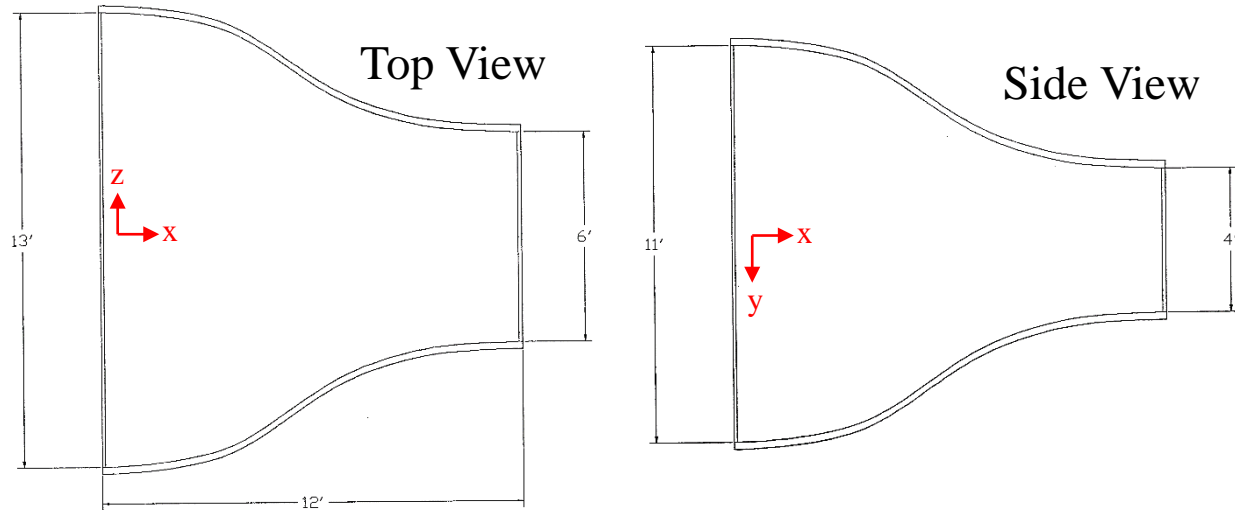


Figure 2.8: Contraction dimensions

The shape of the contraction contour show in Figure 2.9, follows a cubic fit with $X = 0.45$ [12]:

$$H(x) = \begin{cases} (H_{in} - H_{out}) \left[1 - \frac{1}{X^2} \left(\frac{x}{L} \right)^3 \right] + H_{out} & \rightarrow \frac{x}{L} < X \\ (H_{in} - H_{out}) \left[\frac{1}{(1-X)^2} \left(1 - \frac{x}{L} \right)^3 \right] + H_{out} & \rightarrow \frac{x}{L} > X \end{cases} \quad 2.1$$

where H_{in} and H_{out} are the equivalent radii of the inlet and exit, respectively, x is the distance from the inlet along flow direction, and L is the length of contraction.

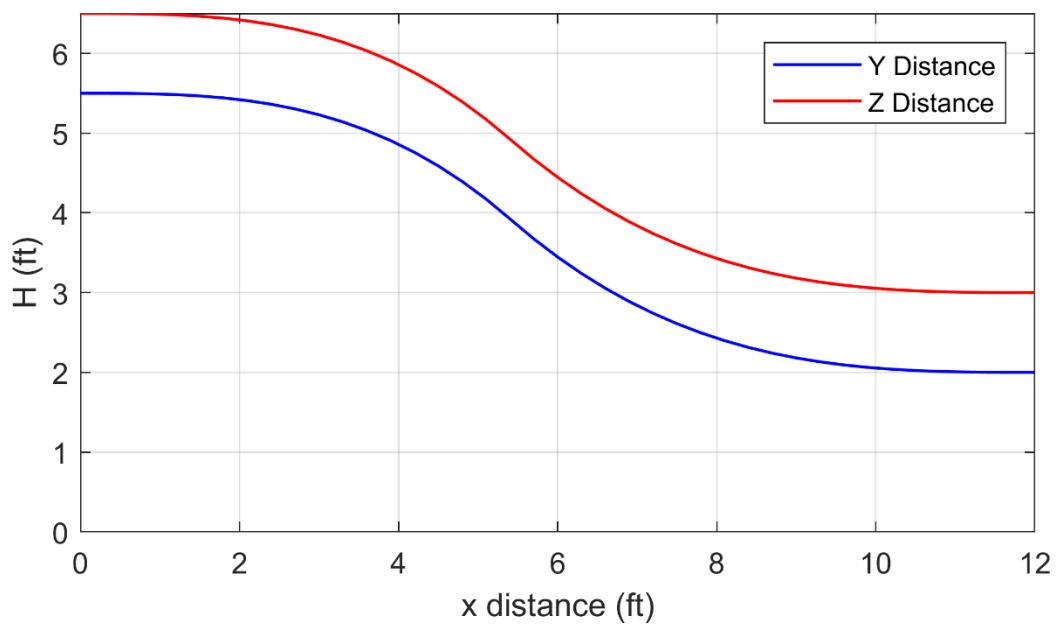


Figure 2.9: Contraction contour profile

The walls of the contraction are made of a three-layer fiberglass laminate construction as shown in Figure 2.10. The middle layer of the wall contains a Divinycell H-60 foam core and is sandwiched between six layers of cloth, which are 60% resin.

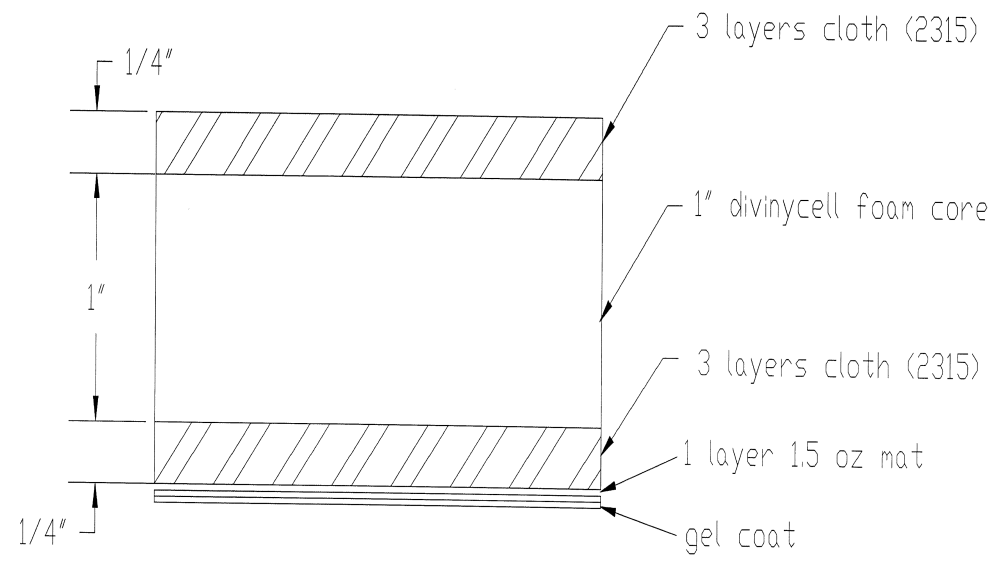


Figure 2.10: Contraction wall fiberglass construction

2.3 Wind Tunnel Performance

Currently the tunnel is able to reach speeds up to 43 m/s with an uncertainty of 1%. A calibration plot of test section flow speed vs. motor frequency is shown in Figure 2.11, and can be used as a baseline for setting the flow speed.

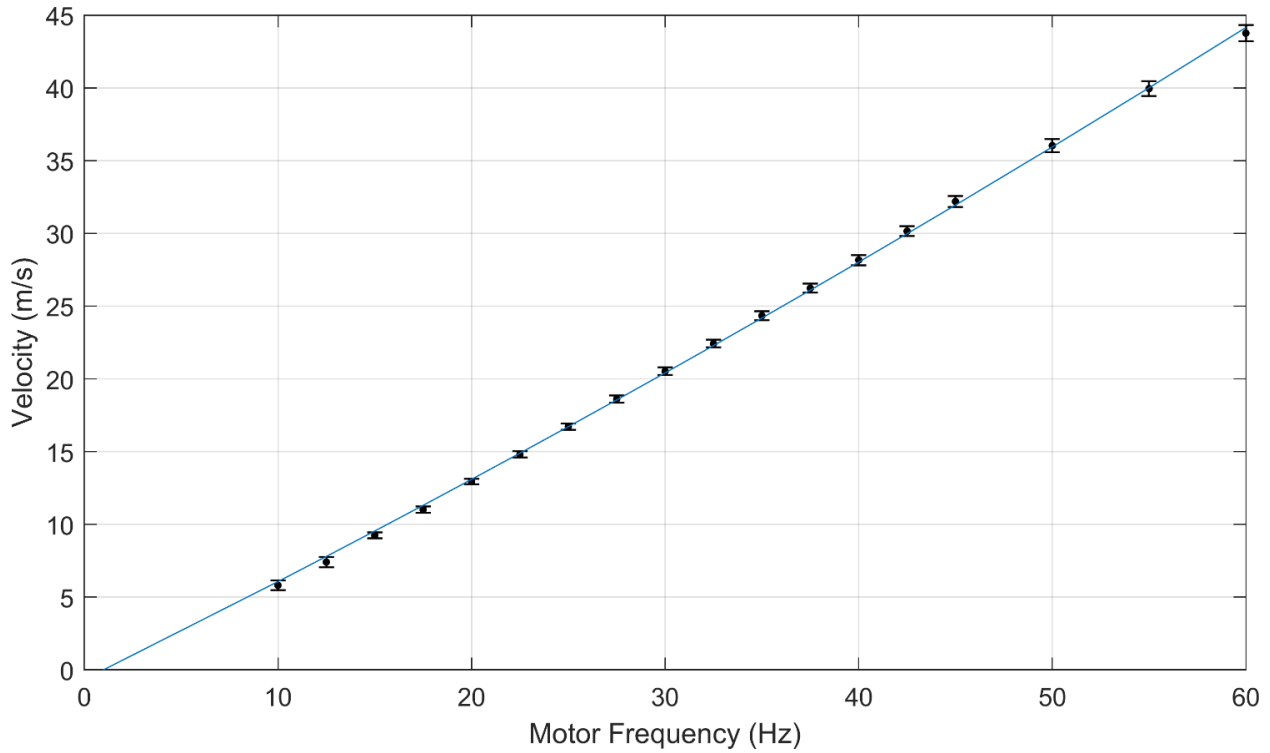


Figure 2.11: Wind tunnel test-section flow speed

3. INSTRUMENTATION AND DATA REDUCTION

Some of the instrumentation available for use with the wind tunnel is detailed in this chapter. These instruments were used to characterize the flow in the tunnel and the results are discussed in the following chapter.

3.1 Reference Velocity

In order to facilitate convenient and fast hot-wire calibration in the test section of the wind tunnel, the contraction section differential pressure is first correlated to the free stream velocity, U_∞ . The free stream velocity is measured using a pitot static probe. Using this correlation, the contraction section differential pressure can be used to calibrate hot-wire anemometry measurements without installing the pitot static probe in the test section. The calibration is performed by installing the pitot static probe at the center of a plane 2.2 m (86") downstream of the test-section entrance as shown in Figure 3.1. The probe is connected to a differential pressure transducer (Validyne PS309) and the differential pressures are used to determine a reference velocity of the flow using Equation 3.1.

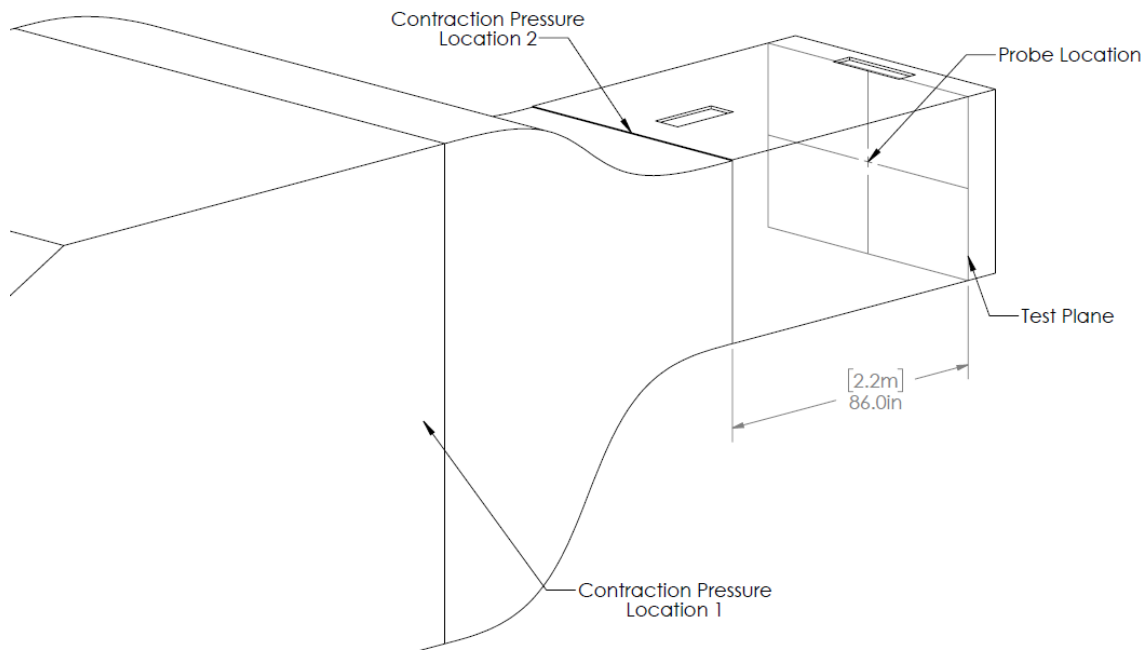


Figure 3.1: Pitot-static tube placement and contraction pressure tap locations

$$u_2 = \sqrt{\frac{2\Delta P_{pitot}}{\rho_{air}}} \quad 3.1$$

This speed calculated by Equation 3.1 is correlated to the pressure drop across the tunnel contraction measured using pressure taps connected to a differential pressure transducer (OMEGA PX653), which allowed a reference speed to be determined solely from the contraction pressure drop [11]. This could be achieved by including losses in Bernoulli's equation and solving for u_2 (test plane speed). The pressure loss through the contraction was modeled with loss coefficient k , yielding Equation 3.2.

$$P_1 + \frac{1}{2}\rho u_1^2 = P_2 + \frac{1}{2}\rho u_2^2 + \frac{1}{2}\rho u_2^2 k \quad 3.2$$

Where P is the static pressure, u is the velocity and $\frac{1}{2}\rho u_2^2 k$ represents the pressure losses. Subscript 1 denotes the upstream contraction parameters and subscript 2 denotes the test-section parameters.

Given the contraction ratio ($A_1:A_2$) of 5.96:1, conservation of mass for incompressible flow (Equation 3.3) is used to determine u_1 as a function of u_2 :

$$\begin{aligned} A_1 u_1 &= A_2 u_2 \\ u_1 &= \left(\frac{1}{5.96}\right) u_2 \end{aligned} \quad 3.3$$

With u_1 in terms of u_2 , Equation 3.2 can be rewritten as Equation 3.4.

$$P_1 - P_2 = \frac{1}{2}\rho u_2^2 \left(1 + k - \frac{1}{5.96^2}\right) \quad 3.4$$

For convenience, the constant coefficients are grouped into a single term $K = \left(1 + k - \frac{1}{5.96^2}\right)^{-1}$.

Using this notation, Equation 3.4 can be written as Equation 3.5 which gives an explicit relationship between the contraction pressure drop and the test section velocity.

$$K(P_1 - P_2) = \frac{1}{2}\rho u_2^2 \quad 3.5$$

The wind-tunnel flow was set to various speeds and the resulting velocity in the test-section calculated using Equation 3.1.

Using a linear regression model, the coefficient (K) of the contraction (based on test plane center velocity) was calculated to be 1.127. Shown in Figure 3.2, this solution gave an extremely close match to the experimental data with an R-square value of 0.99. A plot of the effect of not including losses in the correlation between the contraction pressure drop and the test section speed can be found in Appendix A.

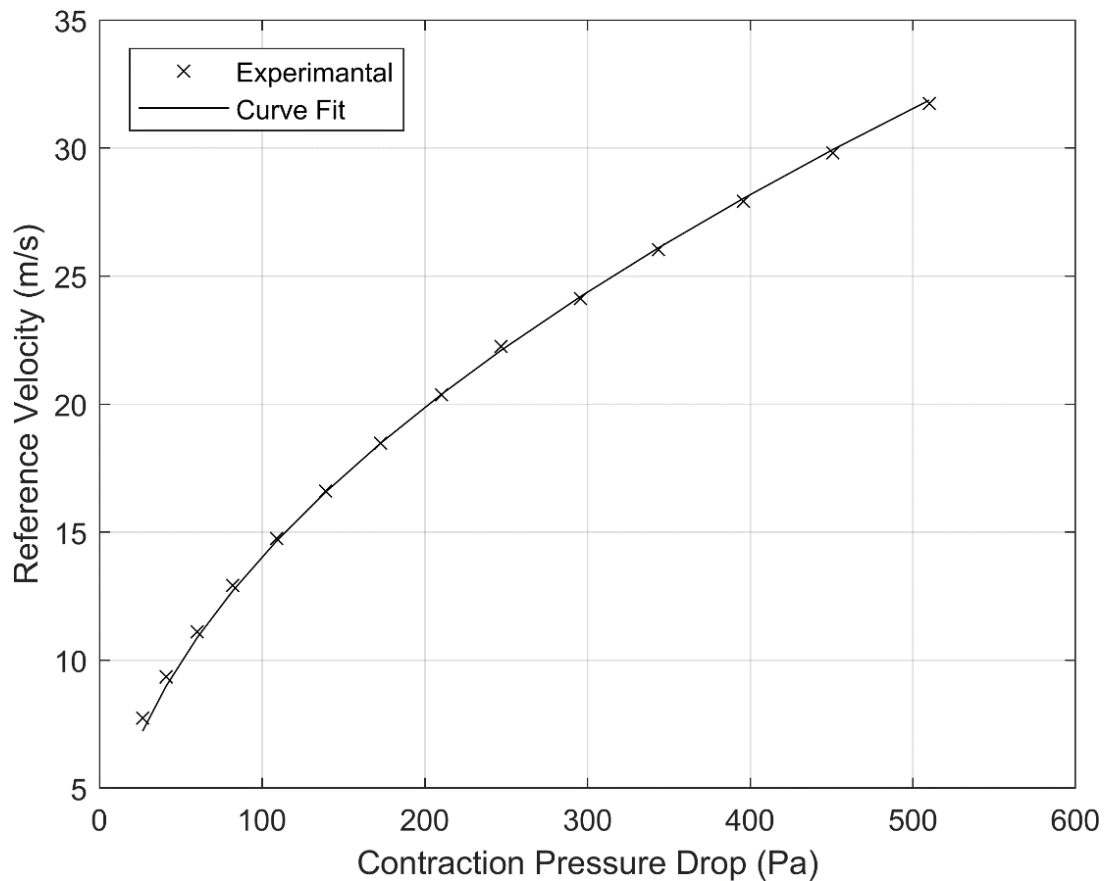


Figure 3.2: Test-section reference velocity vs contraction pressure drop

3.2 Hot-Wire Anemometry

A hot-wire system was used to measure the velocity and turbulence intensity distributions in the tunnel. A hot-wire system was used because hot wires have good spatial resolution and high frequency response and are relatively easy to setup. A Bruhn 6 constant temperature anemometer was used [13] with TSI hot-wire probes.

3.2.1 Theory of Operation

Constant temperature anemometry works on the principle that the convection coefficient and thus the heat transfer rate of a fluid is proportional to the speed at which the fluid is moving over an object. When a heated wire is placed in a flow as shown in Figure 3.3, the voltage flowing through the wire must increase as the speed of the fluid moving over the wire increases in order to keep the temperature of the wire constant. King's Law [14] can be used to correlate the applied voltage (V) to the fluid velocity (U) using calibration coefficients A and B :

$$\sqrt{U} = AV^2 + B \quad 3.6$$

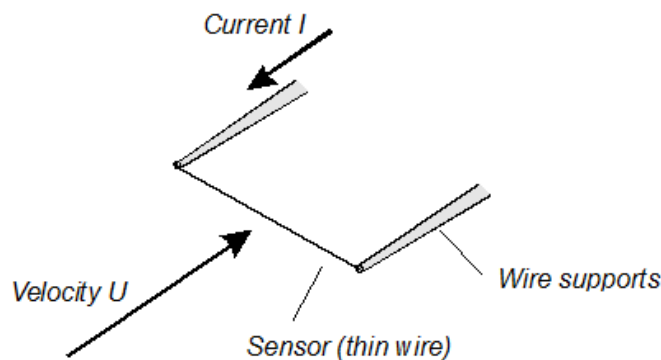


Figure 3.3: Hot-wire sensor operation schematic

The voltage in the anemometer is also sensitive to the temperature of the fluid and can be partially corrected using Equation 3.7 [15]. Where T_w is the operating temperature of the wire, T_{ref} is the temperature of the flow during the hot wire calibration, T_{acq} is the temperature of the flow during testing, V_{acq} is the measured voltage, and V_{corr} is the corrected voltage.

$$V_{corr} = \left(\frac{T_w - T_{ref}}{T_w - T_{acq}} \right)^{0.5} V_{acq} \quad 3.7$$

3.2.2 Instrumentation

A schematic of the instrumentation used with the hot-wire system is shown in Figure 3.4. The probe used for measuring the velocity and turbulence intensity across the cross-section of the tunnel and in the boundary layers was a TSI 1222 shown in Figure 3.5. This probe is a single-direction, 90° angled probe. The 90° angle of the end of the probe allows for easier measurements near the walls of the wind tunnel. Both hot-wire probes used 1.27 mm long, 5 μm diameter platinum wires. The probe used for measuring the velocity and turbulence intensity at the center of the tunnel over a range of flow speeds, was a TSI 1210 shown in Figure 3.6. The probe was attached to a 15 cm (6") long TSI 1150 probe holder and connected to the Bruhn anemometer located on the top of the test section via a 4.5 m (15 ft.) long coaxial cable. The signal from the anemometer was received by a National Instruments NI-9215 A/D converter (100 kS/s/ch, 16 bit) via a 3 m (10 ft.) long and read using a LabVIEW virtual instrument (VI).

When connecting the hotwire to the Bruhn anemometer [13], which was constructed at Purdue, the cold resistance of the hotwire and the 4.5 m (15 ft.) long coaxial cable was first measured using a low-current ohmmeter. This resistance was multiplied by 0.625 to get the operating resistance which was set on the anemometer by adjusting the potentiometer.

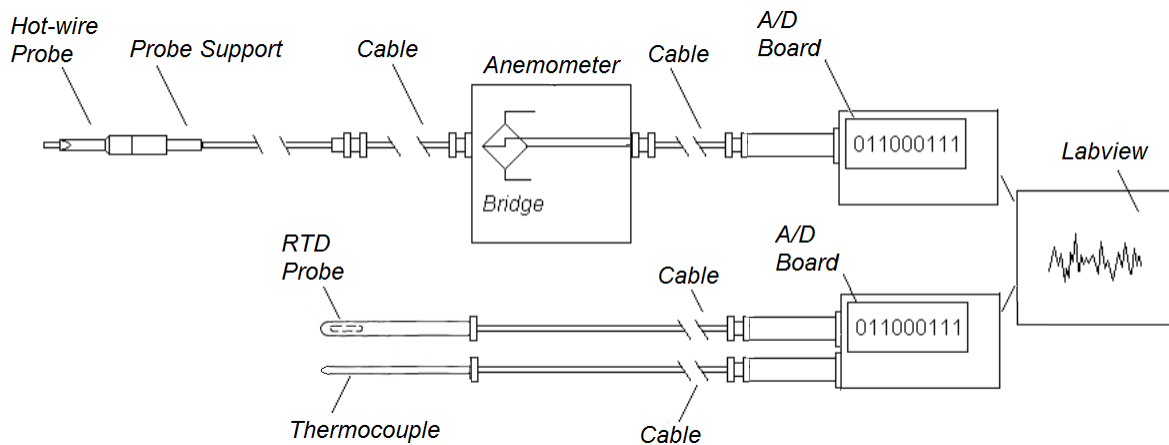


Figure 3.4: Schematic of the wind tunnel measurement system

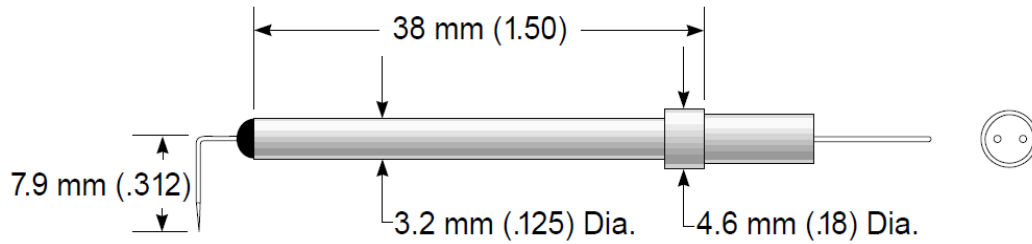


Figure 3.5: 90° hot-wire probe used for boundary layer and cross-section survey measurements [16]

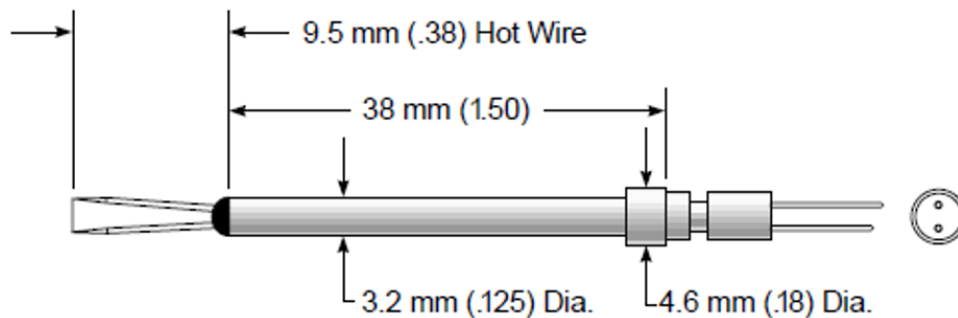


Figure 3.6: Straight hot-wire probe used for measuring turbulence over the entire tunnel speed range [16]

3.2.3 Probe Calibration

The hot-wire probe had to be re-calibrated prior to every test. For every calibration, the probe was positioned in the center of the wind tunnel cross-section, 2.2 m (86") downstream of the test-section entrance. To calibrate the probe, the hot-wire voltage was measured over a range of wind-tunnel speeds and compared to the reference velocity (U_∞) obtained from the contraction pressure drop (ΔP) located at the entrance of the test-section using Equation 3.8.

$$U_\infty = \sqrt{\frac{2K\Delta P}{\rho_{air}}} \quad 3.8$$

The density ρ_{air} was calculated using the ideal gas law where the pressure term came from the atmospheric pressure recorded by a digital barometer (OMEGA DPI 740) located beside the wind tunnel and the temperature term from stilling section temperature in the tunnel. The

pressure drop is obtained from a differential pressure transducer (OMEGA PX653). Table 3.1 shows one example of the calibration parameters for Equation 3.6 using a least-squares-fit linear relation. The calibration curves can be found in Appendix A.

Table 3.1: Sample hot-wire calibration results

A	B	R ²
1.103 ± 0.007	-2.898 ± 0.046	0.9997

3.3 Temperature Measurement

The temperature of the flow in the tunnel was measured using two temperature probes. One was stationary and located in the stilling section of the tunnel, and one was moving with the hot-wire probe in the test-section of the tunnel.

The fixed probe was a 12" long, 3/16" diameter Omega 100 Ohm resistance temperature detectors (RTD) probe and was used to measure the static temperature of the flow as it was in the lower-velocity stilling section. The signal from the RTD probe was sampled by a NI-9219 A/D converter.

The moving probe was a 6" long, 1/16" diameter Omega K-type thermocouple and was placed in situ with the hot-wire probe to measure the temperature profile over the cross section of the tunnel. The probe is also used to take temperature measurements for use in the voltage correction correlation in Equation 3.7. The signal from the thermocouple was sampled by a NI-9211 A/D converter.

3.4 Traverse System

The hot-wire probe is moved across the test-section via a Velmex traverse system. The probe-mounting arm shown in Figure 3.7 is attached to the vertical-axis plate on the traverse. The arm extends down into the flow through a slot in the top of the tunnel. The probe arm is enclosed in an aluminum aerodynamic strut, and the probe was mounted at the end of the arm. The hole in the top of the tunnel is only 24" long. To allow for positioning of the probe outside of this region, a probe-arm extension (80/20 beam) was used. The configuration of the probe shown in

Figure 3.7 was used for measuring the flow parameters only at the center of the test plane. The configurations used for measuring the entire cross-section area can be found in Appendix A.

The aerodynamic strut is hollow which allows any probe cabling/tubes to be routed up through the center of the strut to the top of the tunnel. With the mounting arm extended into the tunnel, two covers are secured around the strut to cover the hole in the top of the tunnel.

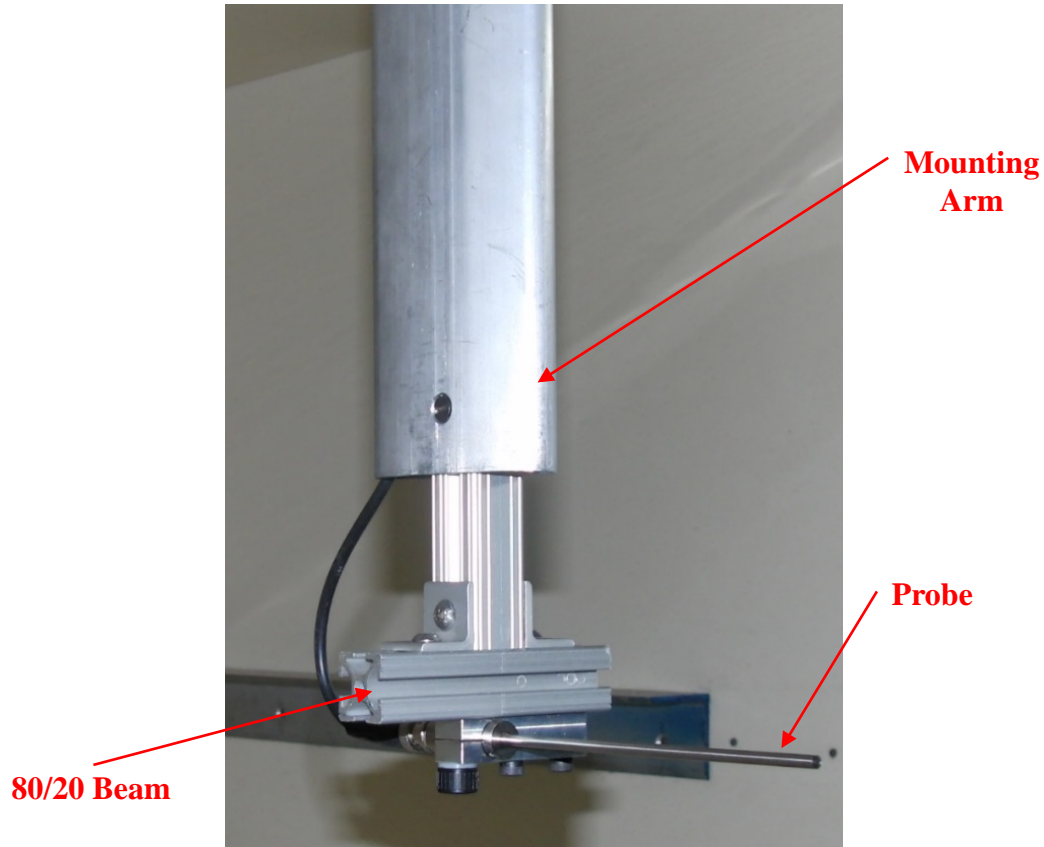


Figure 3.7: Traverse probe mounting configuration used for center measurements

3.5 Survey Grid

The measurement plane was located 86" downstream of the test-section inlet as shown in Figure 3.8. The entire 72" x 48" cross-section of the wind tunnel could not be traversed in a single run and thus the 17 x 15 point survey of the full cross-section was split into smaller sections and the probe arm reconfigured for each section. Each smaller section overlapped measurement points with adjacent sections as shown in Figure 3.9 so that the changes in the probe-mounting configuration could be accounted for during post-processing. The spacing between the

measurement points in the span-wise direction was 4.5", while the spacing in the height direction was 3". A full table of the point locations can be found in Appendix A.

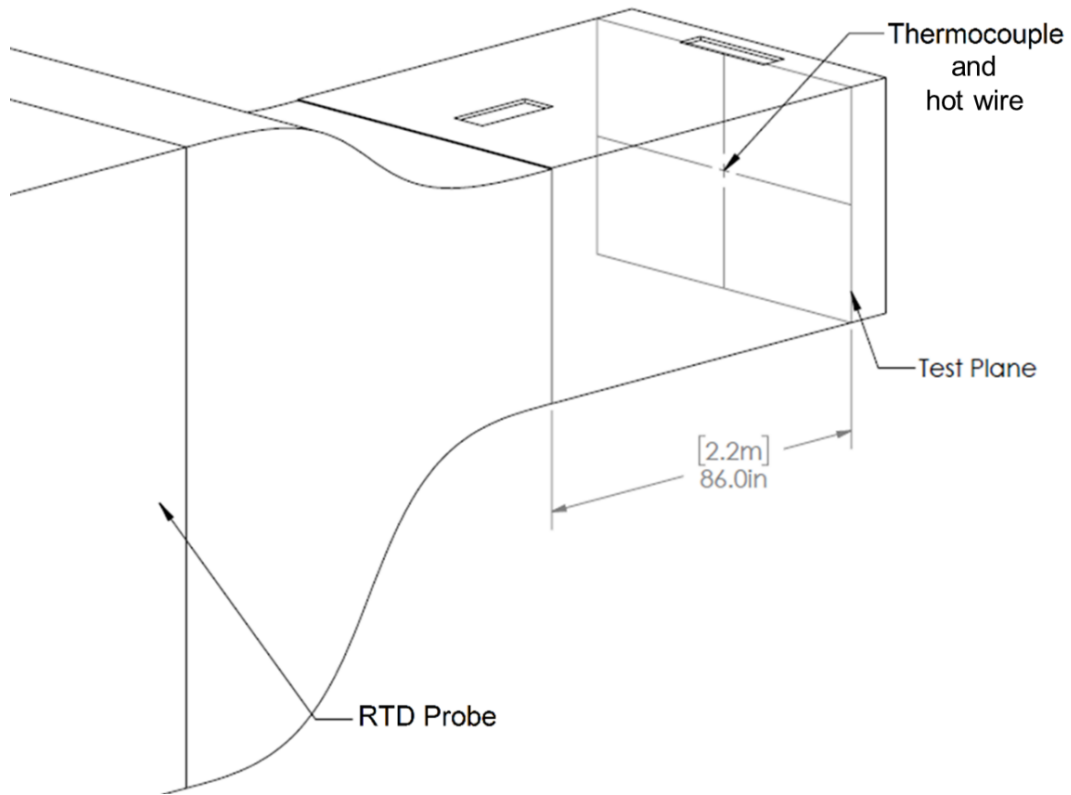


Figure 3.8: Location of measurement instruments in the wind tunnel

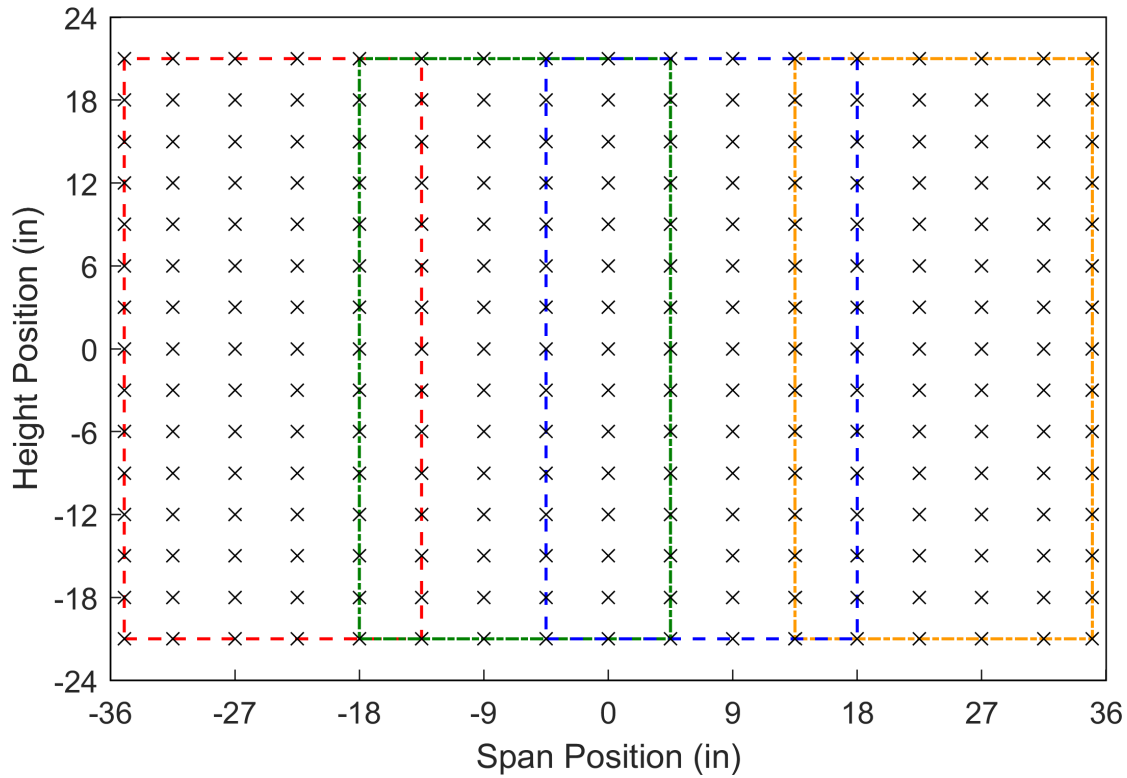


Figure 3.9: Flow measurement grid, each colored box contains the points measured in a single test

3.6 Measurement Parameters

An important flow characteristic in the wind tunnel is the turbulence intensity (Tu). It is defined as the root-mean-square (RMS) value of the fluctuating velocity component (u), normalized by the mean of the velocity component (\bar{u}) and is calculated using Equations 3.9 – 3.11.

$$\bar{u} = \frac{1}{N} \sum_{i=1}^N u_i \quad 3.9$$

$$u'_{rms} = \sqrt{\frac{1}{N-1} \sum_{i=1}^N (u_i - \bar{u})^2} \quad 3.10$$

$$Tu = \frac{u'_{rms}}{\bar{u}} \quad 3.11$$

where \bar{u} and u'_{rms} are calculated using the local flow velocity, and N is the number samples recorded over a single period at one spatial location.

3.7 Correlating tests

Due to the survey grid having to be split into sections, the sections had some overlapped measurement points as shown in Figure 3.10, so that the changes in the probe-mounting configuration could be accounted for during post-processing. Overlapping regions were related using a multiplication factor η shown in Equation 3.12, where $\bar{u}_{old,j}$ is the previous velocity value at point j , $\bar{u}_{new,j}$ is the new velocity value at point j , and N is the total number of overlapping points. Using η , all the points in the new section could be corrected using Equation 3.13. If the corrected sub-section were then used to correlate another section, the \bar{u}_{corr} values would be used as $\bar{u}_{old,j}$.

$$\eta = \frac{1}{N} \sum_j^N \frac{\bar{u}_{old,j}}{\bar{u}_{new,j}} \quad 3.12$$

$$\bar{u}_{corr} = \eta \cdot \bar{u}_{new} \quad 3.13$$

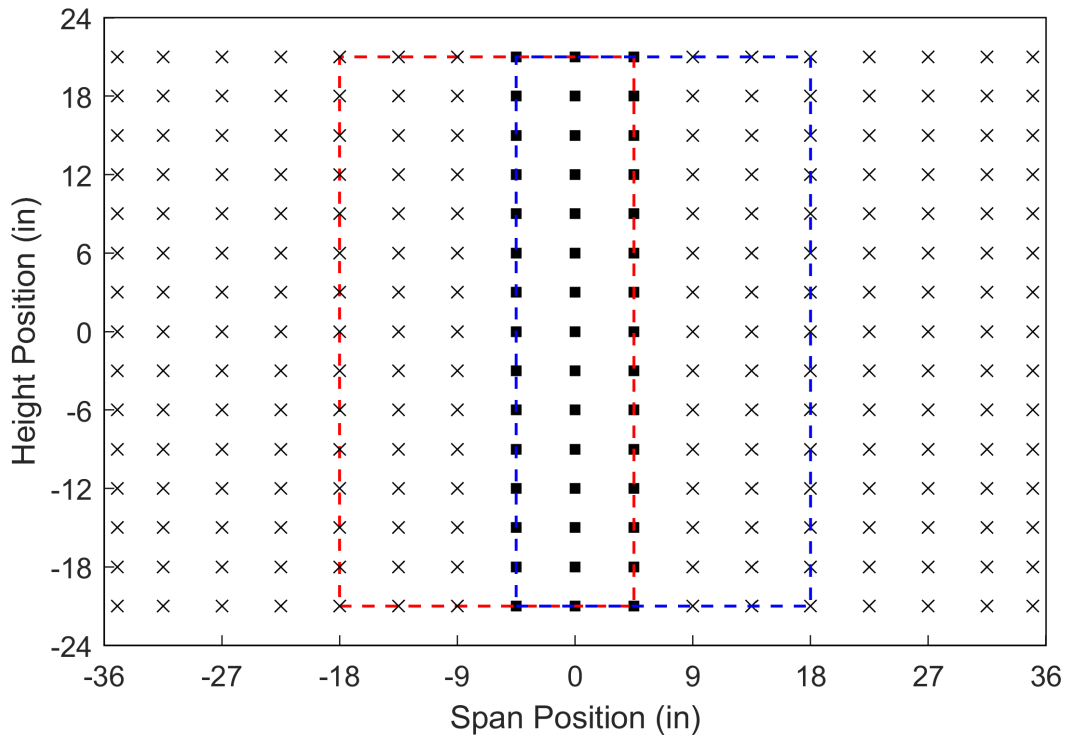


Figure 3.10: Overlapping test regions where the red box is first old and the blue box is new test, (◼) overlapping points

4. RESULTS AND DISCUSSION

The flow quality discussed in the following sections was measured only in the axial direction of the flow. The measurement plane was located 86" downstream of the test-section inlet and covered the entire 4 ft. x 6 ft. cross section of the tunnel. Flow data was acquired at each point of the measurement grid shown in Figure 3.7 at a sampling frequency of 25 kHz for 60s at a tunnel motor frequency of 30 Hz ($U_\infty = 20$ m/s). This is the speed at which the tunnel is primarily run for student projects.

The contours in the following sections are viewed looking downstream with the flow, so that positive span wise positions correspond to the outside half of the tunnel. The contours omit the near wall regions for clarity. The contours which include the near wall regions can be found in Appendix B.

4.1 Velocity Distribution

The velocity distribution for a reference velocity of 20 m/s is shown in Figure 4.1. Away from the walls, the minimum to maximum mean velocity difference is equal to 3% of the reference velocity from 19.9 – 20.5 m/s with a mean velocity RMS value over the test plane of 0.03 m/s. From the contour it can be seen that the flow on the right (inside) side of the tunnel tends to be slightly faster than on the left side, which was also seen before the modifications to the tunnel [1]. The slower flow at the top center of the tunnel is due to the covers over the hole in the top of the tunnel. The width of the hole location is between the two red lines in the figure. The faster flow at the bottom center of the tunnel is thought to be caused by a combination of two things. The first is the model mounting cover (shown in Figure 4.2) allowing air to leak into the tunnel around the edge of the cover. At 36" wide, the hole cover diameter is roughly equal to the higher velocity region and therefore thought to be its possible cause. The second results from a slight velocity overshoot, due to the contraction which is explained more in Section 4.4. Plots of velocity across constant height positions and span positions can be found in Appendix B.

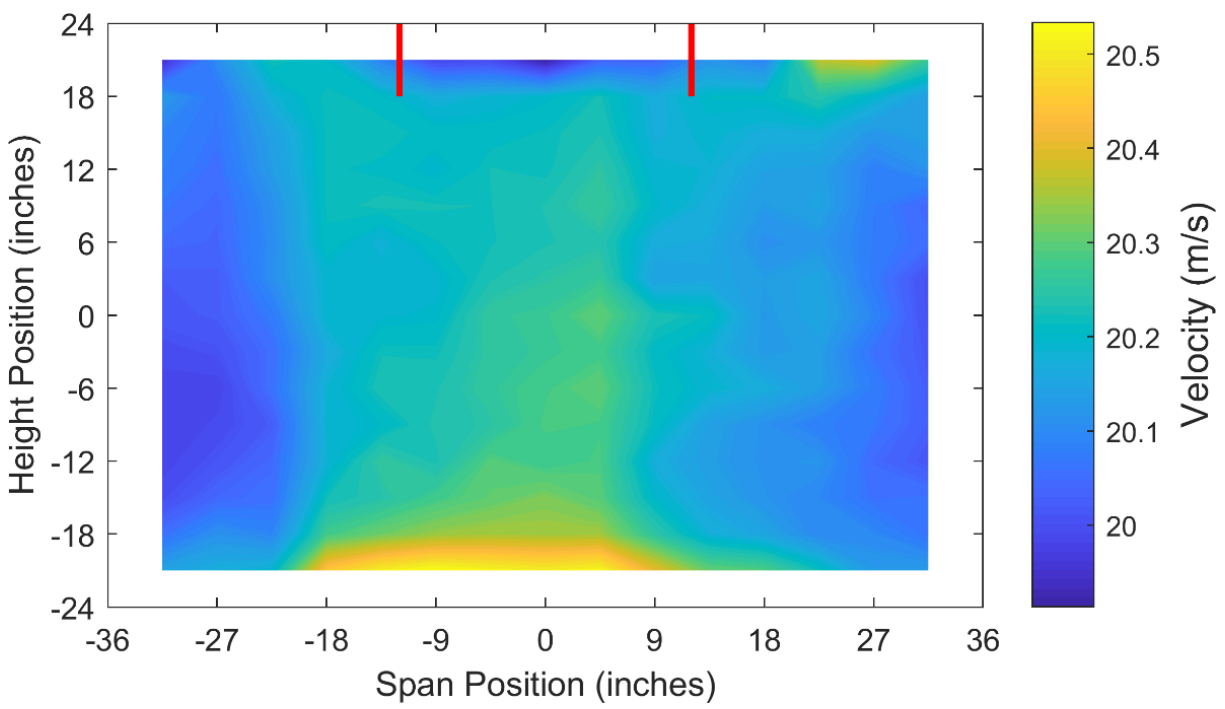


Figure 4.1: Cross-section velocity contour (core region) at 20m/s. The red lines show the boundary of the covered hole in the top of the tunnel

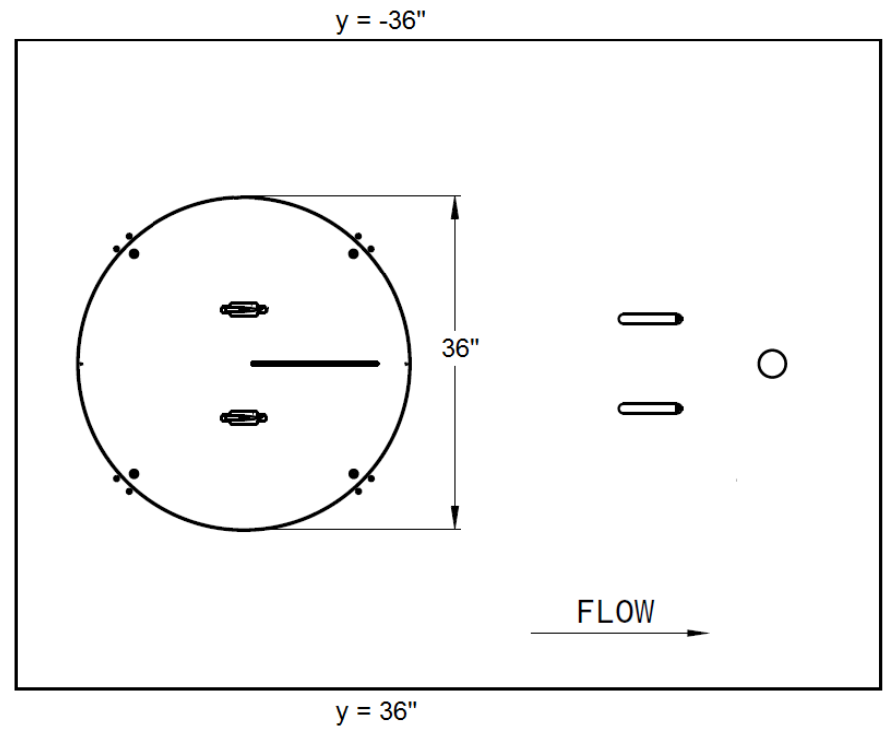


Figure 4.2: Schematic of the floor of the test section showing the model mounting hole cover. Note that during tests the slots in both the cover and the test section floor were sealed.

The percentage deviation from the free-stream velocity (20 m/s) is shown in Figure 4.3. Comparing the magnitudes of these deviations to those of the similar-sized National Diagnostic Facility (NDF) at IIT [7] shown in Figure 4.4, it can be seen that the NDF tunnel has a percentage deviation an order of magnitude smaller than the Boeing Subsonic Wind Tunnel.

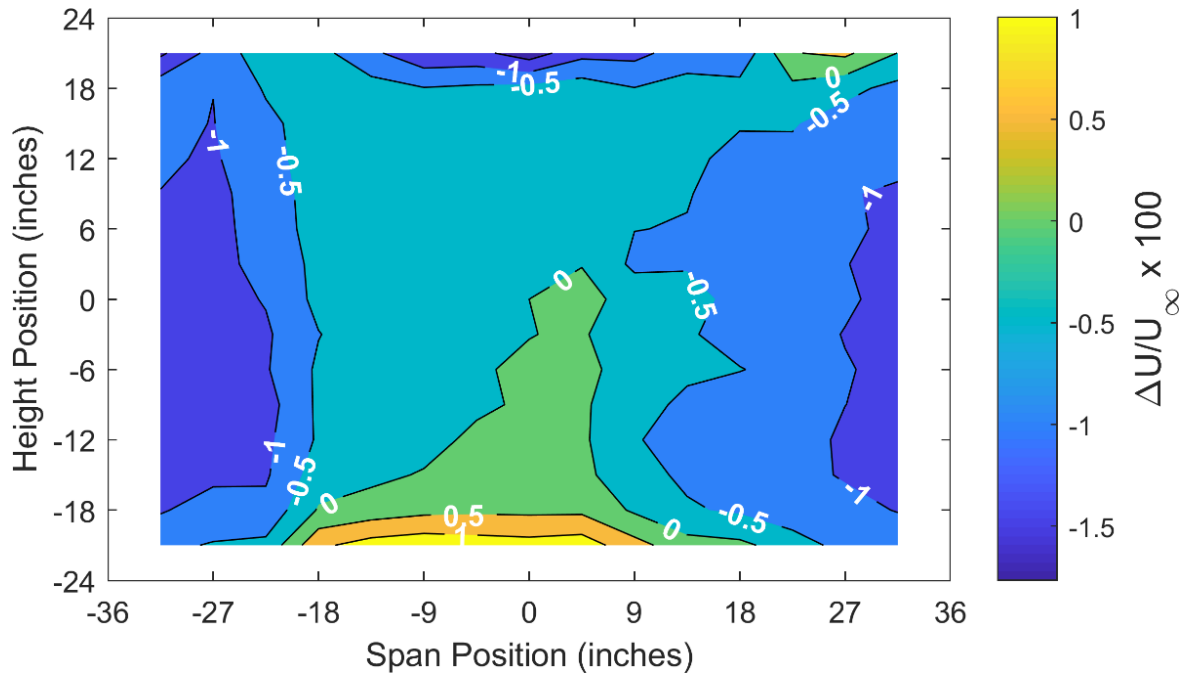


Figure 4.3: Percentage deviation of the mean velocity across the BSWT test section for a free-stream speed of 20 m/s, 86" from the test-section inlet

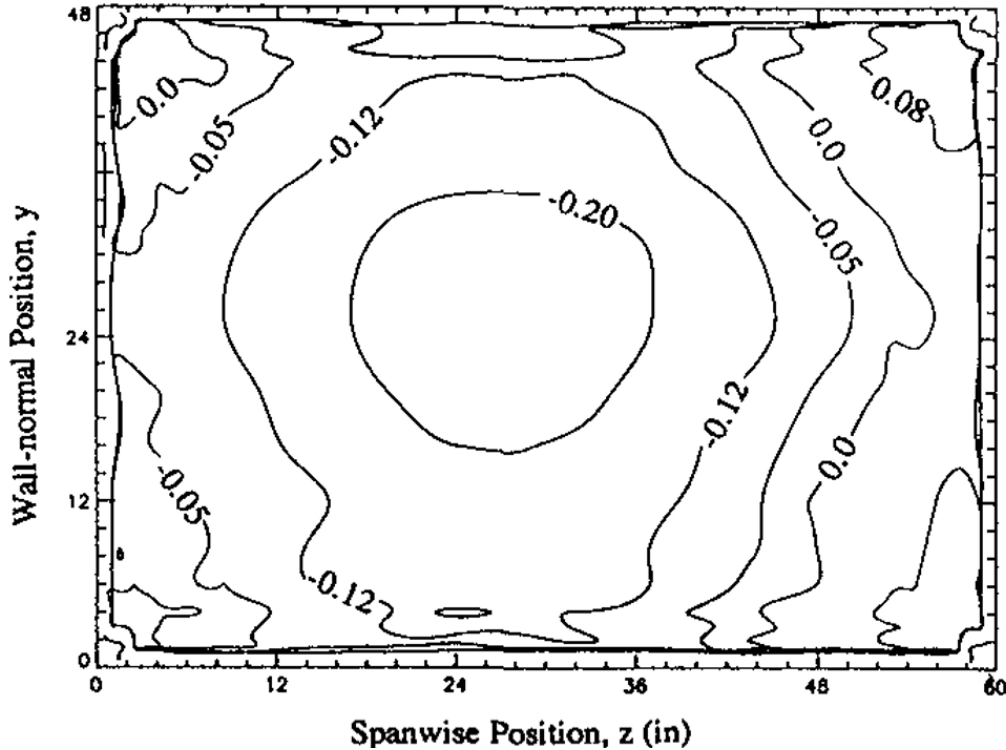


Figure 4.4: Percent deviation of the mean velocity across the NDF test section for a free-stream speed of 20 m/s, 8" inches from the test-section inlet [7]

4.2 Turbulence Intensity

When reporting turbulence intensities, care needs to be taken in how these values are calculated. Parameters such as sample length and the filters applied to those samples can have a large impact on measured turbulence intensity [17], and the effects of these parameters on the calculated turbulence intensities must be considered.

The same set of measurements obtained at the center of the measurement plane with a free-stream speed of 20 m/s and a sampling frequency of 25 kHz for 5 minutes, were used for all analysis in Sections 4.2.1 – 4.2.3.

4.2.1 Sampling Length

To test the effect of sampling length on the reported turbulence, the turbulence intensity of the flow was calculated for sampling lengths ranging from 0.5 s to 180 s with no filtering applied to the data. Figure 4.5 shows the turbulence intensities calculated for the range of sampling lengths.

As the sampling time increases so does the calculated turbulence intensity. The plot shows that around 60 s the calculated turbulence intensity approaches a constant value and therefore, all full cross section hot-wire tests were conducted with a sampling length of 60 s.

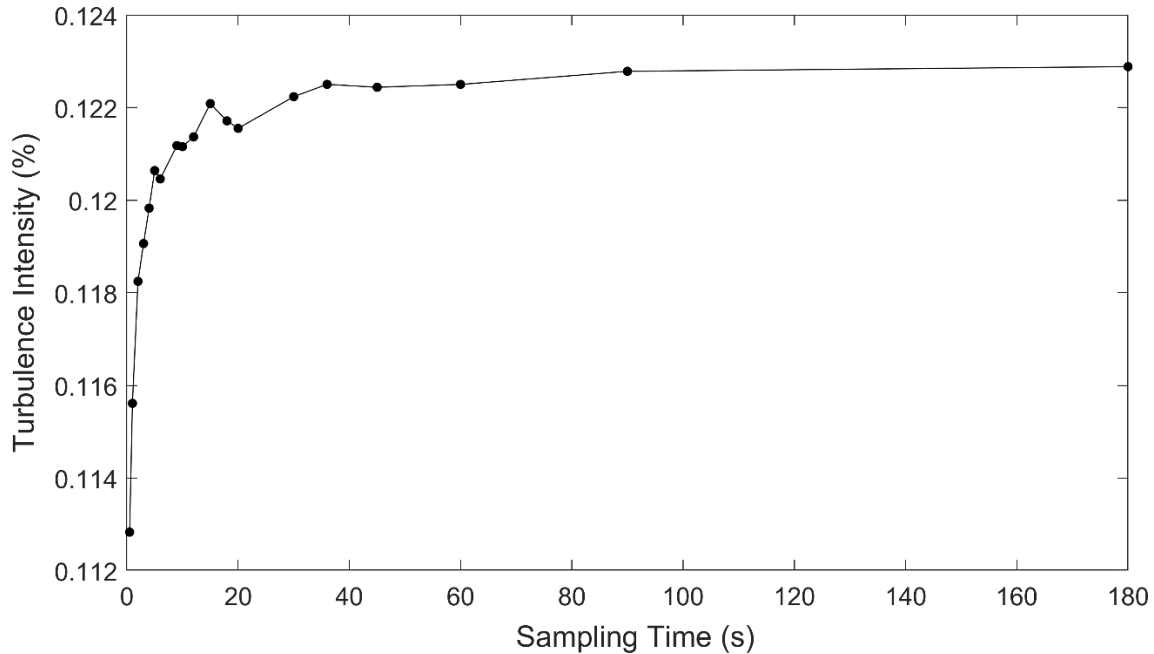


Figure 4.5: Turbulence intensity for various sampling times, at a free-stream speed of 20 m/s

4.2.2 High-Pass Filter

Preliminary analysis of the raw velocity data presented in Appendix B, showed that the turbulence spectra energy began to decay monotonically beyond approximately 200 Hz, and reached the noise floor around 1 kHz. Thus, a 2 kHz low-pass filter was applied to subsequent data and only the effect of the adding a high-pass filter was studied.

Using the filters used in other wind-tunnel turbulence studies (Table 1.1) as a basis, the effect of changing the high-pass filter in conjunction with a 2 kHz low-pass filter was studied. Saric [4] suggested that, when considering frequencies above 0.1 Hz, the turbulence levels in low-turbulence wind tunnels should be below a 0.05% limit. However, the studies listed in Table 1.1 mostly used a high-pass filter at 1 Hz, and the MTL tunnel [6] used a high-pass filter frequency ($f_c = \frac{U_\infty}{\lambda_c}$) obtained from a cut-off wavelength (λ_c) equal to the sum of the lengths of the two

test-section sides. For the Boeing Subsonic Wind Tunnel at a free-stream speed of 20 m/s this would be equal to 6.67 Hz. The results of applying these filters on the calculated turbulence intensity are shown below in Figure 4.6

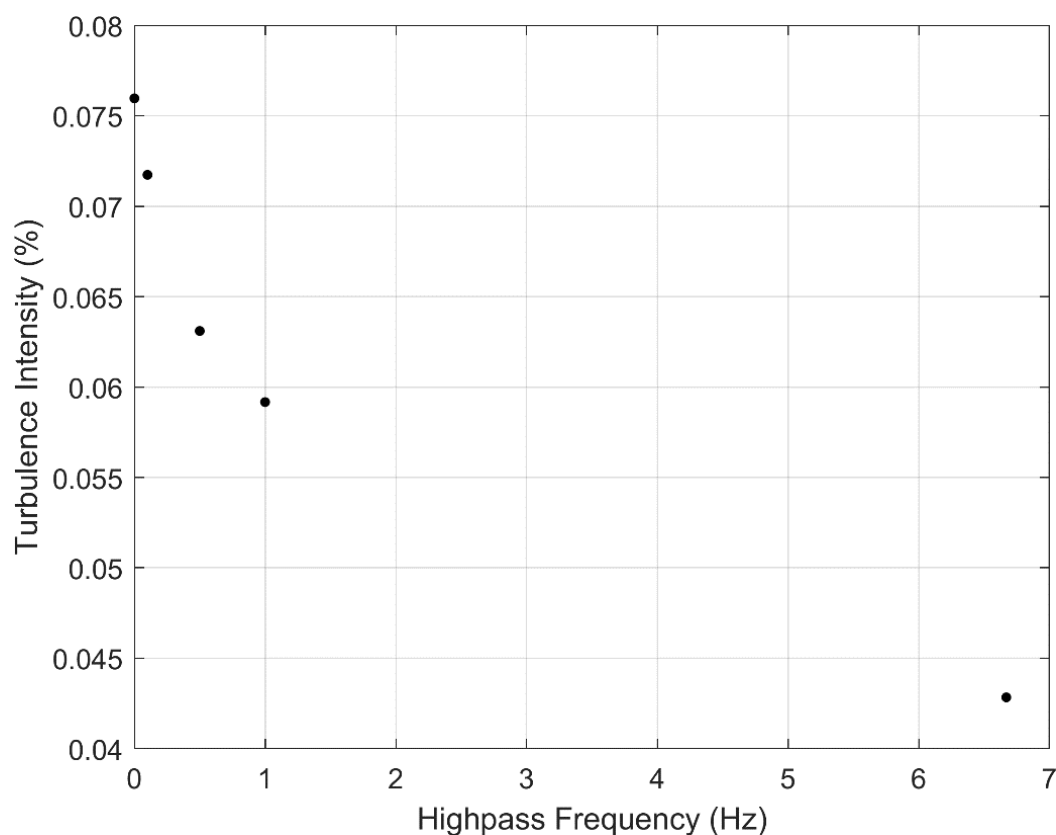


Figure 4.6: Turbulence intensity vs high-pass filter frequency for $U_{\infty} = 20\text{m/s}$

Applying a high-pass filter did reduce the reported turbulence intensity by ~22% for a 1 Hz filter. It did not reduce the turbulence intensity by as much as was observed at the NDF tunnel which saw a decrease in turbulence intensity to 0.032% from 0.085% with a 0.1 Hz high-pass filter and to 0.028% with a 1 Hz high-pass filter. This suggests that a much larger proportion of the Boeing Wind Tunnel turbulent energy lies above 1 Hz than at the NDF tunnel, and is discussed more in Section 4.3.1.

To see how the Boeing Subsonic Wind Tunnel turbulence levels compared to Klebanoff-Saric Wind Tunnel [5] at 20 m/s, a 1Hz – 10 kHz band-pass filter was applied. With this filter the

Boeing Subsonic Wind Tunnel had a turbulence intensity of 0.098% compared to Klebanoff-Saric Wind Tunnel value of 0.091%.

4.2.3 Turbulence Variation with Tunnel Speed

While most research and student projects in the tunnel are run at a free-stream speed of ~ 20 m/s some are run at different speeds. To account for this, the centerline turbulence intensity over the range of tunnel speeds was measured as shown in Figure 4.7. For this test, each flow speed was sampled at 25 kHz for 5 minutes, and the measurements were analyzed with 2 kHz low-pass filter. Turbulence intensities were approximately 0.08% between 20 and 36 m/s and increased to $\sim 0.095\%$ when the tunnel was operated at maximum speed and $\sim 0.09\%$ at 13 m/s. The floor of the test section was noticeably shaking at the top two tunnel speeds, which may be a reason for the increase in turbulence intensity seen at these speeds.

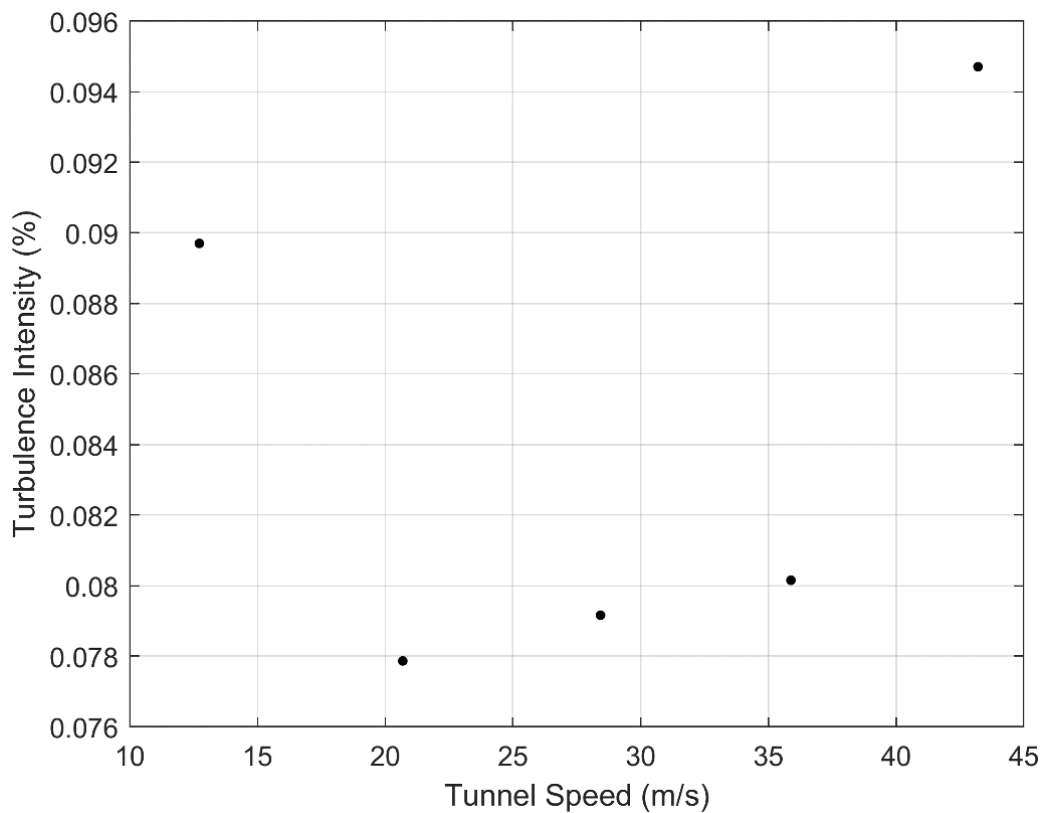


Figure 4.7: Tunnel center turbulence intensity across the entire range of wind tunnel speeds

4.2.4 Turbulence Intensity Distribution

Using the data collected from the velocity distribution tests, the stream-wise turbulence intensities across the cross-section of the wind tunnel were calculated.

As the probe was mounted perpendicular to the flow direction in order to span the tunnel, it vibrated more than it did for the centerline measurements in Section 4.2.3. With the probe mounted perpendicularly, its tip was observed to be moving approximately 0.25 mm in the flow direction, and 0.51 mm up and down. As such, the reported turbulence intensities in the contour plot are higher than in Figure 4.7. A comparison of the two power spectra for the different mounting configurations is shown in Appendix B. The turbulence intensity distribution over the tunnel cross-section is shown in Figure 4.8. The turbulence intensities were less than 0.15% in most of tunnel with a minimum value of 0.09%. At the edges of the core region, the turbulence intensity rose to 0.4%. The contour plot legend is limited to 0.3% turbulence intensity for clarity.

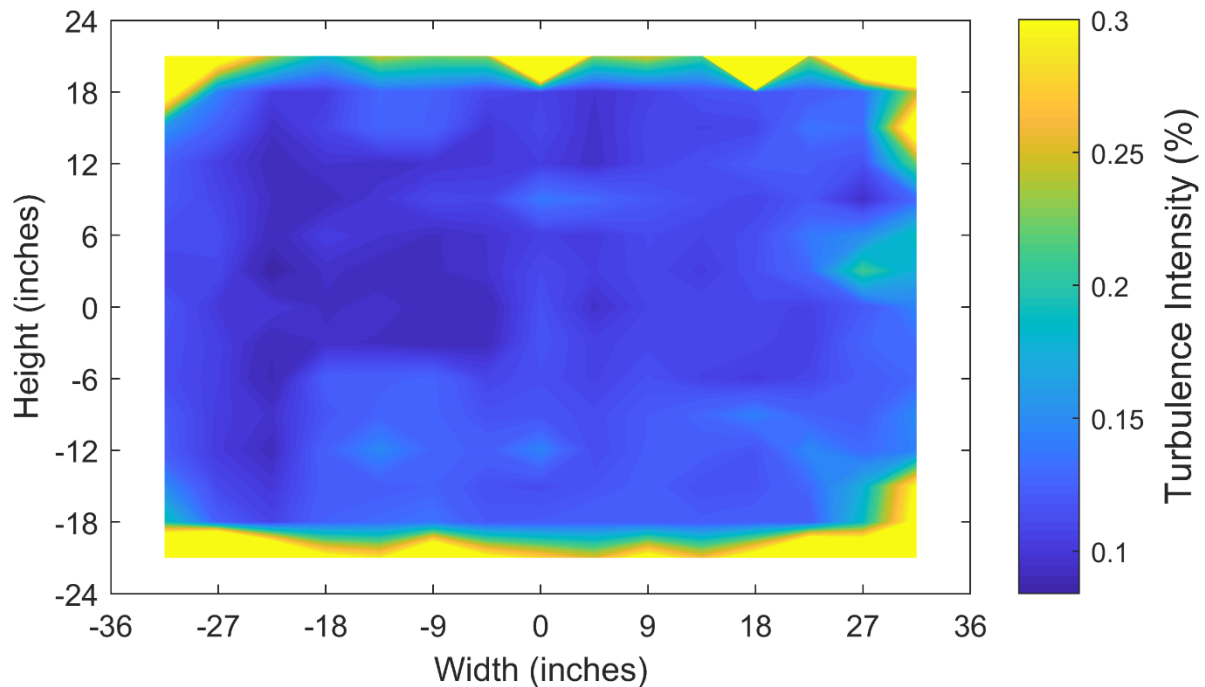


Figure 4.8: Cross-section turbulence intensity contour – core region

The lower turbulence level section located between $22.5'' \leq y \leq -4.5''$, and $3'' \leq z \leq 6''$, was caused by the last screen of the stilling section having been cleaned in that area and is discussed further in the next section.

4.2.5 Effect of Dirty Screens

A higher turbulence level spot (0.27%) located at $y = -13.5''$, $z = 6''$, and shown in Figure 4.9, was initially present for every measurement in this area. One possible reason for this could have been the probe configuration. To rule out the effect of the probe mounting configuration, this region of the test section was studied using four different mounting configurations. For these tests the higher turbulence spot remained. To investigate this region further, a study with a refined $1'' \times 1''$ grid was completed and the results are shown in Figure 4.10. This study showed that there was a region of about 25 square inches centered around $y = -13''$, $z = 5$, that had higher turbulence levels than the rest of the tunnel cross-section.

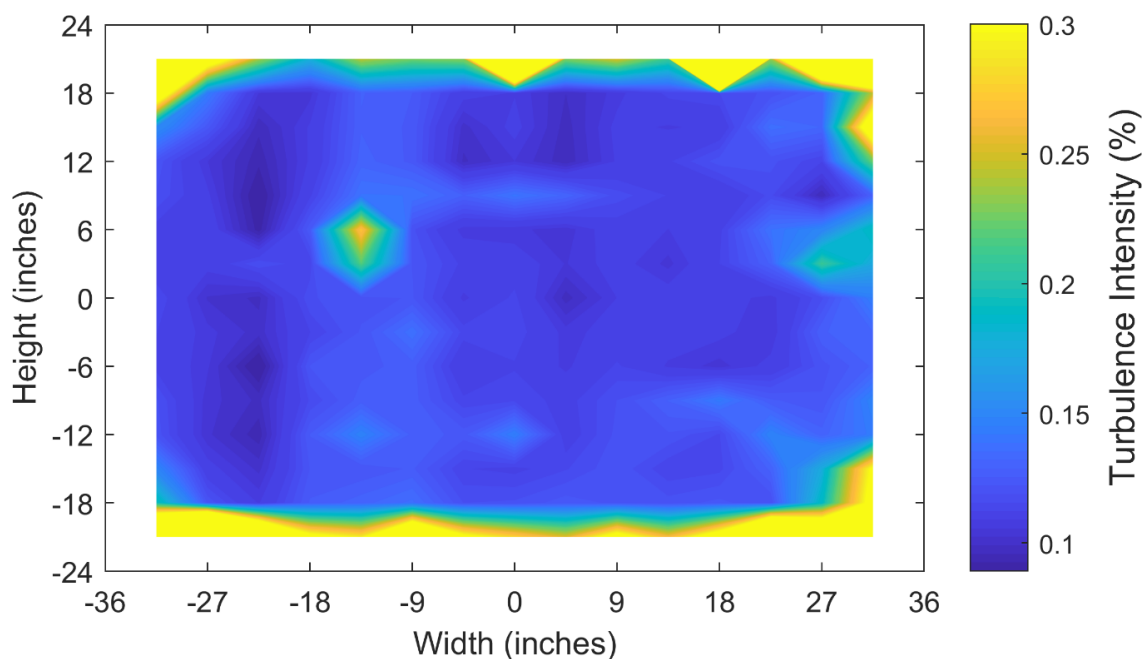


Figure 4.9: Cross-section turbulence intensity contour with high turbulence spot before screen cleaning

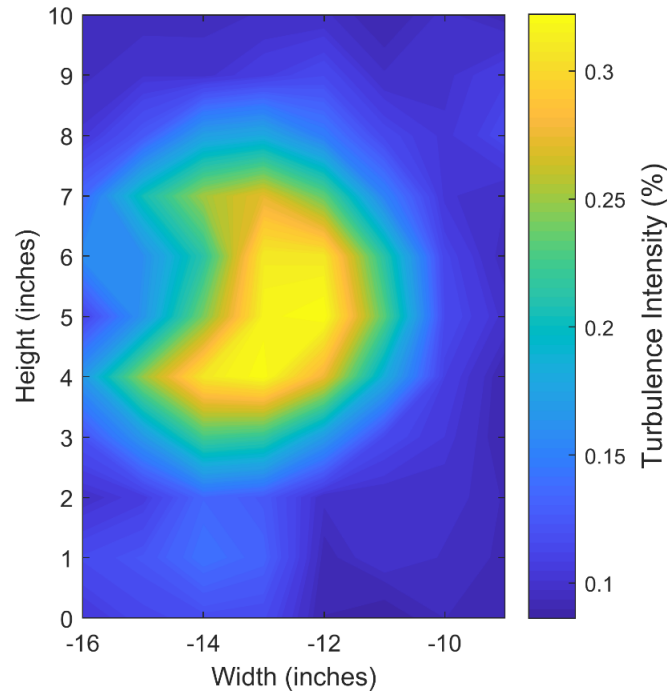


Figure 4.10: Higher turbulence intensity spot – before cleaning

The screens in the stilling section of the tunnel were also examined to see whether there were any holes or large sections of dust that could cause the higher turbulence spot. A section of the last screen was found to have a dirty spot that aligned with the turbulent spot in the test section. After cleaning the spot on the screen, the higher turbulent spot in the test section was no longer present, indicating that cleaning of the screens can reduce the turbulence intensity levels in the test section.

4.3 Turbulence Power Spectral Density

The turbulence power spectral density (PSD) was calculated for several wind tunnel speeds using Welch's Method normalized by the reference velocity U_∞ . Each spectrum was calculated when the hot wire was at the center of the tunnel for the same flow and sampling conditions as in Section 4.1. Figure 4.11 shows the spectra from the unfiltered velocity data for five different flow speeds. The power spectra across all flow speeds show that much of the turbulent energy occurs in the low frequency range and the power spectra reaches the noise floor around 1 kHz. This low frequency energy is likely due to pressure fluctuations caused by the first diffuser. The Arizona State University wind tunnel had a similar diffuser design, and also showed higher

energy levels at low frequencies [18]. The f^2 magnitude increases that occur at the highest frequencies of the spectra are due to the anemometer and are not a property of the flow [19].

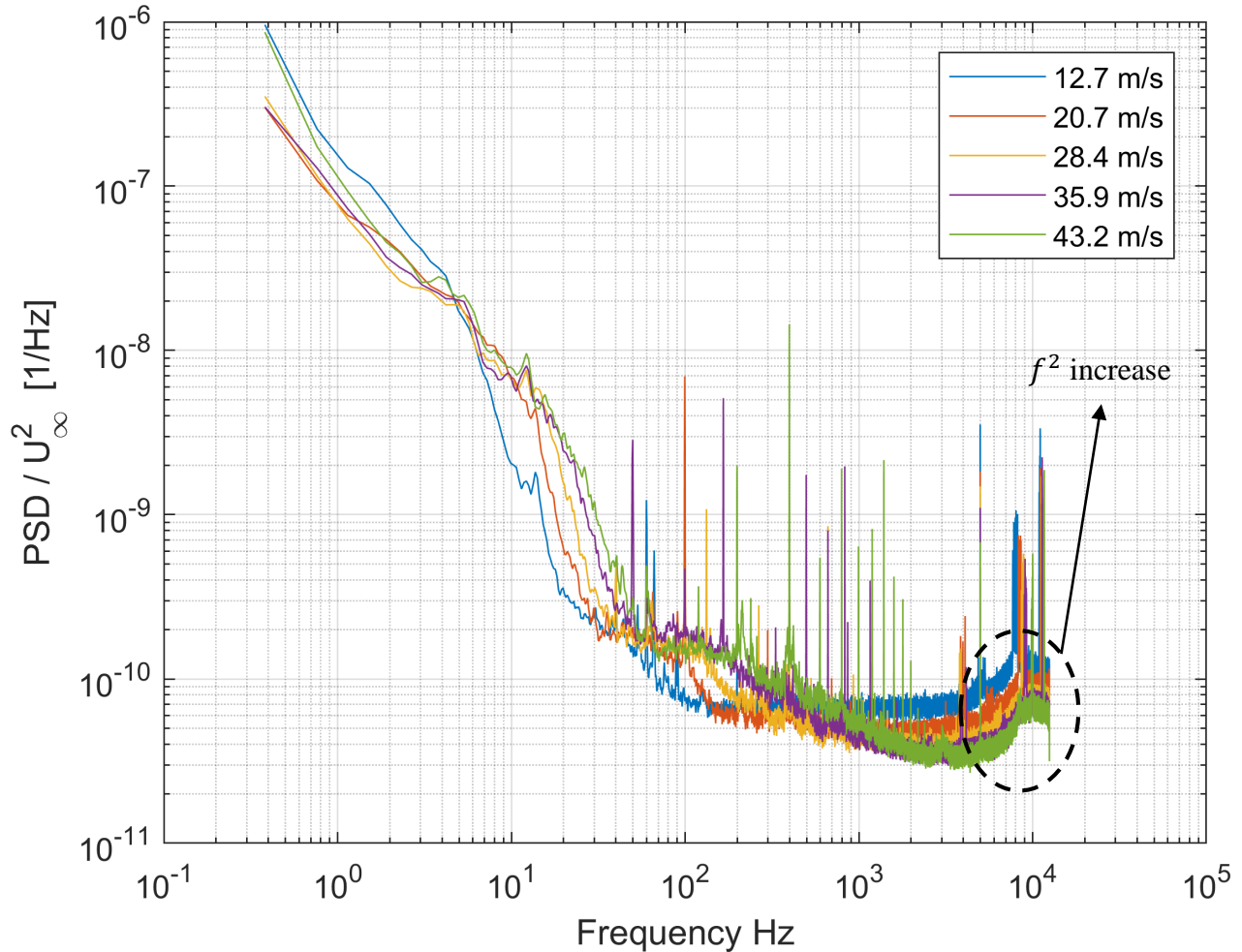


Figure 4.11: Velocity power spectra at the center of the test plane

4.3.1 Hot-wire Signal Noise

As discussed in Section 4.2.2, a larger proportion of the Boeing Wind Tunnel turbulent energy lies above 1 Hz than at the NDF tunnel. One of the causes of this high-frequency energy is due to the anemometer that is being used, as its signal to noise ratio is quite high when compared to other anemometers. Figure 4.12 shows the power spectral densities of flow at 20 m/s in the Klebanoff-Saric Wind Tunnel and the Boeing Subsonic Wind Tunnel where it can be seen that the AA Labs AN-1003 anemometers used for the Klebanoff-Saric Wind Tunnel [5] has a lower

noise floor than the anemometer in the Boeing Subsonic Wind Tunnel. Around 200 Hz, the Boeing Subsonic Wind Tunnel plot data diverges from the Klebanoff-Saric Wind Tunnel data. The amount of energy lying between 200 Hz and 2000 Hz was calculated to be 16% of the total turbulent energy between 0 and 2000 Hz. This higher noise floor leads to the calculated turbulence intensity levels in the tunnel to be higher than if a more sensitive anemometer were to be used.

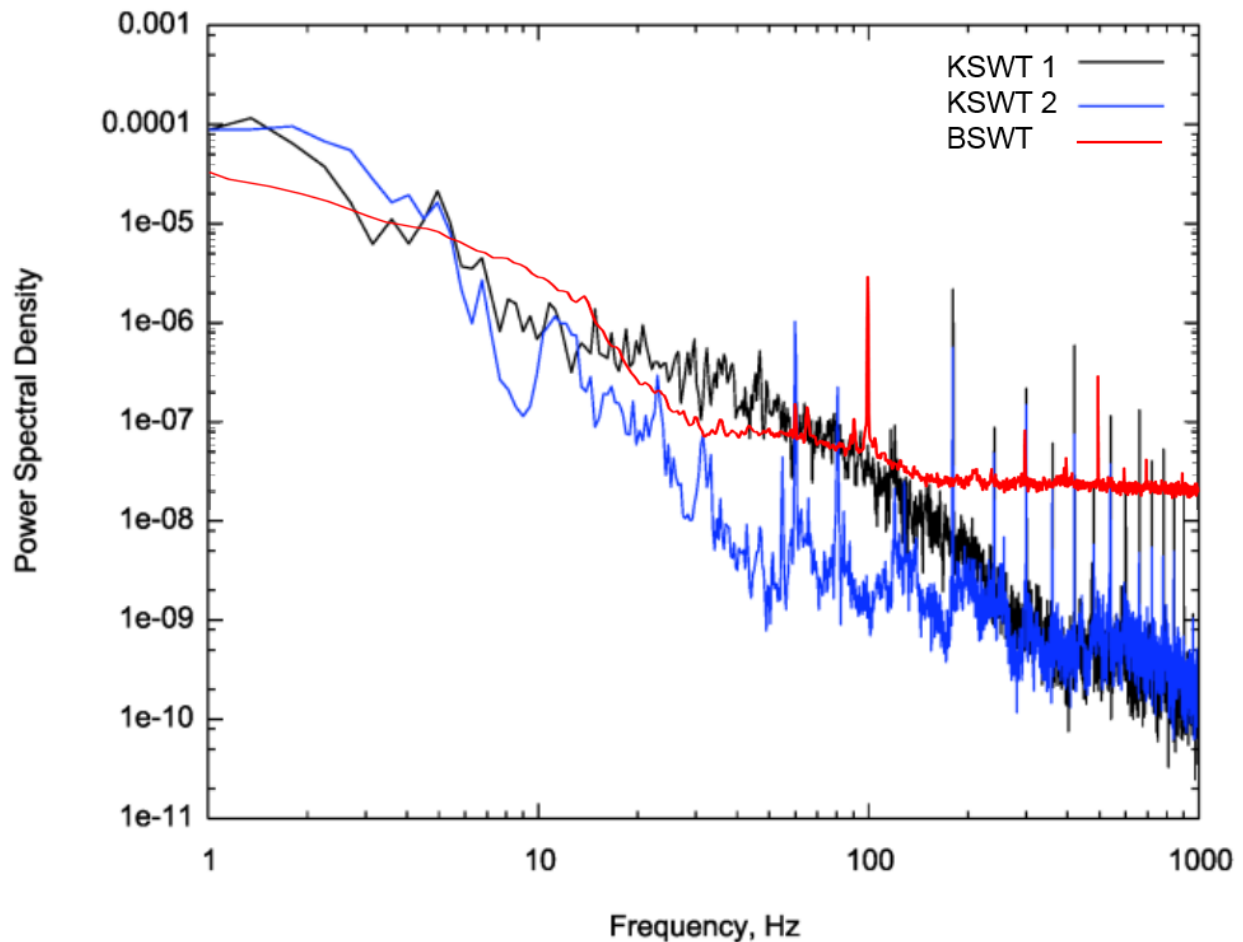


Figure 4.12: Comparison of velocity power spectral densities at 20 m/s for the KSWT and the BSWT [5]

4.3.2 Blade-Passing Frequency

Results shown in Figure 4.13 show peaks in the power spectra between 100 Hz and 1000 Hz, which correspond to the blade-passing frequency (BPF) and its harmonics. The BPF noise

corresponds to the frequency at which a fan blade passes a fixed point. For example, at 30 Hz and 596 rpm, the 10-blade fan has a theoretical BPF of 99.3 Hz. The BPF shown in the power spectra of 99.6 Hz matches very closely to the theoretical value. The BPF and harmonic noise is common to the power spectra through the range of tunnel speeds, which can be found in Appendix B. While the BPF and harmonic energy levels are high with respect to the surrounding frequencies, these peaks are so narrow that they do not significantly contribute to the turbulence levels in the tunnel.

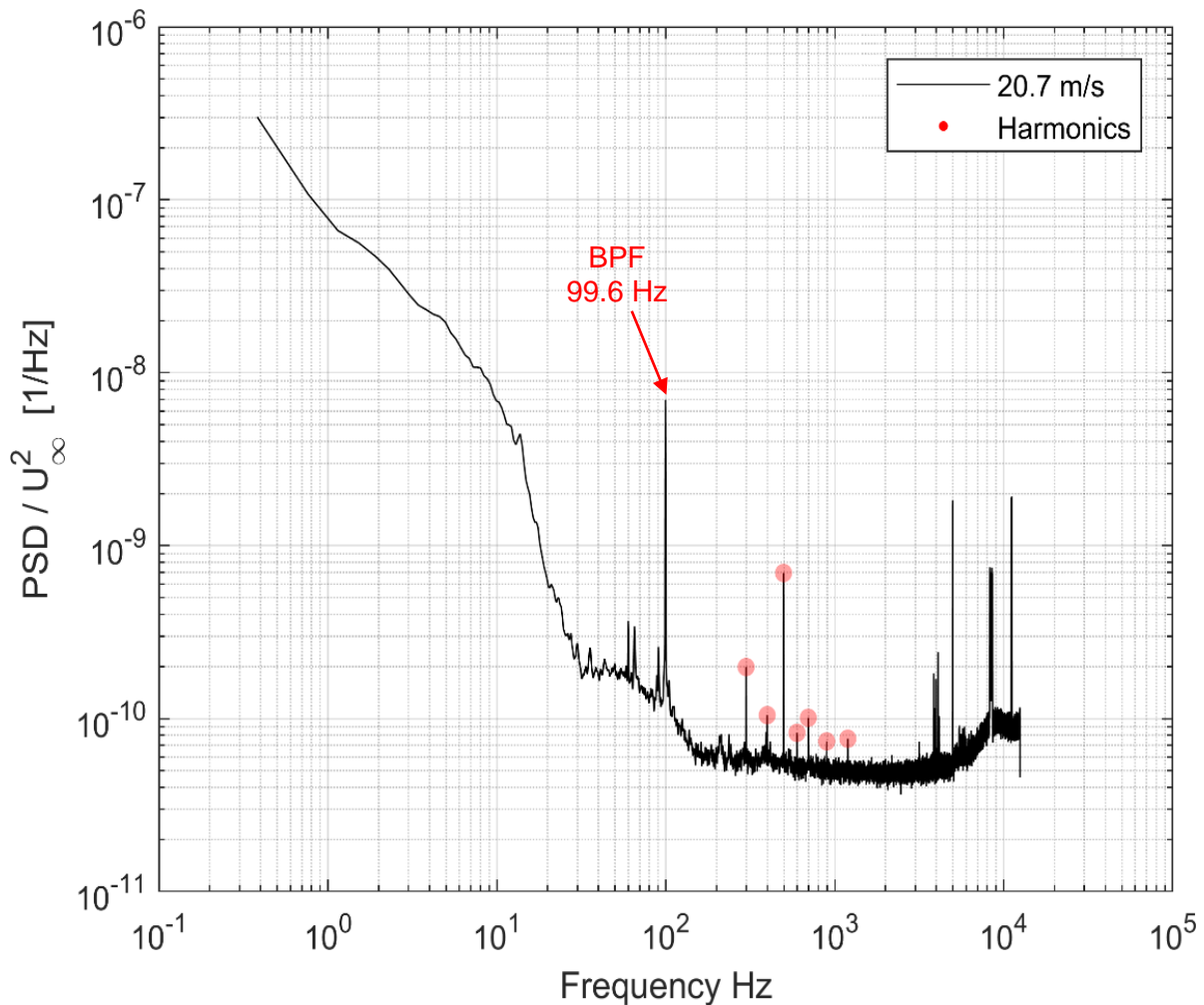


Figure 4.13: Blade-passing frequency noise at a tunnel motor frequency of 30 Hz (20 m/s)

4.4 Boundary Layer

The boundary-layer profile was measured along the center line of the bottom on the test-section for a free-stream speed of 20.3 m/s. The resulting profile shown in Figure 4.14 shows that the boundary-layer thickness at $U/U_\infty = 99\%$ (δ_{99}) is approximately 1.5" thick, with a momentum thickness of $\theta^* = 0.11$ ", and a displacement thickness of $\delta^* = 0.18$ ". For reporting turbulence intensities in the boundary layer, the turbulence intensity was calculated by dividing the point turbulence fluctuations u'_{rms} by the mean free-stream velocity U_∞ , rather than by the mean of the point measurements, as done in previous sections. The boundary layer profile shows that there is a velocity overshoot, which can also be seen in Figure 4.1. This overshoot is caused by having a finite length contraction [20] and cannot be avoided, only minimized through proper contraction design. The maximum velocity overshoot of only 0.4% of the freestream velocity shows that the contraction design in the current tunnel is very good.

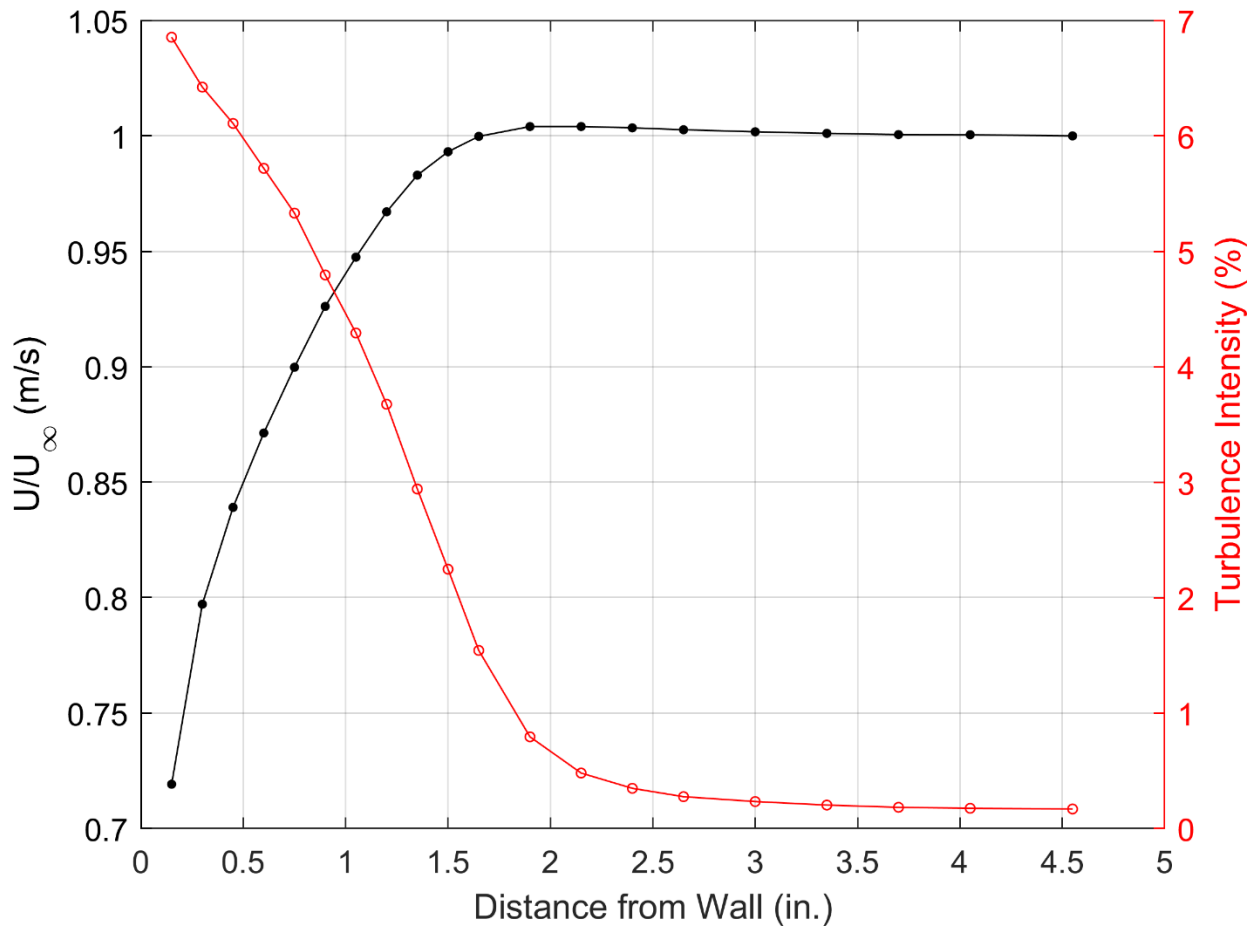


Figure 4.14: Bottom-wall boundary-layer profile and turbulence intensity

4.5 Temperature Variation

4.5.1 Temporal Temperature Variation

Using an RTD probe, the temperature in the stilling section of the tunnel was measured. Measurements were taken here because the flow speed is lower than in the test-section and therefore included less of a dynamic temperature influence. The temperature rise in the tunnel was measured for an ambient temperature of 24.8°C at a free-stream speed of 20 m/s and is shown in Figure 4.15.

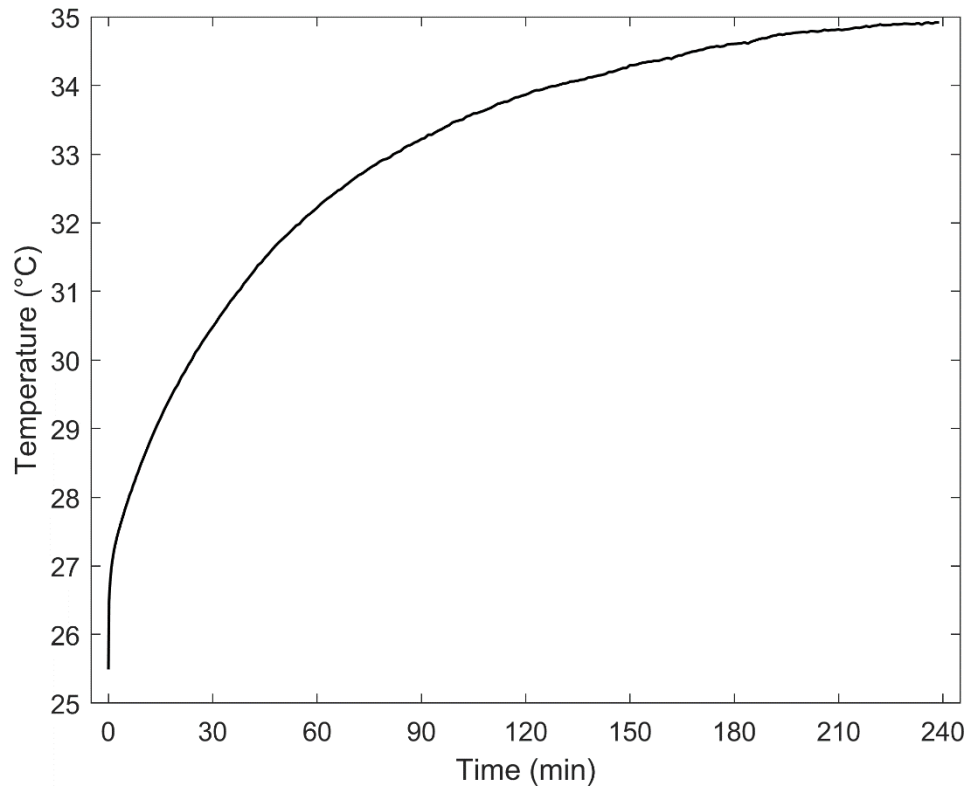


Figure 4.15: Temperature rise measured in the stilling section of the tunnel

After the initial steep increase in temperature for the first five minutes, temperature rose about 5°C within the first hour, 2°C in the second hour, and eventually flattened out after about four hours with an increase of only 1°C in the last two hours. For the majority of tests that are run in tunnel, there is no need to wait for the tunnel temperature to level out. However, the temperature rise should be monitored and kept in mind when analyzing results of future tests.

4.5.2 Spatial Temperature Variation

Due to the large temporal temperature variation shown in Figure 4.15, a profile of the magnitude of the temperature across the cross-section of the tunnel could not be correctly calculated as the time-varying temperature gradient is much larger than the spatial temperature gradient. Instead, the temperature obtained by the thermocouple that traversed the test section was normalized by the temperature in the stilling section of the tunnel. Both temperatures were measured in degrees Celsius. The plot of the spatial temperature variation, shown in Figure 4.16, shows that the cross-section of the tunnel only has about $\pm 0.7\%$ variation in the temperature. The repeatability in the temperature contour over the center of the tunnel was not very high, that is to say the location of the higher temperature contours varying between repeated tests. However, all tests did show that the temperatures near the walls of the tunnel were lower than in the center region. This is important to note when test articles span the entire width of the tunnel.

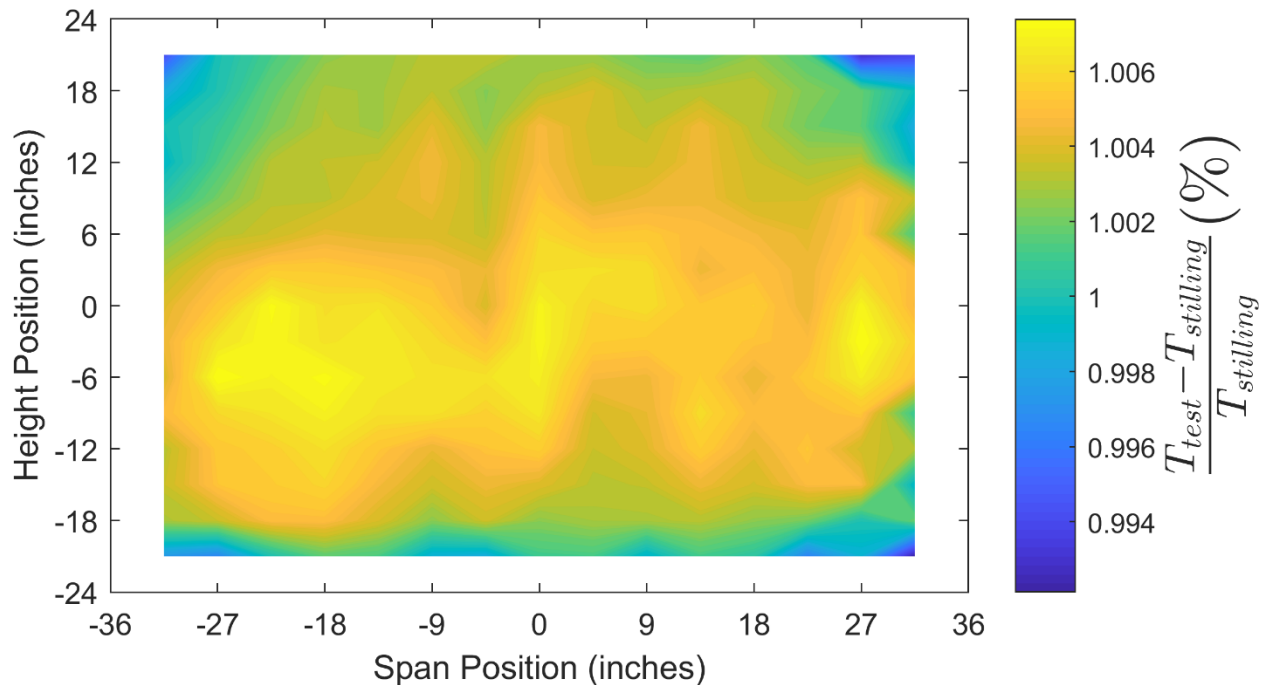


Figure 4.16: Spatial temperature variation – core region – temperature measured in Celcius

5. CONCLUSIONS AND RECOMMENDATIONS

The Boeing Subsonic Wind Tunnel underwent major construction to improve the tunnel flow quality. Before modifications, there was a maximum of a 3% velocity profile gradient and a 0.7% turbulence intensity in the test section of the tunnel.

Post-modification measurements have shown a reduction in the turbulence intensity to less than 0.08% at a U_∞ of 20 m/s. The tunnel is also capable of reaching speeds of up to 43 m/s with a turbulence intensity of less than 0.1%. These turbulence levels are larger than those for low-turbulence tunnel designs ($\sim 0.04\%$). However, the Boeing wind tunnel was not designed as a low-turbulence tunnel and its turbulence levels fall at the lower end of turbulence levels for similar purpose tunnels (0.14% - 1.0%) [8].

The flow uniformity in the free-stream cross-section away from the walls of the tunnel at 20 m/s has a mean flow RMS variance of 0.03 m/s. The velocity profile over that same region has shown a minimum to maximum velocity difference of 3% of the mean flow speed from 19.9 – 20.5 m/s.

With these turbulence levels the Boeing Subsonic Wind Tunnel can be used for a wide array of wind tunnel experiments. Such experiments would include flows that are expected to transition via bypass transition as these types of flows are triggered by mechanisms such as wall roughness or pressure gradient rather than by free-stream turbulence.

The turbulence intensity measurement results can also be used to determine whether specific experiments can be conducted. For example, experiments on laminar separation bubbles can be conducted as studies have shown that bypass transition in these flows does not start until free-stream turbulence intensities of 0.5% are reached, which is far above the levels in the tunnel [21].

The Boeing Subsonic Wind Tunnel is capable of reaching flow speeds ranging from 6 m/s (limited by the tunnel fan motor) to 43 m/s which. These speeds correspond to unit Reynolds numbers (U_∞/ν_∞) ranging from 4.2×10^5 to 30×10^5 . Higher Reynolds numbers can be obtained

if test objects are extended into the 24 ft. long straight section directly downstream of the test section.

The Boeing Subsonic Wind Tunnel is not suitable for experiments involving natural transition where extremely low-turbulence intensity levels are needed. It is also unsuitable for stability experiments as the turbulence intensity levels do not fall below the recommended 0.05% threshold [4].

If more improvements are to be made to the wind tunnel, the following modifications are suggested:

- Clean the screens in the wind tunnel: The screens in the stilling section have, over time, become partially filled with dust. Before the 1991 reconstruction of the tunnel [1], cleaning of the screens caused a 1% decrease in the velocity gradient in the flow. As well, cleaning the area of the last screen – which corresponded to the higher turbulent intensity region in the tunnel – removed the higher turbulence levels. Therefore, cleaning the screens could help to improve the flow uniformity and turbulence intensity levels in the test-section of the tunnel. A procedure for removal of the screens for cleaning can be found in [2].
- Redesign the first diffuser: While flow visualization did not show any flow separation in the diffuser, there are still concerns that this first diffuser may have intermittent separation that is causing flow instabilities. The first diffuser is the best design for how the tunnel is currently arranged, i.e. where the cross-sectional area of the tunnel changes very quickly. However, this fast change is not ideal as it can cause flow separation that will affect the upstream flow in the test-section. Thus, if the first diffuser is to be redesigned, the straight section upstream of the diffuser would need to be shortened to allow for a longer diffuser section.

REFERENCES

- [1] R. D. Behrens, "An Experimental Investigation of Wind Tunnel Quality," Purdue University, 1988.
- [2] D. L. Mains, "Boeing Wind Tunnel Report," Purdue University, 1991.
- [3] M. R. Abbassi, W. J. Vaars, N. Hutchins and I. Marusic, "Skin-friction drag reduction in a high-Reynolds-number turbulent boundary layer via real-time control of large-scale structures," *International Journal of Heat and Fluid Flow*, vol. 67, pp. 30-41, 2017.
- [4] W. Saric and K. Reshotko, "Review of flow quality issues in wind tunnel testing," *AIAA Paper 98-2613*, June 1998.
- [5] L. E. Hunt, R. S. Downs III, M. S. Kuester, E. B. White and W. S. Saric, "Flow Quality Measurements in the Klebanoff-Saric Wind Tunnel," *AIAA Paper 2010-4538*, June 2010.
- [6] B. Lindgren and A. V. Johansson, "Evaluation of the flow quality in the MTL wind-tunnel," *KTH/MEK Report No. TR-02/13-SE*, 2002.
- [7] H. Nagib, M. Hites, J. Won and S. Gravante, "Flow Quality Documentation of the National Diagnostic Facility," *AIAA Paper 94-2499*, June 1994.
- [8] M. K. Goodrich and J. Gorham, "Wind tunnels of the western hemisphere," Federal Research Division Library of Congress, Washington, DC, 2008.
- [9] Y. Kohama, R. Kobayashi and H. Ito, "Tohoku University Low-Turbulence Wind Tunnel," *AIAA Paper 92-3913*, July 1992.
- [10] A. Premi, M. Maughmer and C. Brophy, "Flow-Quality Measurements and Qualification of the Pennsylvania State University Low-Speed, Low-Turbulence Wind Tunnel.," *AIAA Paper 2012-1214*, January 2012.
- [11] W. H. Rae Jr. and A. Pope, *Low-Speed Wind Tunnel Testing*, John Wiley & Sons, Inc., 1984.
- [12] S. M. Batill and J. J. Hoffman, "Aerodynamic Design of High Contraction Ratio, Subsonic Wind Tunnel Inlets," *AIAA Paper 84-0416*, January 1984.
- [13] S. R. Norris and S. P. Schneider, "Bruhn 6 Manual - AAE 520: Experimental Aerodynamics," 29 July 1996. [Online]. Available: <https://engineering.purdue.edu/~aae520/bruhn6-manual.pdf>. [Accessed 07 July 2019].
- [14] H. Bruun, N. Nabhani, A. Fardad and H. H. Al-Kayiem, "Velocity component measurements by X hot-wire anemometer," *Measurement Science and Technology*, vol. 1, pp. 1314-1321, 1990.
- [15] H. H. Bruun, *Hot-wire anemometry : principles and signal analysis*, Oxford University Press, 1995.
- [16] TSI Incorporated, *Innovation In Thermal Anemometry*, St. Paul, MN.

- [17] P. Bradshaw and R. C. Pankhurst, "The design of low-speed wind tunnels," *Progress in Aerospace Sciences*, vol. 5, pp. 1-69, 1964.
- [18] W. Saric, S. Takagi and M. Mousseux, "The ASU unsteady wind tunnel and fundamental requirements for freestream turbulence measurements," *AIAA Paper 88-0053*, January 1988.
- [19] S. G. Saddoughi and S. V. Veeravalli, "Hot-wire anemometry behaviour at very high frequencies," *Measurement Science and Technology*, vol. 7, no. 10, p. 1297, 1996.
- [20] T. Morel, "Comprehensive Design of Axisymmetric Wind Tunnel Contractions," *Journal of Fluids Engineering*, vol. 97, no. 2, pp. 225-233, 1975.
- [21] M. S. Istvan and S. Yarusevych, "Effects of free-stream turbulence intensity on transition in a laminar separation bubble formed over an airfoil," *Experiments in Fluids*, vol. 59, no. 3, p. 52, 2018.

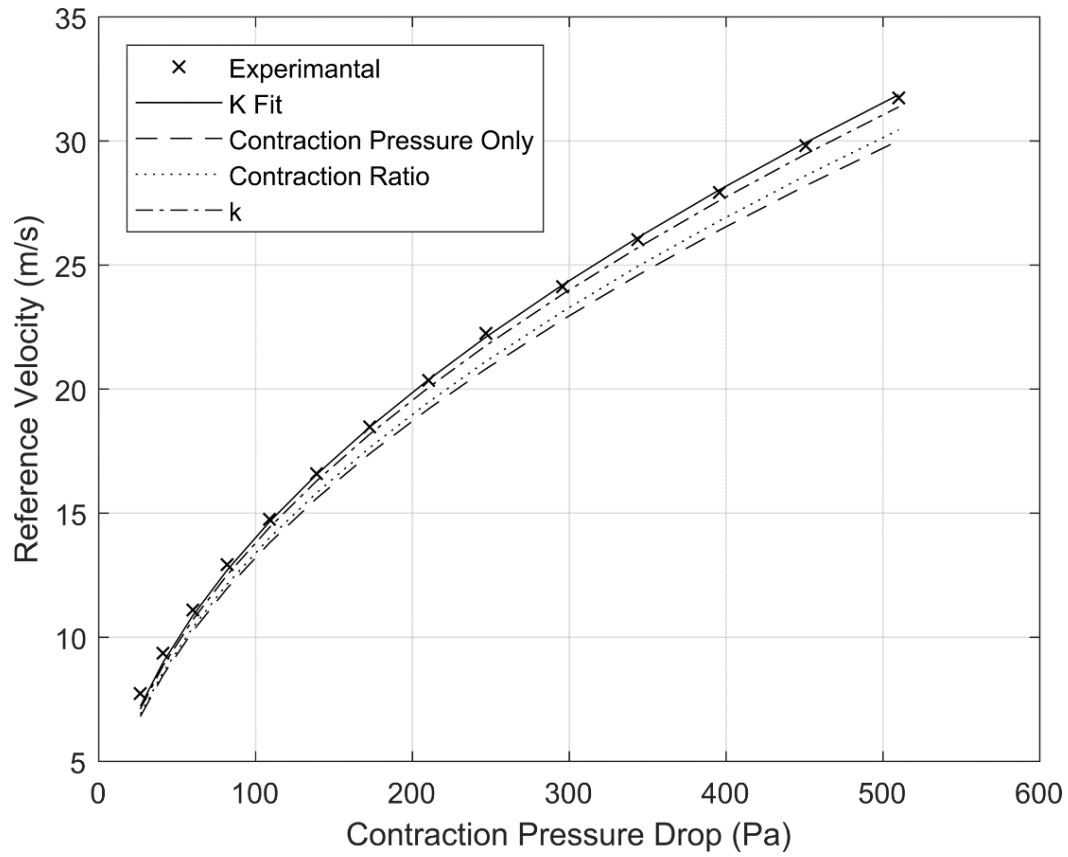
APPENDIX A. TEST SETUP

Figure A.1: Comparison of the effect of including different correction factors on the reference velocity using Equation 3.4

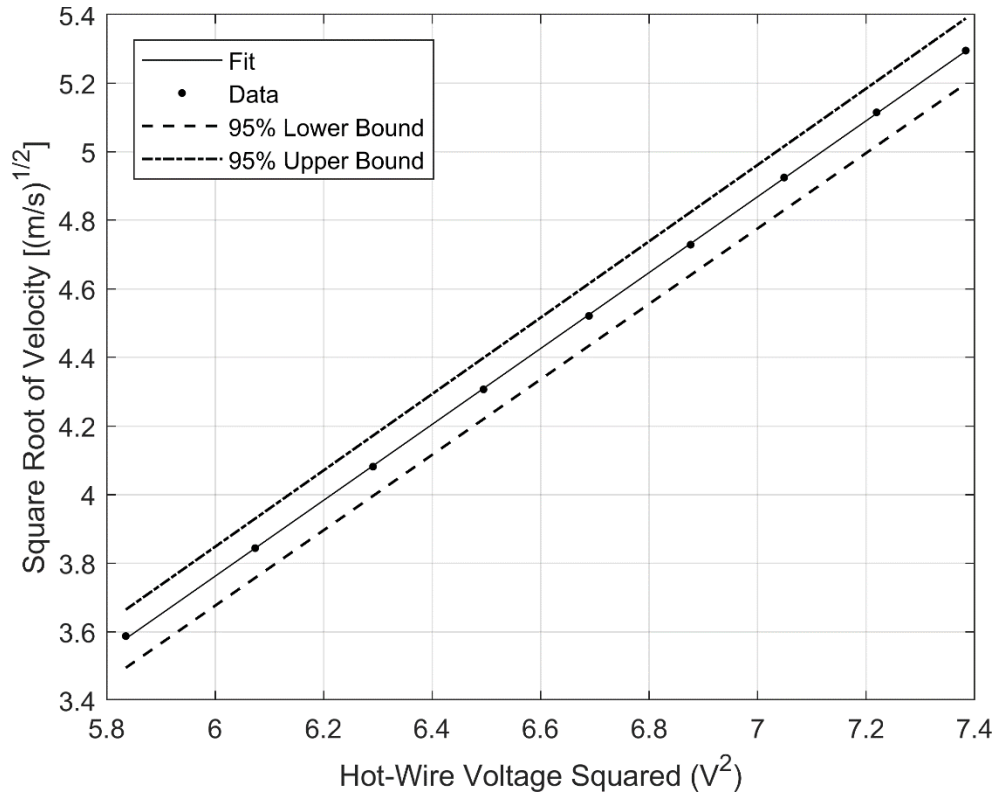


Figure A.2: Hotwire calibration curve showing 95% confidence interval

Table A.1: Cross-section survey measurement locations

Y Measurement Locations (inches)	Z Measurement Locations
-35.0	-21.0
-31.5	-18.0
-27.0	-15.0
-22.5	-12.0
-18.0	-9.0
-13.5	-6.0
-9.0	-3.0
-4.50	0.0
0.0	3.0
4.50	6.0
9.0	9.0
13.5	12.0
18.0	15.0
22.5	18.0
27.0	21.0
31.5	
35.0	

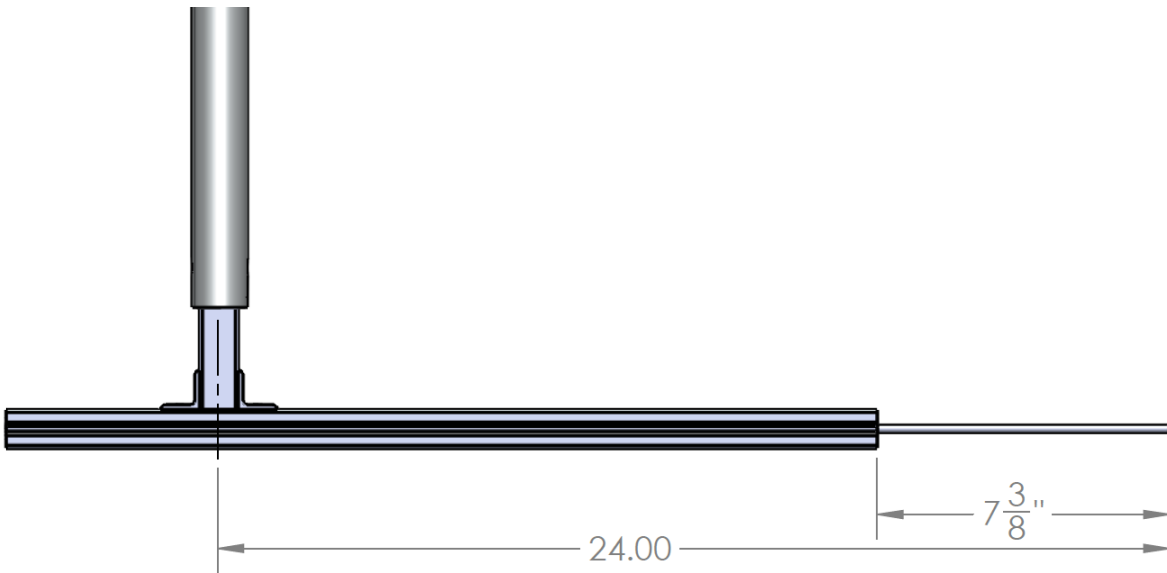


Figure A.3: Probe holding configuration for measurement locations where $Y \leq -13.5''$ or $Y \geq 13.5''$

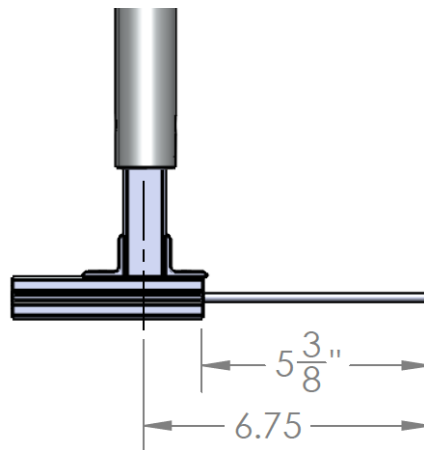


Figure A.4: Probe holding configuration for measurement locations where $-18.0'' \leq Y \leq 18.0''$

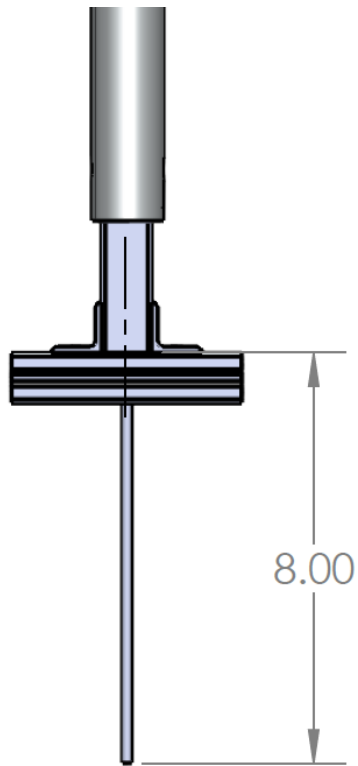


Figure A.5: Probe holding configuration for boundary layer measurements

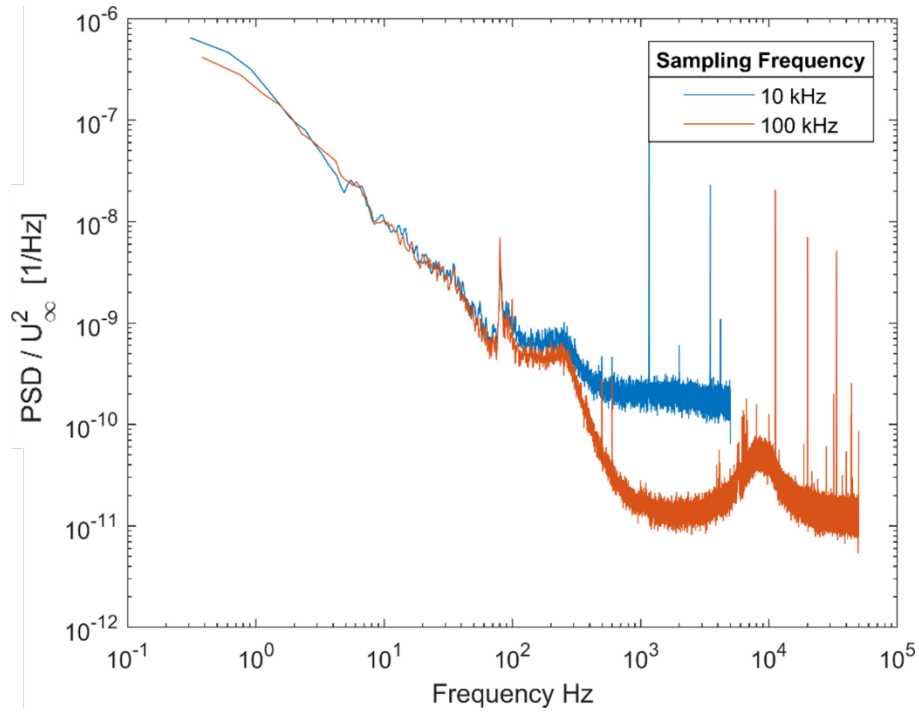
APPENDIX B. SUPPLEMENTARY FLOW QUALITY DATA

Figure B.1: Preliminary test data of tunnel running at 20 m/s for 1 minute

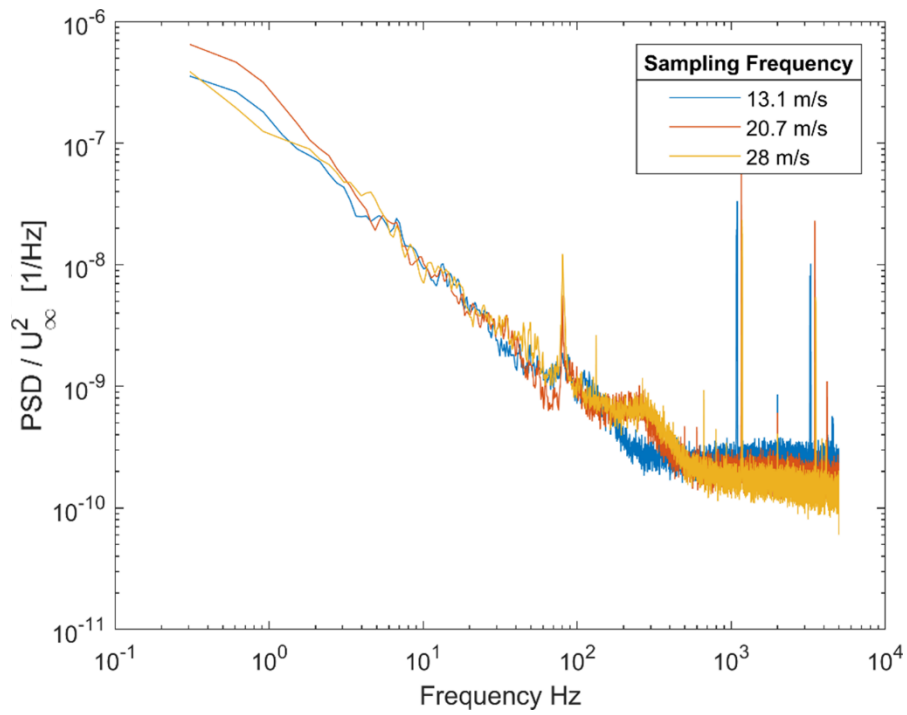


Figure B.2: Preliminary test data of tunnel running for 1 minute for a sampling rate of 10 kHz

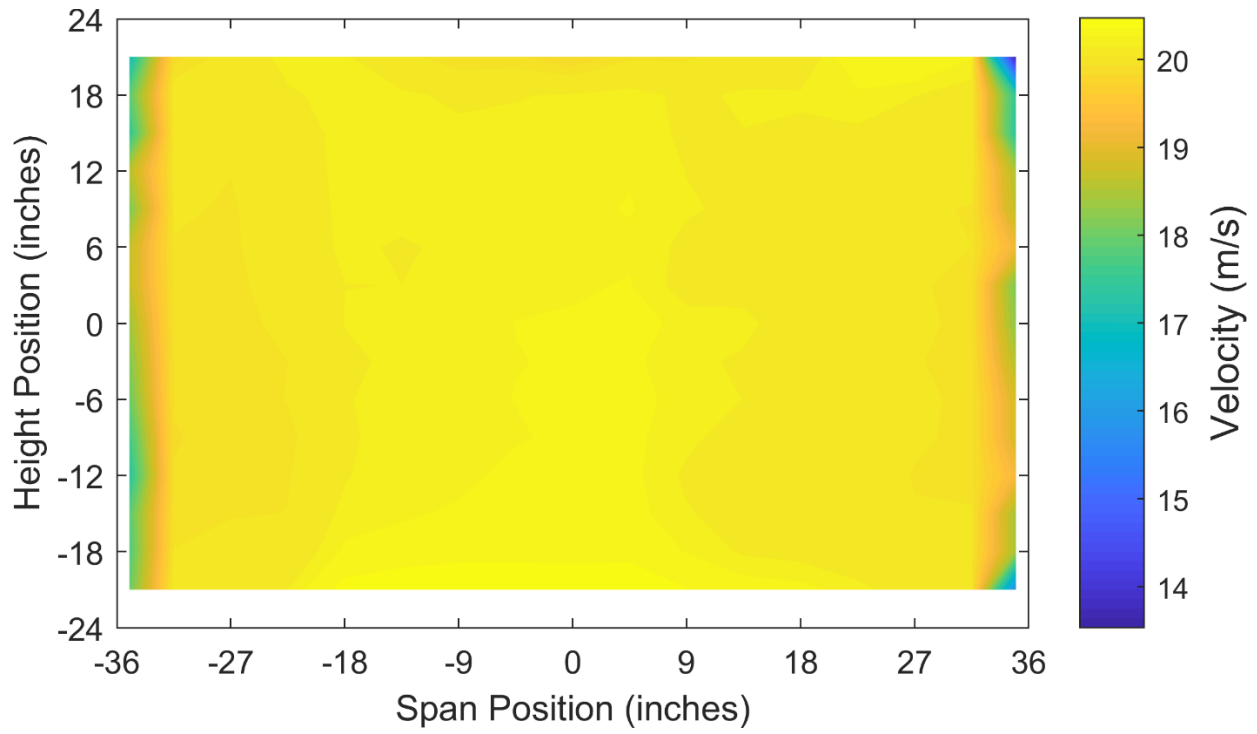


Figure B.3: Cross-section velocity contour – complete test section

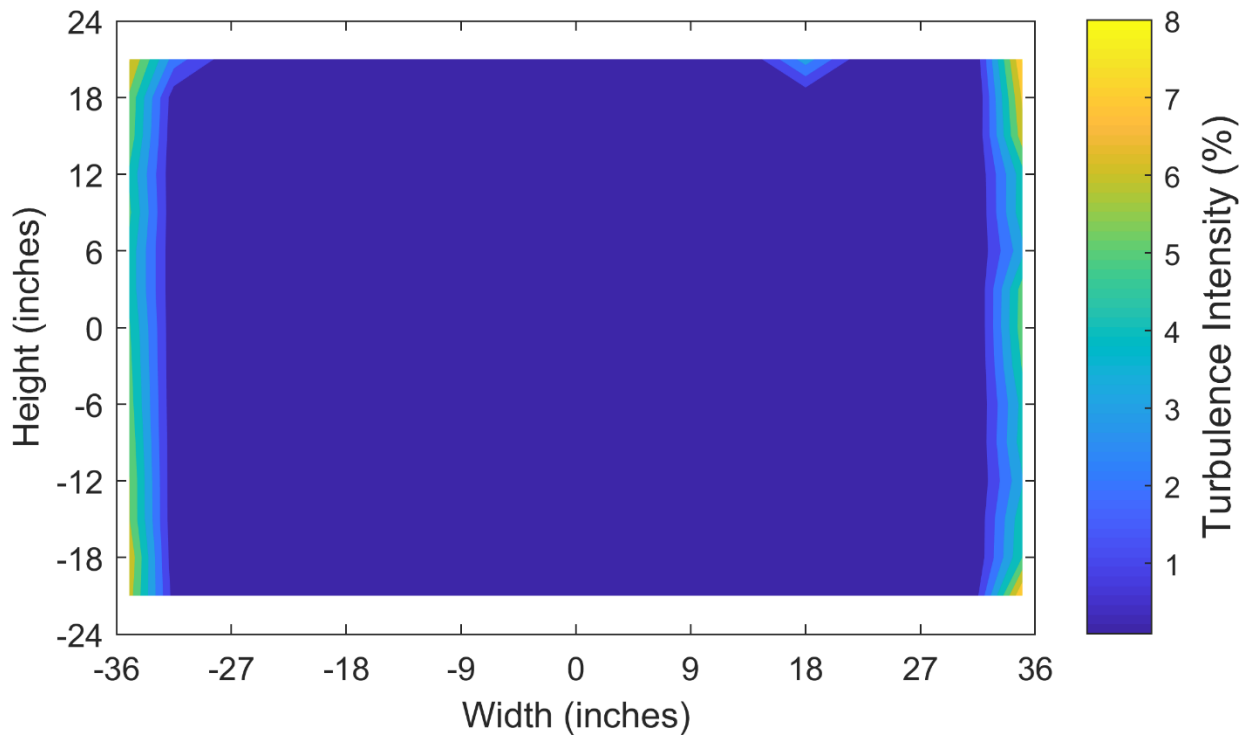


Figure B.4: Cross-section turbulence intensity contour – complete test section

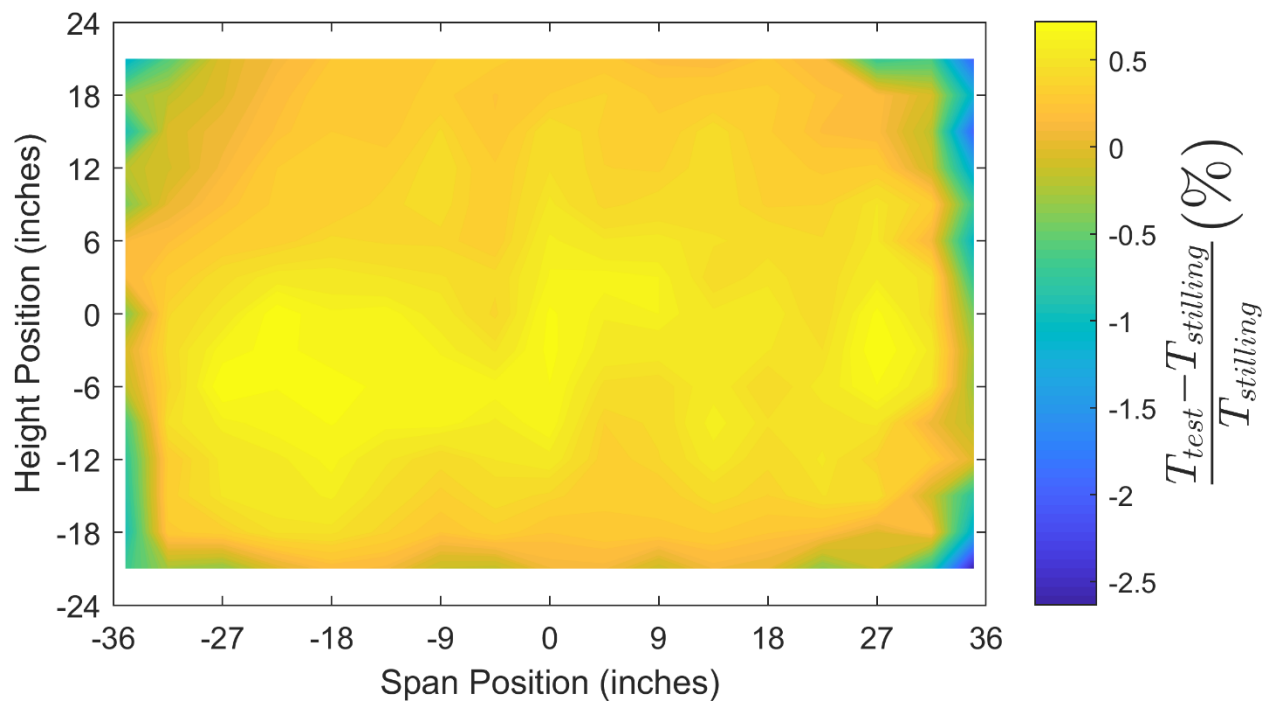


Figure B.5: Cross-section temperature contour – complete test section

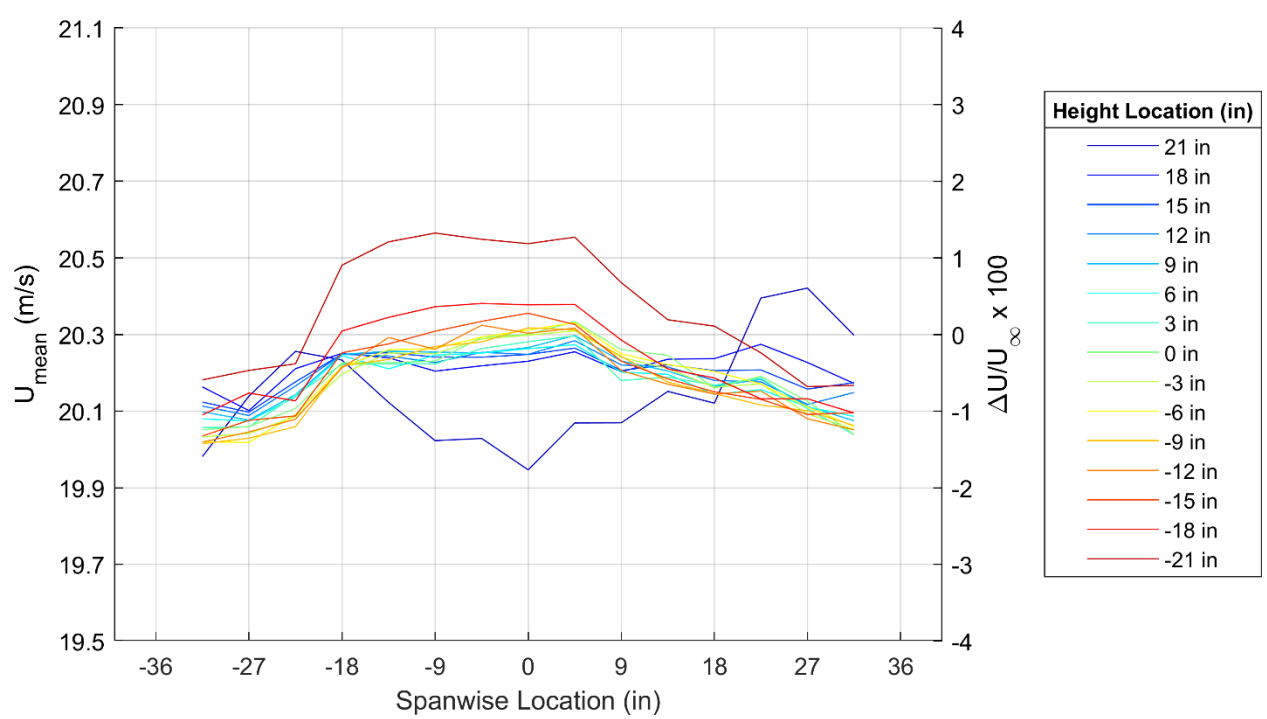


Figure B.6: Velocity profiles for varying height locations over the cross-section core region

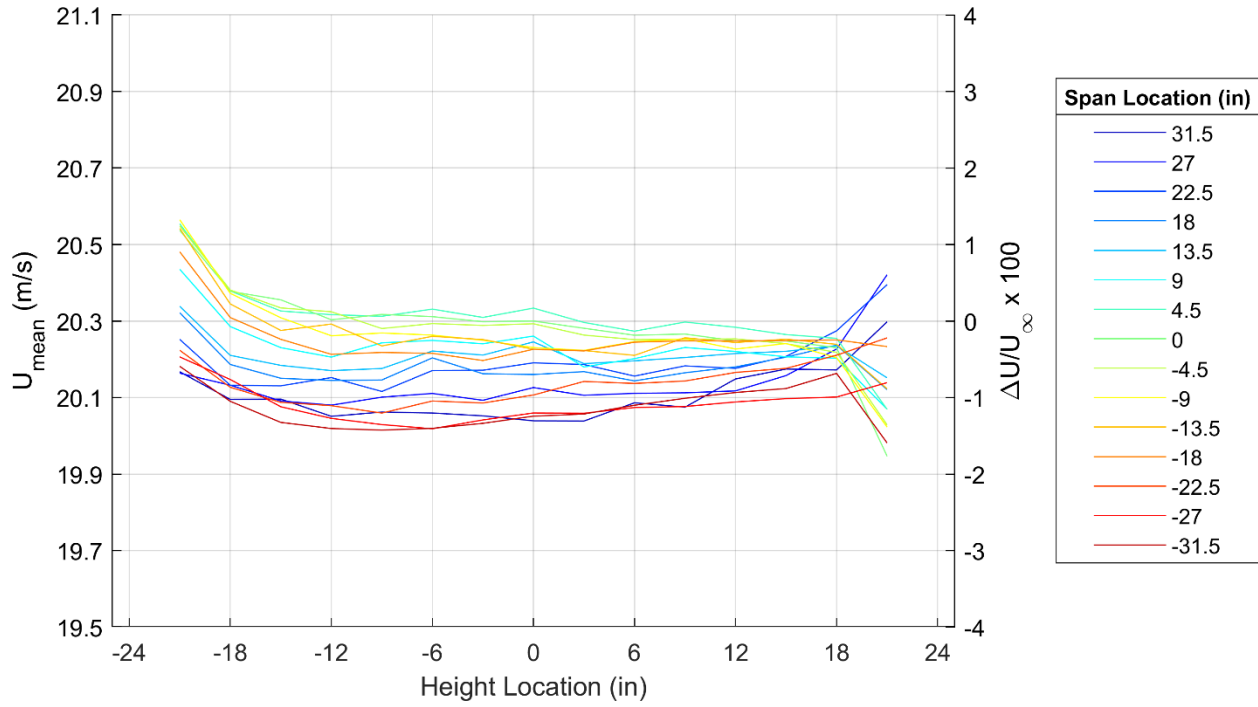


Figure B.7: Velocity profiles for varying spanwise locations over the cross-section core region

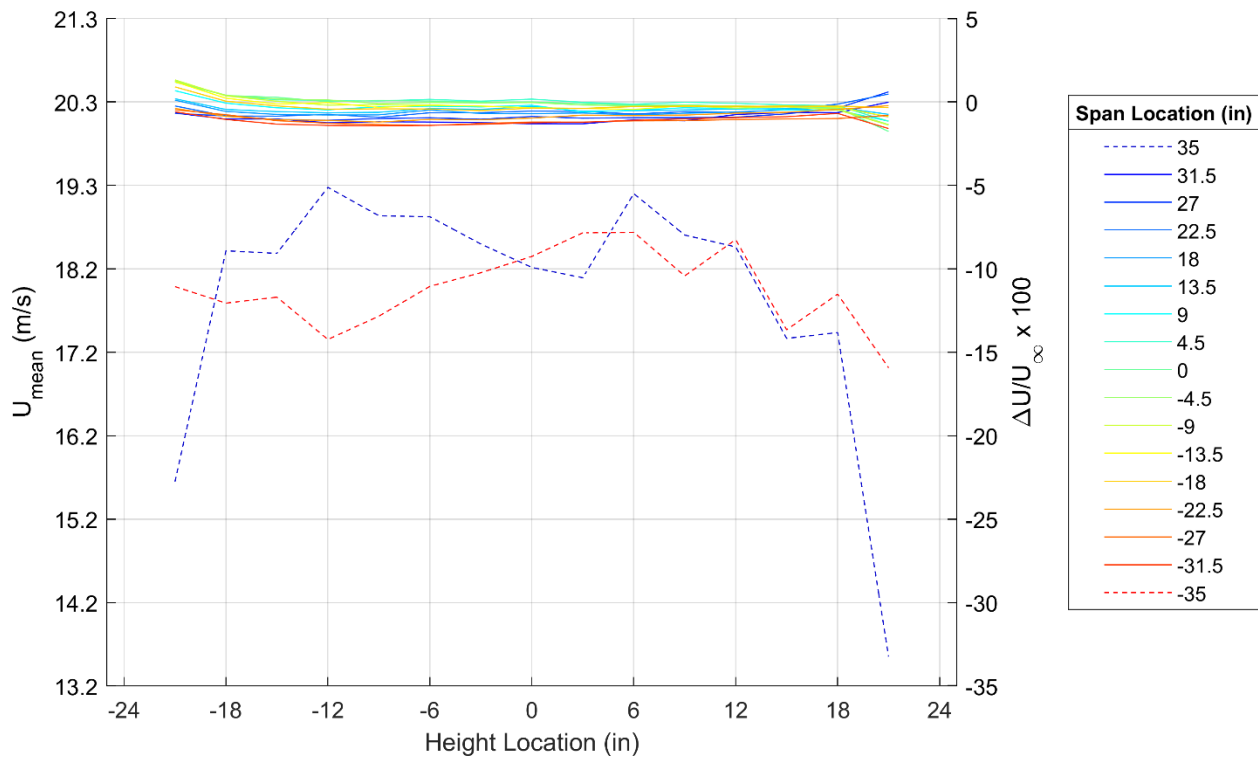


Figure B.8: Velocity profiles for varying height locations over the entire cross-section

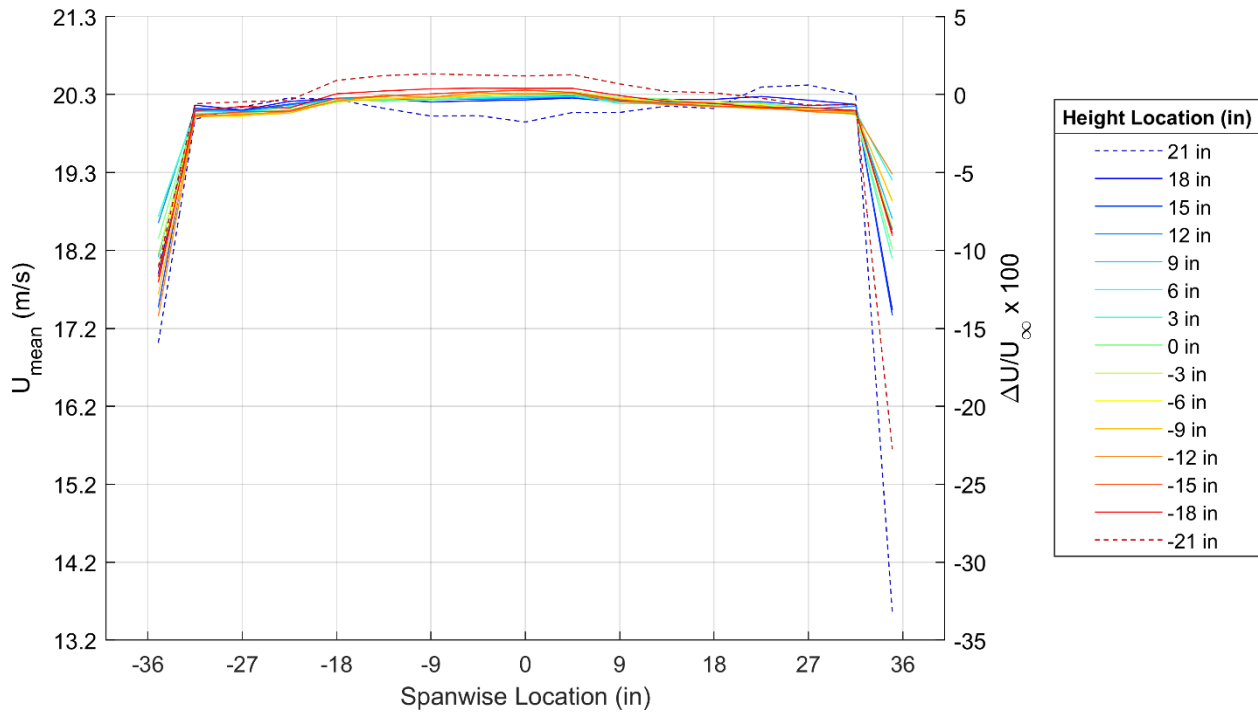


Figure B.9: Velocity profiles for varying spanwise locations over the entire cross-section

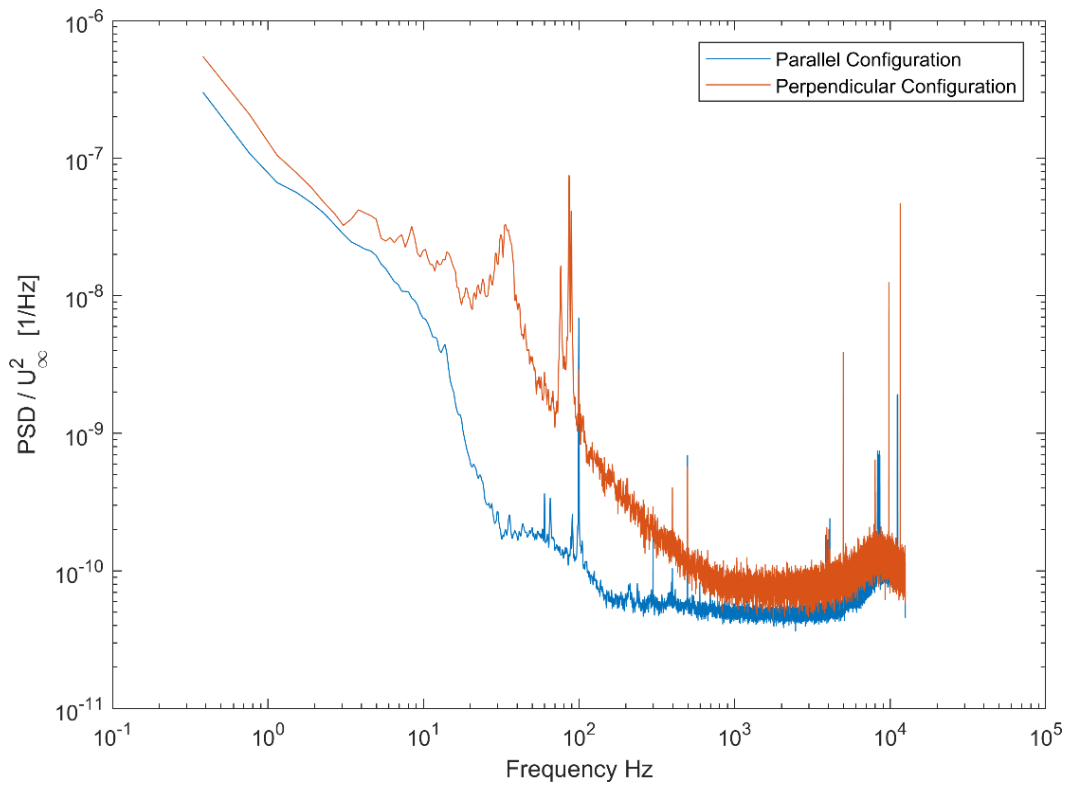


Figure B.10: Comparison of the PSDs for two different probe configurations. Data was measured at the center of the test section for $U_{\infty} = 20$ m/s

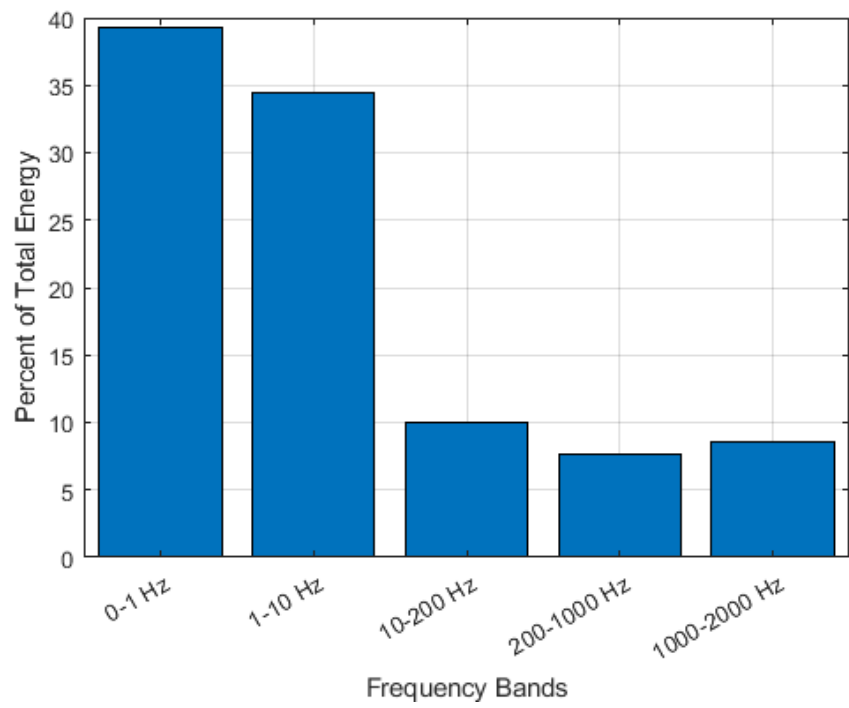


Figure B. 11: Percent of turbulent energy lying between different frequency bands. Data was measured at the center of the test section for $U_{\infty} = 20$ m/s

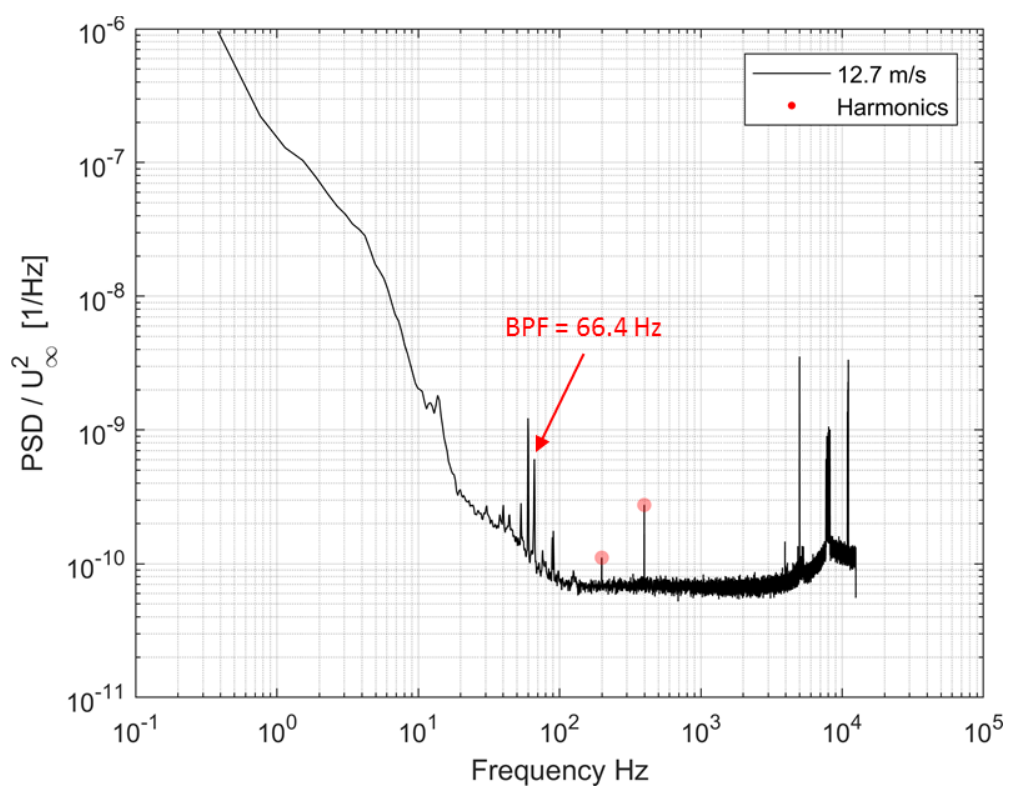


Figure B.12: Power spectrum at a tunnel motor frequency of 20 Hz

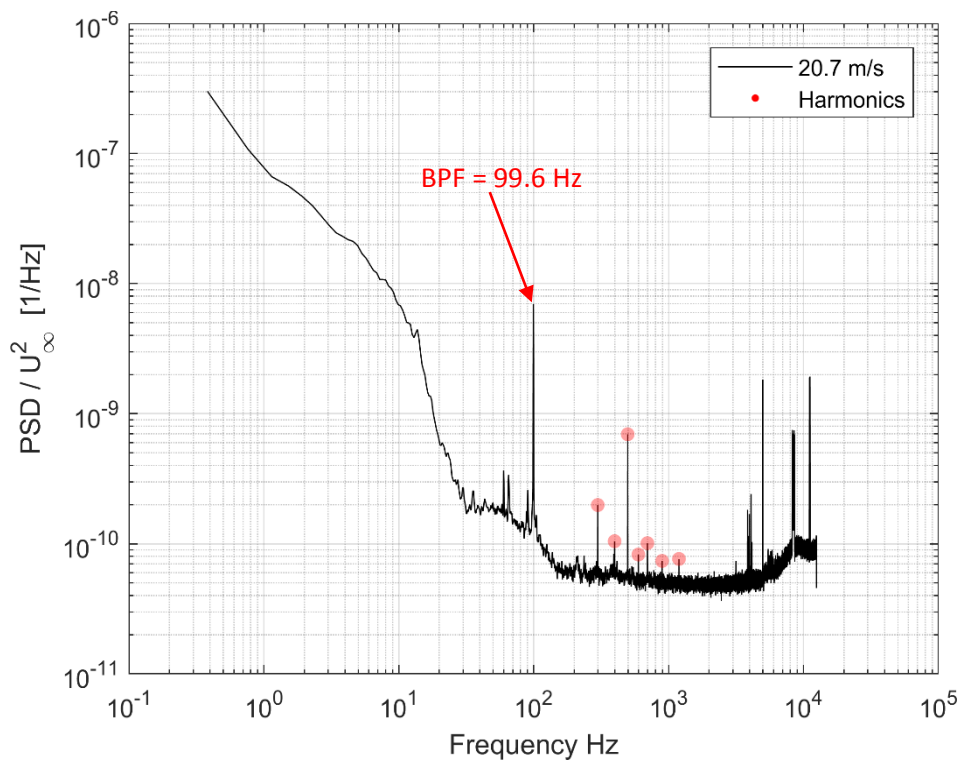


Figure B.13: Power spectrum at a tunnel motor frequency of 30 Hz

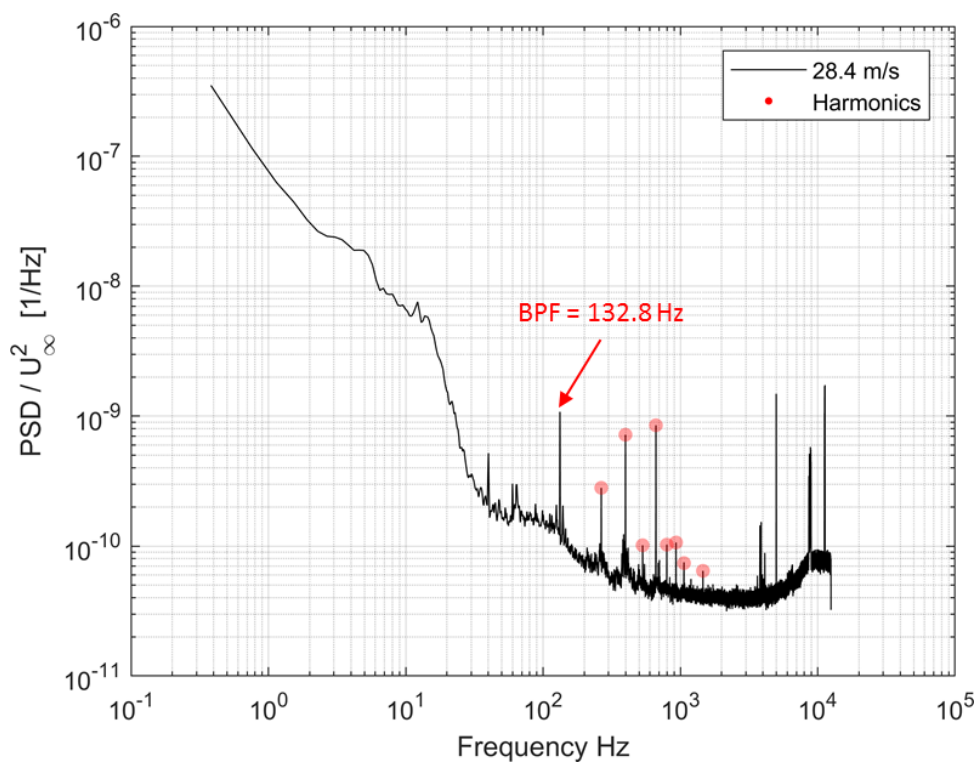


Figure B.14: Power spectrum at a tunnel motor frequency of 40 Hz

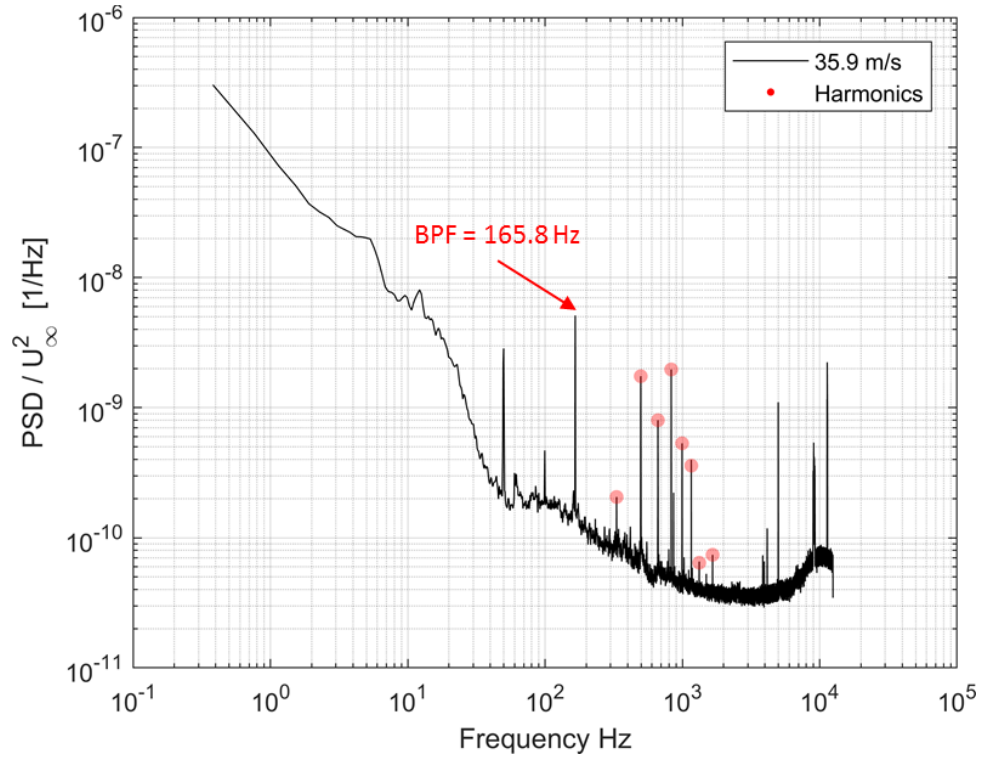


Figure B.15: Power spectrum at a tunnel motor frequency of 50 Hz

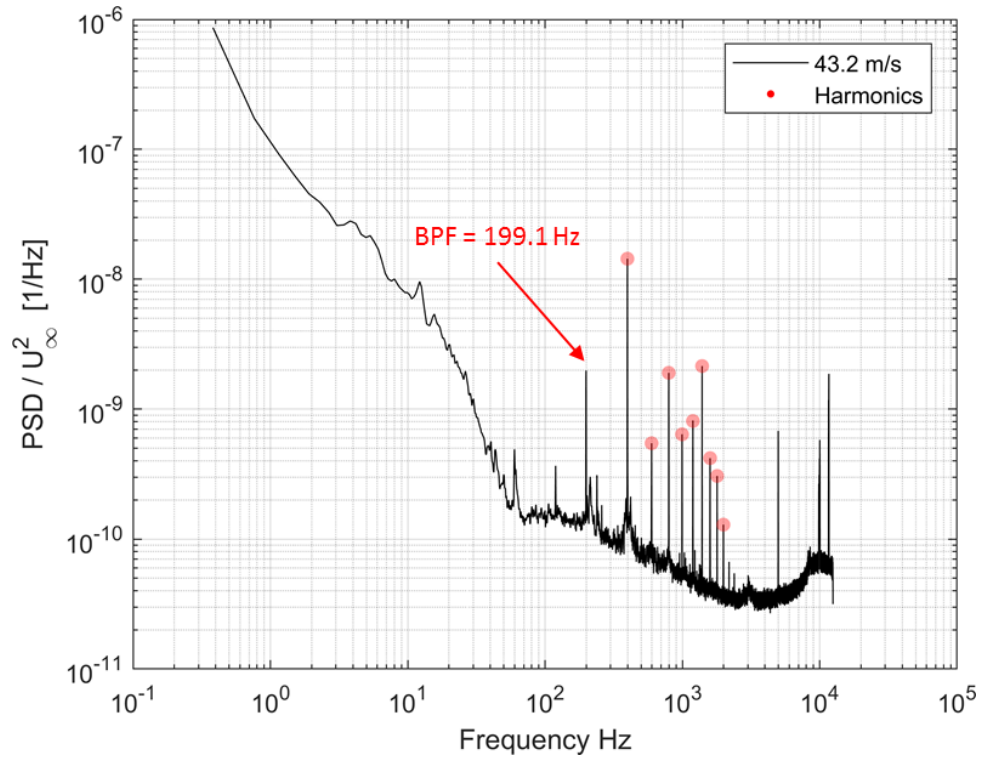


Figure B.16: Power spectrum at a tunnel motor frequency of 60 Hz

APPENDIX C. BOEING SUBSONIC WIND TUNNEL MANUAL

The following contains the Boeing Subsonic Wind Tunnel manual, which was written to be a standalone document and contains information from various different sources

TABLE OF CONTENTS

Figures	iii
Introduction.....	1
Wind Tunnel Performance.....	2
Operating the Wind Tunnel	4
Startup.....	4
Shutdown	4
Main Tunnel Components.....	5
Safety Exit from Tunnel.....	5
Stilling Section – Screens and Honeycomb	5
Contraction.....	7
First Diffuser.....	9
Breather.....	9
Turning Vanes.....	10
Wind Tunnel Fan	10
General Maintenance	11
Model Mounting and Installation.....	13
Strut Installation.....	13
AOA Control Arm Installation	14
Four Component Force Balance	15
Platform/Parallelogram Balance Overview	15
LabVIEW Implementation.....	17
Calibration.....	17
Force Transducers.....	19
Instrumentation	19
LabVIEW Implementation.....	19
Location and Installation.....	19
Temperature Measurements.....	22
Instrumentation	22
LabVIEW Implementation.....	22
Location and Installation.....	22
Air Velocity Transducer	25
Instrumentation	25
Transducer Configuration	25
LabVIEW Implementation.....	25

Location and Installation.....	25
Contraction Pressure Drop.....	29
Instrumentation	29
LabVIEW Implementation.....	29
Location and Installation.....	29
Two-Axis Traverse	33
Instrumentation	33
Probe Mounting	34
Running the Traverse.....	35
LabVIEW Implementation.....	37
Smoke Wand.....	43
Instrumentation	43
Location and Installation.....	43
Instruction Manual	43
Selected Part Drawings	63

FIGURES

Figure 1: Boeing Subsonic Wind Tunnel overview	1
Figure 2: Wind tunnel speed (m/s).....	2
Figure 3: Wind tunnel speed (mph)	3
Figure 4: Variable frequency drive	4
Figure 5: Wind tunnel speed controller.....	4
Figure 6: Safety Exit Location	5
Figure 7: Honeycomb and screen configuration	6
Figure 8: Contraction dimensions	7
Figure 9: Contraction contour profile	7
Figure 10: Contraction wall construction.....	8
Figure 11: Diffuser.....	9
Figure 12: Top view of corner turning-vanes showing flow direction	10
Figure 13: Wind tunnel motor power curve.....	10
Figure 14: Fan motor lubrication instructions.....	11
Figure 15: Tunnel Fan Plate.....	12
Figure 16: Tunnel Fan Motor Plate.....	12
Figure 17: Latched hole cover position.....	13
Figure 18: Unlatched hole cover position	13
Figure 19: Wind-tunnel hole cover design.....	13
Figure 20: Mount strut installation locating method.....	14
Figure 21: AOA control arm installation	14
Figure 22: Platform balance setup	15
Figure 23: Free body diagram for lift, drag and pitch.....	16
Figure 24: Free body diagram for roll (Section A-A).....	16
Figure 25: Free body diagram LabVIEW implementation	17
Figure 26: Force transducer virtual channel block.....	19
Figure 27: Temperature probe virtual channel block.....	22
Figure 28: Temperature probe installation.....	22
Figure 29: Temperature probe DAQ wiring	23
Figure 30: Analog voltage virtual channel block.....	25
Figure 31: Air velocity transducer protection	25
Figure 32: Hot-wire anemometer rubber sheath	26
Figure 33: Air velocity transducer probe installation	26
Figure 34: Analog voltage virtual channel block.....	29
Figure 35: Contraction pressure tap locations.....	29
Figure 36: Pressure tap installation.....	30
Figure 37: Pressure transducer connection	30
Figure 38: Two-axis traverse layout	33
Figure 39: Traverse probe mounting configuration	34
Figure 40: Traverse lubrication points	35
Figure 41: Traverse movement LabVIEW Interface	35
Figure 42: Hole cover lifting points.....	36
Figure 43: LabVIEW program - manually inputted traverse movement	37
Figure 44: Traverse configuration setup	37
Figure 45: Traverse movement configuration.....	38
Figure 46: AEROLAB smoke generator.....	43

INTRODUCTION

The Boeing Subsonic Wind Tunnel shown in Figure 1, located in the Aerospace Sciences Laboratory (ASL) at Purdue University, is a closed-return, closed test-section wind tunnel with a 4 ft. x 6 ft. x 8 ft.-long test section. With an empty test section, the wind tunnel is able to reach speeds of 96 mph (43 m/s).

The tunnel is equipped with the following instrumentation:

- Four component force balance
 - Lift, drag, pitch, roll
 - Computer-controlled angle of attack
- Computer-driven two-axis traverse
 - 80 in horizontal travel x 60 in vertical travel
- Pitot probes, seven hole probe, air velocity transducer, temperature transducer
- Smoke wand
- LabVIEW data acquisition system

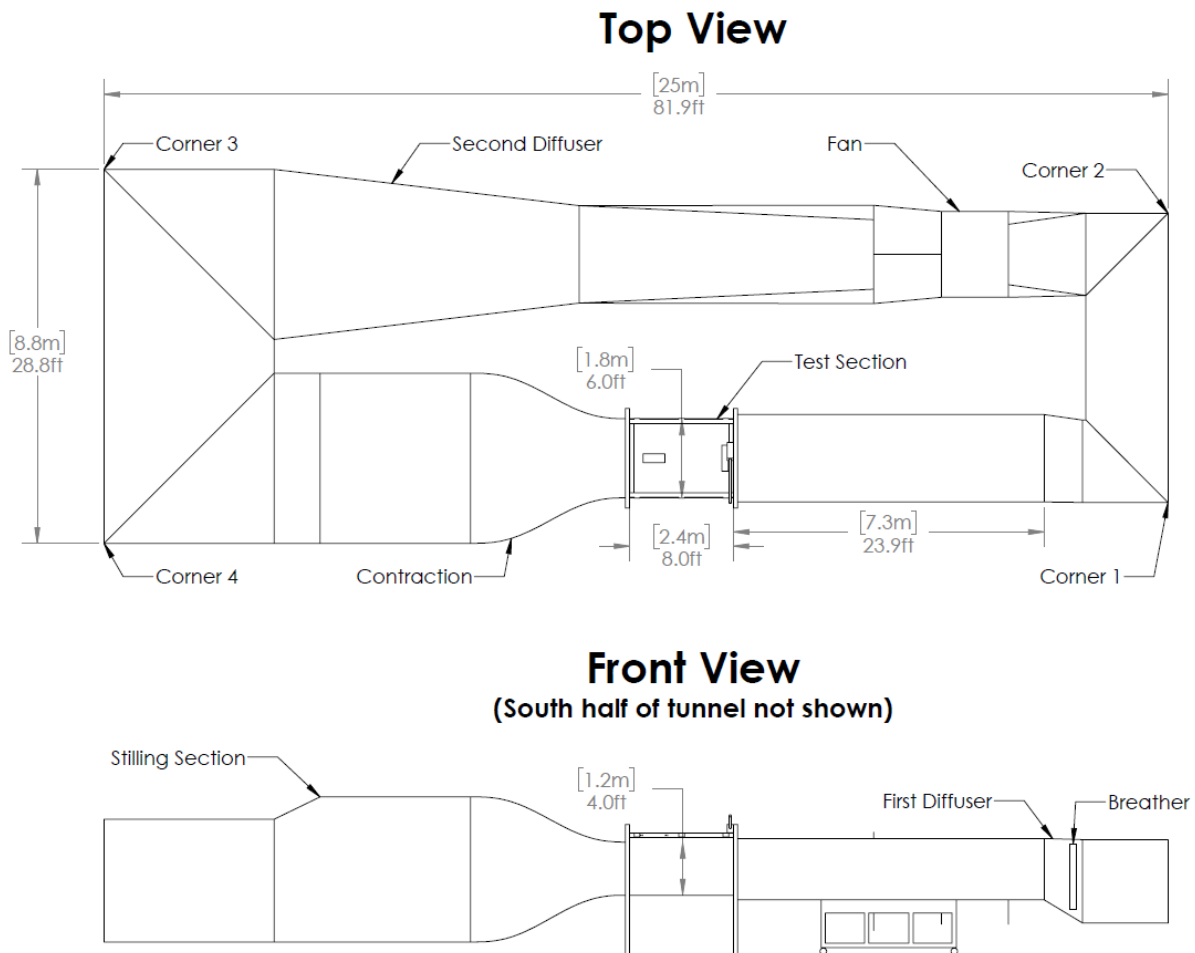


Figure 1: Boeing Subsonic Wind Tunnel overview

WIND TUNNEL PERFORMANCE

Currently the tunnel is able to reach speeds of up to 96 mph (43 m/s). A calibration plot of test section flow speed vs. motor frequency is shown below, and can be used as a baseline for setting the flow speed.

The speed of the flow in the test section (u_2) can be calculated using the equation below, where $(P_1 - P_2)$ is equal to the pressure drop across the contraction and $K = 1.127$ is a calibration constant. For $K = 1.127$ metric units must be used.

$$K(P_1 - P_2) = \frac{1}{2}\rho u_2^2$$

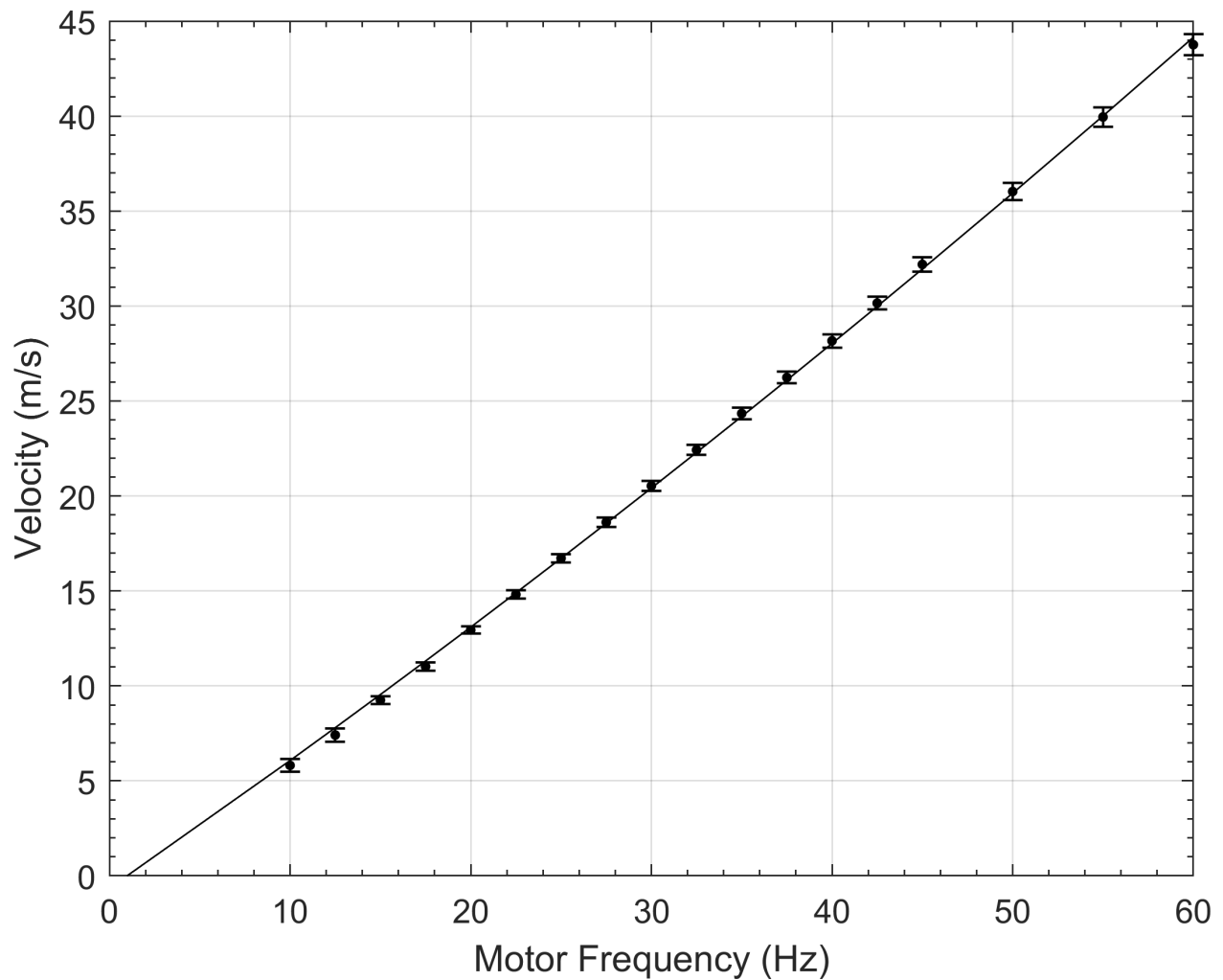


Figure 2: Wind tunnel speed (m/s)

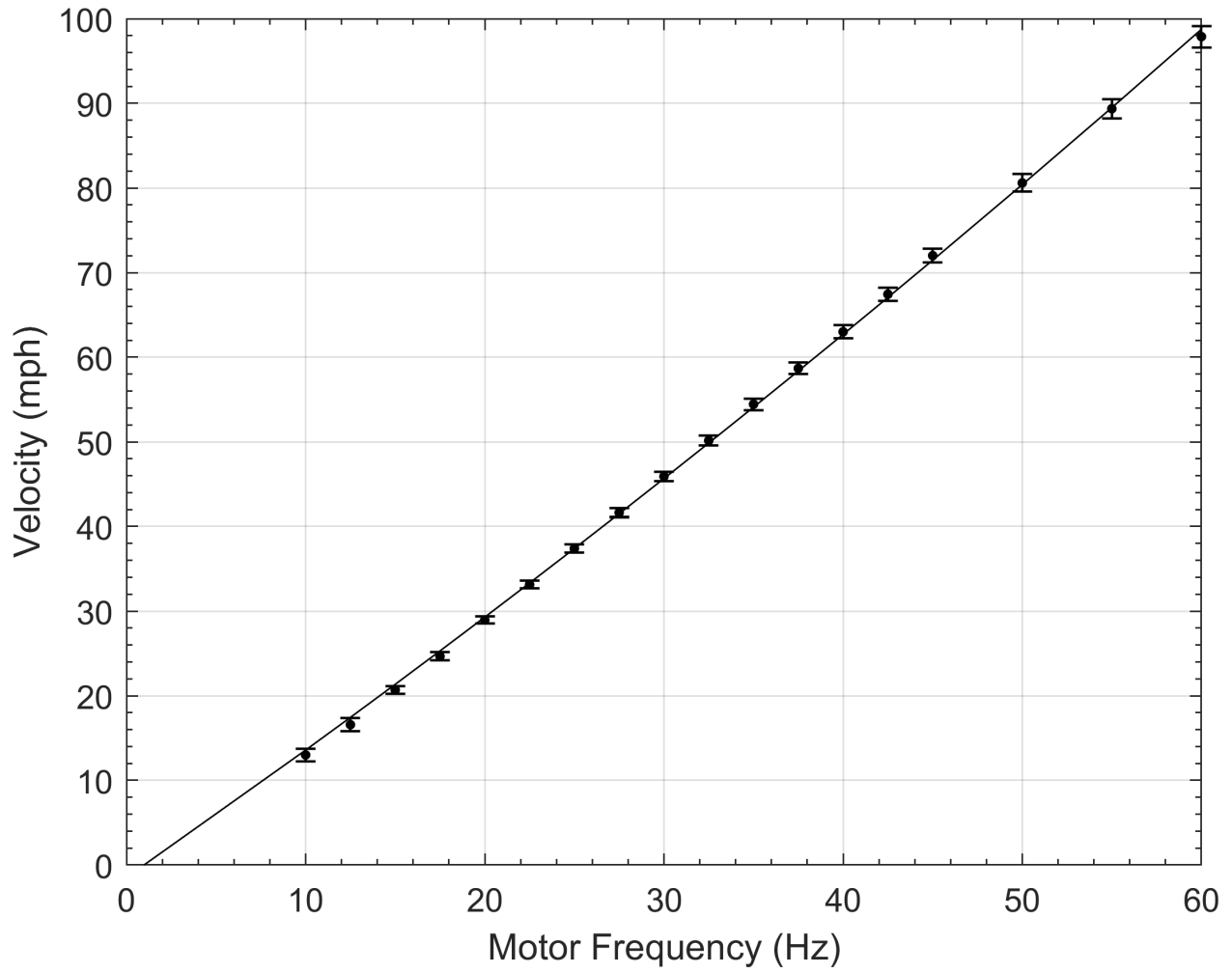


Figure 3: Wind tunnel speed (mph)

OPERATING THE WIND TUNNEL

Startup

At the variable frequency drive (located on the SW corner of the wind tunnel on the concrete platform):

1. Turn the handle clockwise 90 degrees to turn on (cooling fan should turn on)



Figure 4: Variable frequency drive

CAUTION Before turning on the tunnel:

2. Make sure the circular hole cover is tightly secured
3. Make sure that all tools have been removed from the tunnel and that there are no loose items (nuts, bolts, etc.) in the tunnel

At the controller (located across from the test section)

4. Pull out emergency button
5. Set frequency to 10 Hz using the up arrow
6. Press the green hand button (tunnel will start)
7. Set tunnel speed using arrows (25 Hz max for teaching labs)



Figure 5: Wind tunnel speed controller

Shutdown

At the controller

1. Lower frequency to zero
2. Push red OFF button
3. Push emergency button in

At the variable frequency drive

4. Rotate handle 90 degrees counter clockwise to OFF position

MAIN TUNNEL COMPONENTS

Safety Exit from Tunnel

In the unlikely situation that a person is in the test section of the tunnel and the main door cannot be opened, a safety exit door is available at the bottom of the contraction section, near the stilling section of the tunnel.

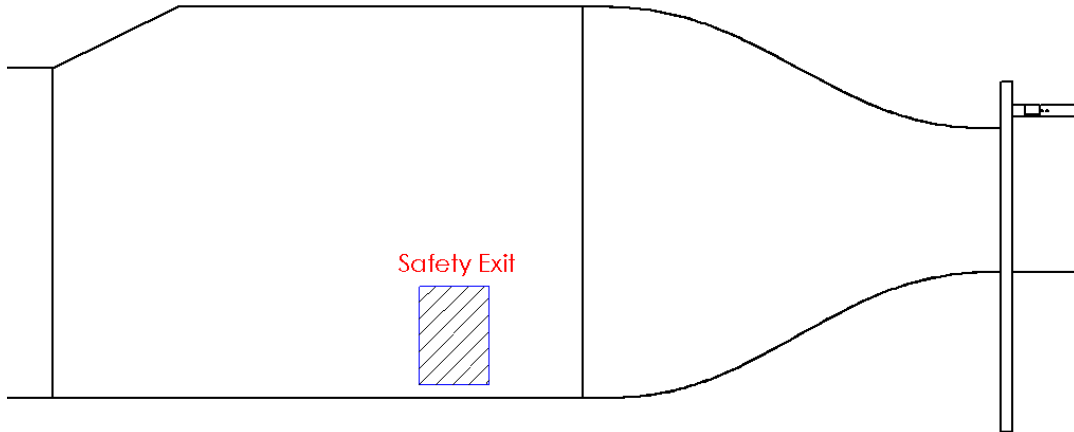


Figure 6: Safety Exit Location

The safety exit door is equipped with a Southco rotatory latch to keep the door closed. The door can be opened from the inside of the tunnel using a push button actuator, which is flush mounted to the tunnel wall next to the safety exit door. The latch can also be opened from the outside of the tunnel by pulling up on the latch cable.

When closing the safety exit door, insure that the latch is fully engaged by lightly pulling on the door. The latch does feature a two-stage engagement to provide latching if the door is not fully closed, but the tunnel should only be run if the door is fully closed.

Stilling Section – Screens and Honeycomb

The stilling section of the wind tunnel is designed to reduce the size of the turbulent fluctuations and straighten and increase the uniformity of the flow entering the test-section. The honeycomb is used to reduce any large swirl components of the upstream flow. The screens reduce turbulence and establish a uniform test-section profile [1]. This part of the tunnel is divided into the seven sections as shown below, where the first two stations are not part of the stilling section, but are part of the diffuser used to increase the tunnel cross section size to the size of the contraction inlet. The dotted lines represent screens made from aluminum wire cloth with the properties as follows in Table 1. The honeycomb wall at Station 3 is 4 inches thick and made of polycarbonate, with a 1/2-inch cell diameter. This honeycomb was supplied by Plascore and has a total density of 3lbs/ft³.

Table 1: Stilling Section Screen Sizes

Mesh Size (wires/inch)	Wire Diameter (in)	Porosity
8M	0.035	51.8%
16M	0.011	67.9%
28M	0.0075	62.4%
43M	0.005	61.6%
50M	0.0045	60.1%

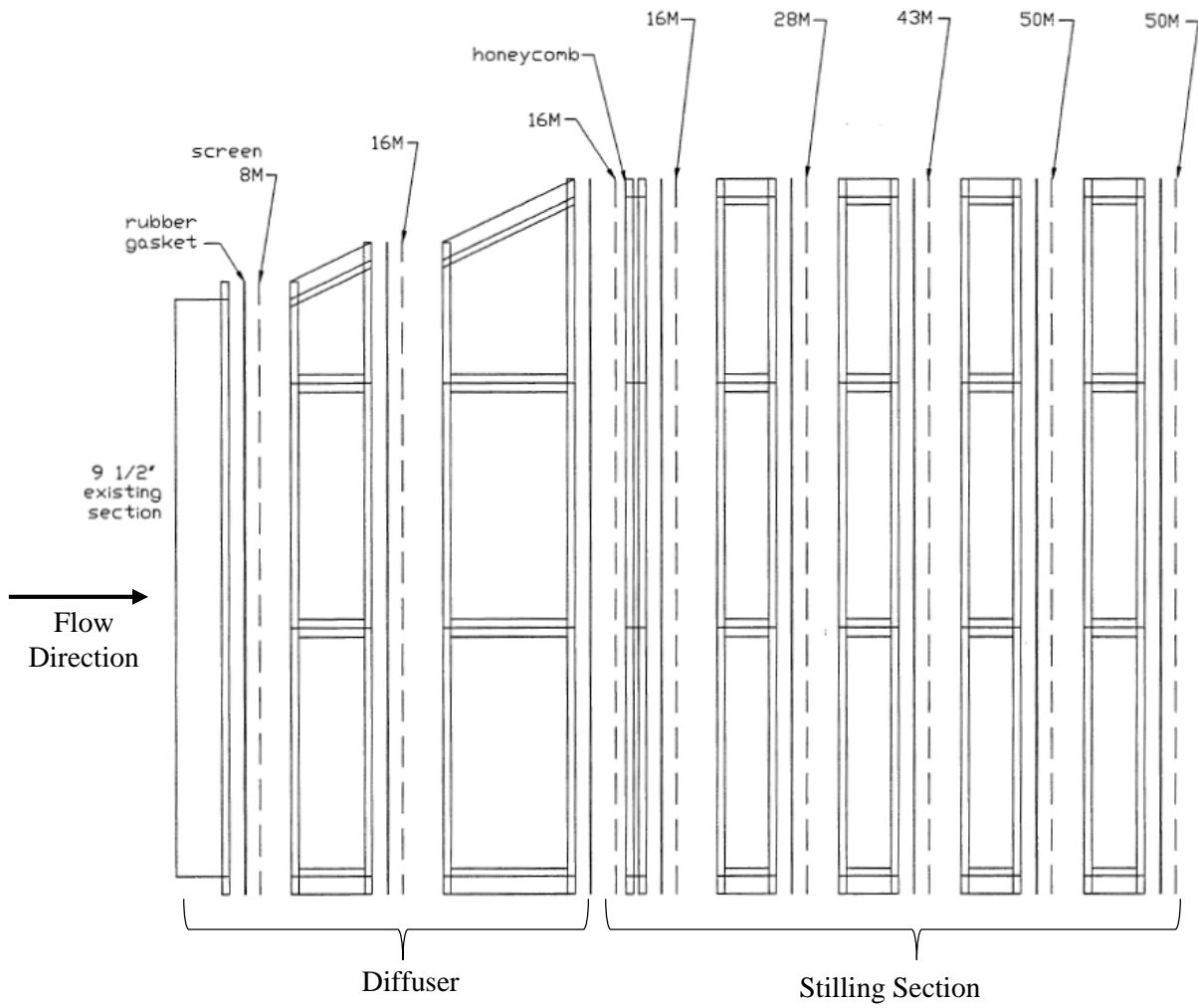


Figure 7: Honeycomb and screen configuration

Contraction

The contraction section of the tunnel is used to increase the air speed entering the test section and has a total contraction ratio (A_{in}/A_{out}) of 5.96:1. It is constructed of four individual fiberglass sides, which are fastened together at the corners.

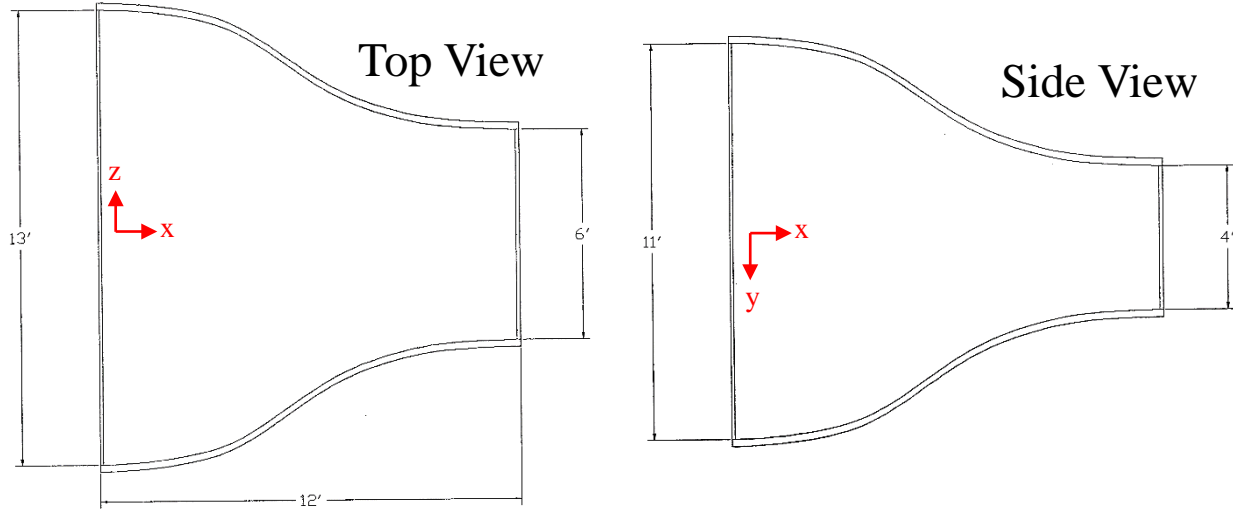


Figure 8: Contraction dimensions

The shape of the contraction contour follows a cubic fit with $X = 0.45$ [2]

$$H(x) = \begin{cases} (H_{in} - H_{out}) \left[1 - \frac{1}{X^2} \left(\frac{x}{L} \right)^3 \right] + H_{out} & \rightarrow \frac{x}{L} < X \\ (H_{in} - H_{out}) \left[\frac{1}{(1-X)^2} \left(1 - \frac{x}{L} \right)^3 \right] + H_{out} & \rightarrow \frac{x}{L} > X \end{cases}$$

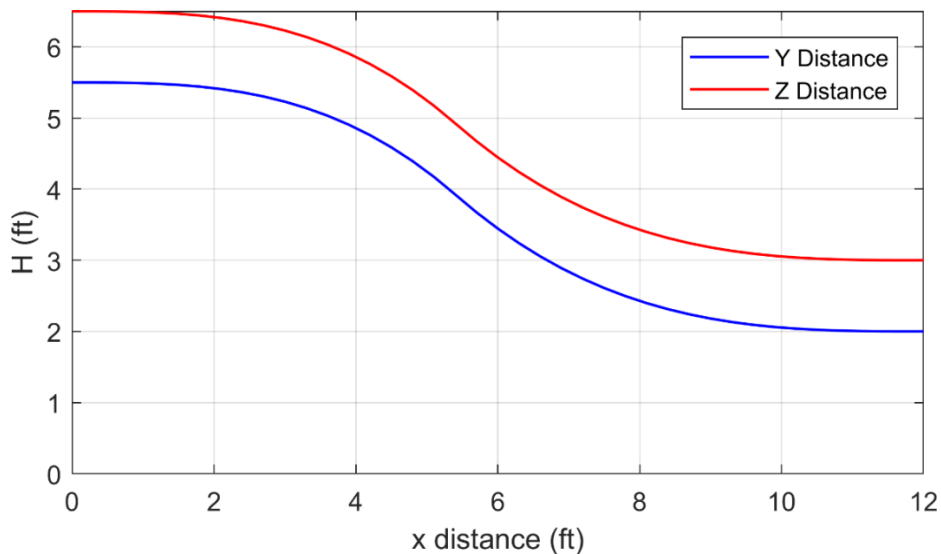


Figure 9: Contraction contour profile

The walls of the contraction are made of a three-layer fiberglass laminate construction as shown below. The middle layer of the wall contains a Divinycell H-60 foam core and is sandwiched between six layers of cloth, which are 60% resin.

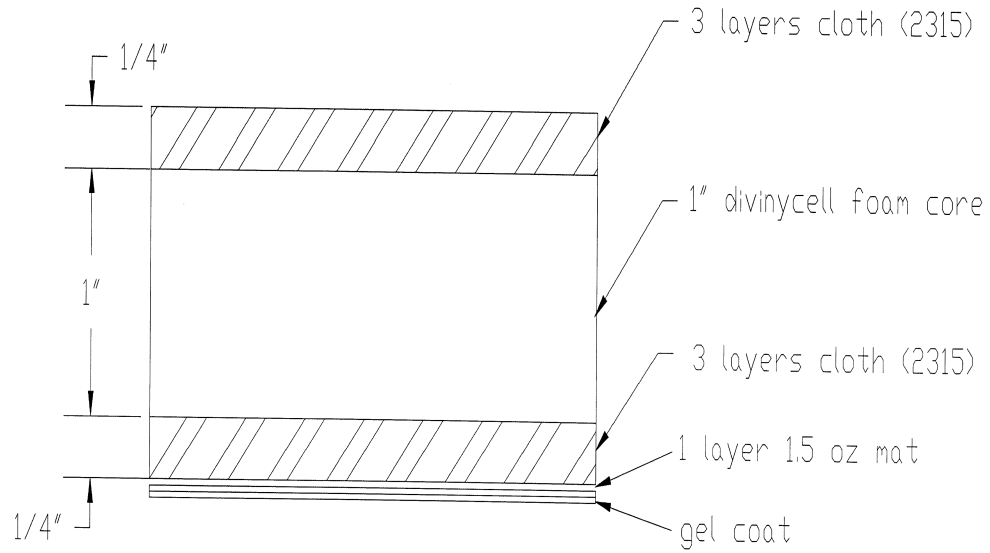


Figure 10: Contraction wall construction

First Diffuser

The first diffuser is situated between the downstream end of the test-section and the first corner. It contains five angled plates to prevent the flow from separating, shown below.

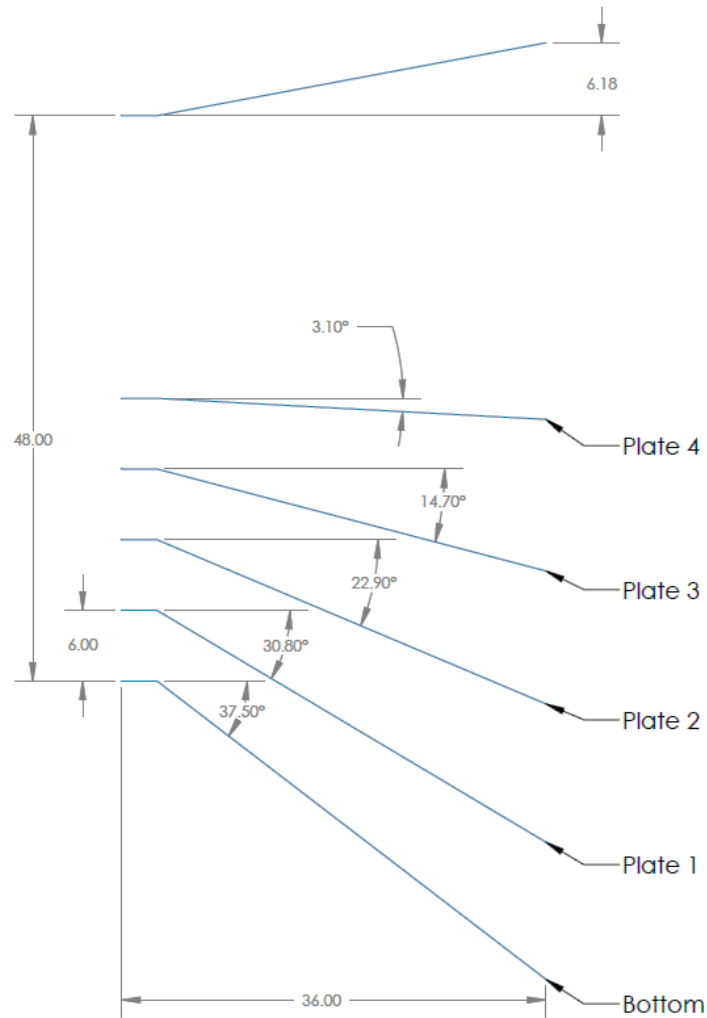
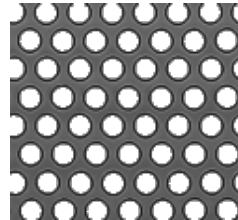


Figure 11: Diffuser

Breather

The downstream end of the diffuser contains a breather section, which is constructed from a perforated aluminum sheet with the following characteristics:

- 3/16" hole diameter
- 51% open area
- Staggered arrangement
- 1/4" center-to-center spacing



The breather section allows air into the tunnel. This keeps the static pressure within the tunnel close to atmospheric pressure and also helps to control the temperature in the tunnel.

Turning Vanes

In Corners 1, 2, and 3 of the wind tunnel, there are turning vanes that span the entire height of the tunnel. These turning vanes are used to minimize pressure losses as the air turns the corner and to mitigate separation of the boundary layer through the turn. The turning vanes in Corners 1 and 3 both contain support bars that link the individual turning vanes, reducing any fluttering of the turning vanes.

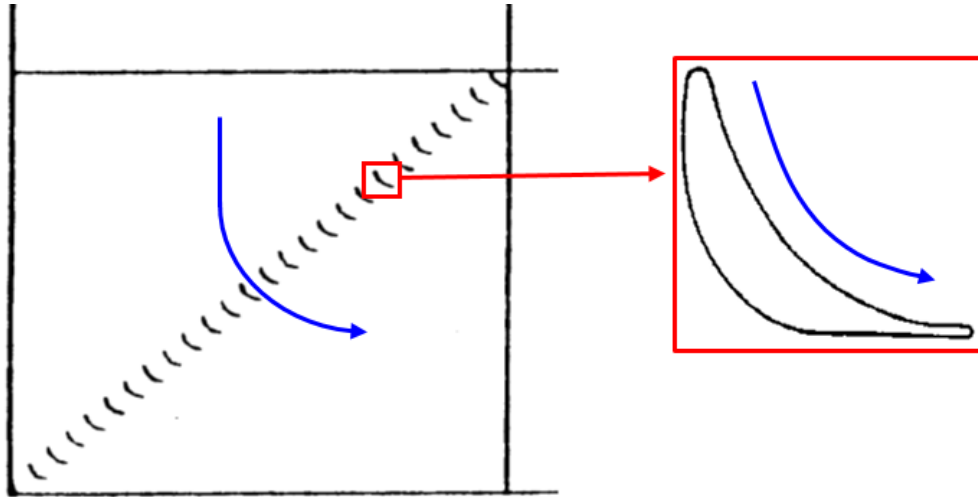


Figure 12: Top view of corner turning-vanes showing flow direction

Wind Tunnel Fan

The wind-tunnel fan unit consists of an Axico Anti-Stall Vaneaxial Fan, run by an MAX-E1 AC Motor with a variable-speed drive. The fan (FPDA-2-200-8-10-1160-300) consists of 10 blades with variable pitch, which allows for changing the fan rpm vs tunnel flow speed curve. The maximum manufacturer service for this fan is 1188 RPM (60 HZ). The motor manufacturer's maximum power is 300 HP. The wind tunnel fan is run by an ABB drive (ACH550- PDR-368A-4+B055) located at the southwest corner of the wind tunnel

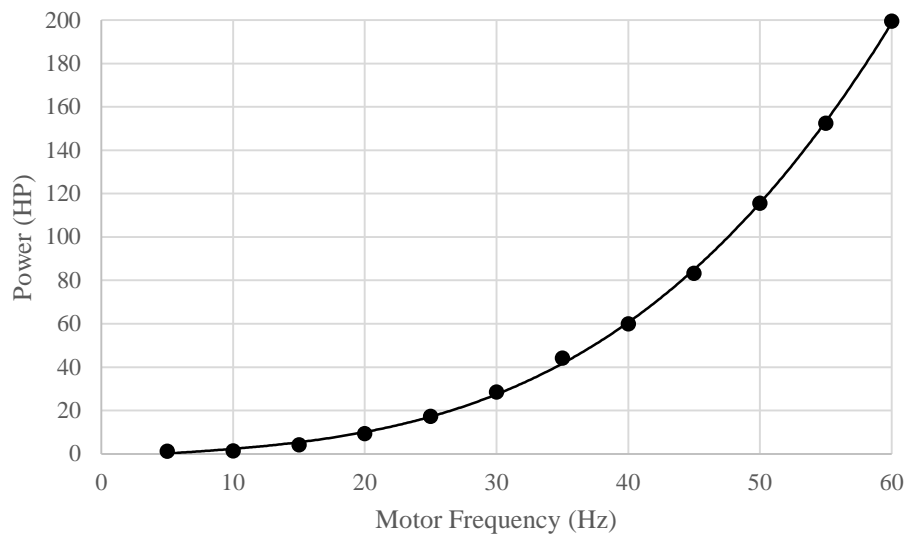


Figure 13: Wind tunnel motor power curve

General Maintenance

The propeller in an axial flow fan must be kept reasonably clean if it is to perform properly. Fans handling fresh air for ventilating purposes will seldom need cleaning. Fans exhausting process air should be cleaned as required. Dirt or chemical deposits will usually build up evenly on a propeller and although performance is affected, vibration is usually acceptable until the deposits become thick enough to break away in crust-like pieces. When this happens, the propeller may be thrown out of balance and the resulting vibration could be serious. Accumulations should be removed by solvent cleaning or scraping. If the propeller has been coated, be careful not to cut through this protective covering. The vaneaxial fan is constructed with a set of guide vanes adjacent to the propeller. These should be cleaned at the same time the propeller is cleaned. The guide vanes are important to the performance of the fan and should be inspected carefully. They may accumulate dirt even under conditions where the propeller remains clean.

Per the manufacturer's instructions, the fan motor should be lubricated every 3000 hrs. or every five years. The motor was last greased on May 8, 2019.

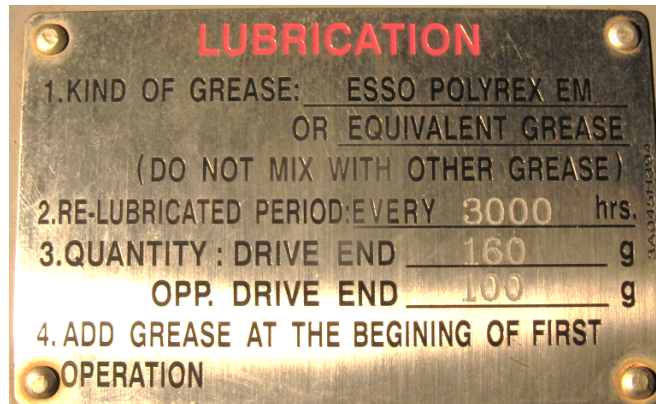


Figure 14: Fan motor lubrication instructions

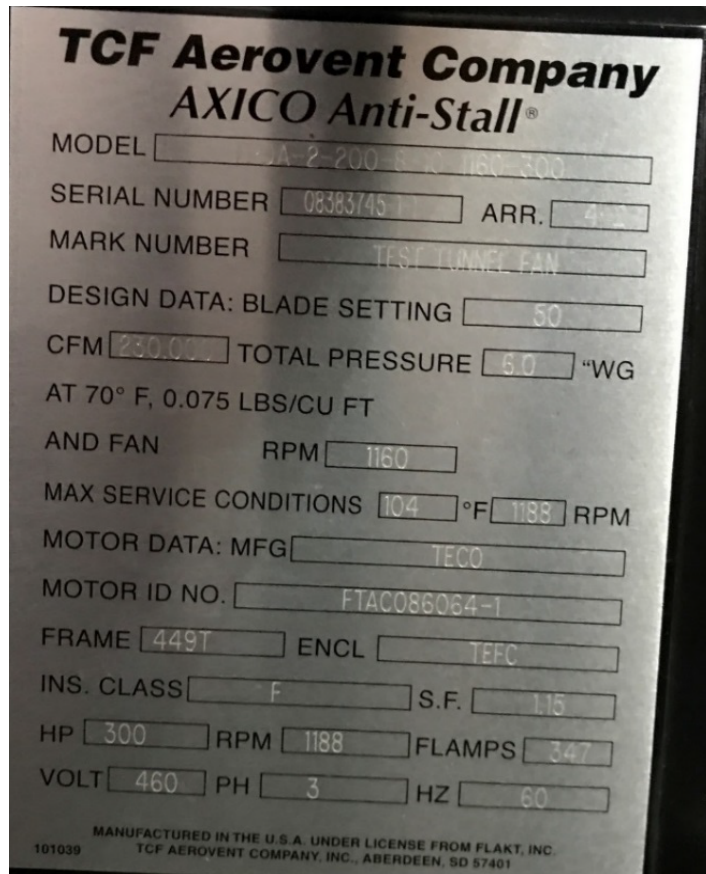


Figure 15: Tunnel Fan Plate

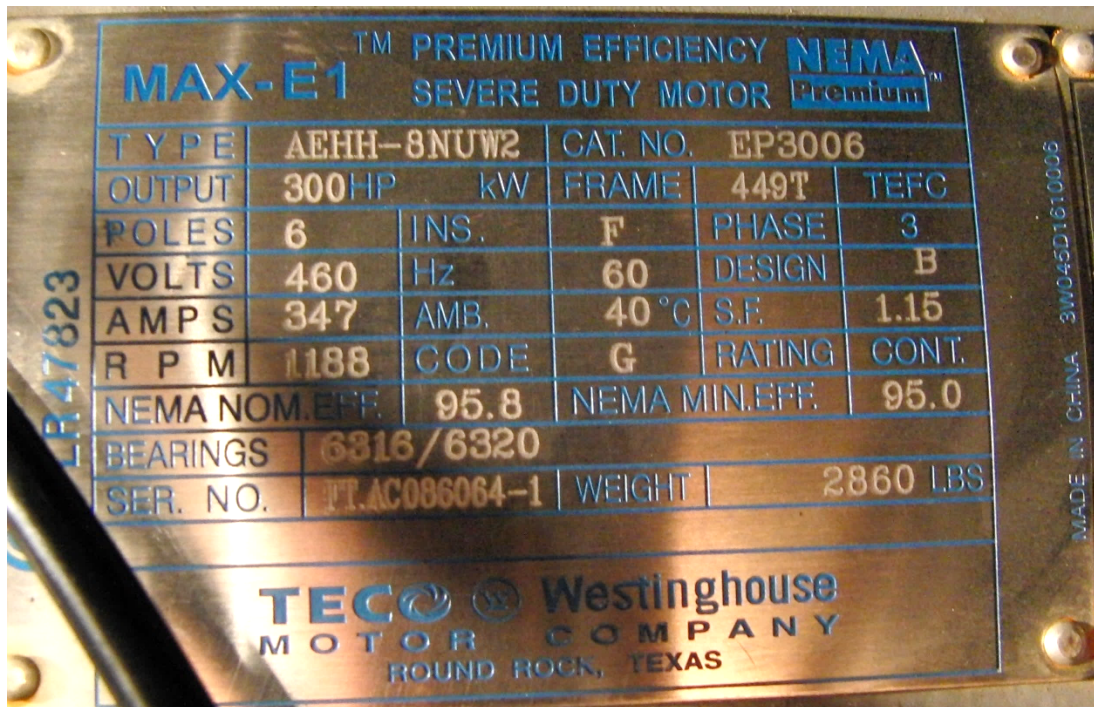


Figure 16: Tunnel Fan Motor Plate

MODEL MOUNTING AND INSTALLATION

Although the force balance is designed to allow for different mounting strut positions, it is strongly recommended that the standard mounting positions be used whenever possible. If other mounting positions are needed, the wooden hole covers should be used, rather than putting holes in the standard Plexiglas hole cover.

For dimensioned drawings of the test section and mounting struts, see “Selected Part Drawings” at the end of this manual.

Strut Installation

1. Turn all four latches from the latched to the unlatched position

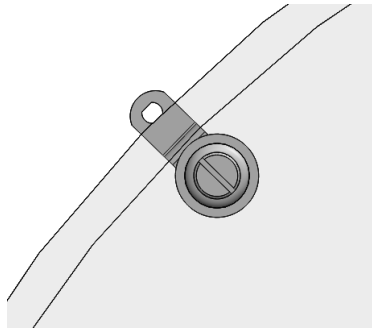


Figure 17: Latched hole cover position

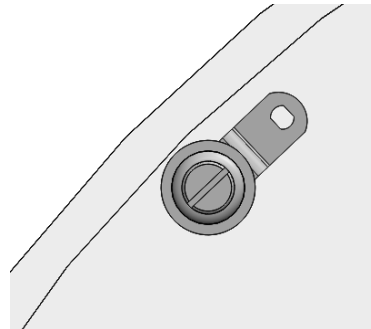


Figure 18: Unlatched hole cover position

2. Grabbing the Plexiglas hole cover by the strut holes, lift and remove the cover from the floor of the tunnel.

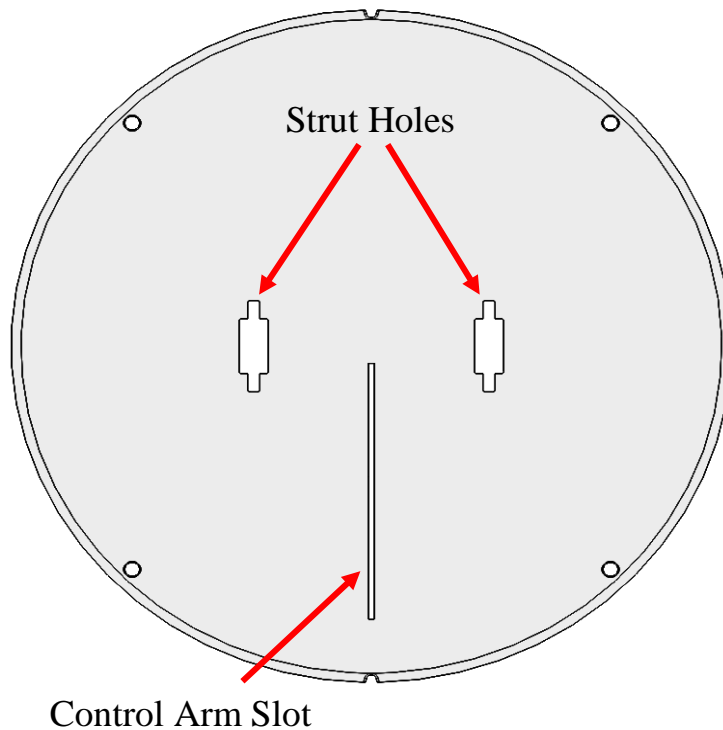


Figure 19: Wind-tunnel hole cover design

- Using the locating pins on the bottom of the struts, place the struts onto the force balance mounting plate
 - The blunt ends of the struts should be facing forward.

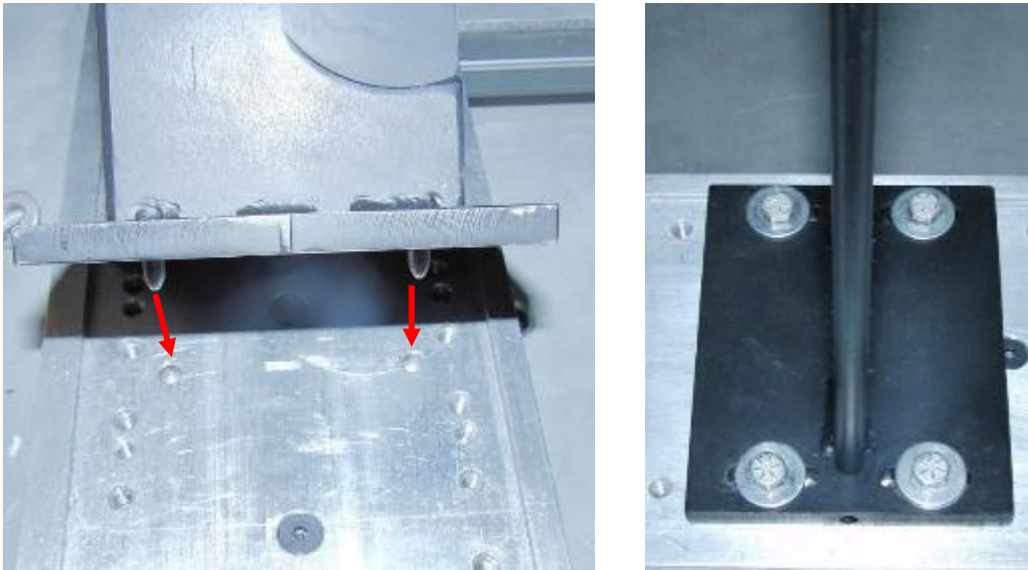


Figure 20: Mount strut installation locating method

- Secure each strut with four bolts and washers
- Lower the hole cover over the struts so that the control arm slot is downstream of the struts
 - The hole cover should be lying flush with the tunnel floor.
- Turn all four latches to the latched position

AOA Control Arm Installation

- Slide the thin end of the AOA control arm through the control arm slot in the hole cover

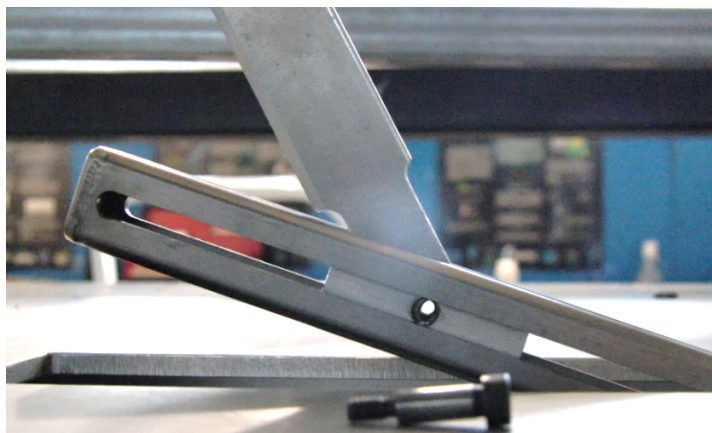


Figure 21: AOA control arm installation

- On the back side of the test section, attach the control arm to the force balance using a 1/8"-24 shoulder bolt and finger tighten

FOUR COMPONENT FORCE BALANCE

Platform/Parallelogram Balance Overview

The platform balance is used to measure the lift, pitching moment and rolling moment produced on a model in the wind tunnel. It consists of three FUTEK Force Transducers located under the top balance plate. These are labeled F1, F2, and F3. The fourth transducer, located outside the parallelogram balance, measures the drag produced, and is labeled F0. All transducers are connected to the National Instruments Channel Amplifiers. A schematic of the setup is shown below.

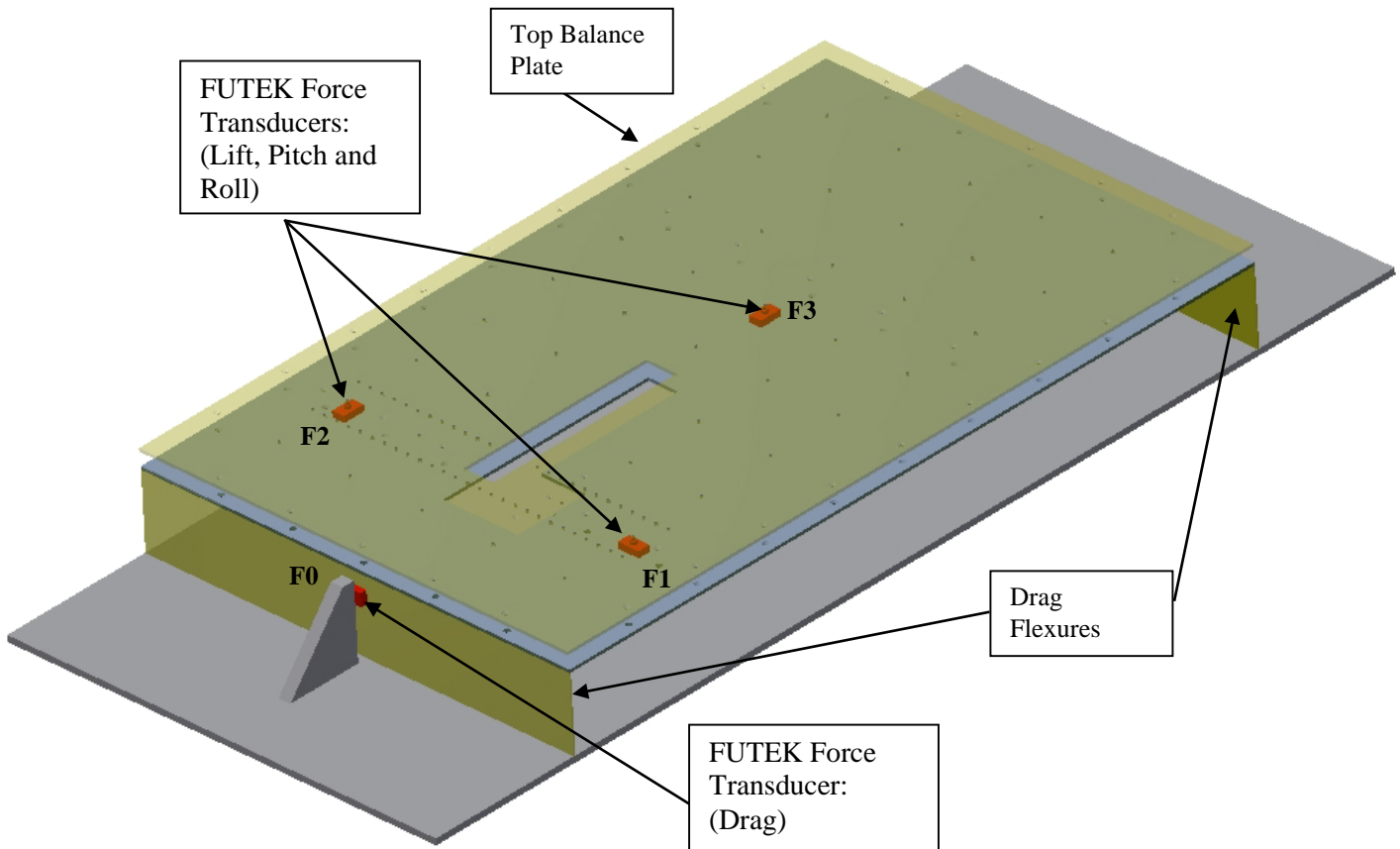


Figure 22: Platform balance setup

The balance works by taking the readings from the different transducers and manipulating them with the proper equations to output the lift, drag and pitching moment respectively.

- **The Drag** – is measured by the F0 transducer reading inside the parallelogram. It measures the force induced between the top plate and the bottom plate.

$$D = F0$$

- **The Lift** – is measured by the F1, F2, and F3 transducers located beneath the top plate. When the airfoil is placed in the wind tunnel, the lift force pulls up on the balance. This lift force is the sum of the transducers.

$$L = F1 + F2 + F3;$$

- **The Pitching Moment** – is measured by the F3 and F0 transducers. It is measured from the moments created by the lift and drag forces on the airfoil.

$$P = -L_p * F_3 + h * F_0;$$

(where L_p is the distance from the airfoil base on the top plate (30.0 inches), to the F3 transducer, and h is the distance from the top plate to the airfoil 32 inches).

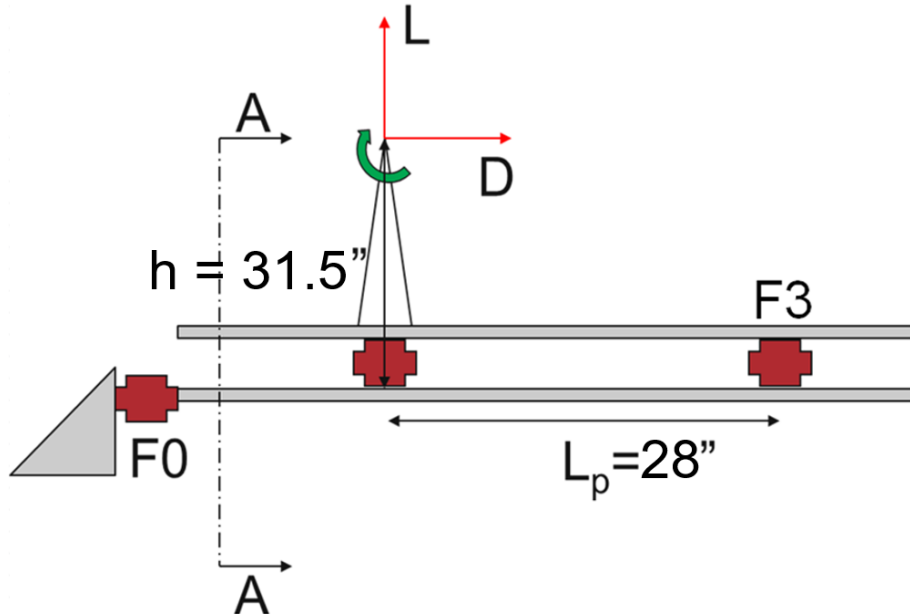


Figure 23: Free body diagram for lift, drag and pitch

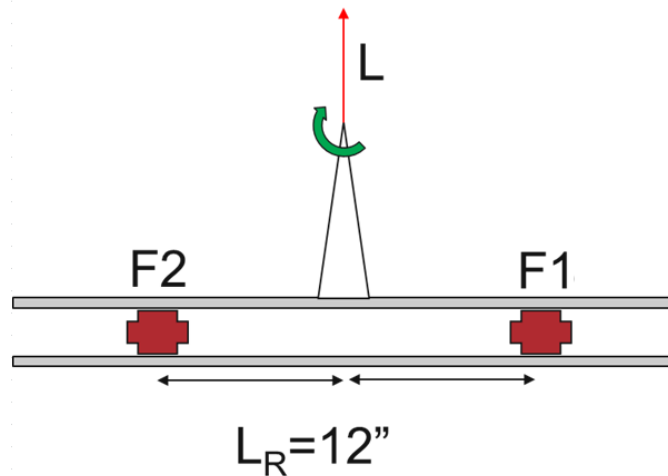


Figure 24: Free body diagram for roll (Section A-A)

- **The Rolling Moment** – is measured by the F1 and F2 transducers.

$$R = L_r * (F_1 - F_2)$$

(where L_r is the distance from the airfoil base on the top plate (12.0 inches), to the F2 and F1 transducer).

LabVIEW Implementation

When implementing the free body diagram equations above into LabVIEW, the units for the values of h , L_r and L_p are in feet.

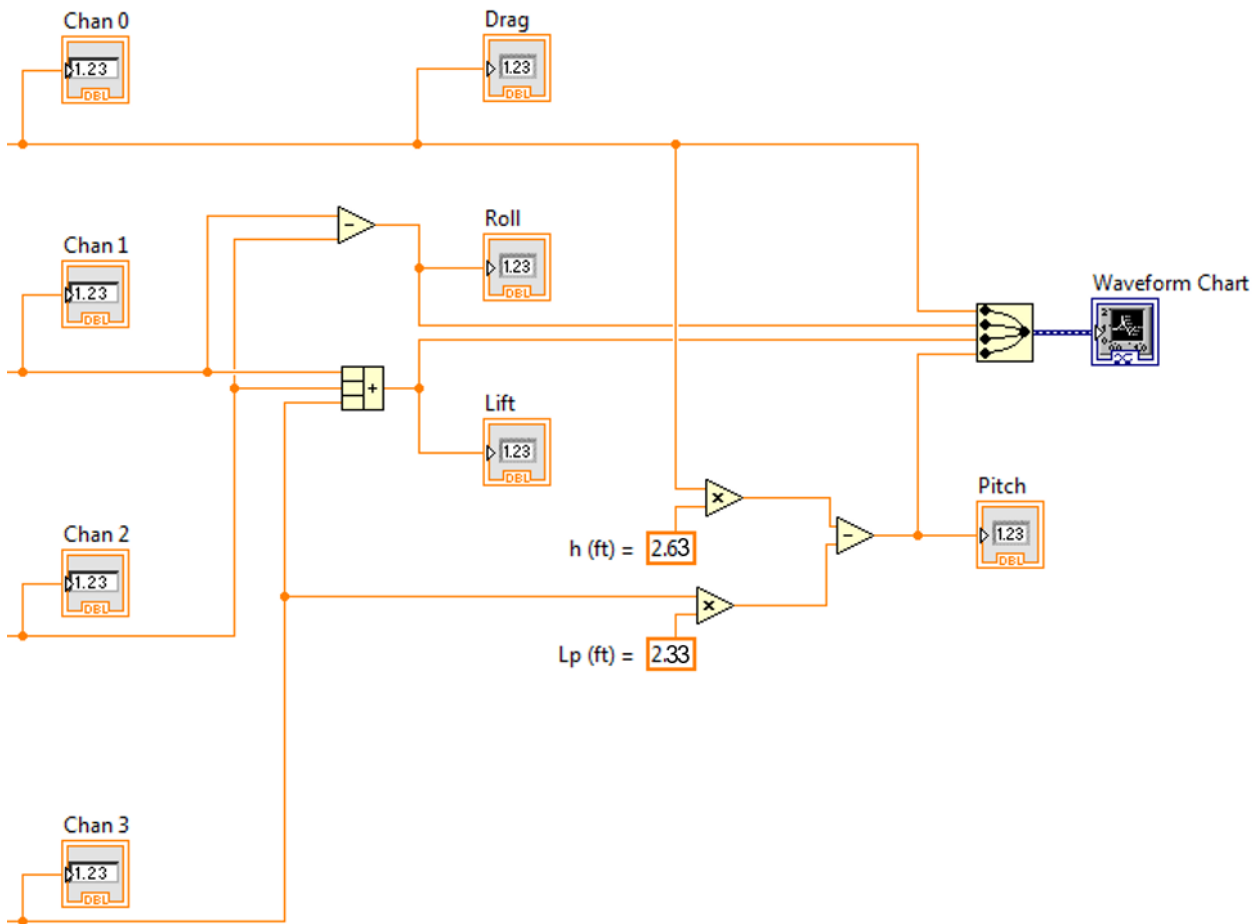


Figure 25: Free body diagram LabVIEW implementation

Calibration

To calibrate the four transducers on the platform balance, it is necessary to apply a known load at three different locations on the balance to measure lift, drag and pitching moment respectively.

To Calibrate the Lift

1. Open the *Wind Tunnel Balance* LabVIEW program located in the *C:\Temp\AAE 334I-Fall2017* folder. Once opened, select a folder and text file where you would like the output readings to be saved. (You only need to create one text file for the calibrations, the program sets a separate time stamp for each reading you take)
2. Run the balance program and click the tare values button
3. Apply one of the known weights from the weight box to the middle of the Top Balance Plate and let the balance even out before recording data. A circle is marked on the top balance plate with L written on it; place weights on this circle for lift
4. The transducer lift measurements are located in the text file to which you created the path. The text file includes 11 columns of data which are: Pitot pressure, wind speed, temperature, AoA,

drag, lift, pitch, F0 (force from 0 transducer), F1, F2, and F3 respectively. The lift is calculated using the equation shown in the introduction.

5. Use 1-10lb weights to get 10-point calibration
6. In Excel or MATLAB, compare this value to the actual value of the weight you used, and scale appropriately.

To Calibrate the Drag

1. Remove the weight used to calibrate the lift.
2. Place a known weight on the pulley platform located just behind the F2 transducer and let the balance even out before writing data.
3. The transducer drag measurements are located in the text file to which you created the path. The drag measured is the fifth column of data.
4. Use 1-10lb weights to get 10 point calibration
5. In Excel or MATLAB, compare this value to the actual value of the weight you used, and scale appropriately.

To Calibrate the Pitching Moment

1. Remove the weight used to calibrate the drag
2. Place a known weight on the same circle where you placed the lift weight.
3. The transducer data is located in the same text file with new timestamp. The pitching moment is the seventh column of data.
4. Use 1-10lb weights to get 10 point calibration
5. The pitching moment is calculated using the equation shown in the introduction. In Excel or MATLAB, compare this value to the actual value of the weight you used and scale appropriately.

FORCE TRANSDUCERS

Instrumentation

FUTEK Low Profile Tension & Compression Load Cell (F0 Transducer)

- Model No. LRF325
- 75 lb. capacity
- 1/4-28 thread connector

FUTEK Low Profile Tension & Compression Load Cell (F1-F3 Transducers)

- Model No. LRF350
- 150 lb. capacity
- 3/8-24 thread connector

LabVIEW Implementation

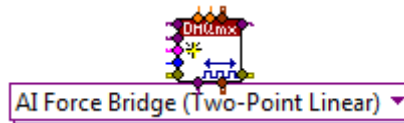


Figure 26: Force transducer virtual channel block

Table 2: Temperature probe channel configuration

Channel	Value		Units
	F0	F1-F3	
Physical Channels	cDAQ2Mod2/ai0	cDAQ2Mod2/ai1:3	
Bridge Configuration	Full bridge (10182)		
Voltage excitation source	Internal (10200)		
Voltage excitation value	3.3		V
Nominal bridge resistance	350		Ohms
Minimum value	-75	-150	lbs.
Maximum value	75	150	lbs.
Units	Pounds (15876)		
First electrical value	0	0	
Second electrical value	2	1.65	
Electrical units	mVolts/Volt (15897)		
First physical value	0	0	
Second physical value	75	150	
Physical units	Pounds (15876)		

Location and Installation

At the DAQ platform

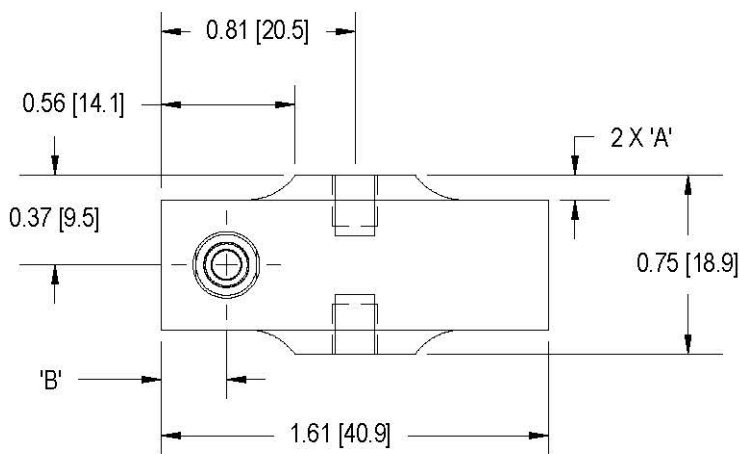
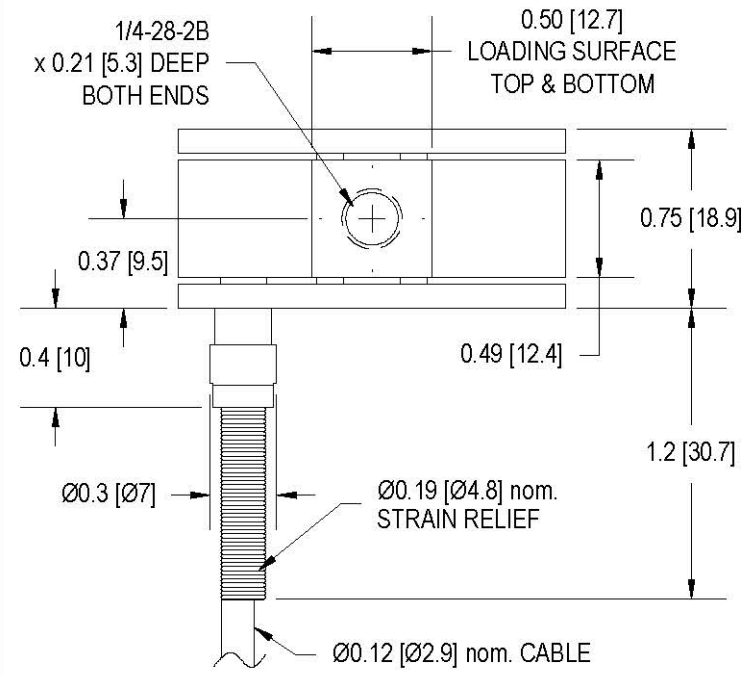
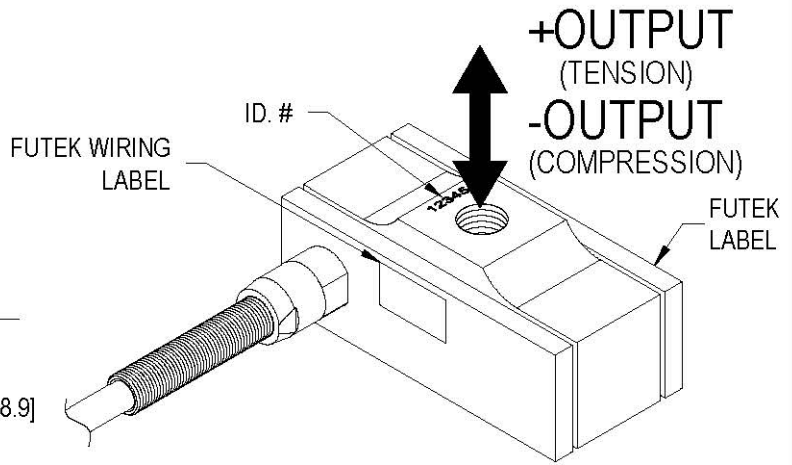
Connect the black BNC connector from the force transducers to the corresponding MOD2 ports (i.e. F1 to Ch1) on the input module (NI-9237)

FUTEK MODEL LRF325 (L2320) *LOW PROFILE TENSION AND COMPRESSION LOAD CELL*

Drawing Number: F11069-A

INCH [mm] | R.O.= Rated Output

WIRING CODE (WC1)			
+Excitation	-Excitation	+Signal	-Signal
RED	BLACK	GREEN	WHITE
Shield			
FLOATING			

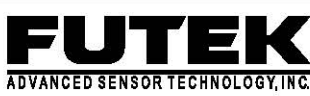


STK#	CAPACITY		A	B
	lb	N		
FSH00073	25	111	0.10 [2.5]	0.27 [6.9]
FSH00074	50	222		0.29 [7.4]
FSH00075	75	334	0.09 [2.3]	0.30 [7.6]
FSH00076	100	445	0.07 [1.8]	0.31 [7.9]

SPECIFICATIONS:

RATED OUTPUT	2 mV/V <i>nom.</i>
SAFE OVERLOAD	150% of R.O.
ZERO BALANCE	±1% of R.O.
EXCITATION (VDC OR VAC)	15 MAX
BRIDGE RESISTANCE	350 Ω <i>nom.</i>
NONLINEARITY	±0.1% of R.O.
HYSTERESIS	±0.1% of R.O.
NONREPEATABILITY	±0.05% of R.O.
CREEP	±0.05% of LOAD
TEMP. SHIFT ZERO	±0.005% of R.O./°F [0.01% of R.O./°C]
TEMP. SHIFT SPAN	±0.005% of LOAD/°F [0.01% of LOAD/°C]

COMPENSATED TEMP.	60 to 160°F [15 to 72°C]
OPERATING TEMP.	-60 to 200°F [-50 to 93°C]
WEIGHT	1.8oz [51g]
MATERIAL	ALUMINUM
DEFLECTION	0.002 [0.05] <i>nom.</i>
CABLE:	#28 AWG, 4 Conductor, Spiral Shielded Clear PVC Cable 10 ft [3 m] Long
ACCESSORIES AND RELATED INSTRUMENTS AVAILABLE	
CERTIFICATE OF CONFORMANCE (STD)	TENSION
CALIBRATION (AVAILABLE)	5 pt. TENSION/COMPRESSION
	60.4 K Ω SHUNT CAL. VALUE
	10 VDC
CALIBRATION TEST EXCITATION	



This drawing is submitted solely for the information and exclusive use of the original addressee. It is not to be divulged in whole or in part, by any firm or individual without written permission from FUTEK

10 THOMAS
IRVINE, CA 92618 USA
1-800-23-FUTEK (38835)

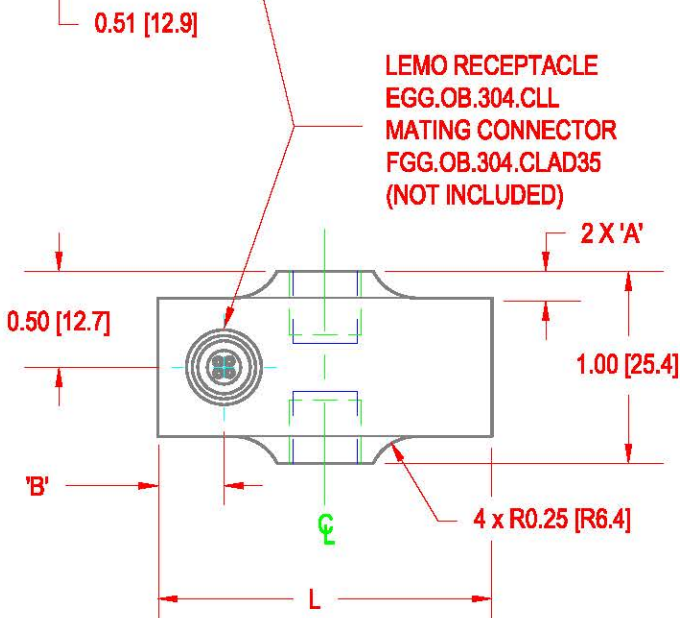
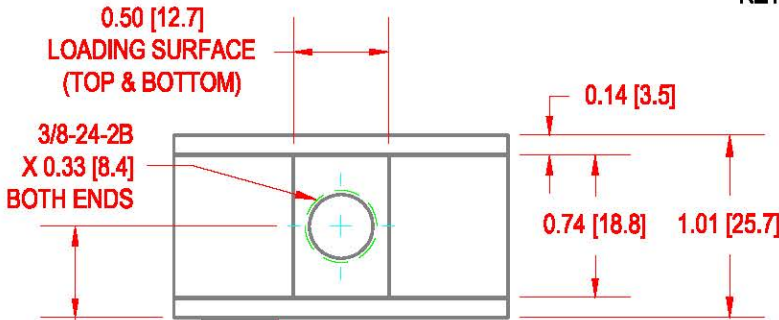
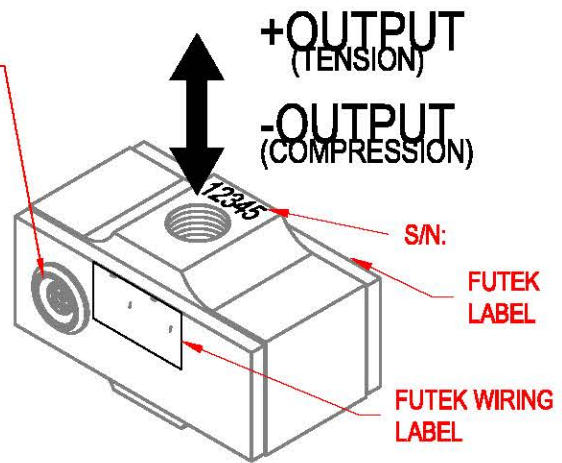
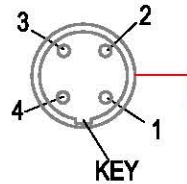
INTERNET:
<http://www.futek.com>

FUTEK MODEL LRF350 (L2320) LOW PROFILE TENSION AND COMPRESSION LOAD CELL

Drawing Number: FI1070-C

INCH [mm] R.O.= Rated Output

CONNECTOR CODE (CC4)			
+Excitation	-Excitation	+Signal	-Signal
1 RED	4 BLACK	2 GREEN	3 WHITE

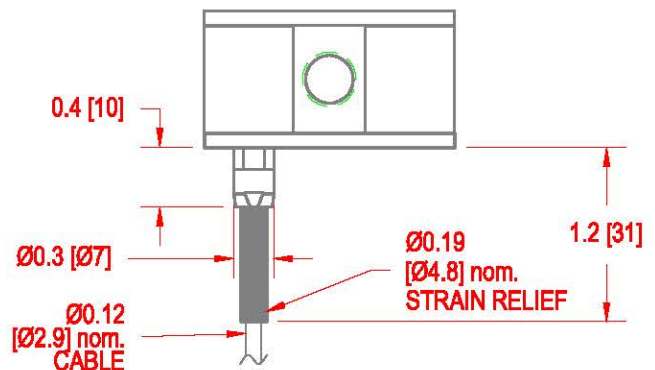
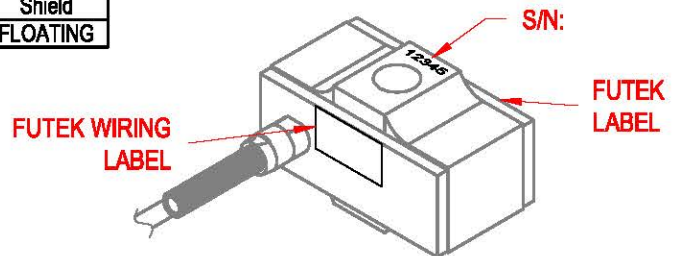


ITEM#	CAPACITY		A	B	L	MATERIAL	CABLE OPTION
	lb	N					
FSH00083	150	667	0.16 [4.1]	0.35 [8.9]	1.74 [44.2]	ALUMINUM 2 oz [57 g]	
FSH00077							X
FSH00084	200	890	0.14 [3.6]	0.36 [9.1]			X
FSH00078							
FSH00085	300	1334	0.12 [3.0]	0.39 [9.9]	X		
FSH00079							
FSH00086	500	2224	0.16 [4.1]	0.34 [8.6]	1.70 [43.2]	17-4PH S.S. 5 oz [142 g]	X
FSH00080							
FSH00087	750	3336	0.14 [3.6]	0.36 [9.1]			X
FSH00081							
FSH00088	1000	4450	0.11 [2.8]	0.39 [9.9]	1.74 [44.2]		
FSH00082					X		

SPECIFICATIONS:

RATED OUTPUT	2 mV/V nom.
SAFE OVERLOAD	150% of R.O.
ZERO BALANCE	±1% of R.O.
EXCITATION (VDC OR VAC)	18 MAX
BRIDGE RESISTANCE	350 Ω nom.
NONLINEARITY	±0.1% of R.O.
HYSTERESIS	±0.1% of R.O.
NONREPEATABILITY	±0.05% of R.O.
CREEP	±0.05% of LOAD
TEMP. SHIFT ZERO	±0.005% of R.O./°F [0.01% of R.O./°C]
TEMP. SHIFT SPAN	±0.005% of LOAD/°F [0.01% of LOAD/°C]
COMPENSATED TEMP.	60 to 180°F [15 to 72°C]
OPERATING TEMP.	-60 to 200°F [-50 to 93°C]
MATERIAL(FLEXURE)	SEE CHART
MATERIAL(COVER)	ALUMINUM, Red Anodized After S/N:400511
DEFLECTION	0.002[0.05] nom.
CONNECTOR:	LEMO 4 Pin Receptacle (EGG.OB.304.CLL)
CABLE:	#28 AWG, 4 Conductor, Spiral Shielded Clear PVC Cable 10 ft [3 m] Long
ACCESSORIES AND RELATED INSTRUMENTS AVAILABLE	
CALIBRATION (STD)	5 pt. TENSION; 60.4 KΩ SHUNT CAL. VALUE
CALIBRATION (AVAILABLE)	COMPRESSION
CALIBRATION TEST EXCITATION	10 VDC

CABLE OPTION (WC1)			
+Excitation	-Excitation	+Signal	-Signal
RED	BLACK	GREEN	WHITE
Shield			
FLOATING			



FUTEK
ADVANCED SENSOR TECHNOLOGY, INC.

This drawing is submitted solely for the information and exclusive use of the original addressee. It is not to be divulged in whole or in part, by any firm or individual without written permission from FUTEK

10 THOMAS
IRVINE, CA 92618 USA
1-800-23-FUTEK (38835)

INTERNET:
<http://www.futek.com>

TEMPERATURE MEASUREMENTS

Instrumentation

Omega quick disconnect RTD probe

- Model No. PR-13-2-100-3/16-12-E
- 12" sheath length
- 3/16" probe diameter
- -200 to 500°C range

LabVIEW Implementation

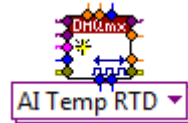


Figure 27: Temperature probe virtual channel block

Table 3: Temperature probe channel configuration

Channel	Value	Units
Physical Channels	cDAQ2Mod4/ai0	
Current excitation value	5.00e-4	V
r0	100	Ohm
Resistance configuration	3-Wire (3)	
Minimum value*	15	°C
Maximum value*	50	°C
Current excitation source	Internal (10200)	
RTD type	Pt3851 (10071)	
Output units	°C	

*Can be changed to better match the bounds of the expected temperature measurements

Location and Installation

The RTD probe is located directly upstream of the contraction section on the north side of the wind tunnel.

At the probe hole

1. Insert the probe all the way through the plastic hole in the side of the wind tunnel
2. Tighten the set screw onto the probe just enough so the probe doesn't slide out
 - NOTE: do not over-tighten the setscrew

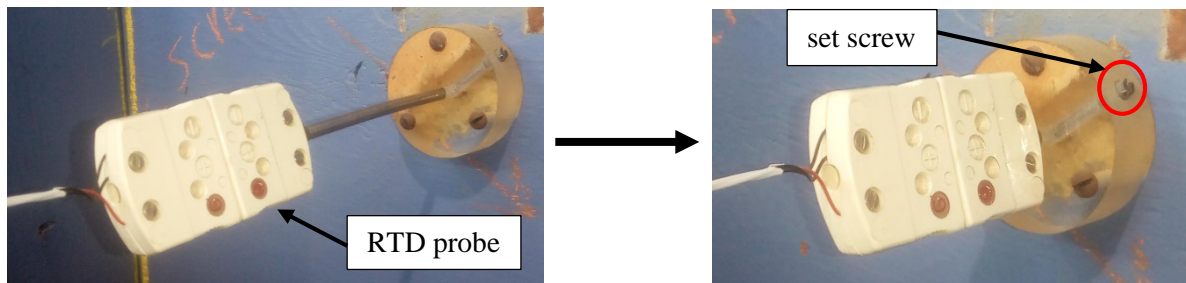


Figure 28: Temperature probe installation

At the DAQ platform

1. Connect the three wires coming from the white wire to the analog input module (NI-9219)
2. Connect the red wire to CH0-3
3. Connect one of the black wires to CH0-6
4. Connect the other black wire to CH0-5

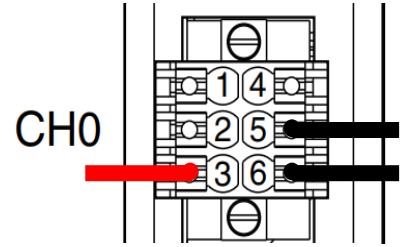


Figure 29: Temperature probe DAQ wiring

Platinum RTD Probes



Standard Dimension PR-13 Series Quick Disconnect Probes

A general purpose probe with electrical connections made via a standard size OTP 3-prong connector. Each unit is supplied with mating connector. Available in 1/16", 1/8", 3/16", or 1/4" diameters, with standard probe lengths from 6" to 24". Custom lengths available on request.

Type PR-13 Mating Female Connector Included.

Shown actual size.

Red lead attaches to this pin for Style 2.

Also Available with PFA Coating

To Order

Model Number	Lead Style†	Ω at 0°C	Sheath Length**
PR-13-2-100-(*)-6-E	2	100	6"
PR-13-2-100-(*)-9-E	2	100	9"
PR-13-2-100-(*)-12-E	2	100	12"
PR-13-2-100-(*)-18-E	2	100	18"
PR-13-2-100-(*)-24-E	2	100	24"

* Specify: 1/16, 1/8, 3/16 or 1/4 for probe diameter in inches.

** Add additional cost per inch for lengths over 24" (1/4" diameter 24" max).

† 3-wire lead configuration standard; contact sales for other configurations.

RTD Probes cannot be bent in the field. OMEGA offers custom bending; consult our Sales Department.

Ordering Example: PR-13-2-100-1/4-6-E, quick disconnect PR-13 probe with mating connector, style 2 wiring, 100 Ω @ 0°C, 1/4" diameter, 6" long, European curve ($\alpha = 0.00385$).

- ✓ Includes a Precision 100 Ω , Class "A" DIN Platinum Wire Wound RTD Element
- ✓ Easily Connect to Your Meter or Measurement System via Our Standard 3-Prong OTP Connector and Extension Cords or Cables
- ✓ Variable Diameters and Lengths Available
- ✓ Temperature Range is -200 to 500°C (220°C Max at Connector)

Metric Dimension PR-13 Series Quick Disconnect RTD Probes

A general purpose probe with electrical connections made via a standard size OTP 3-prong connector. Each unit is supplied with mating connector. Available from 1.5 to 6 mm diameters, with standard probe lengths from 150 to 600 mm. Other lengths available on request.

Model Number	Lead Style†	Ω at 0°C	Sheath Length**
PR-13-2-100-(*)-150-E	2	100	150 mm
PR-13-2-100-(*)-225-E	2	100	225 mm
PR-13-2-100-(*)-300-E	2	100	300 mm
PR-13-2-100-(*)-450-E	2	100	450 mm
PR-13-2-100-(*)-600-E	2	100	600 mm

* Specify: M15 for 1.5 mm, M30 for 3 mm, M45 for 4.5 mm or M60 for 6 mm, for probe diameter in mm.

** Add additional cost per 25 mm for lengths over 600 mm (1.5 mm diameter 600 mm max).

† 3-wire lead configuration standard; others available, contact sales for other configurations.

RTD Probes cannot be bent in the field. OMEGA offers custom bending; consult our Sales Department.

Ordering Example: PR-13-2-100-M60-150-E, quick disconnect PR-13 probe with mating connector, style 2 wiring, 100 Ω @ 0°C, 6 mm diameter, 150 mm long, European curve ($\alpha = 0.00385$).

Options



HH804U meter.

BRLK fitting.



RECU1-OTP-TAF extension coil cable.

AIR VELOCITY TRANSDUCER

Instrumentation

TSI air velocity transducer

- 8455 series
- 12" probe length
- 1/4" probe diameter
- 25–10,000 ft./min (0.125–50 m/s) range

Transducer Configuration

Current settings for the transducer (can be changed by opening the box)

Units = m/s

Full scale = 50.0 m/s

Output = 0 – 5 V

Time Constant = 1 s

Adjust Zero = 0

Span = +0.05 (+5%)

LabVIEW Implementation

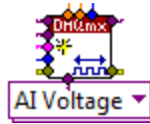


Figure 30: Analog voltage virtual channel block

Table 4: Air velocity transducer channel configuration

Channel	Value	Units
Physical Channels	cDAQ2Mod3/ai1	
Input Terminal Configuration	Differential (10106)	
Minimum value	0	V
Maximum value	5	V
Output Units	0.1 m/s	

Location and Installation

The air velocity transducer is located on the top of the upstream end of the test section.

Before Installation

1. Make sure that the probe is covered with heat shrink tubing longer than the metal sheath



Figure 31: Air velocity transducer protection

2. The heat shrink should cover the black plastic part of the probe

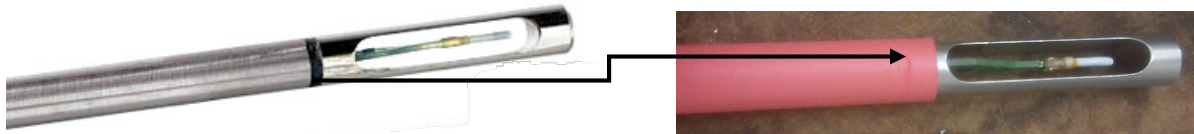


Figure 32: Hot-wire anemometer rubber sheath

At the probe hole – on top of the wind tunnel

3. Install the cord grip fitting into the 3/8-NPT hole in the top of the wind tunnel
 - The bottom of the fitting should be flush with the inner roof of the wind tunnel.
4. Slide the hot-wire probe through the top of the fitting, and into the tunnel
5. Tighten the top of the fitting just enough that the probe doesn't fall through

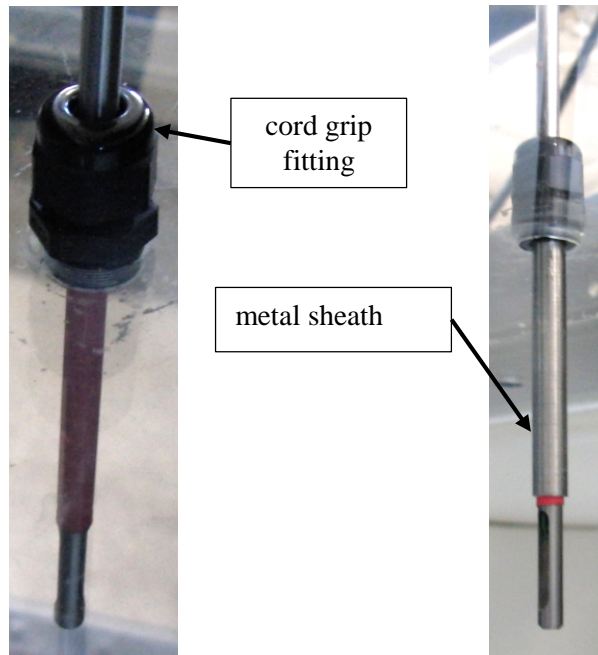


Figure 33: Air velocity transducer probe installation

In the wind tunnel

6. Slide the metal protective sheath over the probe and fully into the cord grip fitting
 - The end of the sheath will butt against the fitting when fully in
7. Slide the probe up or down so that end of the heat shrink just peeks out of the metal sheath.
 - **The metal sheath is used to protect the plastic part of the probe from snapping and thus must fully encase this section**
8. Carefully turn the probe so that the opening of the probe tip is aligned with the direction of flow

At the probe hole – on top of the wind tunnel

9. Tighten the top of the fitting so that probe has very little wiggle room

At the DAQ platform

10. Connect the black BNC connector from the air velocity transducer box to MOD3-CH1 of the voltage input module (NI-9215)

AIR VELOCITY TRANSDUCERS MODELS 8455, 8465, AND 8475



The 8455, 8465, and 8475 Air Velocity Transducers are ideal for both temporary and permanent installations for air velocity measurements in research and development labs, manufacturing processes, and other applications. The full-scale range, signal output, and time constant are user selectable and can be easily changed to meet the needs of your application.

Applications

- + Comfort and draft studies
- + Critical environment installations (e.g., clean rooms and hospitals)
- + Diffuser design analysis
- + Monitoring drying processes
- + Monitoring air flows in tunnels and subways
- + Used as a standard in wind tunnels and calibration facilities
- + Environmental monitoring in greenhouses and IAQ applications
- + General engineering applications

General Purpose (8455)

- + Protected probe tip
- + Rugged ceramic sensor
- + Wide range of measurement applications
- + Fast response time

Windowless (8465)

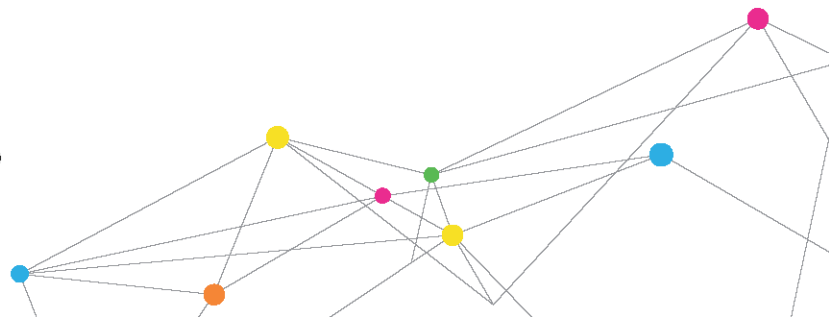
- + Less flow blockage
- + Ideal for measuring in confined spaces
- + Fast response time

Omnidirectional (8475)

- + Omnidirectional probe tip
- + Accurate at low velocities from 10 to 100 ft/min (0.05 to 0.5 m/s)
- + Ideal for unknown or varying flow direction



UNDERSTANDING, ACCELERATED



SPECIFICATIONS

AIR VELOCITY TRANSDUCERS MODELS 8455, 8465, AND 8475

Accuracy

8455	±2.0% of reading ¹ , ±0.5% of full scale of selected range
8465	±2.0% of reading ¹ , ±0.5% of full scale of selected range
8475	±3.0% of reading ² , ±1.0% of full scale of selected range

Field Selectable Range

8455 and 8465	25 ft/min to 200, 250, 300, 400, 500, 750, 1,000, 1,250, 1,500, 2,000, 2,500, 3,000, 4,000, 5,000, 7,500, 10,000 ft/min (0.125 m/s to 1.0, 1.25, 1.50, 2.0, 2.5, 3.0, 4.0, 5.0, 7.5, 10.0, 12.5, 15.0, 20.0, 25.0, 30.0, 40.0, 50.0 m/s)
8475	10 ft/min to 100, 125, 150, 200, 250, 300, 400, 500 ft/min (0.05 m/s to 0.5, 0.75, 1.0, 1.25, 1.50, 2.0, 2.5 m/s)

Repeatability

8455 and 8465	< ±1.0% of reading ³
8475	N/A

Response to Flow

8455 and 8465	0.2 sec ⁴
8475	5 sec ⁵

Temperature Range

Compensation	32 to 140°F (0 to 60°C)
Operating (electronics)	32 to 200°F (0 to 93°C)
Operating (sensor)	32 to 200°F (0 to 93°C)
Storage	32 to 200°F (0 to 93°C)

Resolution (minimum)

0.07% of selected full scale

Input Power

11 to 30 VDC or 18 to 38 VAC, 350 mA max⁶

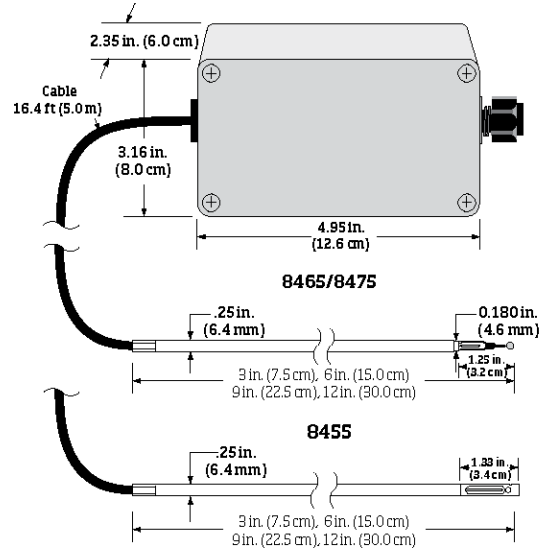
Output

Impedance	Voltage mode: less than 1 ohm, 20 mA max source current
Resistance	Current mode: 500 ohms maximum load
Signal	Field selectable 0 to 5V, 0 to 10V, 0 to 20, 2 to 10V, mA, 4 to 20 mA
Time Constant	Field selectable 0.05 to 10 seconds

Probe length

3 in., 6 in., 9 in., 12 in. (7.5 cm, 15 cm, 22.5 cm, or 30 cm)

All models contain on-board electronics and calibration curves that provide a linear signal output. This linear signal is sent out as either a current (mA) or a voltage (V) signal, allowing output to a variety of data loggers or data acquisition systems. In addition, the current and voltage output ranges are user-selectable for your convenience.



	8455/8465	8475
Range	25 to 10,000 fpm (0.127 to 50.8 m/s), selectable	10 to 500 fpm (0.05 to 2.54 m/s), selectable
Accuracy	±(2% of reading at 64.4 to 82.4°F (18-28°C) +0.5% of full scale of selected range)	±(3% of reading at 68.0-78.8°F (20 to 26°C) +1% of full scale of selected range)
Response time	0.2 seconds	5.0 seconds
Input power	11 to 30 VDC or 18 to 28 VAC, 350 mA maximum	

¹From 64.4 to 82.4°F (18 to 28°C), outside this range and within temperature compensation range add 0.11% per °F (0.2% per °C).

²From 68 to 78.8°F (20 to 26°C), outside this range and within temperature compensation range add 0.28% per °F (0.5% per °C). Directional sensitivity of the Model 8475 is +5%/-20% of reading +0/-10 ft/min (+0/-0.05 m/s) over 270° solid angle regardless of flow direction.

³Standard deviation based on one minute average from 100 to 1,000 fpm (0.5 to 5.0 m/s).

⁴For 63% of final value, tested at 1,500 fpm (7.5 m/s).

⁵For 63% of final value, tested at 500 fpm (2.5 m/s).

⁶Input voltage must be maintained within specifications at the transducer.

Specifications are subject to change without notice.

TSI and the TSI logo are registered trademarks of TSI Incorporated.



UNDERSTANDING, ACCELERATED

TSI Incorporated - Visit our website www.tsi.com for more information.

USA	Tel: +1 800 874 2811	India	Tel: +91 80 67877200
UK	Tel: +44 149 4 459200	China	Tel: +86 10 8251 6588
France	Tel: +33 4 91 11 87 64	Singapore	Tel: +65 6595 6388
Germany	Tel: +49 241 523030		

CONTRACTION PRESSURE DROP

Instrumentation

Omega differential pressure transducer

- Model No. PX653-10D5V
- 0 – 10 in.H₂O (0 – 2.49 kPa) range
- DP41-E-S4 meter

LabVIEW Implementation

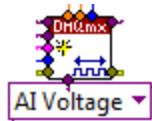


Figure 34: Analog voltage virtual channel block

Table 5: Air velocity transducer channel configuration

Channel	Value	Units
Physical Channels	cDAQ2Mod3/ai0	
Input Terminal Configuration	Differential (10106)	
Minimum value	1	V
Maximum value	5	V
Output Units	in.H ₂ O	

Location and Installation

Two lengths of tubing connect the pressure transmitter to pressure taps at stations 1 and 2.

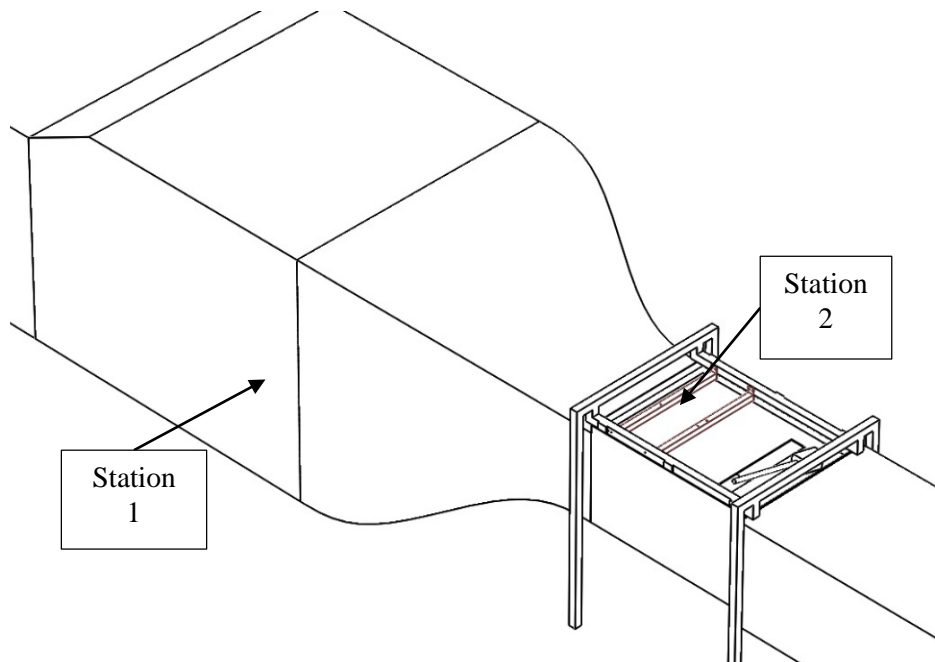


Figure 35: Contraction pressure tap locations

At the pressure taps

1. Connect the long length of tubing to the brass fitting at Station 1.
2. Connect the short length of tubing to the brass fitting at Station 2.
 - If this fitting is loose, reseal it into the wind tunnel with RTV

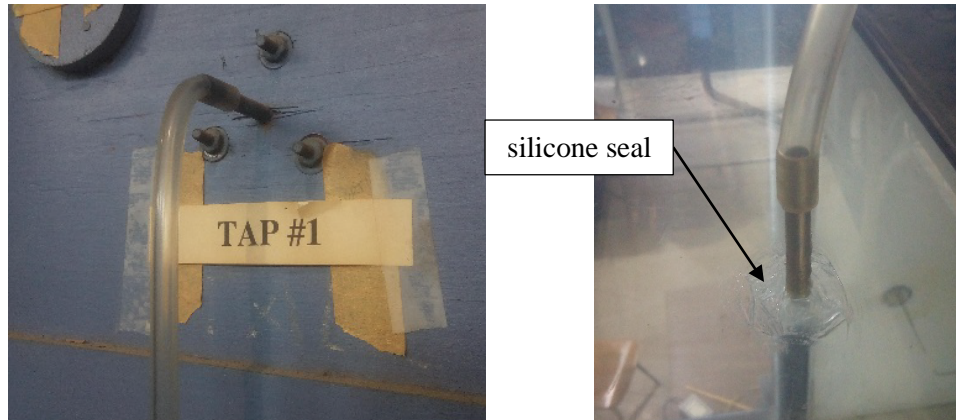


Figure 36: Pressure tap installation

At the pressure transmitter

3. Connect the tubing from Station 1 to the high pressure fitting
4. Connect the tubing from Station 2 to the low pressure fitting

At the DAQ platform

5. Connect the black BNC connector from the pressure transmitter to MOD3-CH0 of the voltage input module (NI-9215)

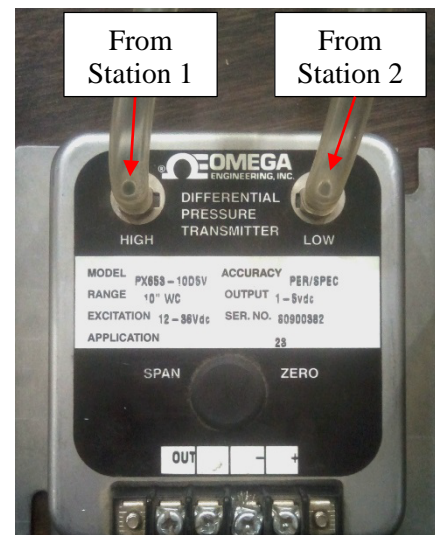


Figure 37: Pressure transducer connection

HIGHLY ACCURATE, LOW-PRESSURE LABORATORY TRANSDUCER

0-0.1 to 0-50 inH₂O
0-25 Pa to 0-12.5 kPa

PX653 Series



Ideal Applications:

- ✓ Clean Rooms
- ✓ HVAC
- ✓ Laboratory Fume Hoods

SPECIFICATIONS

Excitation: 12 to 36 Vdc
Output: 1 to 5 Vdc (3 wire)
Linearity: 0.3% FS (BFSL)
Hysteresis: 0.02% FS
Repeatability: 0.05% FS
Operating Temperature: -29 to 72°C (-20 to 160°F)
Compensated Temperature: 2 to 57°C (35 to 135°F)
Thermal Effects:
Zero: 0.015% FS/°F
Span: 0.015% rdg/°F
Proof Pressure: 15 psi
Burst Pressure: 20 psi
Static Pressure: 25 psi
Gage Type: Capacitance
Supply Current: <5 mA
Calibration Report: NIST cal at 25, 50, 75 and 100% FS; upscale and downscale provided
Response Time: 250 ms
Wetted Parts:
Dry, clean, non-corrosive gases only
Enclosure: NEMA 2 (IP62)
Dimensions: 107 H x 117 W x 53 mm D (4.2 x 4.6 x 2.1")
Pressure Port: 1/8" barbed fittings (tubing TY-316-100)
Electrical Connections: Screw terminal
Weight: 368 g (13 oz)



PX653-10D5V, with DP3002-E meter, shown smaller than actual size.

DIFFERENTIAL PRESSURE TRANSDUCERS **B**

To Order

RANGE		MODEL NO.	COMPATIBLE METERS
inH ₂ O	Pa/kPa		
0 to 0.1	0 to 25	PX653-0.1D5V	DP25B-E, DP41-E, DP460-E
0 to 0.25	0 to 62	PX653-0.25D5V	DP25B-E, DP41-E, DP460-E
0 to 0.50	0 to 125	PX653-0.5D5V	DP25B-E, DP41-E, DP460-E
0 to 0.75	0 to 187	PX653-0.75D5V	DP25B-E, DP41-E, DP460-E
0 to 1	0 to 249	PX653-01D5V	DP25B-E, DP41-E, DP3002-E
0 to 2	0 to 498	PX653-02D5V	DP25B-E, DP41-E, DP460-E
0 to 3	0 to 748	PX653-03D5V	DP25B-E, DP41-E, DP460-E
0 to 5	0 to 1.25	PX653-05D5V	DP25B-E, DP41-E, DP460-E
0 to 10	0 to 2.49	PX653-10D5V	DP25B-E, DP41-E, DP3002-E
0 to 25	0 to 6.23	PX653-25D5V	DP25B-E, DP41-E, DP460-E
0 to 50	0 to 12.5	PX653-50D5V	DP25B-E, DP41-E, DP460-E
BI-DIRECTIONAL RANGES			
±0.1	25	PX653-0.1BD5V	DP25B-E, DP41-E, DP460-E
±0.25	62	PX653-0.25BD5V	DP25B-E, DP41-E, DP460-E
±0.50	125	PX653-0.5BD5V	DP25B-E, DP41-E, DP460-E
±1	249	PX653-01BD5V	DP25B-E, DP41-E, DP460-E
±2.5	623	PX653-2.5BD5V	DP25B-E, DP41-E, DP460-E
±5	1.25	PX653-05BD5V	DP25B-E, DP41-E, DP460-E
±10	2.49	PX653-10BD5V	DP25B-E, DP41-E, DP460-E
±25	6.23	PX653-25BD5V	DP25B-E, DP41-E, DP460-E
±50	12.5	PX653-50BD5V	DP25B-E, DP41-E, DP460-E

Comes complete with NIST traceable calibration certificate and operator's manual.
Ordering Examples: PX653-01D5V, 0 to 1 inH₂O range with 1 to 5 Vdc output.
PX653-01BD5V, ±1 inH₂O range, 1 to 5 Vdc output with 0 = 3 Vdc.



PX653, PX654, PX655, PX656
 Pressure Transducer
 M1436/0902



PX654, PX656



PX653, PX655*



COMMON SPECIFICATIONS FOR ALL UNITS

Accuracy: (Based on best fit straight line, although NIST cal. sheet is based on terminal point, therefore NIST cal. sheet could report a max. accuracy of 0.5% TP)	±0.25% FS (BFSL)	Static Pressure: PX653, PX655: PX654, PX656: Process Media:	15 PSI 100 PSI Clean, dry clean non-corrosive gases
Linearity:	±0.25% FS (BFSL)	Thermal Effects: Zero: Span:	0.02% FS/°F 0.02% FS/°F
Hysteresis:	±0.02% FS	Sensor Type:	Capacitance
Repeatability:	±0.05% FS	Response Time:	250 ms
Operating Temp.:		Enclosure:	
PX653, PX655:	-20° to 160°F (-29° to 72°C)	PX653, PX655:	NEMA 2
PX654, PX656:	-20° to 185°F (-29° to 85°C)	PX654, PX656:	NEMA 4X
Compensated Temp.:		Pressure Port:	
PX653, PX655:	35° to 135°F (2° to 57°C)	PX653, PX655:	1/8 and 1/4 barbed fittings
PX654, PX656:	0° to 160°F (-18° to 72°C)	PX654, PX656:	1/4 NPTF
Storage Temp.:		Electrical Connection:	Screw terminal
PX653, PX655:	-40 to 180°F	PX654, PX656:	Two 1/2 NPTF conduit
PX654, PX656:	-40 to 210°F		
Proof Pressure:	PX653 15 PSI PX654 20 PSI		
Burst Pressure:	PX655 25 PSID PX656 50 PSID		

PX653 & PX654 (VOLTAGE OUTPUT)

EXCITATION:	12-36Vdc
OUTPUT:	1-5Vdc
SUPPLY CURRENT:	<5mA
WEIGHT:	
PX653:	13 oz. (368 g)
PX654:	2.1 lb. (955 g)

PX655 & PX656 (ANALOG OUTPUT)

EXCITATION:	12-36Vdc
OUTPUT:	4-20mA (2 wire)
MAX. LOOP RES.:	(supply voltage -10) x 50 ohms
WEIGHT:	
PX655:	13 oz. (368 g)
PX656:	2.1 lb. (955 g)

HANDLING PRECAUTIONS

This sensor has a high insulation resistance. It can be damaged when exposed to high static discharges. Good instrumentation grounding practices should be used during handling, testing and installation.

*CE Approval is only available on PX655 and valid if connected per the wiring diagram see reverse.

CALIBRATION REPORT

All models are tested to meet or exceed the published specifications. Calibration testing was performed using NIST traceable instrumentation. all sensors come calibrated. **DO NOT ATTEMPT TO RECALIBRATE SENSOR, UNLESS YOU HAVE A KNOWN PRESSURE SOURCE THAT IS AT LEAST 5 TIMES MORE ACCURATE THAN THE SENSOR.**

TWO-AXIS TRAVERSE

The two-axis traverse system, consists of two Velmex BiSlides controlled by a Velmex VXM stepper-motor controller.

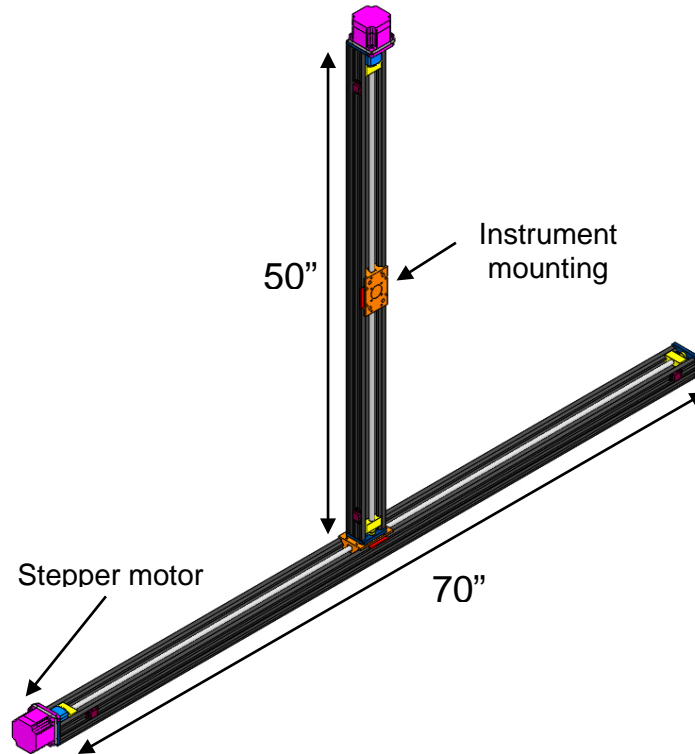


Figure 38: Two-axis traverse layout

Instrumentation

Two Velmex Precision Lead Screw BiSlides

- Model No. MN10-0700-E04-31 (70 inch travel)
- Model No. MN10-0500-E04-31 (50 inch travel)
- 0.4 in/rev travel
- Limit switches
- Fail safe brake on vertical slide
- 4 in/sec speed
- 0.001 inch resolution

Two Vexta Type 34T1 stepper motors

- Model No. PK296-03AA-A6-3/8
 - o Single shaft
 - o Controls horizontal slide
- Model No. PK296-03BA-A3-3/8
 - o Double shaft
 - o With fail safe brake
 - o Controls vertical slide
- Two-phase
- accuracy of ± 3 arc minutes (0.05°)
 - o This error does not accumulate from step to step

Probe Mounting

The probe mounting arm is attached to the vertical axis plate on the traverse, and extends down into the flow through a slot in the top of the tunnel. The probe arm is enclosed in an aluminum aerodynamic strut, and probes can be mounted at the end of the arm. The hole in the top of the tunnel is only 24" long, so to allow for positioning of the probe outside of this region, a probe arm extension (80/20 beam) can be used.

The aerodynamic strut is hollow which allows routing of any probe cabling/tubes up through the center, to the top of the tunnel. With the mounting arm extended into the tunnel, the two hole covers must be secured around the strut to cover the hole in the top of the tunnel.

For dimensioned drawings of the probe mounting parts, see "Selected Part Drawings" at the end of this manual.

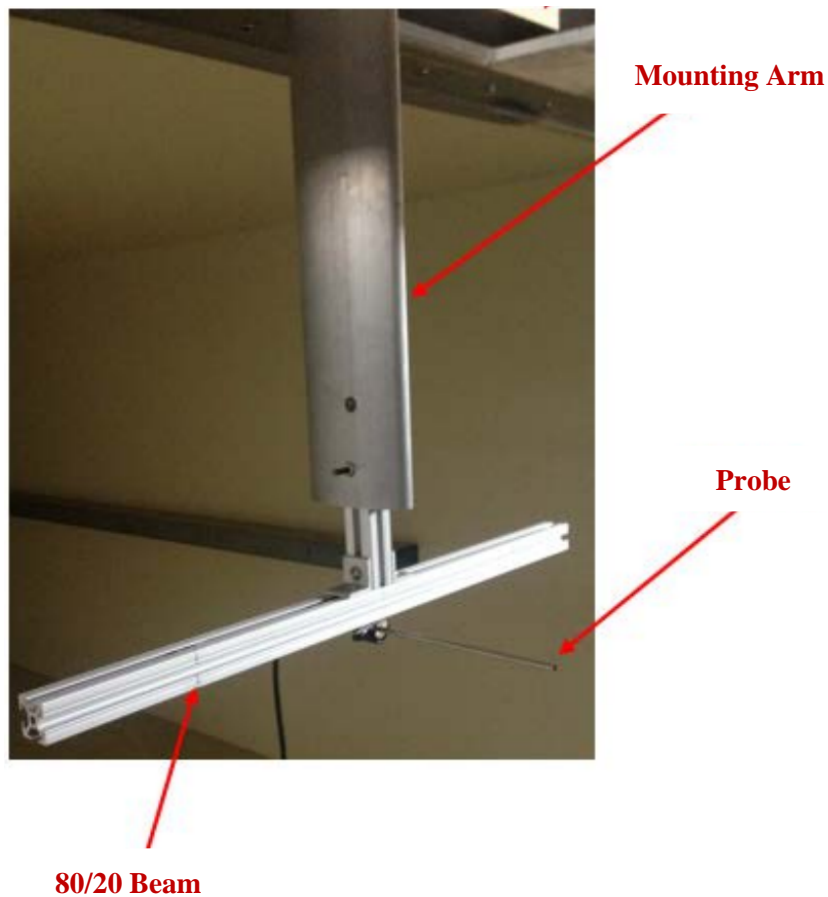


Figure 39: Traverse probe mounting configuration

Running the Traverse

Setup

If the traverse has not been used for some time or the lead screw and ways appear dry of lubricant, lubricate with Velmex BL-1 oil.

- Continuous use applications with heavy loads may necessitate daily lubrication.
- To lubricate, traverse carriage near center of travel and apply 3 to 4 drops of oil to the end of carriage at the way surfaces and on the lead screw threads.
- Apply oil to both ends of carriage

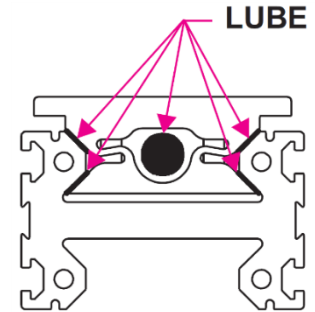


Figure 40: Traverse lubrication points

Moving the Traverse

If the traverse needs to be stopped immediately press red STOP button

1. Switch on the traverse using the switch mounted above the computer desk
2. Open the “Move Traverse.vi” code which runs the traverse.
3. Ensure that the hole on top of the tunnel for the mounting arm is open
4. Run the vi code but do not move the traverse yet
5. Center the mounting arm over the hole
 - Use the horizontal movement value selector and *move* button to do this
 - **DO NOT press “center” button while arm is above the tunnel**
6. Once the arm is centered it can be lowered into the tunnel
 - Use the vertical movement value selector and *move* button to do this

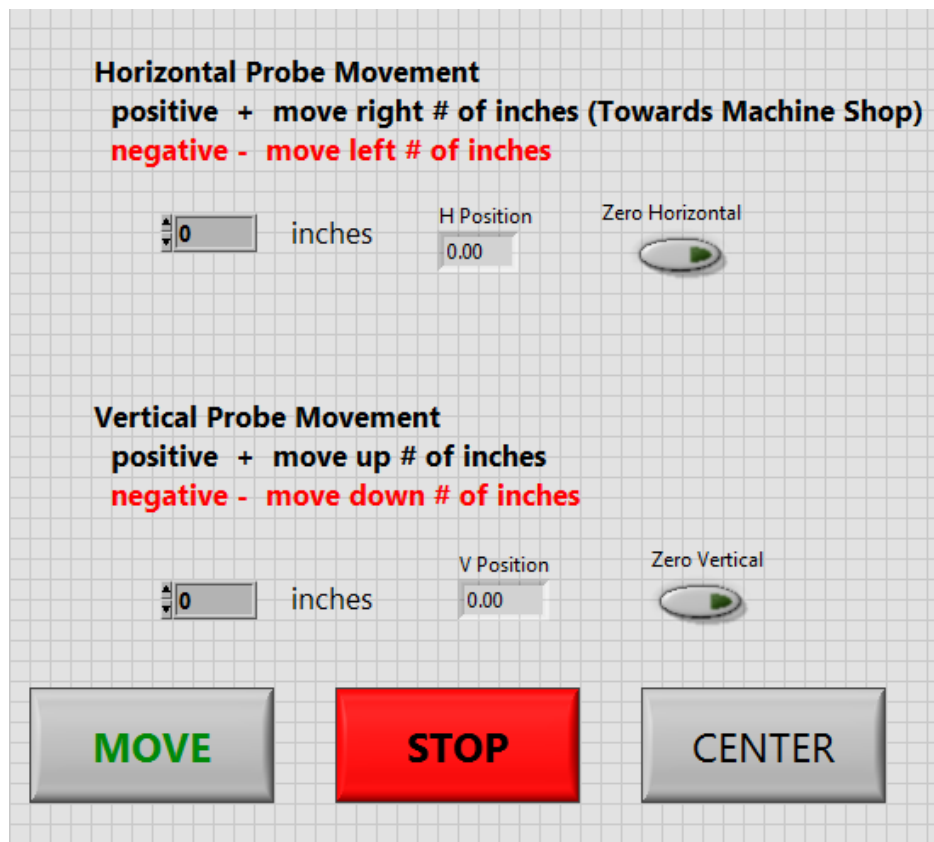


Figure 41: Traverse movement LabVIEW Interface

7. Secure the hole cover around the mounting arm
8. When using the hole cover
 - Ensure the strings holding the ends of the cover are not worn or broken
 - If broken or worn replace the strings
 - The ends of the cover must lift up when the traverse is at the ends of its travel and must stay down when over the hole in the tunnel
 - This may take some adjustment in string length.

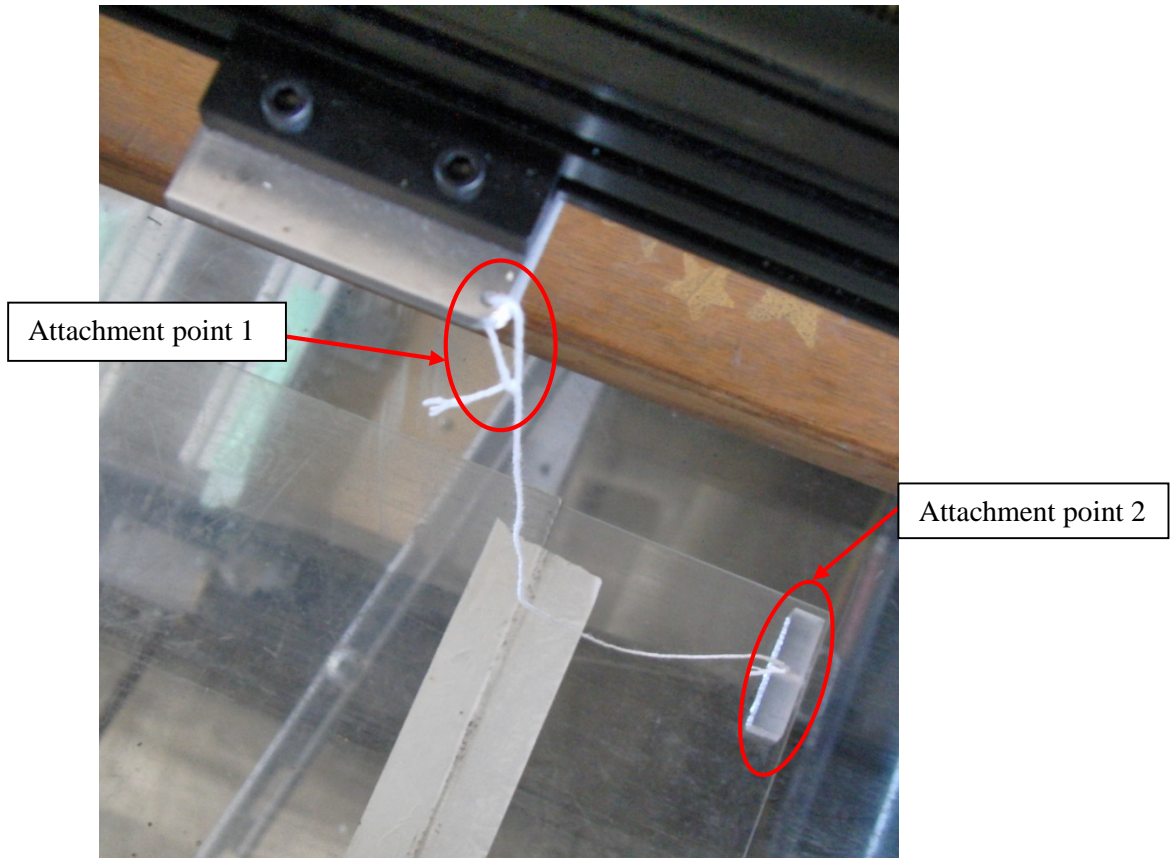


Figure 42: Hole cover lifting points

LabVIEW Implementation

The following information outlines a basic LabVIEW implementation of manually inputted traverse movements. The structures within this simple program can be extrapolated for programs that are more complex.

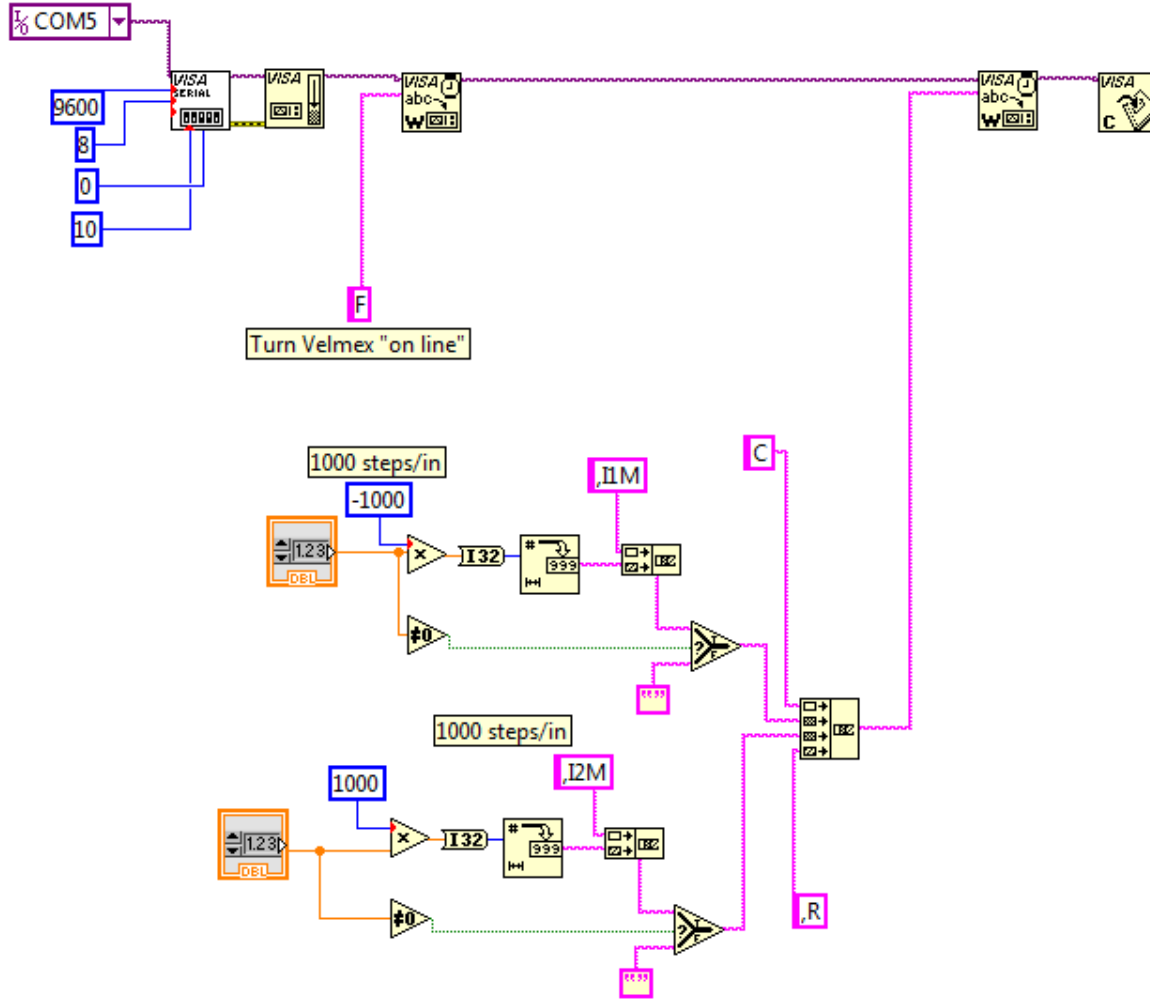


Figure 43: LabVIEW program - manually inputted traverse movement

The upper half of the program is where the traverse is configured. Currently the traverse system is connected to COM5, which controls both axis of the traverse.

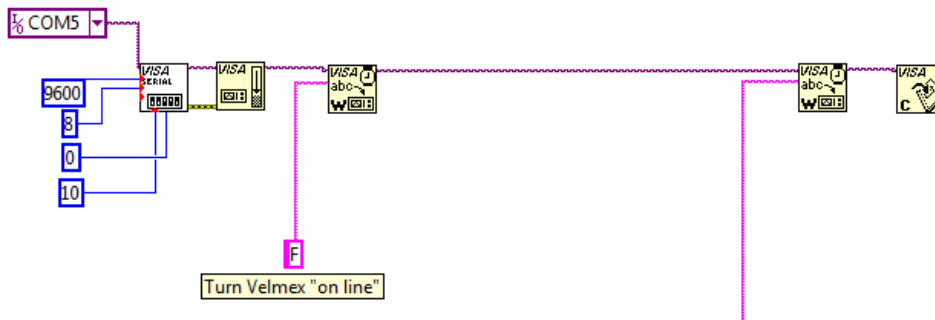


Figure 44: Traverse configuration setup

The lower half of the program controls the movement of the traverse. The program takes in two values, in inches, from the front panel and moves the horizontal and vertical axis by their respective amounts. Both user inputs have to be multiplied by 1000 because the Velmex control works in motor steps rather than absolute distances (1 step = 0.001 inch).

I1M controls the vertical axis movement, and the input distance is multiplied by -1000, which allows a positive input to correspond to an upward movement of the traverse. I2M controls the horizontal axis movement, where a positive input moves the traverse towards the north side of the test section.

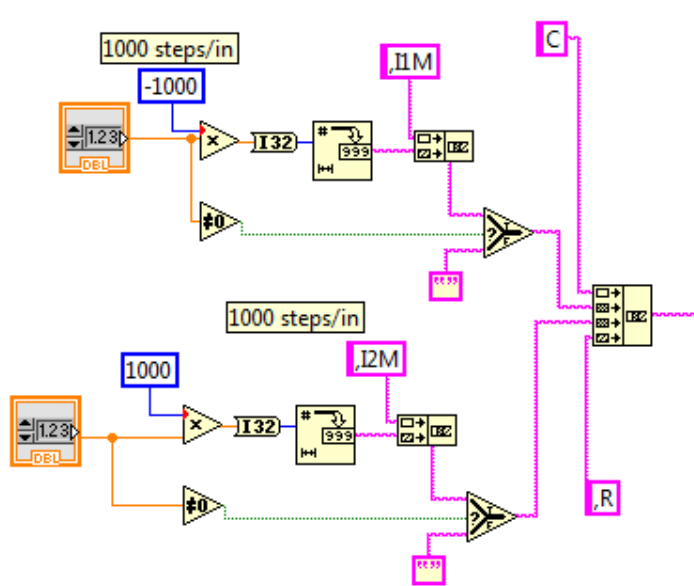


Figure 45: Traverse movement configuration

If the Velmex controller were to receive a value of zero for the distance, the traverse would move continuously in one direction until it hit the limit switches rather than not moving at all. The true/false block is critical in mitigating this, and allows for a true zero distance input at the front panel.

BiSlide Construction Delivers High Precision and Long Life

Large, Versatile Carriage – provides a 4.6" x 3.1" mounting surface suitable for carrying anything from assembly fixture to a measuring probe – eight threaded attachment holes let you securely fasten any kind of payload. Also, there's four accessory holes for limit switch cam or other sensors. Carriage has fit and wear compensation adjustments

Precision Lead Screw – we make our own lead screws to make sure they're the best quality. Precision rolled acme thread, hard nickel plated for smooth, trouble-free operation and long life

Support Bearing – delivers just the right combination of constraint and anti-vibration qualities for the lead screw

StabilNut™ – a Velmex exclusive, is the "solid", low friction connection between the lead screw and carriage. It has an antibacklash design with fine mesh adjustment for responsive rotary to linear translation

End Plate – provides a convenient way to directly mount a BiSlide assembly on end. Four hole pattern mates with other BiSlide carriages and T-slots

Motor Plate – the four bolt design securely attaches the motor

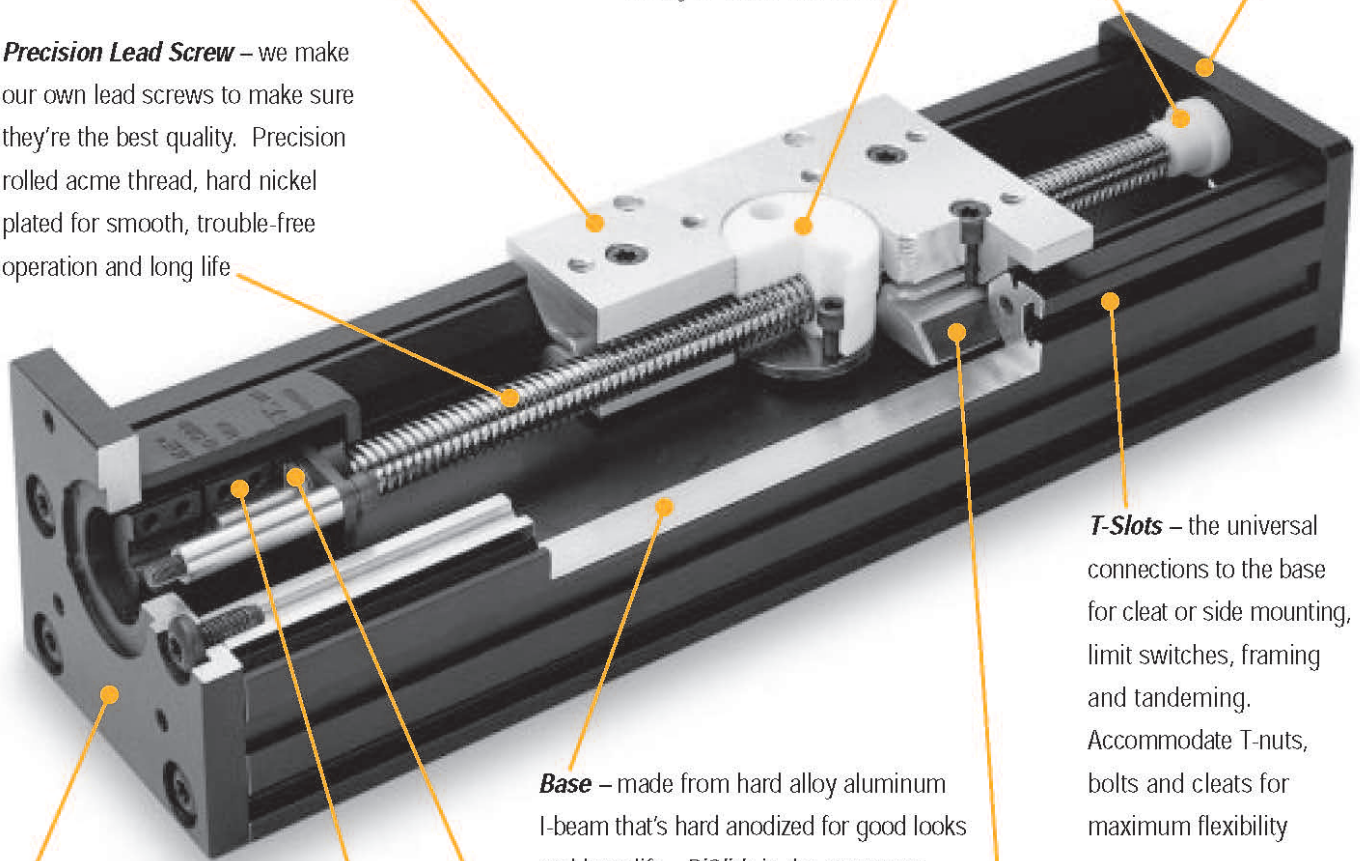
Coupling – precision-honed to provide a rigid motor to lead screw mating

Base – made from hard alloy aluminum I-beam that's hard anodized for good looks and long life. BiSlide is the strongest, lightest, and most durable slide actuator available

Roller Bearings – preloaded to provide axial constraint for the lead screw. Designed for high capacity, for impact resistance and long life

Bearing Pads – super slick PTFE compound for lowest friction, smooth linear motion, and long life

T-Slots – the universal connections to the base for cleat or side mounting, limit switches, framing and tandeming. Accommodate T-nuts, bolts and cleats for maximum flexibility



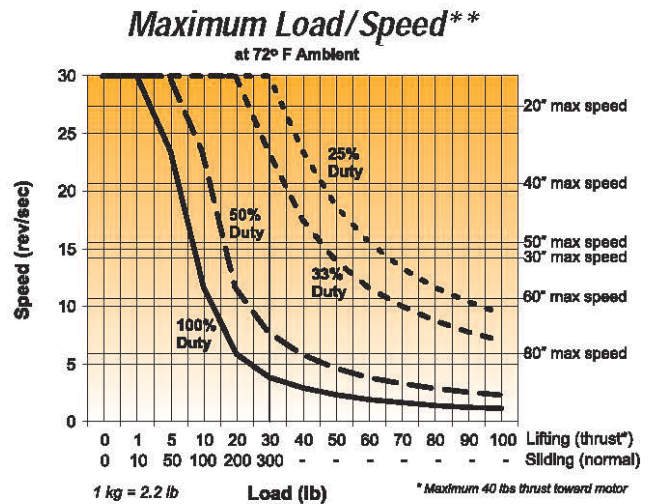
A Versatile, Durable Design

BiSlide Delivers the Accuracy and Load-Carrying Capacity You Need

- Coefficient of friction:** 0.09 typical
- Coefficient range:** 0.04 (Heavy Load Dynamic) to 0.15-0.3 (Lubricated Heavy Load Static>1 hour)
- Minimum motor torque required:** 55 oz-in
- Repeatability:** 0.0002" over short term, long term dependant on wear
- Straight line accuracy:** 0.003" over entire travel distance
- Screw lead accuracy:** 0.003"/10" (0.076 mm/25 cm)
- Operating temperature:** 0 to 180° F (-18 to 82° C)

Finish

- Lead screw:** hard nickel plated
- Carriage:** machined aluminum
- Other surfaces:** black anodized aluminum

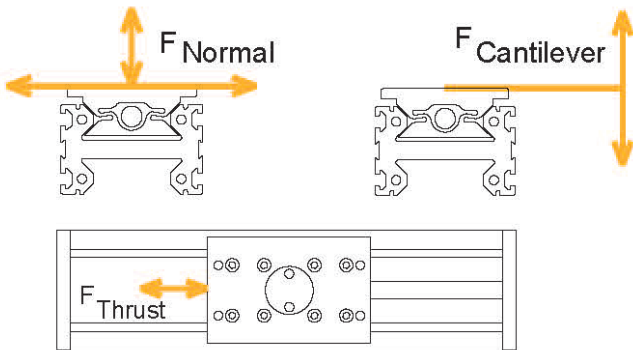


**In other environments contact our technical sales department for recommendations

Maximum Load Carrying Capacity

Load	Dynamic	Static	Momentary
Normal Centered	300 lb.	300 lb.	1000 lb.
Thrust	100 lb*	200 lb.	300 lb.
Cantilevered	500 inch-lb. (See formula below)		

For cantilevered loads: equivalent center load = $(d \times L/2) + L$
where d= distance load is from center in inches, L= Load (lbs.)



How to Specify Your BiSlide Model

M N 1 0 - 0 2 0 0 - E 0 1 - 2 1

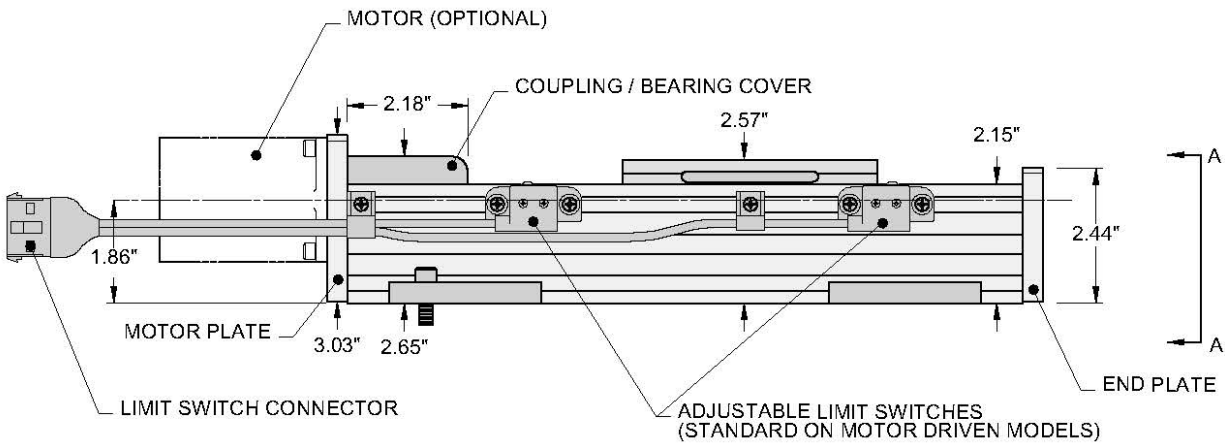
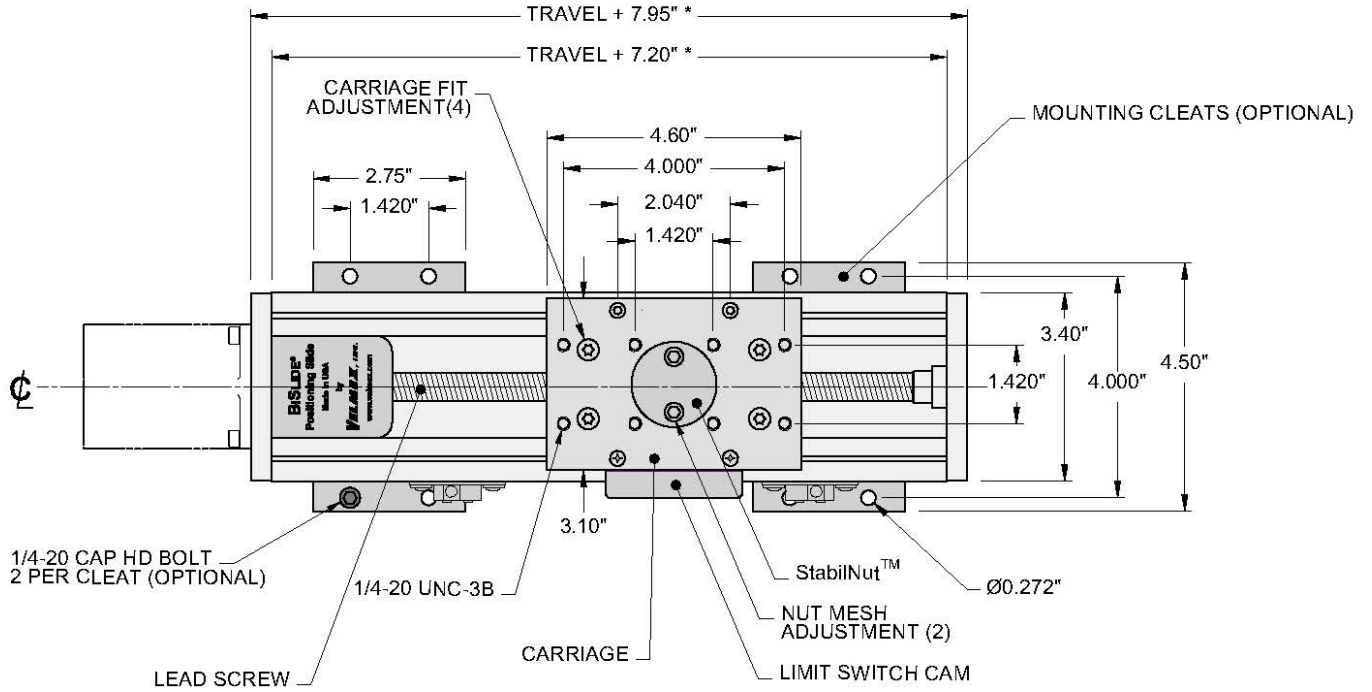
Cross Section M	Design	Lead Screw	Advance/Turn	Mounting
	10=Inch	Blank	None	Blank=None
	11=Inch & Way Cover	M02	2.00 mm	11=Basic Knob
Drive Scheme		E01	0.10 inches	12=Knob/Counter, Horizontal, Increment + from Knob
N=Nut/Screw Drive		E04	0.40 inches	13=Knob/Counter, Vertical, Increment + from Knob**
F=Free Sliding				14=Knob/Counter, Horizontal, Increment - from Knob
				15=Knob/Counter, Vertical, Increment - from Knob**
				20=NEMA 23 Motor Mount
				21=NEMA 23 Mount & Limit Switch
				30=NEMA 34 Motor Mount
				31=NEMA 34 Mount & Limit Switch

Design Travel* (Tenth of Inch)
Standard Travel Lengths (Inches):
5, 10, 15, 20, 30, 40, 50, 60, 80
*Free sliding models have 2.4" longer travel,
way cover models under 40" travel have 1.0" less

**For BiSlides oriented vertically with the knob up.
Use the horizontal reading (-12 or -14) for applications with knob down.

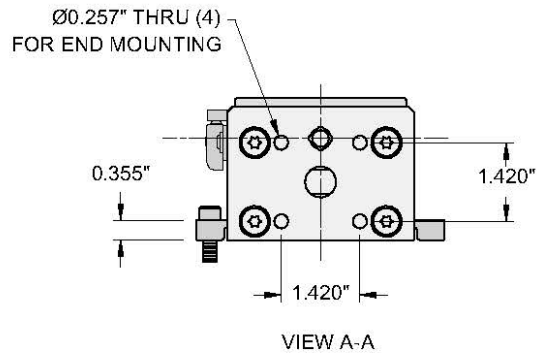
BiSlide Assembly Series M Dimensions

* ADD 2.40" FOR UNITS WITH 40" TRAVEL AND LONGER

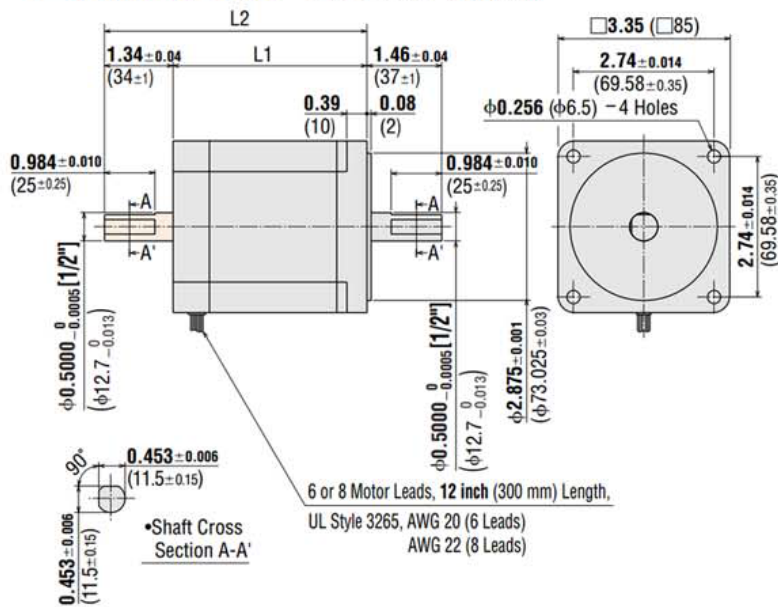


Travel Length (Inches)	Cleats Recommended**
5	4
10	4-6
15	4-8
20	6-10
30	8-12
40	10-14
50	12-16
60	14-18
80	16-20

**Use higher number for heavy loads



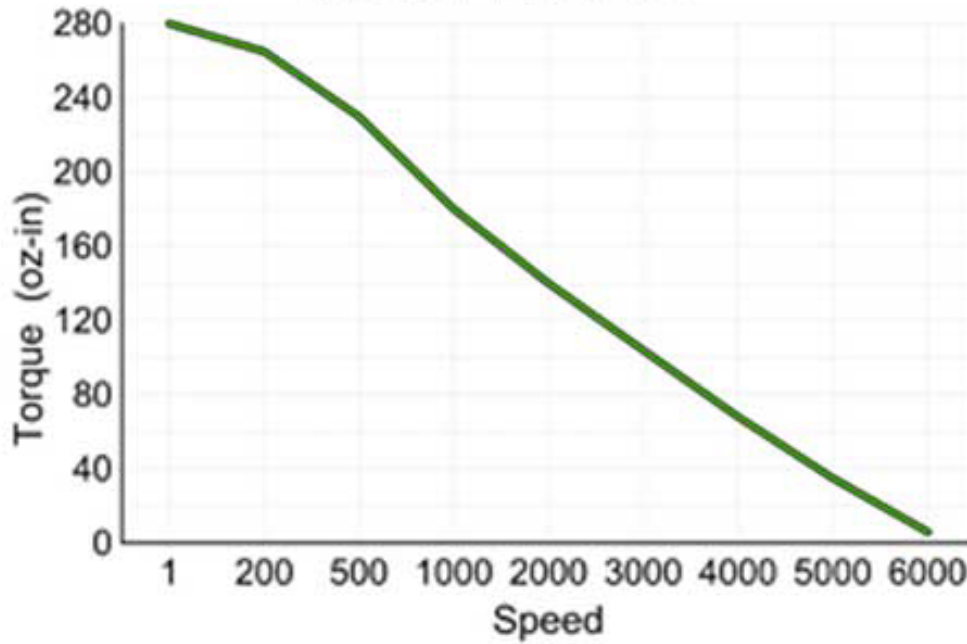
Dimensions Scale 1/4, Unit = inch (mm)



Model	L1 inch (mm)	L2 inch (mm)	Weight lb. (kg)	DXF
PK296-0 □ AA PK296-F4.5A	2.60 (66)	—	3.7 (1.7)	B122U
PK296-0 □ BA PK296-F4.5B		3.94 (100)		

- Enter the winding specification in the box (□) within the model name.
- These dimensions are for double shaft models. For single shaft models, ignore the shaded area.

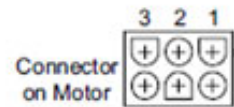
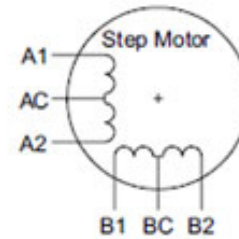
Vexta PK296-03



Motor Wiring (for Velmex installed step motors)

Pin	Motor	Cable (6 wire)	Slo-Syn	Vexta	Pacific Scientific*
1	BC	W	W	W	W/Y & W/R
2	B2	Gn	Gn	Bu	R
3	AC	Bk	Bk	Y	W/Bk & W/O
4	A2	Or	W/R	Bk	O
5	A1	R	R	Gn	Bk
6	B1	Bu	W/Gn	R	Y

* 8 lead motor with wires combined at AC and BC for 6 lead configuration



Amp 1-480705-0
(mates with: 1-480704-0 on Cable)

SMOKE WAND

Instrumentation

AEROLAB electric-powered Smoke Generator

- **White mineral oil fluid**
 - o KAYDOL® White Mineral Oil
 - o Drakeol® 19 MIN OIL USP
 - o Or similar
- 18” long smoke wand
- Compressed air supply: 20 – 150 psig
- Automatic temperature setting
- Electrical power: 110VAC ONLY
- 45 minutes of runtime (full reservoir)
- 1 gallon reservoir



Figure 46: AEROLAB smoke generator

Location and Installation

The access hole for putting the smoke wand into the tunnel is located on the right side of the test section door.

Instruction Manual

The following instruction manual is from AEROLAB; use the instructions from this manual instead of the ones on the side of the smoke generator.

MAKE SURE YOU HAVE THE BUCKET OF GRAVEL TO CATCH ANY DRIPPING OIL

AEROLAB



AEROLAB Complete Smoke Generator System Owner's Manual / Operating Instructions

V11.1

AEROLAB Complete Smoke Generator System - Operating Instructions

Specifications

The AEROLAB Complete Smoke Generator System is supplied with the following items:

- Base/Power Unit
- Corded Smoke Wand (short or long)
- Smoke Wand Protective Cap
- One Gallon (3.70 liter) Smoke Fluid (Propylene Glycol or White Mineral Oil)
- Airline Fitting
- Funnel and Heat-resistant Collector Can
- Owner's / Operator's Manual (this document)

Base/Power Unit

- 14.5 inches (36.8cm) long, 5 inches (12.7cm) deep, 7.25 inches (18.4) tall inclusive of all knobs and fittings
- 9.8 pounds (4.4kg) excluding smoke fluid

Short Smoke Wand

- 18 inches (46cm) long
- 1.8 pounds (0.8kg) including cabling

Long Smoke Wand

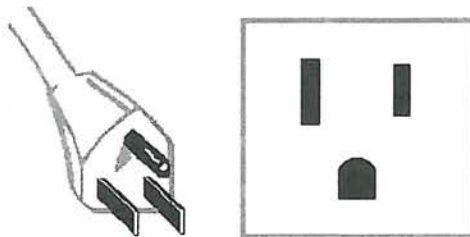
- 45 inches (114cm) long
- 2.2 pounds (1kg) including cabling

Electrical Requirements

- The Smoke Wand must never be plugged directly into domestic power. This is dangerous and permanent damage to the wand will result.
- **110VAC ONLY**
- 375 Watts
- Type B Extension Cord (Not included)

Compressed Air Requirements

- 150 psig (1,034 KPa) maximum
- 1 pint (475cc) per hour



Type B Extension Cord

System Warnings

**** NOTE ****

The AEROLAB Smoke Generator can be used with 110-120VAC 50/60Hz ONLY!

The system draws 375 Watts.

1. Read and understand this manual before operating the unit.
2. NEVER plug the smoke wand directly into a wall outlet. It should ONLY be plugged into the base/power unit.
3. Make sure the unit is sitting in an upright position at all times! It should NEVER be positioned or stored on its side!!
4. Use the recommended smoke fluid only. Failure to do so may cause injury and/or permanent damage to the system. The system is designed for propylene glycol or white mineral oil, only. These fluids are available directly from Aerolab (301)-776-6585.
5. During operation and cool-down, do not touch the wand near the tip. Severe burns may result.
6. If the smoke fluid reservoir runs empty, immediately turn **POWER OFF**. Allow air to pass through the system for at least 10 minutes. Failure to do this may clog the tip and result in costly repairs.
7. To shut down the unit: First, turn Power OFF. Then, allow smoke fluid to drip from the wand for least 7 minutes or until cool.
8. Failure to follow proper shut-down procedure will likely clog the tip and result in costly repairs.
9. Systems Using White Mineral Oil: Never position the wand tip less than 5 inches (13cm) to an object. Vapor combustion could result.

AEROLAB Complete Smoke Generator System - Operating Instructions

Introduction

The AEROLAB Smoke Generator vaporizes a fluid (white mineral oil or propylene glycol) as it flows through an electronically-heated, small-diameter stainless steel tube. Although the system is referred to as a smoke generator, it does not burn the fluid or produce smoke.

The base/power unit (black) consists of a compressed air pressure regulator, a fluid reservoir, a wand tip temperature controller and a fluid flow valve. The system requires compressed air (supplied by your existing compressed air system), a standard electric extension cord and 110-120VAC. The internal regulator ensures the system will not be over pressurized. The regulated compressed air drives the smoke fluid from the reservoir to the wand tip. In the tip, the smoke fluid is vaporized as it passes by a heating element.

AEROLAB Complete Smoke Generator System - Operating Instructions

Controls and Connections



Top View of the Base/Power Unit

PRESSURE REGULATOR – Allows the Operator to adjust the compressed air pressure in the smoke fluid reservoir.

Pressure Gauge – Indicates the current air pressure within the smoke fluid reservoir.

FLUID FILLER PLUG – A screw-in cap for the smoke fluid reservoir.

TEMPERATURE CONTROLLER – Calibrated and set at AEROLAB, this component maintains correct smoke wand temperature.

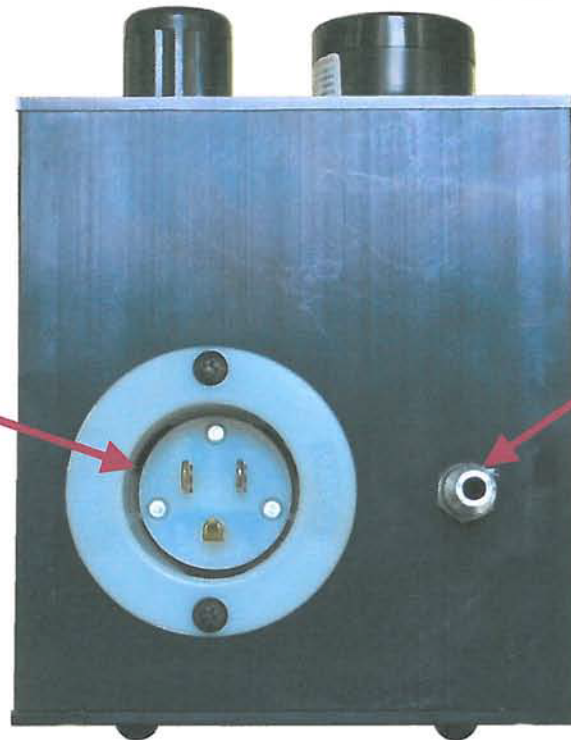
FLUID FLOW – This knob controls smoke fluid flow from the reservoir to the smoke wand.

POWER – This switch powers the base/power unit and the smoke wand.

AEROLAB Complete Smoke Generator System - Operating Instructions

Main Power Input
Type B plug
110-120 VAC ONLY

Compressed Air
Supply Input
150 psig Max.
(1,034 KPa)



Input Side of Base/Power Unit

Wand Temperature
Sensor Plug

Main Fuse
4 Amp Max.

Wand Power Cord
Plug

Wand Fluid Tube
Connection



Output Side of Base/Power Unit

AEROLAB Complete Smoke Generator System - Operating Instructions

Operation

Startup

Note: All Smoke Generator Systems are thoroughly tested at AEROLAB prior to shipment. As such, some residual fluid will be present in the smoke wand tubing and fluid reservoir. This is normal.

1. Ensure:
 - compressed air is **not** connected to the base/power unit
 - electrical power is **not** connected to the base/power unit
 - the **POWER** switch is **OFF**
2. Connect the wand fluid tube to the base/power unit.



3. Connect the wand power cord to the base/power unit.



AEROLAB Complete Smoke Generator System - Operating Instructions

4. Connect the temperature sensor plug to the base/power unit. Note: The plug is polarized – it can be inserted only one way. Do not force the plug.



All Wand Connections Complete

AEROLAB Complete Smoke Generator System - Operating Instructions

5. To remove the smoke wand tip protector cap, pull it off the wand. The protector cap is clearly labeled with a red cloth flag reading, "REMOVE BEFORE FLIGHT". Do not proceed to the next step until the protector cap has been removed. Never attempt to operate the system with the cap installed – permanent damage will result.



6. Remove the **FLUID FILLER PLUG** (turn the filler plug anticlockwise). Note: If pressure exists in the reservoir, a slight hissing sound will be heard as the filler plug is loosened. There is no danger.



AEROLAB Complete Smoke Generator System - Operating Instructions

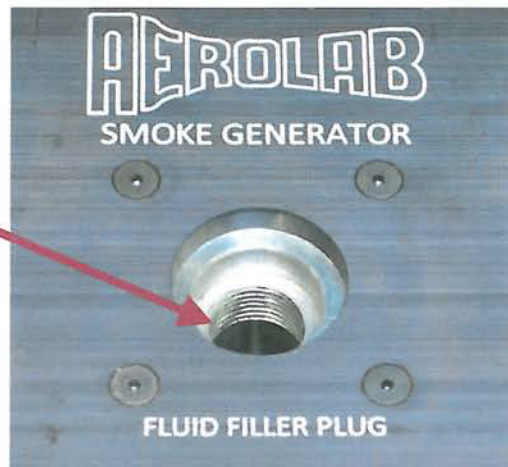


7. Using the supplied funnel, fill the fluid reservoir with an approved fluid. The fluid can be filled up to the bottom of the filler plug threads.



AEROLAB Complete Smoke Generator System - Operating Instructions

Maximum Fluid Fill
Height



8. Reinstall the **FLUID FILLER PLUG** (turn the filler plug clockwise).
9. Close the **FLUID FLOW** valve. To do so, turn the knob clockwise.



AEROLAB Complete Smoke Generator System - Operating Instructions

10. Connect electrical power to the base/power unit.



11. Connect compressed air to the base/power unit. Note: Compressed air supply must not exceed 150 psig (1,034 KPa).



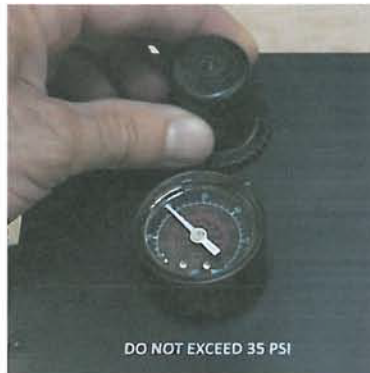
All Input Connections
Complete

AEROLAB Complete Smoke Generator System - Operating Instructions

12. Pull up on the **PRESSURE REGULATOR** knob to unlock it for adjustment.



13. While watching the air pressure gauge, turn the **PRESSURE REGULATOR** knob clockwise or anticlockwise to adjust the reservoir pressure to 20 psig.



14. Press down on the Pressure Regulator knob to lock the setting



Should be fill
with small rocks

15. Position the smoke wand tip over the supplied heat-resistant metal can. Smoke fluid will be discharged in the following steps.

16. Turn the **FLUID FLOW** knob anticlockwise $\frac{1}{8}$ to $\frac{1}{4}$ of a turn. This will begin fluid flow to the smoke wand. (Turning FLUID FLOW knob more than $\frac{1}{4}$ turn will keep unit from heating up fully)

17. Watch the smoke wand tip. Do not proceed to the next step until there is a steady drip of fluid.

18. Turn **POWER ON**. Soon, the steady drip of fluid will become a steady stream and then white vapor.

Notes:

- Upon turning **POWER ON**, the **TEMPERATURE CONTROLLER** will indicate **YCA** and then **rLY**. This is normal.



AEROLAB Complete Smoke Generator System - Operating Instructions



The system is now ready for use.

Notes:

- The smoke wand tip becomes very hot. Do not touch the wand tip to skin or combustible materials – burns or fire will likely result.
- The wand temperature was adjusted and set at AEROLAB during pre-delivery testing. Temperature adjustment is possible, but not recommended (see Temperature Adjustment – Not Recommended)

Normal Shutdown

1. Position the smoke wand tip over a heat-resistant vessel such as a metal can. Smoke fluid will be discharged in the following steps.
2. Turn **POWER** OFF. Soon, the white vapor will become a steady stream and then a steady drip.
3. Allow the wand to drip for at least 7 minutes. After this time, the wand should be cool to the touch.
4. Turn the **FLUID FLOW** knob clockwise until it stops. This will stop the fluid flow to the smoke wand.
5. Disconnect electrical power from the base/power unit.
6. Disconnect compressed air supply from the base/power unit.
7. Reinstall the smoke wand tip protector cap.

The system is now completely shutdown.

AEROLAB Complete Smoke Generator System - Operating Instructions

Notes:

- Do not reinstall the smoke wand tip protector cap until you are certain the wand is cool. Otherwise, burns could result.
- Following normal shutdown, fluid will remain in the smoke wand and delivery tube. This is normal.
- Pressure will remain in the fluid reservoir. It is not necessary to remove this pressure.

Loss of Smoke Fluid / Abnormal Shutdown

If the reservoir becomes empty during use, follow these steps.

1. Turn **POWER OFF**.
2. Allow air to pass through the wand for at least 10 minutes. After this time, the wand should be cool to the touch.
3. Disconnect compressed air supply from the base/power unit.
4. To prepare the system for use, proceed to Startup, step #1.

System Storage

Ensure:

- the **POWER** switch is **OFF**
- the smoke wand is cool
- the smoke wand protector cap is installed
- compressed air is ***not*** connected to the base/power unit
- electrical power is ***not*** connected to the base/power unit
- the wand is not connected to the base/power unit
- the **FLUID FLOW** knob is turned clockwise until it stops

Notes:

- Never position the base/power unit on its side or ends. It must be stored upright.
- It is OK to store the system with fluid in the reservoir.
- It is okay to store the system with pressure in the reservoir.
- To avoid spilled smoke fluid, it is best to hang the smoke wand and cabling above a collector vessel for a period of 1 to 2 days. After this time, store the wand and cabling on a flat surface away from sunlight and heat.

Troubleshooting

If the **TEMPERATURE CONTROLLER** does not become active upon **POWER ON**:

- Ensure power is properly connected to the base/power unit.
- Check the power fuse located on the output side of the base/power unit. If open, replace with similar 4 Amp fuse – never use a larger fuse.
- If these measures do not correct the problem, contact AEROLAB.

If white vapor turns to liquid fluid during use:

- Position the wand tip over a non-combustible collector vessel.
- Ensure the wand temperature sensor plug is properly inserted.
- Ensure the wand power plug is properly inserted.
- Ensure the base/power unit is properly connected to power.
- Ensure the fuse is not open.
- If these measures do not correct the problem, perform a Normal Shutdown and contact AEROLAB.

Temperature Adjustment – Not Recommended

During pre-delivery testing at AEROLAB, every Smoke Generator System is thoroughly tested. Additionally, the **TEMPERATURE CONTROLLER** is set for optimal smoke density. Adjustments to the wand temperature should be completely unnecessary for the majority of the system's service life. Improper adjustment of the wand temperature will result in diminished smoke density and substandard operation.

Over time, a slight increase in wand temperature may be necessary to ensure complete vaporization of the smoke fluid. The following steps are offered for this adjustment.

Note: The thickest smoke density is obtained at a wand temperature just above vaporization. Beyond this temperature, the vapor will become thin and translucent.

1. Startup the system as described in Startup.
2. Quickly touch and release the **MD** button on the **TEMPERATURE CONTROLLER**. Do not hold the button. The display will change to **Su**. Then, it will display the current temperature setting.

AEROLAB Complete Smoke Generator System - Operating Instructions



3. To increase or decrease the temperature setting, press the arrow buttons.
4. To accept the new temperature setting and save it to memory, quickly press and release the **MD** button.

Notes:

- During pre-delivery testing at AEROLAB, a temperature range was determined and programmed into the **TEMPERATURE CONTROLLER**. Do not attempt to increase this range or permanent damage to the wand will result. Attempts to change the original temperature range will void the warranty.
- Temperature settings will not effective until the **MD** button is pressed a second time (exiting the adjustment routine).
- Make **SMALL** temperature changes and then test.
- High wand temperatures do not increase smoke flow or density.



Wand Temperature Too Cool



Wand Temperature Too HOT



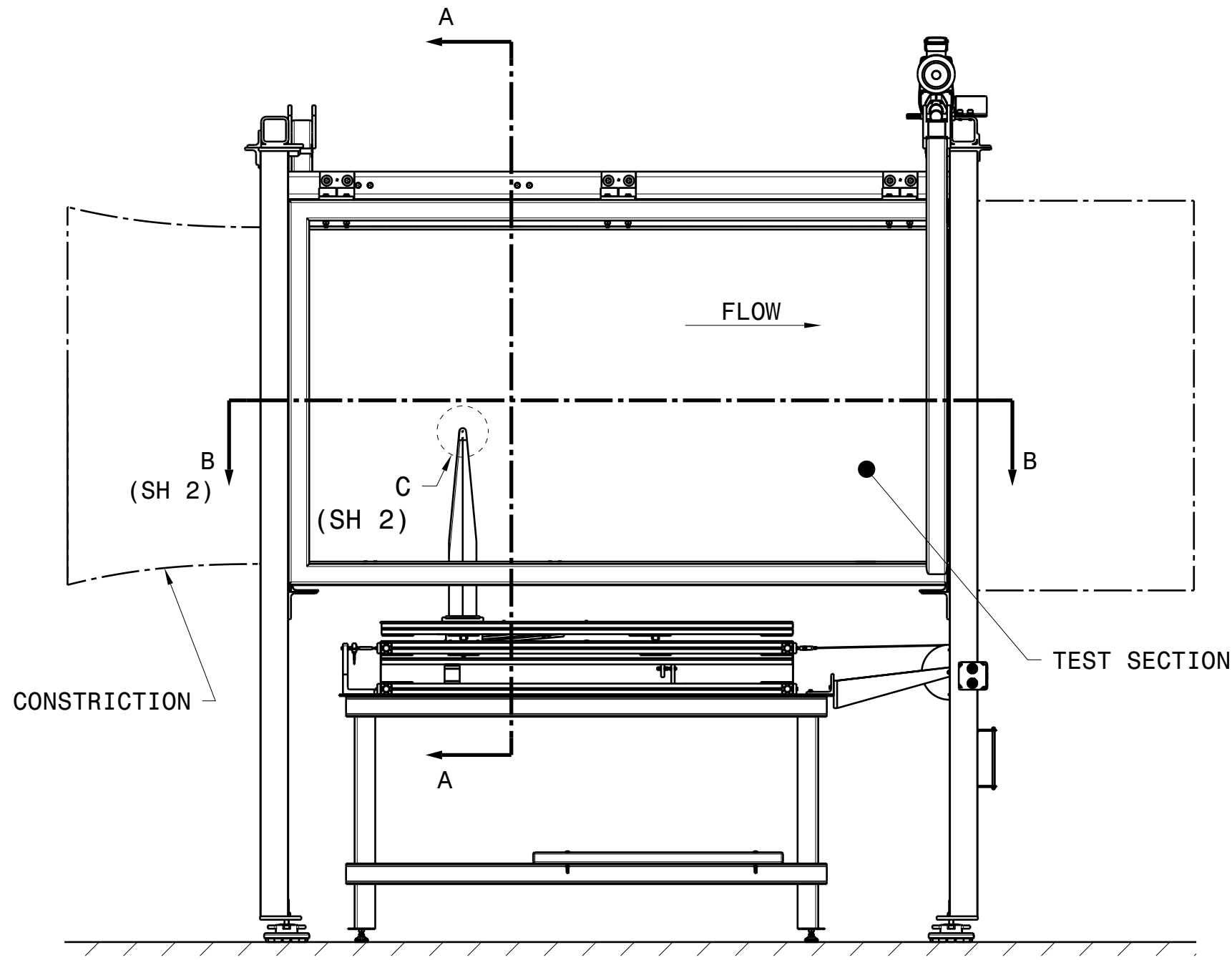
Perfect Wand Temperature

Contact AEROLAB

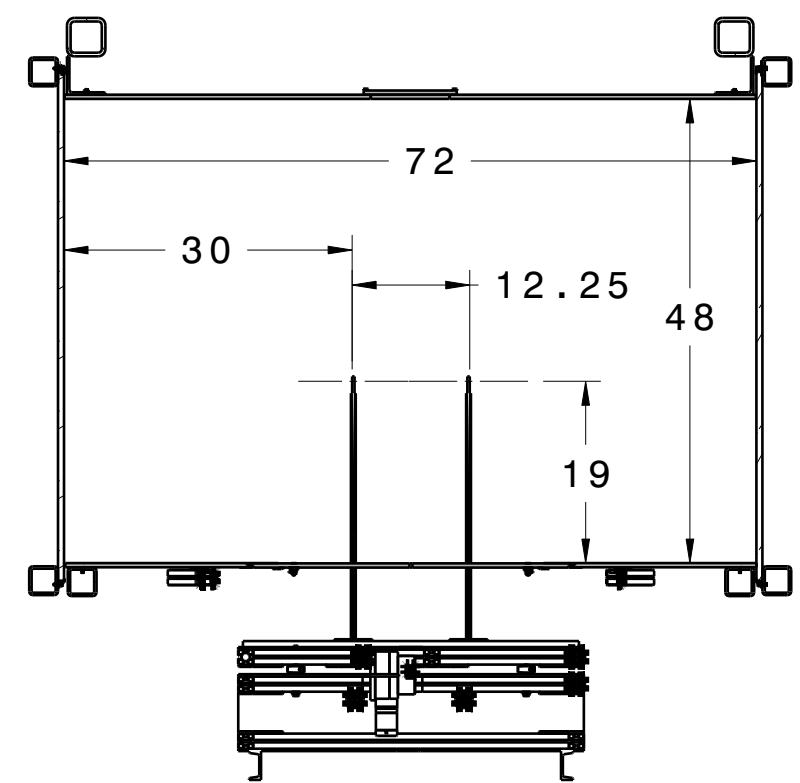
AEROLAB LLC
9580 Washington Boulevard
Laurel, Maryland 20723
(P) 301-776-6585
(F) 301-776-2892

www.aerolab.com
aerolab@aerolab.com

SELECTED PART DRAWINGS



Front view
Scale: 1:20



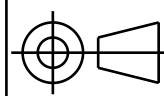
Section view A-A

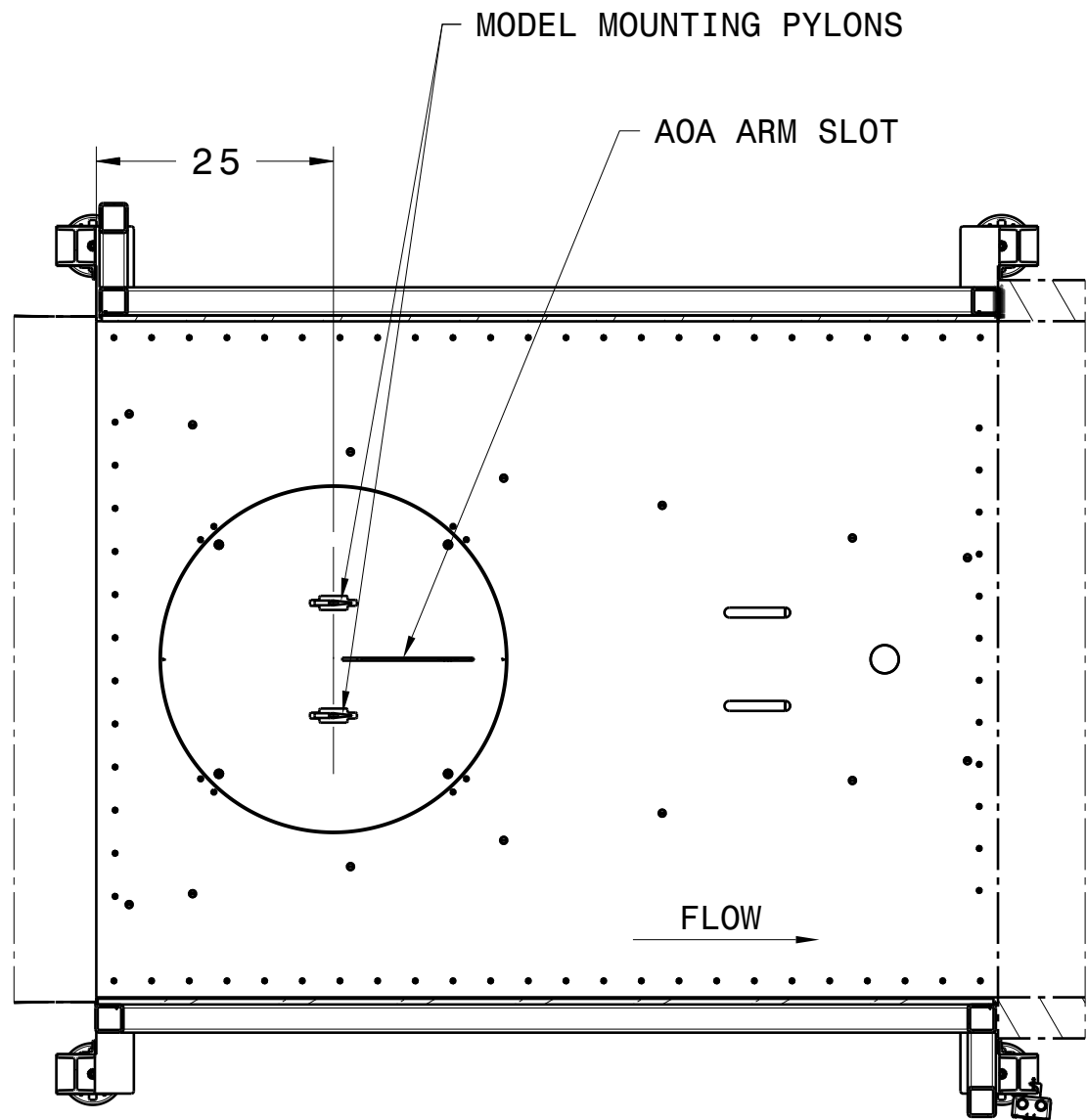
NOTES:

1. IT IS RECOMMENDED TO LEAVE SPACE BETWEEN THE MODEL AND THE TUNNEL DOORS.
2. ANGLE OF ATTACK ARM IS ADJUSTABLE. GENERAL SETUP USES ONE $\varnothing 0.25$ HOLE TO SECURE ARM TO MODEL.

UNLESS OTHERWISE SPECIFIED

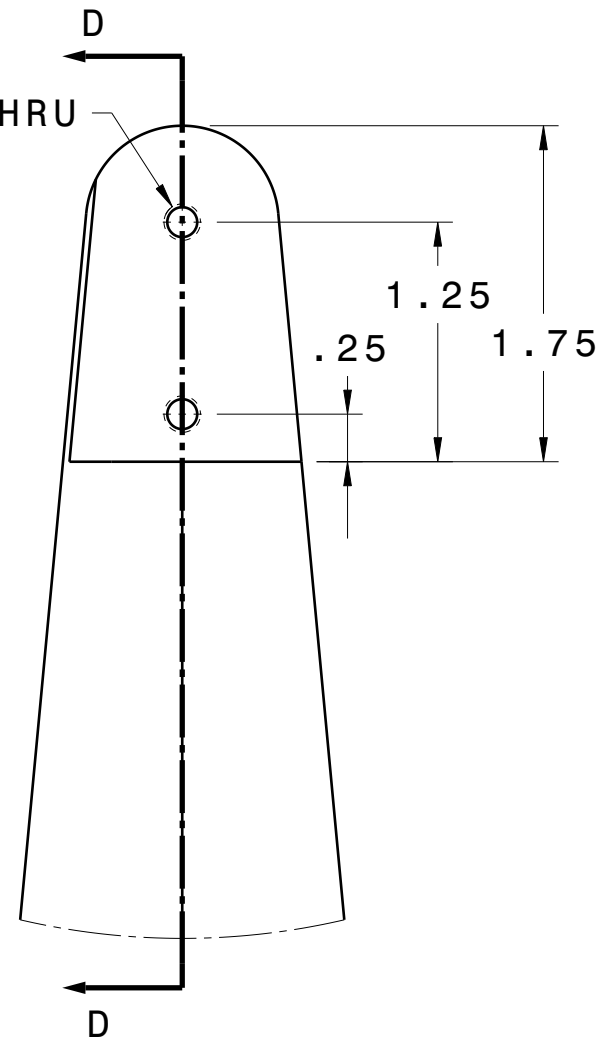
- TOLERANCES
X.X = ± 0.05
X.XX = ± 0.01
X.XXX = ± 0.005
- DEBURR HOLES AND BREAK SHARP EDGES.
- GEOMETRY IS DEFINED BY 3D SOLID MODELS.

DRAWN BY: 7/1/2019 P. BALDWIN		 PURDUE UNIVERSITY AERONAUTICS & ASTRONAUTICS	
SHEET SIZE B			
SCALE 1:20 & NOTED	ALL DIMENSIONS IN INCHES	DRAWING NUMBER XXXXXXXXXXXXXXXXXXXX	SHEET 1/2

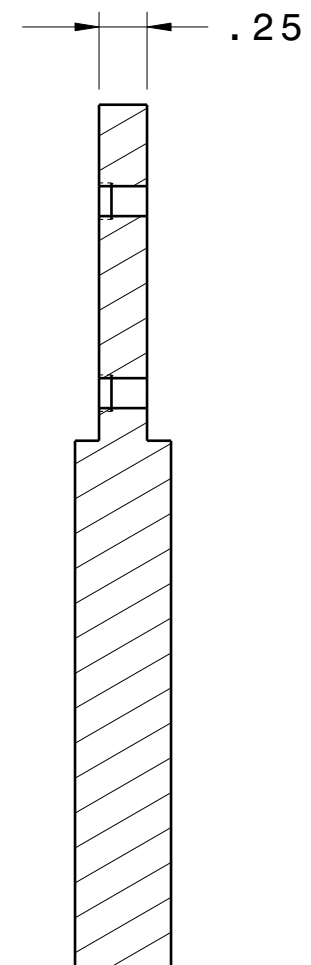


Section view B-B
(SH 1)

2X 10-32 UNF THRU

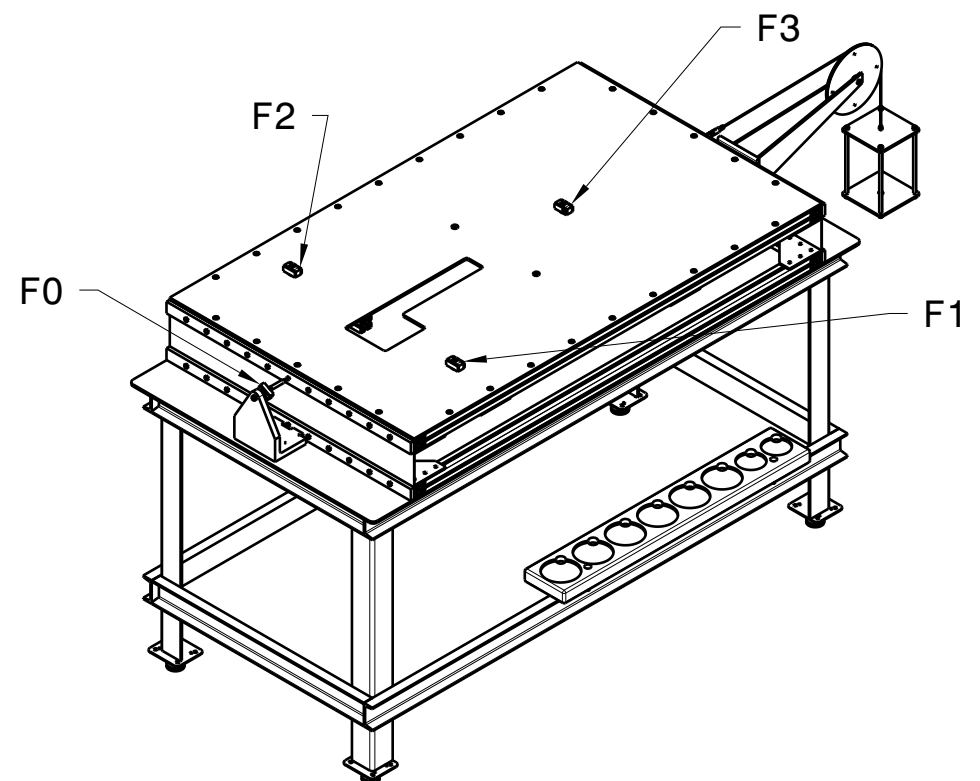
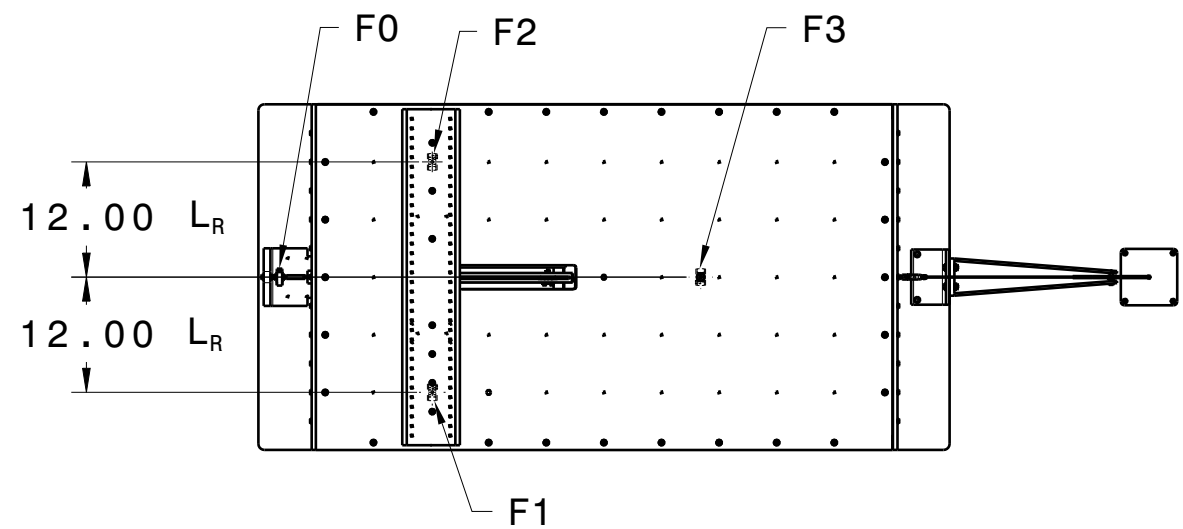


Detail C
(SH 1)
TYP 2 PL
Scale: 1:1

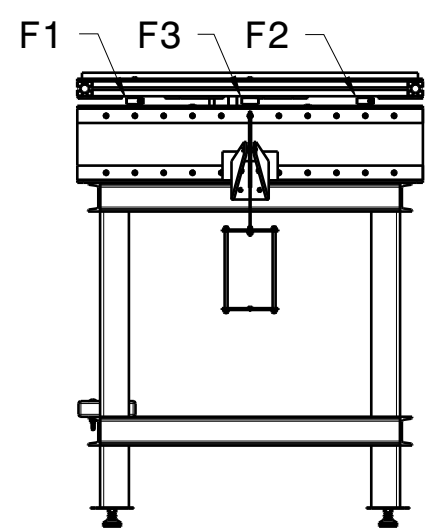
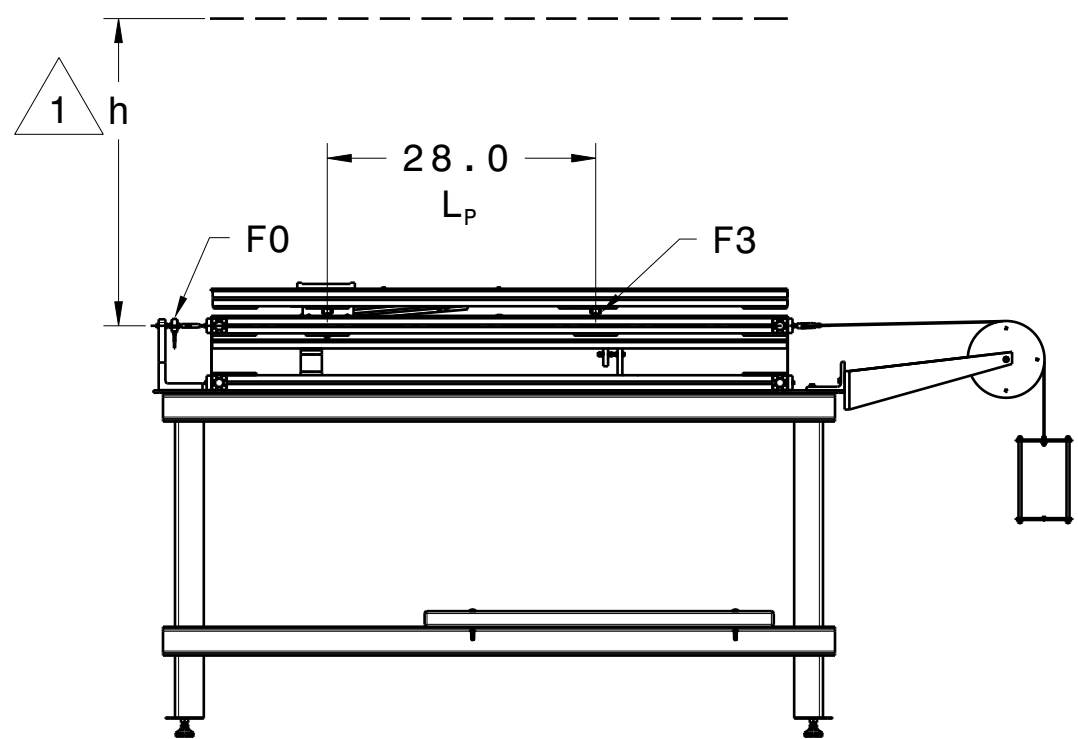
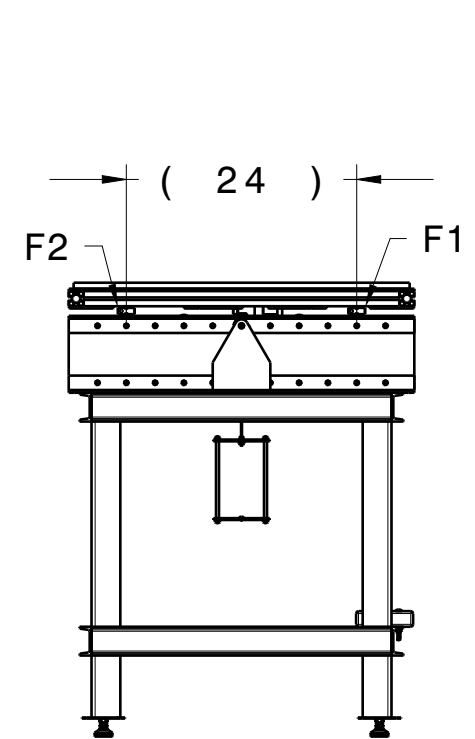


Section view D-D
Scale: 1:1

SHEET SIZE B		DRAWING NAME BOEING WIND TUNNEL - MODEL INTERFACE CONTROL	REVISION -A
SCALE 1:20 & NOTED		DRAWING NUMBER XXXXXXXXXXXXXXXXXXXX	SHEET 2/2
ALL DIMENSIONS IN INCHES			



Isometric view
TOP LEVEL NOT SHOWN FOR CLARITY



NOTES:

- 1 "h" IS THE HEIGHT FROM THE DRAG AXIS TO THE MODEL ROTATION AXIS. FOR THE STANDARD PYLONS, $h = 31.5$ INCHES.
2. FORCES AND MOMENTS ARE CALCULATED AS FOLLOWS:
 DRAG FORCE: $D = F_0$
 LIFT FORCE: $L = F_1 + F_2 + F_3$
 PITCHING MOMENT: $P = -L_p * F_3 + h * F_0$
 ROLLING MOMENT: $R = L_r * (F_1 - F_2)$

UNLESS OTHERWISE SPECIFIED
 TOLERANCES
 X.X = ±.05
 X.XX = ±.01
 X.XXX = ±.005
 DEBURR HOLES AND BREAK SHARP EDGES.
 GEOMETRY IS DEFINED BY 3D SOLID MODELS.

DESIGNED BY:
 DRAWN BY: 7/3/2019
 P. BALDWIN
 SHEET SIZE: B
 SCALE: 1:20
 ALL DIMENSIONS IN INCHES

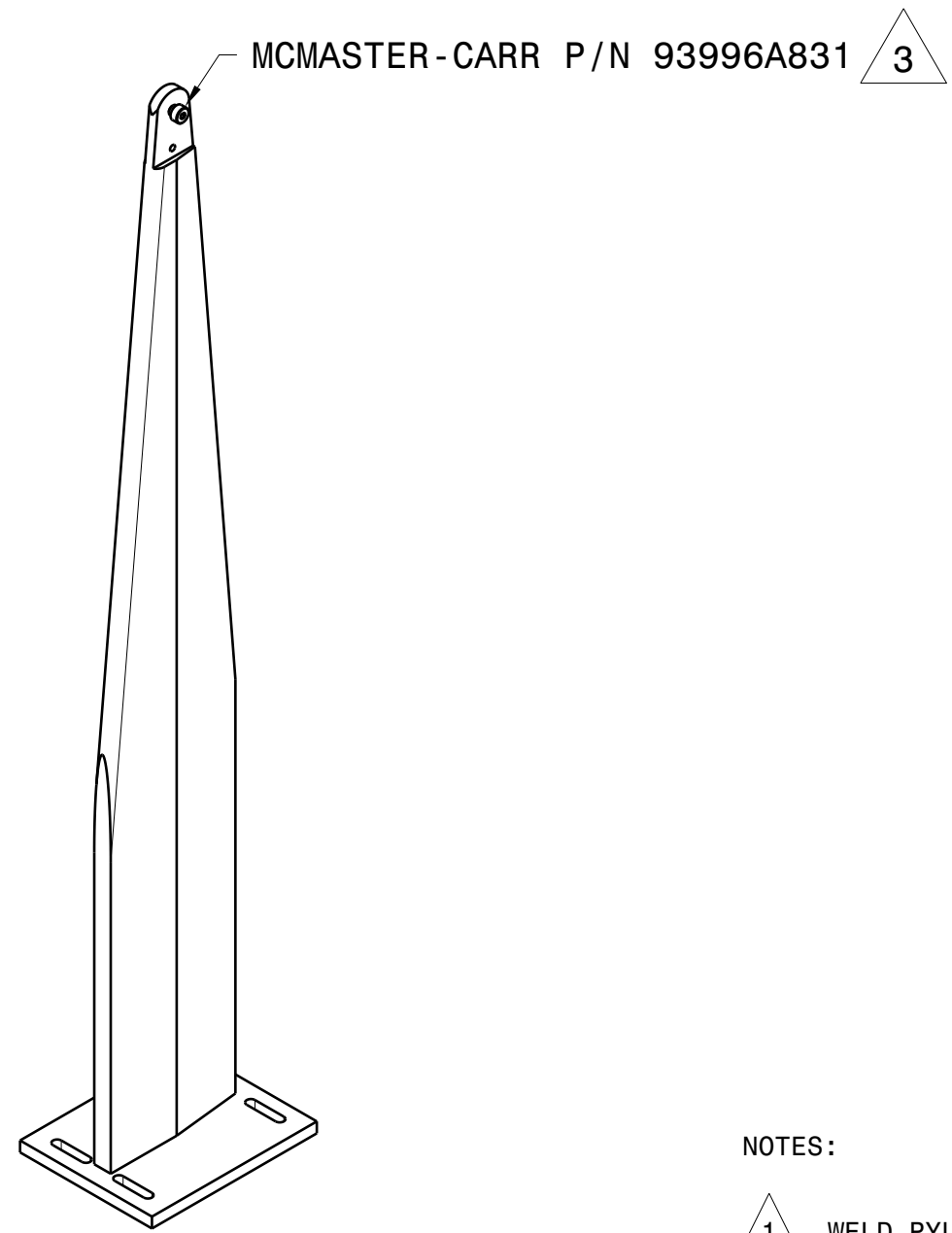
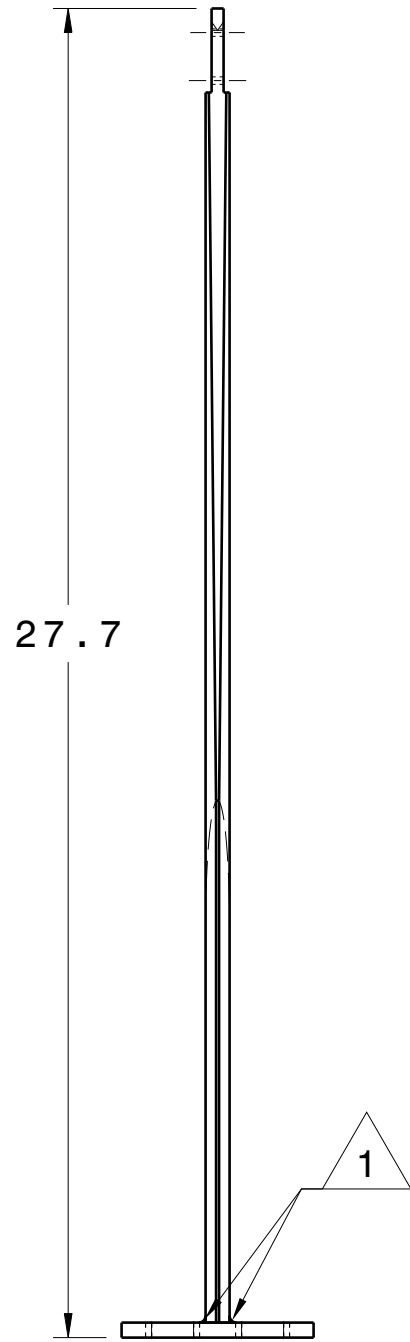
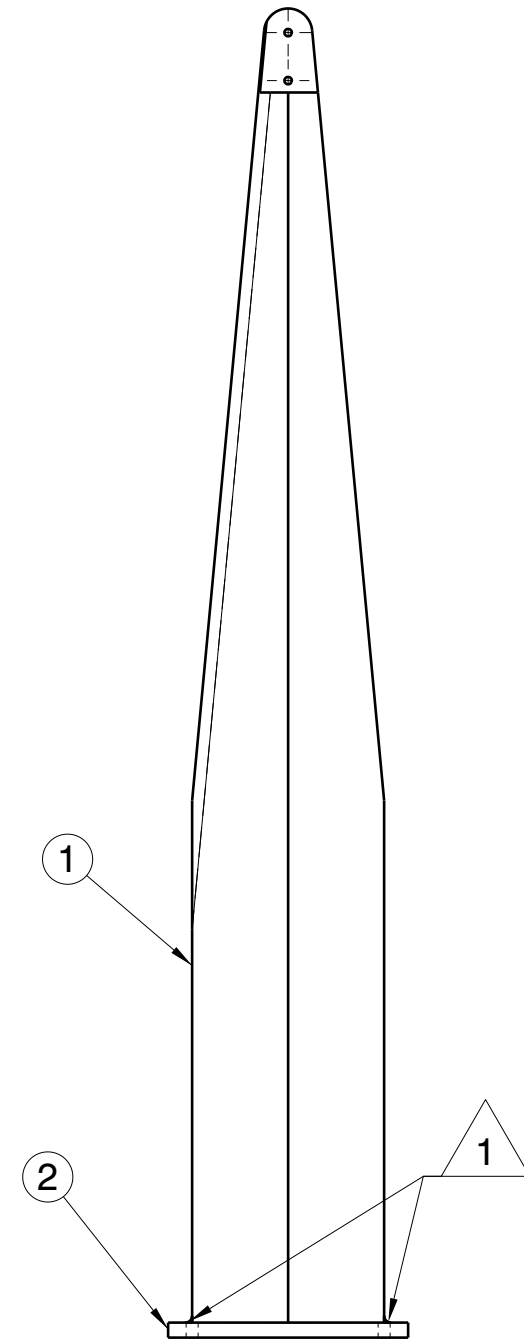
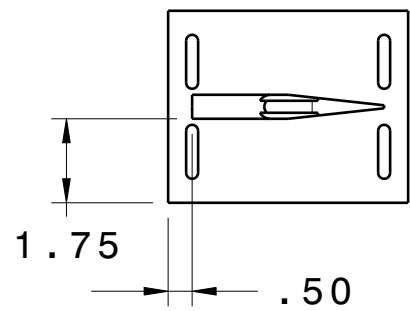


PURDUE UNIVERSITY

AERONAUTICS & ASTRONAUTICS

DRAWING NAME		REVISION
BOEING WIND TUNNEL FORCE BALANCE INSTRUMENTATION		--
DRAWING NUMBER		SHEET
		1 / X

LABEL	MODEL	CAPACITY
F0	FUTEK LRF325	75 LB
F1	FUTEK LRF350	150 LB
F2		
F3		

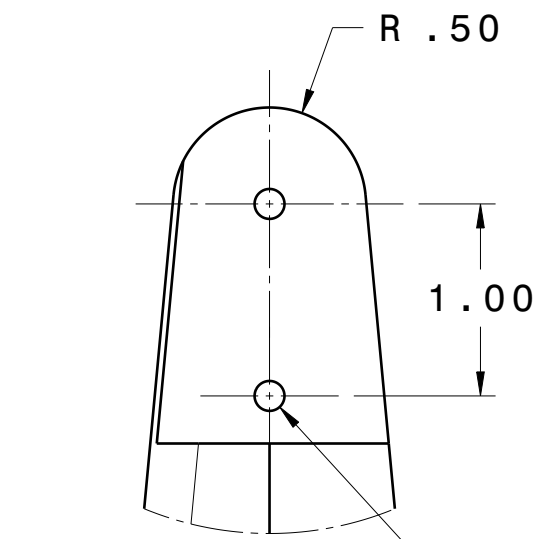


NOTES:

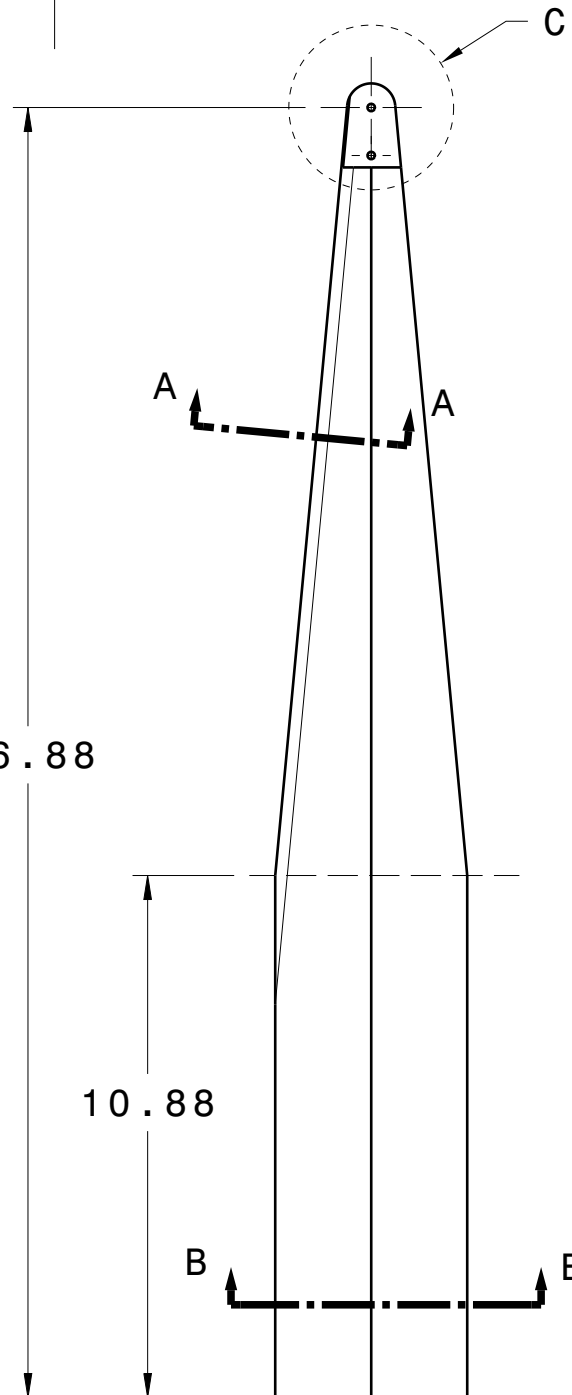
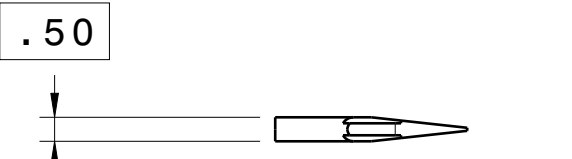
- 1 WELD PYLON TO BASE AT MACHINIST'S DISCRETION.
- 2. TO BE DONE IN THE STYLE OF THE EXISTING PYLONS.
- 3 SHOULDER SCREW FOR MODEL MOUNTING IS TENTATIVE.

UNLESS OTHERWISE SPECIFIED		DESIGNED BY: 2/21/2018		 PURDUE UNIVERSITY AERONAUTICS & ASTRONAUTICS	
TOLERANCES X.X = ±.05 X.XX = ±.01 X.XXX = ±.005		P. BALDWIN			
DEBURR HOLES AND BREAK SHARP EDGES. GEOMETRY IS DEFINED BY 3D SOLID MODELS.		DRAWN BY: 3/7/2018		DRAWING NAME	
		P. BALDWIN		Boeing Wind Tunnel -	
		SHEET SIZE		REVISION	
		B		--	
		SCALE		DRAWING NUMBER	
		1:4		1/3	
		ALL DIMENSIONS IN INCHES			

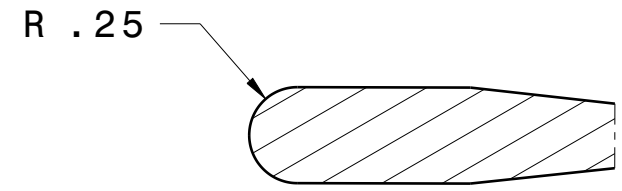
STRUT ASSEMBLY



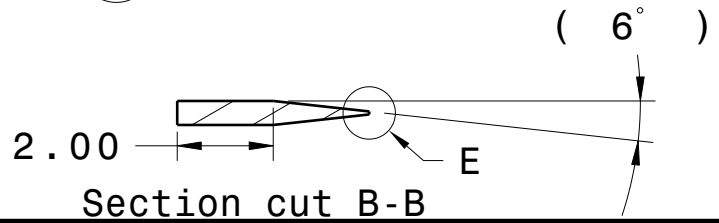
2X 10-32 THRU
Detail C
Scale: 1:1



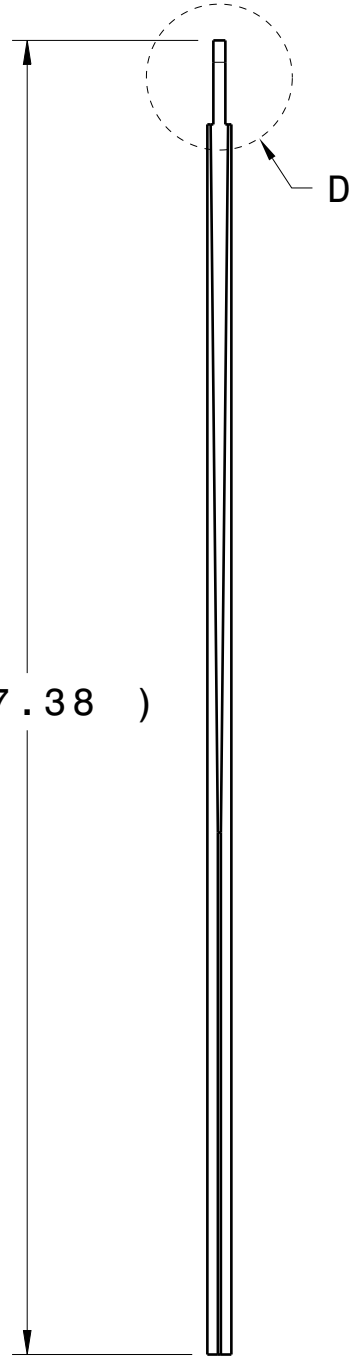
① STRUT ARM



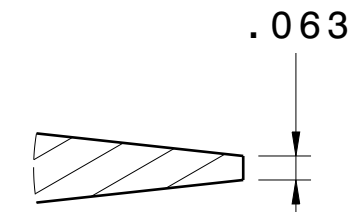
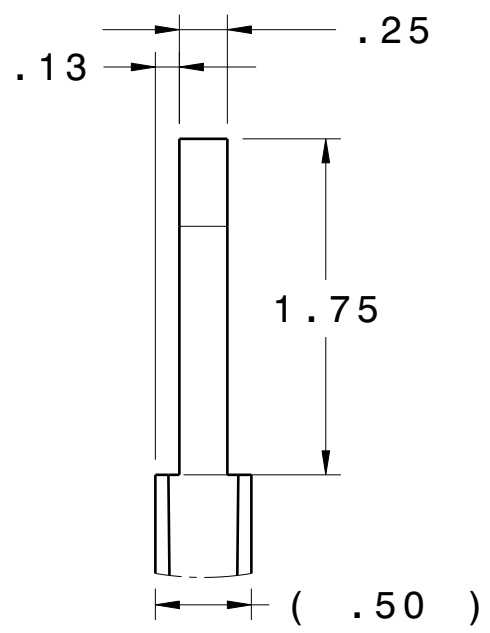
Section cut A-A
Scale: 1:1



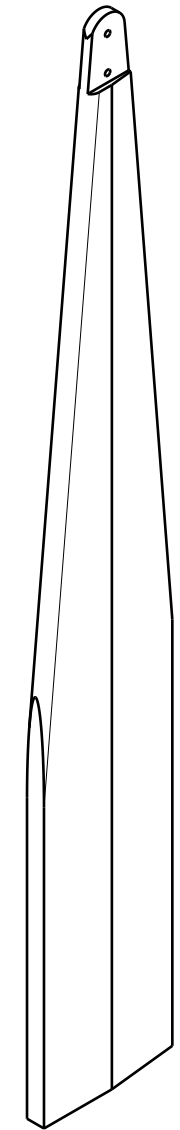
Section cut B-B



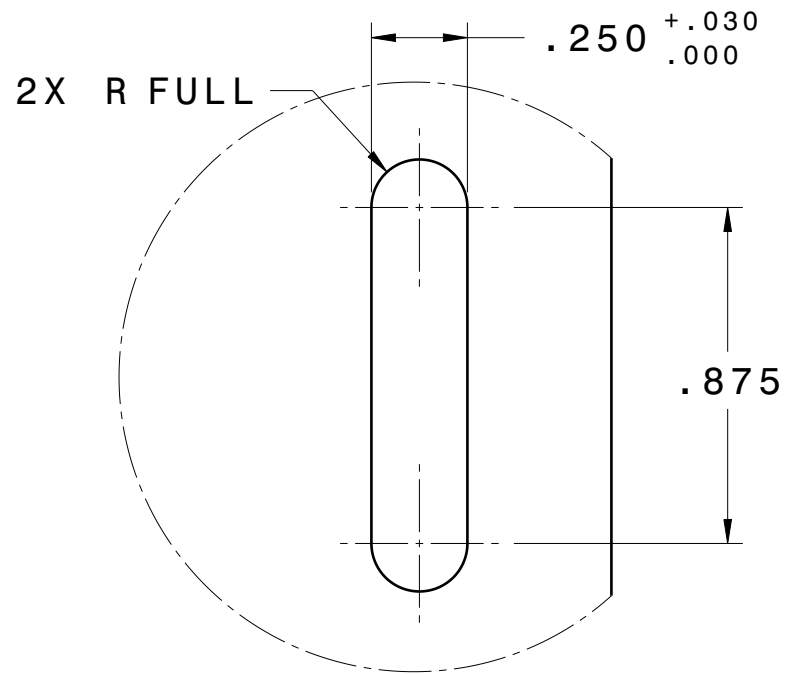
Detail D
Scale: 1:1



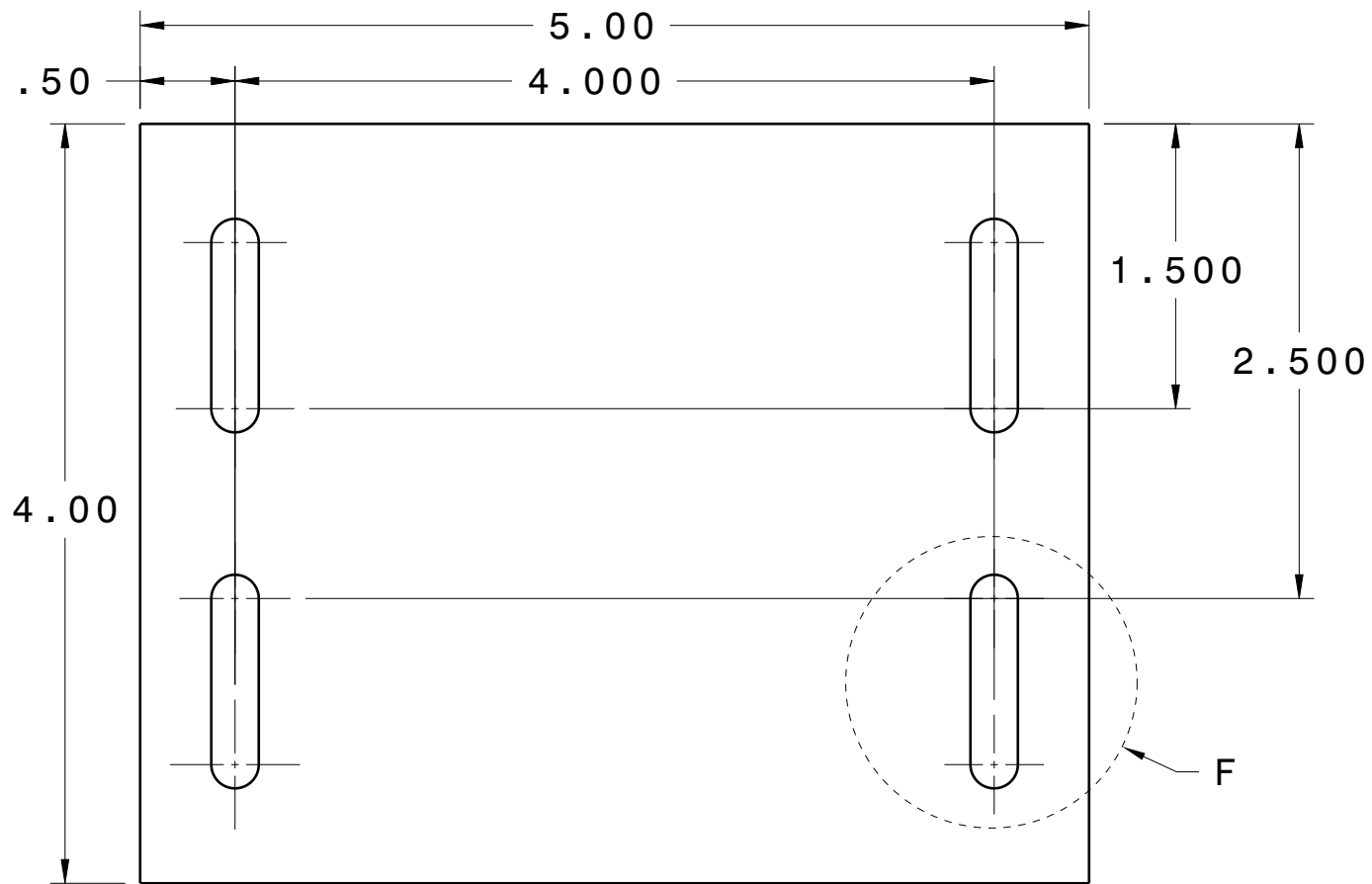
Detail E
Scale: 2:1



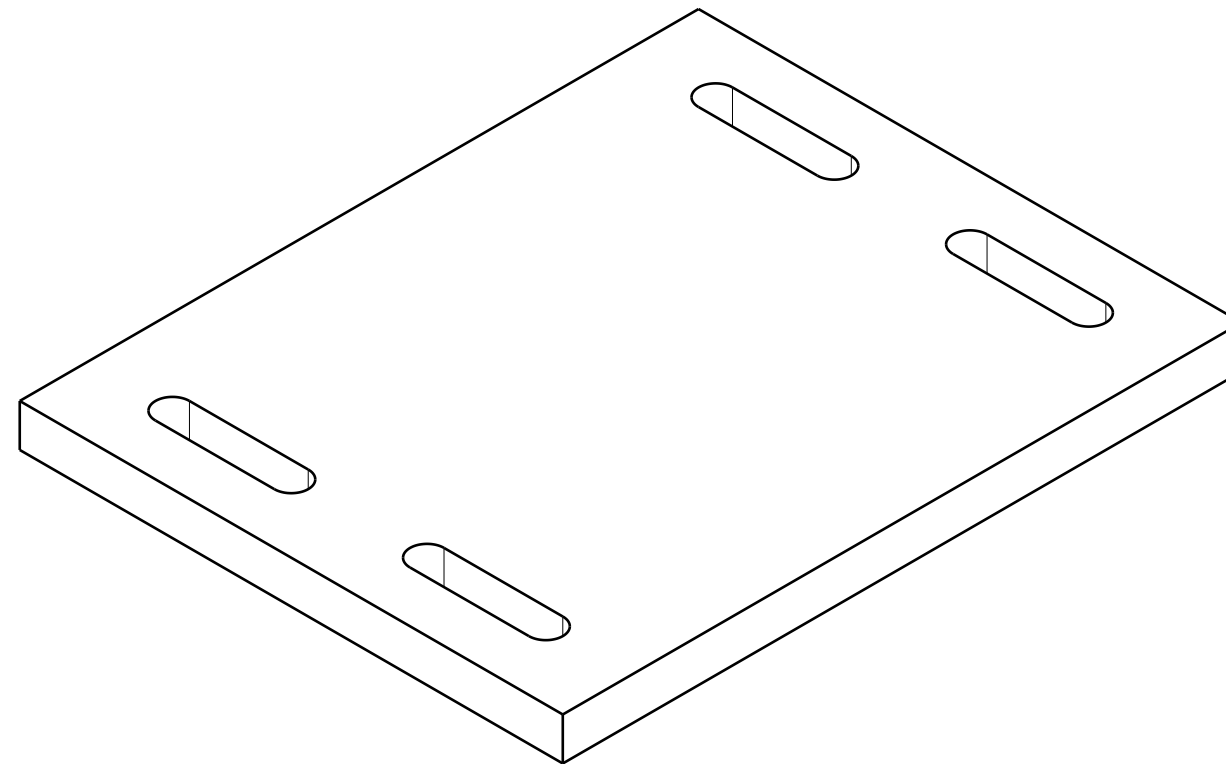
SHEET SIZE B		DRAWING NAME Boeing Wind Tunnel - New Struts	REVISION --
SCALE 1:4 & NOTED		DRAWING NUMBER	SHEET 2/3
ALL DIMENSIONS IN INCHES			



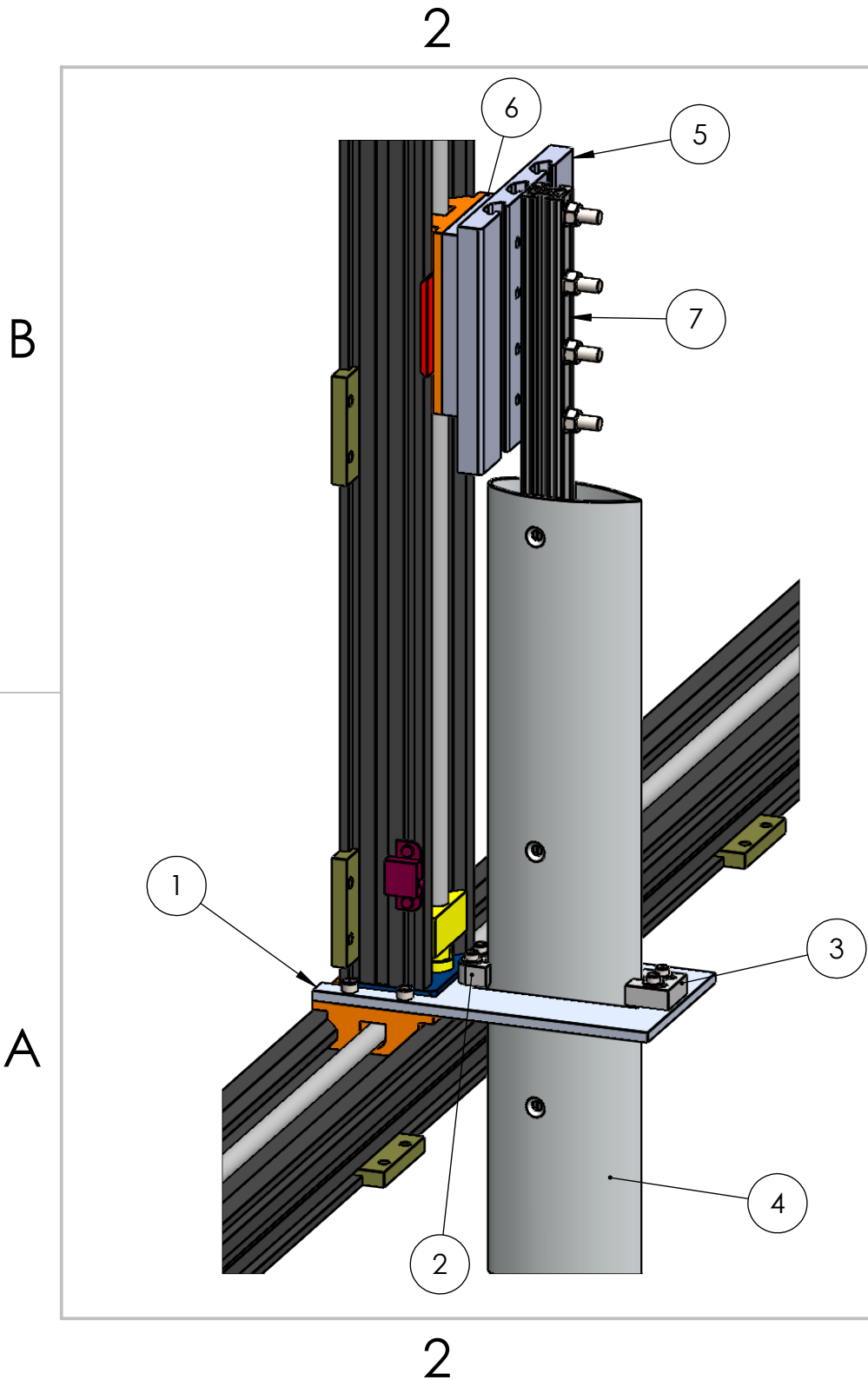
Detail F
Scale: 2:1
TYP 4 PL



② STRUT PLATE

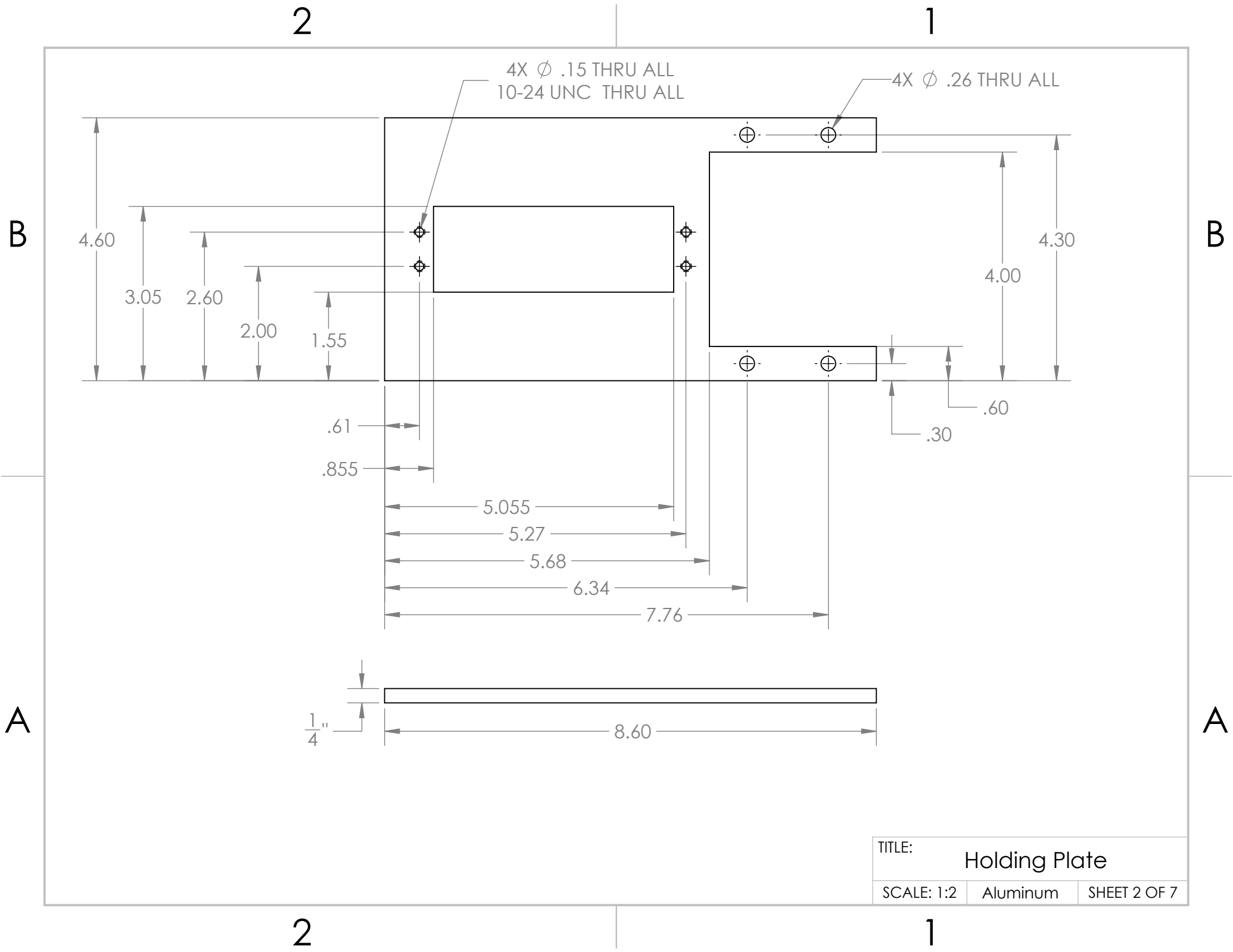


SHEET SIZE B		DRAWING NAME Boeing Wind Tunnel - New Struts	REVISION --
SCALE 1:1 & NOTED		DRAWING NUMBER	SHEET 3/3
ALL DIMENSIONS IN INCHES			

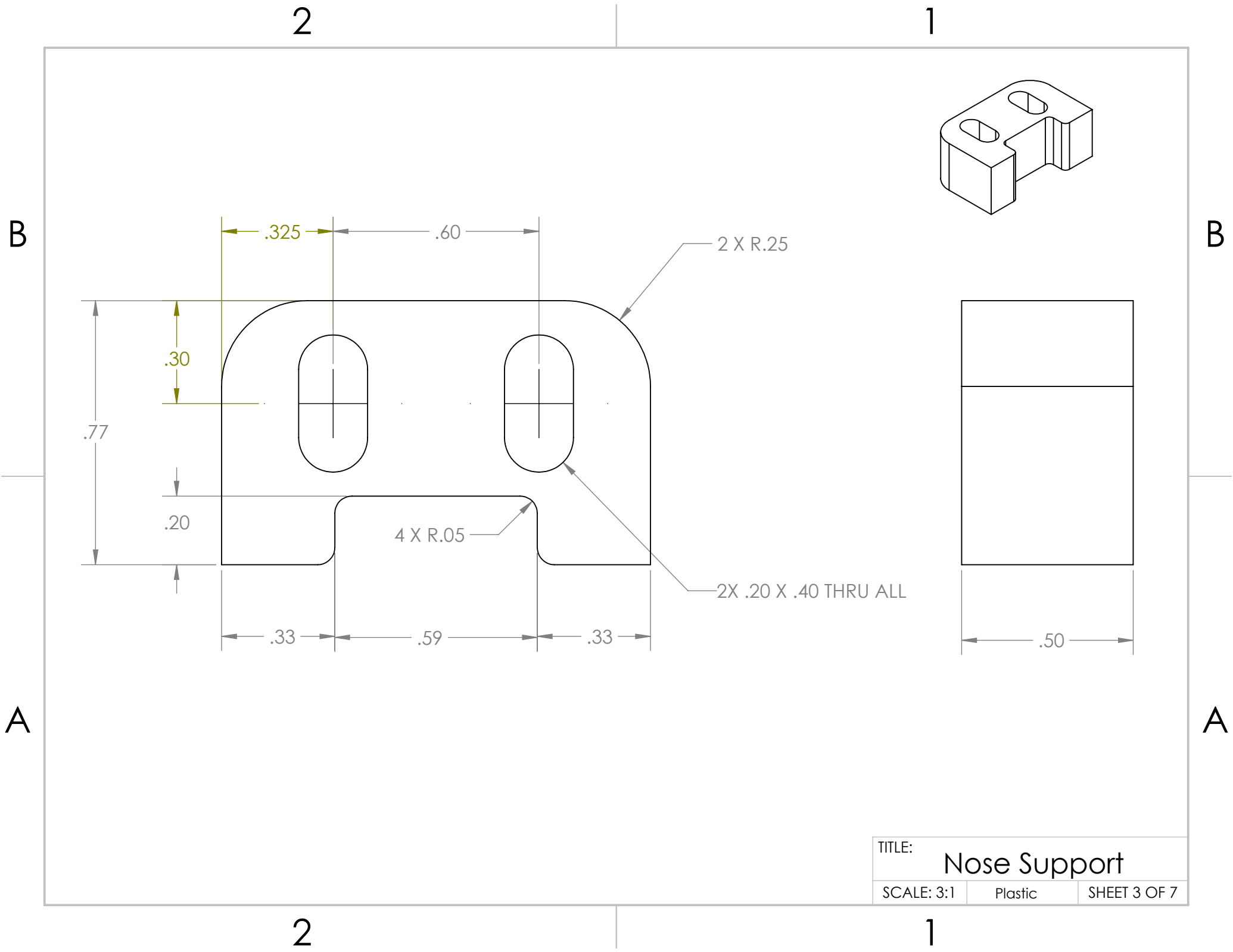


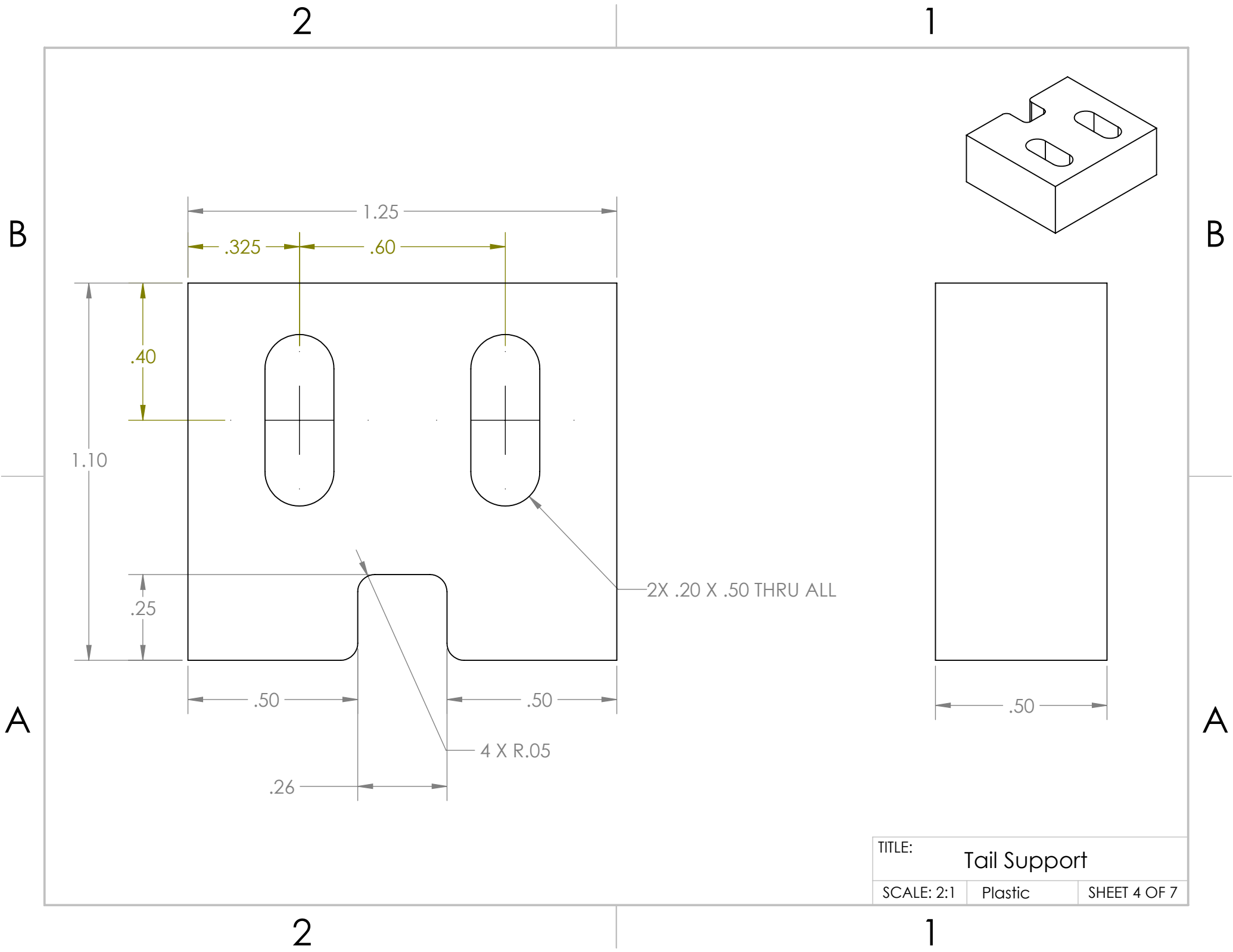
ITEM NO.	PART NUMBER
1	Holding Plate
2	Nose Support
3	Tail Support
4	Hollow Airfoil
5	Mounting Plate
6	Mounting Spacer
7	Support Rod

	NAME	DATE	TITLE:	
DRAWN	C. Diffey	7/2/2019	Traverse Probe Mounting	
COMMENTS:			SIZE	DWG. NO.
			A	--
MATERIAL			SCALE: 1:4	WEIGHT:
			SHEET 1 OF 7	



TITLE:	Holding Plate	
SCALE: 1:2	Aluminum	SHEET 2 OF 7





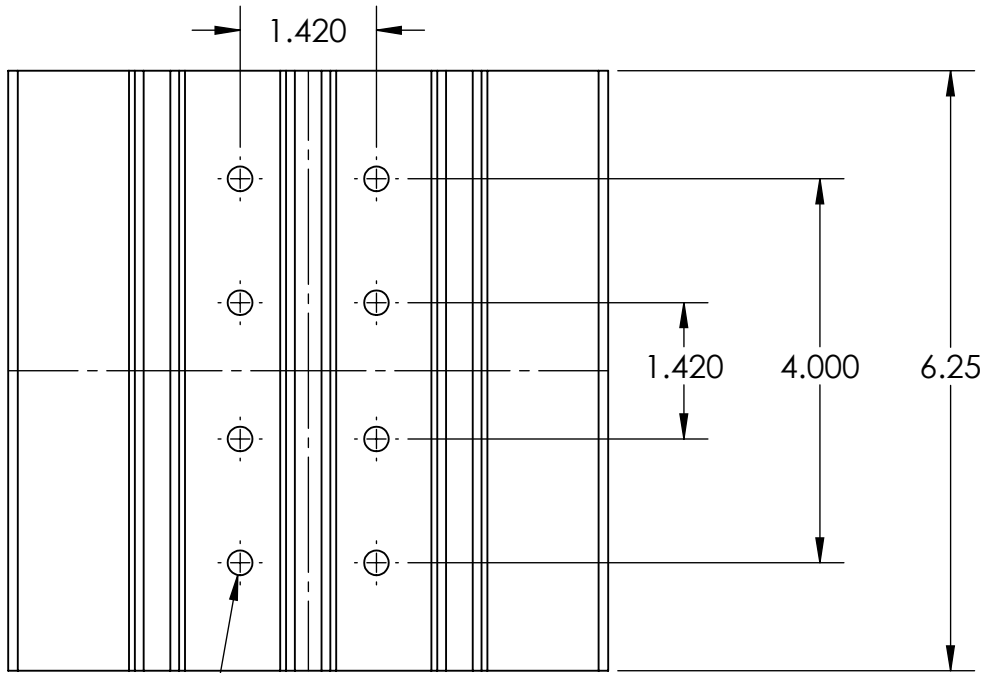
TITLE:	Tail Support	
SCALE: 2:1	Plastic	SHEET 4 OF 7

2

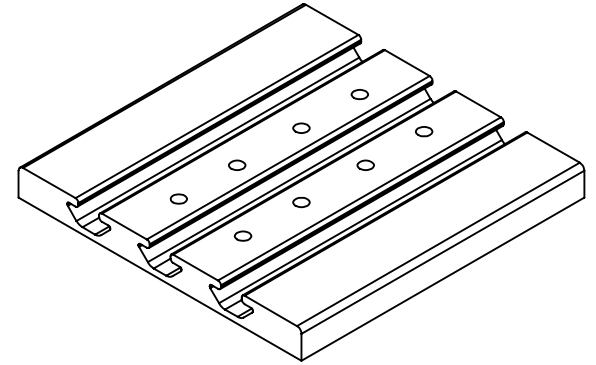
1

B

B

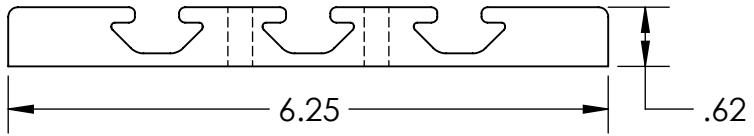


8X \varnothing F THRU ALL



A

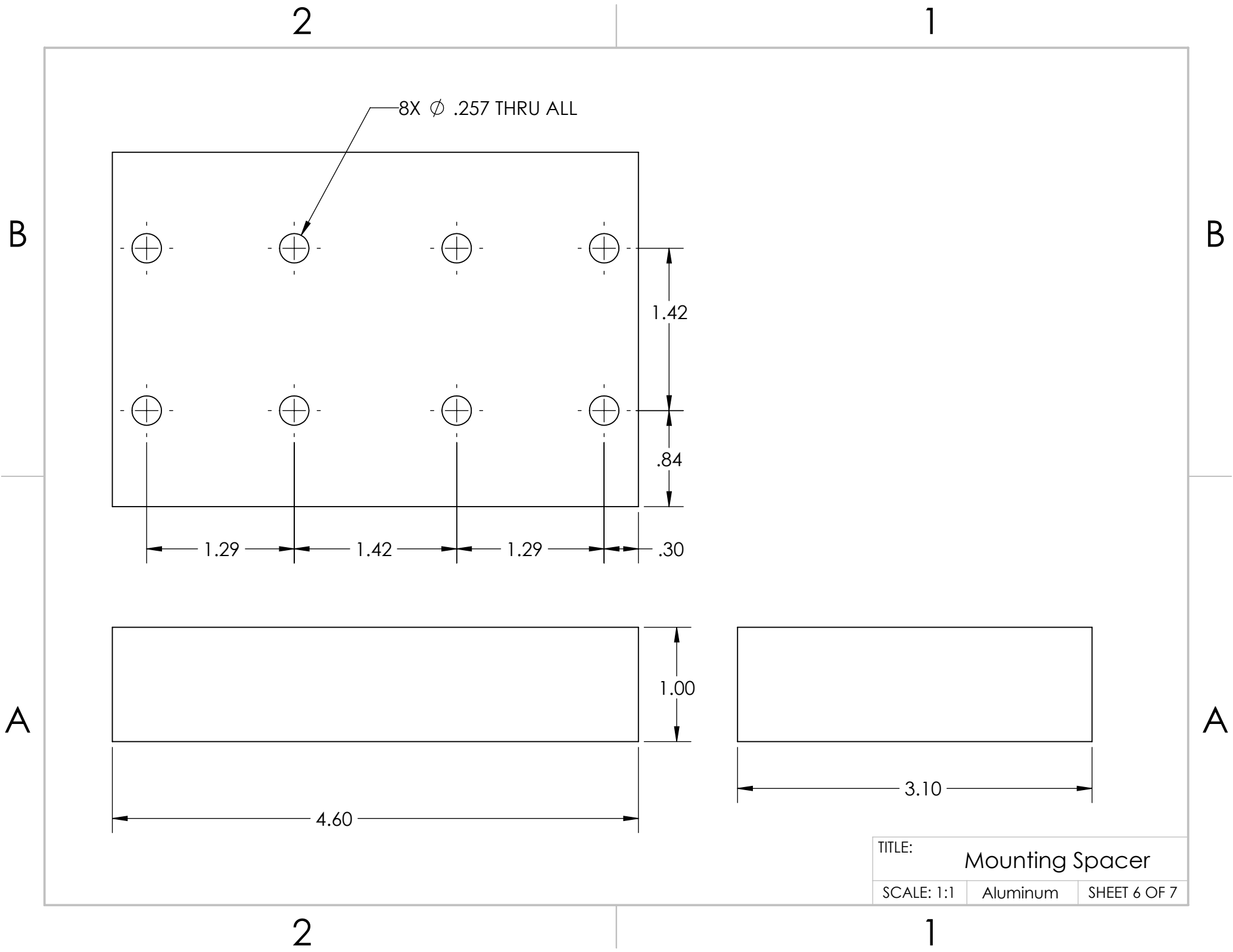
A



TITLE:	Mounting Plate	
SCALE: 1:2	Aluminum	SHEET 5 OF 7

2

1

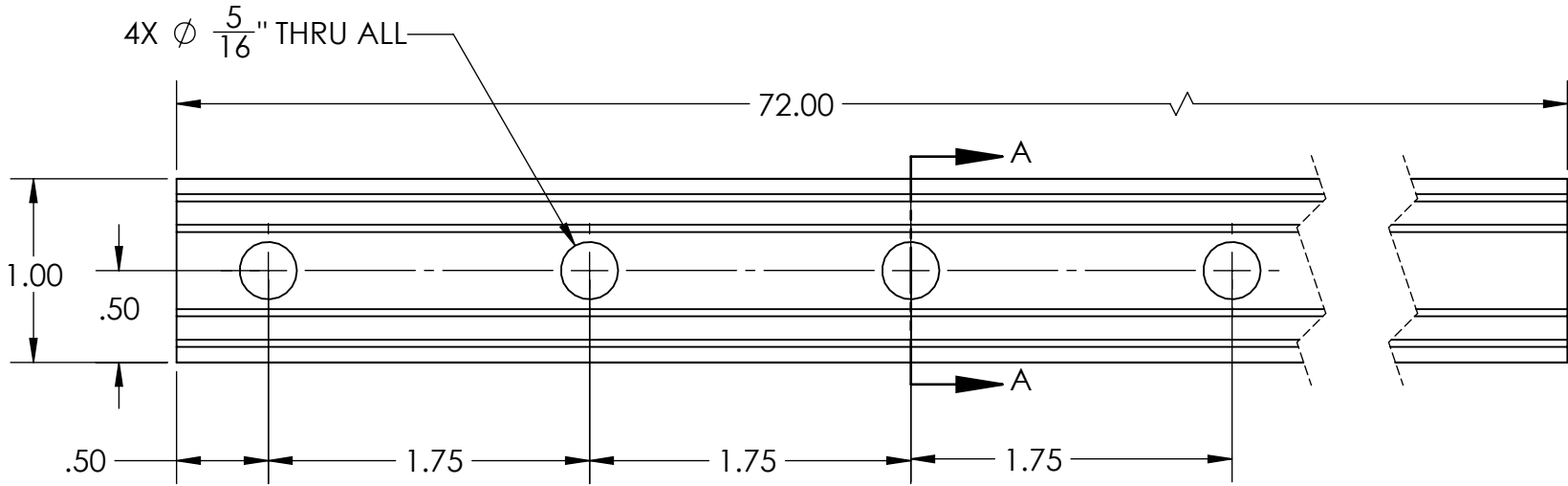


2

1

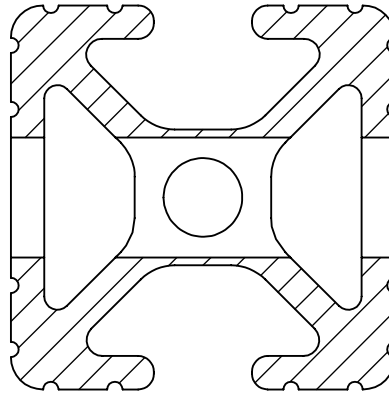
B

B



A

A

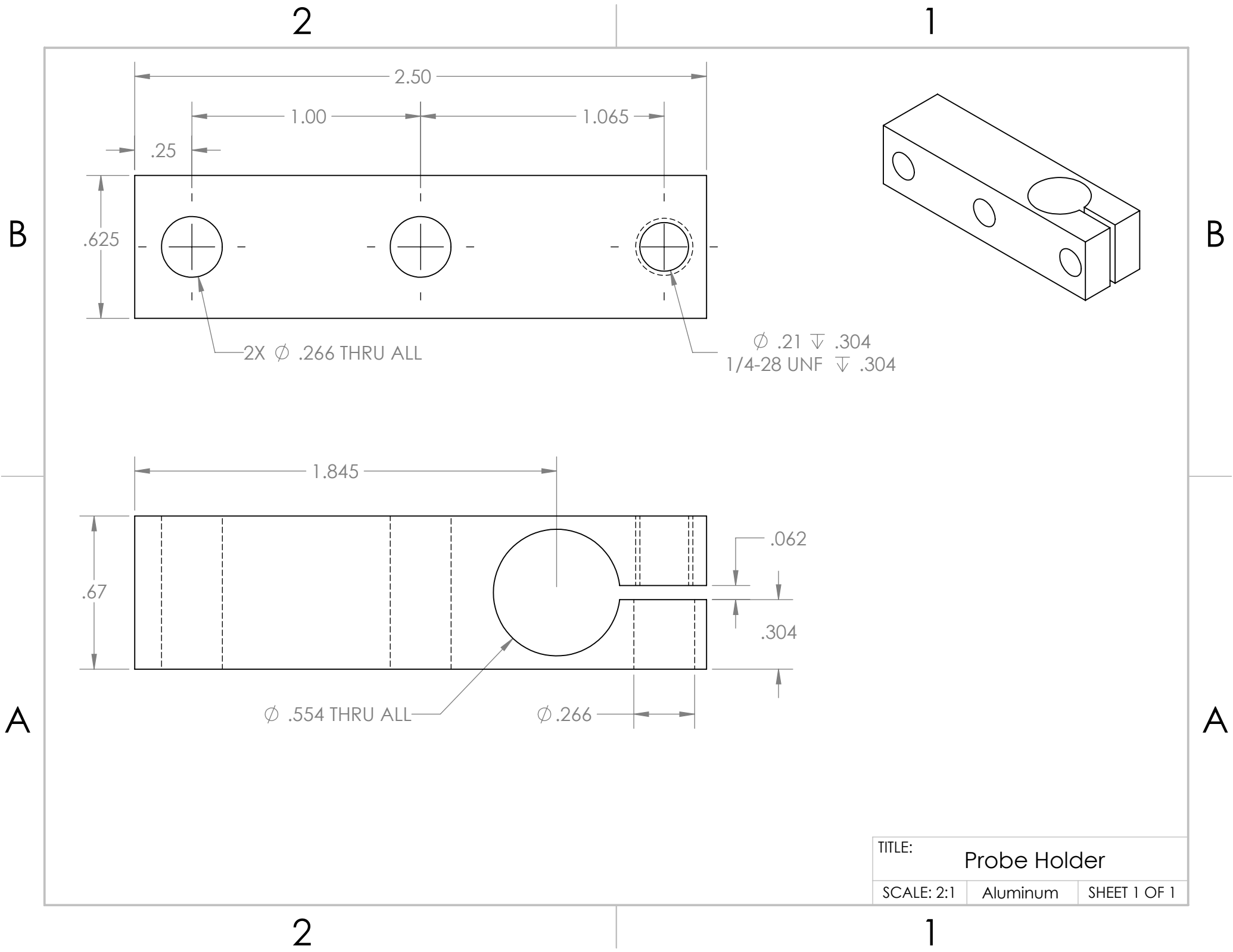


SECTION A-A
SCALE 2 : 1

TITLE:	Support Rod	
SCALE: 1:1	Aluminum	SHEET 7 OF 7

2

1



TITLE:	Probe Holder	
SCALE: 2:1	Aluminum	SHEET 1 OF 1

